# DEVELOPMENT OF RELIABILITY PROGRAM FOR RISK ASSESSMENT OF

# COMPOSITE STRUCTURES TREATING DEFECTS

# AS UNCERTAINTY VARIABLES

by

William Wilson Riddle III

A dissertation submitted in partial fulfillment
of the requirements for the degree

of

Doctor of Philosophy

in

Engineering

MONTANA STATE UNIVERSITY
Bozeman, Montana

November 2013

# APPROVAL

of a dissertation submitted by

William Wilson Riddle III

This dissertation has been read by each member of the dissertation committee and has been found to be satisfactory regarding content, English usage, format, citation, bibliographic style, and consistency and is ready for submission to The Graduate School.

Dr. Douglas S. Cairns

Approved for the Department of Mechanical & Industrial Engineering

Dr. Christopher Jenkins

Approved for The Graduate School

Dr. Ronald W. Larsen

## STATEMENT OF PERMISSION TO USE



William, Wilson, Riddle III

November, 2013

## ACKNOWLEDGEMENTS

There are a number of people that have helped me achieve this work. First, I would like to thank my committee, Dr. Douglas Cairns, Dr. John Mandell, Dr. Paul Veers, Dr. David Miller, and Robb Larson, for their mentorship and support. Dan Samborsky and the Montana State University Composites Group were instrumental in facilitating the comprehensive nature of this effort. Special thanks should be given to Pancasatya "Tiok" Agastra, Patrick Flaherty, Daniel Guest, Julie Muretta, Tammy Ritchey, and all of the undergraduate students who contributed. I am extremely grateful to Dr. Doug Cairns, who probably does not realize the instrumental role he has played on my life, beginning with helping me obtain in internship in 2006, and for his under recognized support since then. Next, I wish to acknowledge the help from Sandia contract monitors Dr. Daniel Laird and Mr. Joshua Paquette (current) while acknowledging the technical help from Mr. Mark Rumsey of Sandia. In addition, I wish to thank Mr. Scott Hughes, Mr. Michael Desmond, Mr. Derek Berry, Mr. Steve Nolet, and the entire BRC for their help and encouragement. Finally, I am extremely grateful to my entire family and especially to my wife, Spring, for all the support she has given me over the last four years.

To Dr. Cairns and Dr. Jared Nelson, many thanks for an amazing journey filled with growth, challenges and excitement. I am grateful to have been a part of this project with you both and I appreciate your friendship.

TABLE OF CONTENTS

TABLE OF CONTENTS - CONTINUED

TABLE OF CONTENTS - CONTINUED

TABLE OF CONTENTS - CONTINUED

LIST OF TABLES

LIST OF TABLES - CONTINUED

Table Page

LIST OF FIGURES

LIST OF FIGURES-CONTINUED

LIST OF FIGURES-CONTINUED

Figure Page

LIST OF FIGURES-CONTINUED

Figure Page

LIST OF FIGURES-CONTINUED

Figure Page

LIST OF FIGURES

# ABSTRACT

It has been reported that a leading cause of repairs and failures in wind turbine blades is attributable to manufacturing defects. The size, weight, shape and economic considerations of wind turbine blades have dictated the use of low cost composite materials. Composite structure manufacturing quality is a critical issue for reliability. While significant research has been performed to better understand what is needed to improve blade reliability, a comprehensive study to characterize and understand the manufacturing flaws commonly found in blades has not been performed. The work presented herein is focused on performing mechanical testing of flawed composite specimen and developing probabilistic models to assess the reliability of a wind blade with defects. The analysis postulates that one should assess defects as a design parameter in a parametric probabilistic analysis. A consistent framework has been established and validated for quantitative categorization and analysis of flaws. Results from this effort have shown that the probability of failure of a wind turbine blade with defects, can be adequately described through the use of Monte Carlo simulation. The two approaches detailed in this analysis have shown that, by treating defects as random variables, one can reduce the design conservatism of a wind blade in fatigue. Reduction in the safe operating lifetime of a blade with defects, compared to one without has shown that the inclusion of defects is critical for proper reliability assessment. If one assumes that defects account for some of the uncertainty in the blade design and these defects are analyzed with application specific data, then safety factors can be reduced. It has been shown that characterization of defects common to wind turbine blades and reduction of design uncertainty is possible. However, it relies on accurate and statistically significant data.

# CHAPTER 1

# INTRODUCTION

## Overview of Motivation

Renewable energy has been on the rise in recent years after its birth in the early 1980s, since then has later decline due to the reduction of oil prices after the oil crisis of the 1970s. Wind energy has lead the way in terms of installed power generation capacity as is evidenced by Figure 1. It can be seen in this figure that Wind Energy dwarfs all other renewable energy sources for new installed capacity and competes directly with non-renewable energy sources. [1]

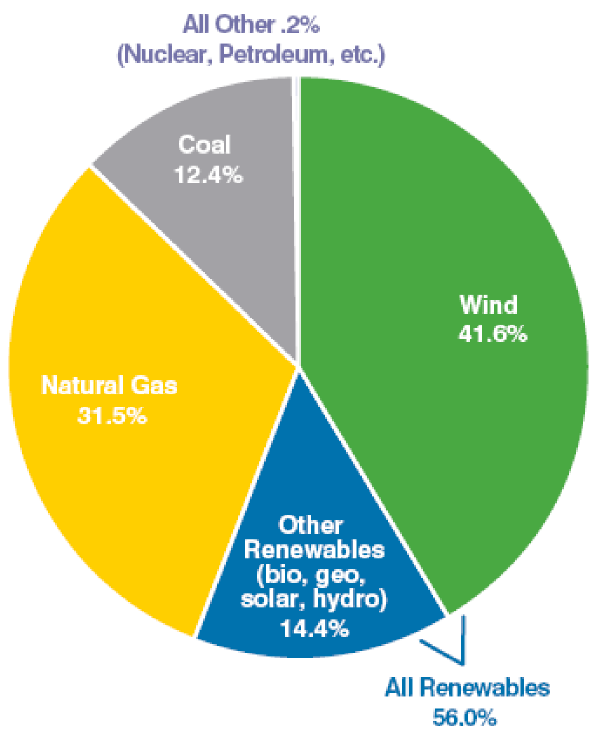


Figure 1: Percentage of New Power Generation Capacity. [1]

The capacity of wind wnergy installed in the United States has grown significantly since the late 1990s as can be seen in Figure 2 [2]. This increase can be attributed to the fact that wind energy is financially feasible which in turn has made it the flagship for renewable energy around the world.

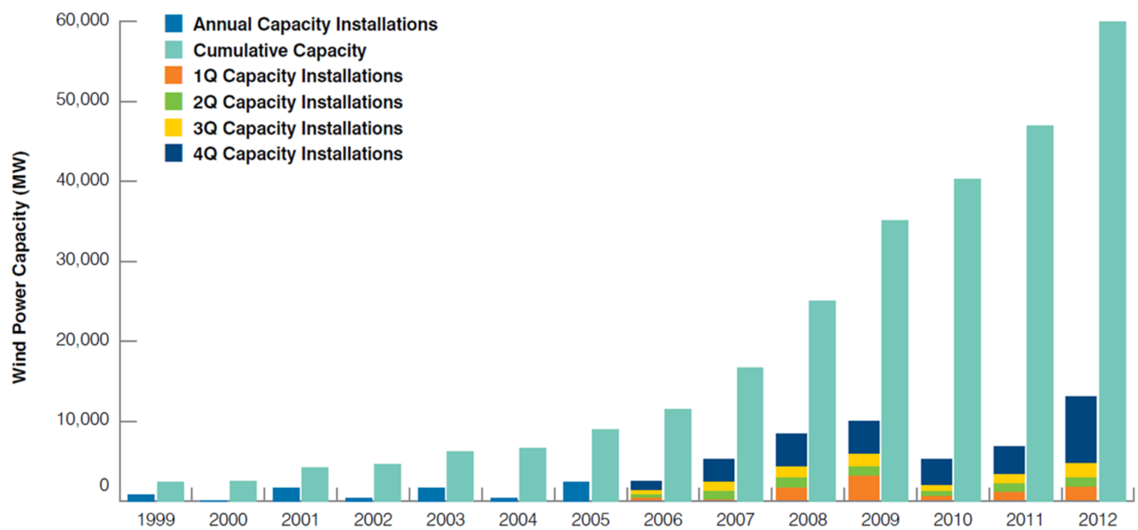

Figure 2: US Wind Capacity Growth. [1]

In an attempt to maintain growth of the wind industry, the US Department of Energy continually invests in research and removing market barriers for wind energy. Moreover, the United States has implemented a policy that targets serving 20% of the country's electricity demands with wind energy by 2030 [3]. Wind power installations must continue at close to current rates in order to achieve this scenario (Figure 3). While the economics are profitable for investors, the growth and wane of installations is consistent with the introduction and removal of subsidies. Wind energy, as with all businesses, is continually looking for more market stability. Top tier locations, with access to transmission lines for farms, are running thin. Moreover, utility companies are often reluctant to accept wind farms due to the natural intermittency of wind. It is important that wind farms achieve maximum availability by reducing down time due to maintenance and failures as much as possible.

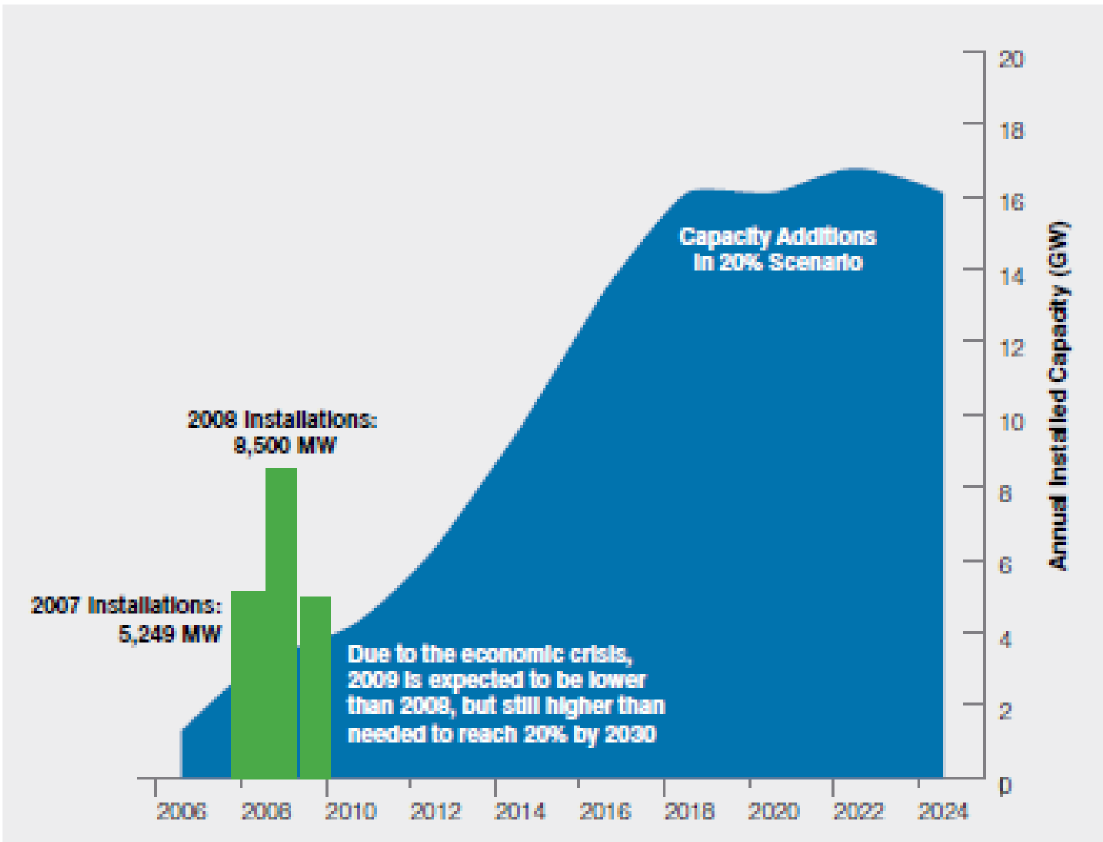

Figure 3: 20% Wind by 2030 Scenario [2].

There are many parts in a wind turbine, and a substantial number of those are located over 80m above the ground. Of particular interest to reliability are the gearbox, generator, and rotor. These systems are often large and it is a complex process to perform repairs on site. In general, repairs to these systems require the turbine to be shut down and a crane brought in to remove the problematic system. As wind farms are intrinsically windy locations, crane service is often delayed. Needless to say, any time a turbine is down it is not generating energy nor is it making money. In summary, a quantifiable and statistically defensible reliability program for wind turbines is required to maintain and achieve the potential of wind energy.

Reliability is an inherent characteristic of a system, therefore it should be considered a design objective and its assessment should be performed as an integral part of the design process. In many low-cost composite manufacturing instances reliability assessment is performed as a subjective and qualitative step, rather than using a quantifiable reliability metric. In order to achieve high system reliability levels, quantitative terms must be allied. The first step in developing improved reliability is to establish which components of the system are prone to failure. According to a study performed by Institut für Solare Energieversorgungstechnik (ISET) on historical wind farm operating data, blades and rotors result in approximately 12% of a wind turbine's down time (Figure 4) [4].

In 2008, a preliminary survey of wind turbine farm operators was performed by Sandia National Laboratories. Data collected from five wind farms showed that approximately 7% of all wind turbines blades had to be replaced prematurely. However, based on discussions with a number of major wind turbine OEMs and blade manufacturers this number is probably higher [5]. The operators surveyed in this study reported that the leading causes of repairs and failures where manufacturing defects and lightning strikes [4].

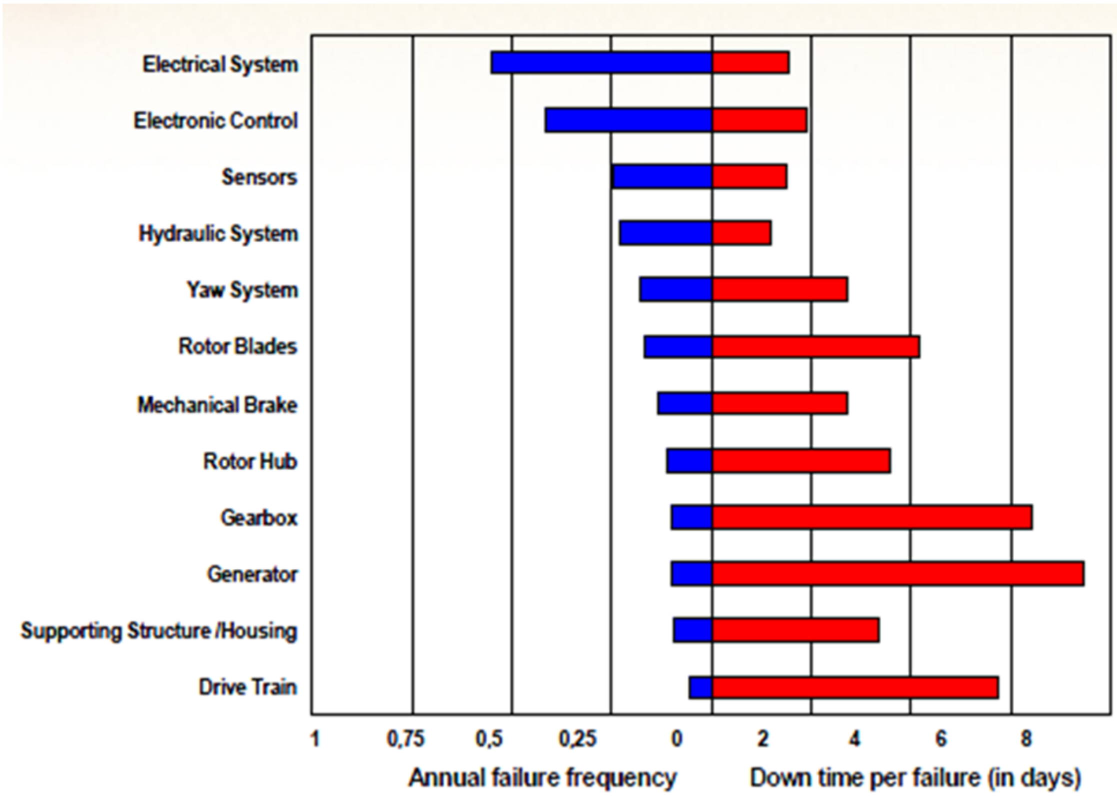


Figure 4: Wind turbine reliability from historical European data [4].

Manufacturing quality is a critical issue for improved reliability. As recently as May 2012 a Vestas turbine in Ohio experienced a very public catastrophic blade failure. A press release issued by Vestas said that the failure was a result of waviness in the carbon fiber spar cap. In  February 2010 Suzlon Energy Ltd., the world's fifth leading wind turbine manufacturer, announced a retrofit program to resolve blade cracking issues discovered during the operations of some of its S88 turbines in the United States. The six-month retrofit program was carried out by maintaining a rolling stock of temporary replacement blades to minimize the downtime for operational turbines. The cost of the retrofit program was estimated to be $25 million USD [6].  Problems such as these are not exclusive to the wind energy industry.  Growing use of composites in the aerospace industry, for example, has led to similar problems. In August of 2009 a Boeing supplier halted manufacturing of the barreled pieces of the 787's mid-section because of a problem in the manufacturing process. This manufacturing problem resulted in macroscopic wrinkles in structural stringer supports along the length of the airframe. Boeing had to develop a patch in order to repair the existing plane sections. Subsequently newer sections were made utilizing a different manufacturing process [7].

The size, weight, shape and economic considerations of wind turbine blades have dictated the use of low cost composite materials. Large blades are likely to use the heaviest possible reinforcing fabrics or prepreg ply thickness to achieve manufacturing efficiency. Increases in fabric weight—and therefore thickness—may affect basic in-plane properties, delamination, and problems associated with ply drops where the thickness is tapered [8]. Moreover, thick composite laminates have an increased likelihood of hidden flaws and multiple flaws being grouped in the same local area. A number of production-related flaws may occur in larger structures which are more easily avoided in smaller structures, and rarely appear in test coupons. Typical of these are fabric joints and overlaps where individual rolls of fabric terminate, as well as flaws in the fabric where individual strands terminate during production. Other factors that are more likely in the manufacture of larger blades include fiber waviness, large scale porosity, large resin rich areas, and resin cure variations through the thickness [9].

Even though composites have desirable engineering qualities, it is not apparent that design and manufacturing within the wind industry are able ensure a 20 year product life. This is in part due to the relative infancy of the industry. Most wind farms are not very old or are retrofitted with larger turbines prior to reaching the full twenty year design life. The most influential economic factor to the wind industry is tax subsidies, and should the industry desire to remain economically productive without subsidies, it will be imperative that every opportunity to improve performance be exploited. Prevention of failures is one area where improvements can be made to support the continued development of the wind turbine industry. While significant research has been performed to better understand what is needed to improve blade reliability, a comprehensive study to characterize and understand the manufacturing flaws commonly found in wind blades has not been performed. The Department of Energy (DOE) sponsored Blade Reliability Collaborative (BRC) is one initiative designed to perform such research.

## General Project Overview

Montana State University (MSU) has taken responsibility for the Effects of Defects portion of the BRC and has split this into two distinct tasks; Flaw Characterization and Effects of Defects. The function of the Flaw Characterization portion of this program has been to provide quantitative analysis for two major directives: (A) acquisition & generation of quantitative flaw data for use in the Effects of Defects numerical modeling program; and, (B) development of a probabilistic approach to establishing flaw severity and reliability of defect laden blades. The Effects of Defects portion is focused on the development of Progressive Damage modeling capabilities to predict the structural implications of common flaws found in composite wind turbine blades.

Testing and analysis are being performed on a specific material system and as such the absolute values presented are only valid for that particular system. However, the framework under development may be reproduced by interested parties on their specific material and structural systems. Moreover, the probabilistic reliability and criticality/severity metrics being developed should be applicable to any composite structure assuming the requisite data is utilized.

The BRC has charged the Montana State University Composites Group (MSUCG) with the goal of "understanding and quantifying the effects of manufacturing discontinuities and defects with respect to wind turbine blade structural performance and reliability." As noted, two coordinated distinct tasks were established to meet this goal: Flaw Characterization and Effects of Defects. The work herein describes the former. However, integral to the overall program is work performed by Jared Nelson on the Effects of Defects task, which has focused on developing coordinated progressive damage models. In his study it was proposed to:

a. Understand critical flaw types.
    i. Critical flaw types determined from flaw database and probabilistic modeling.
    ii. Previous research specific to blades and from other applications.
b. Characterize the mechanical properties of common flaws deemed critical to composite blades.
c. Determine the criteria at criticality threshold of each flaw type.
    i. Flaw type, size, and location.
d. Use a three-round study to develop coordinated 2D analytical and experimental analogs for damage growth and residual strengths necessary for blade reliability.
    i. Develop finite element model initially at individual flaw scale.
    ii. Improve model toward full blade scale with combinations of flaws.
e. Understand and model how these flaws contribute to the entire structure.

f. Complement on-going activities of entire BRC.

The work-flow diagram shown in Figure 5 maps out the progression necessary to achieve each of these individual goals. It is worth noting that the iterative approach allowed for additional physical testing to be continuously integrated into the models, while allowing for the accuracy of each model type to be continuously improved. More details of his effort can be found in Nelson's Doctoral Thesis, ref [10].

The overall process is described in the following flowchart;

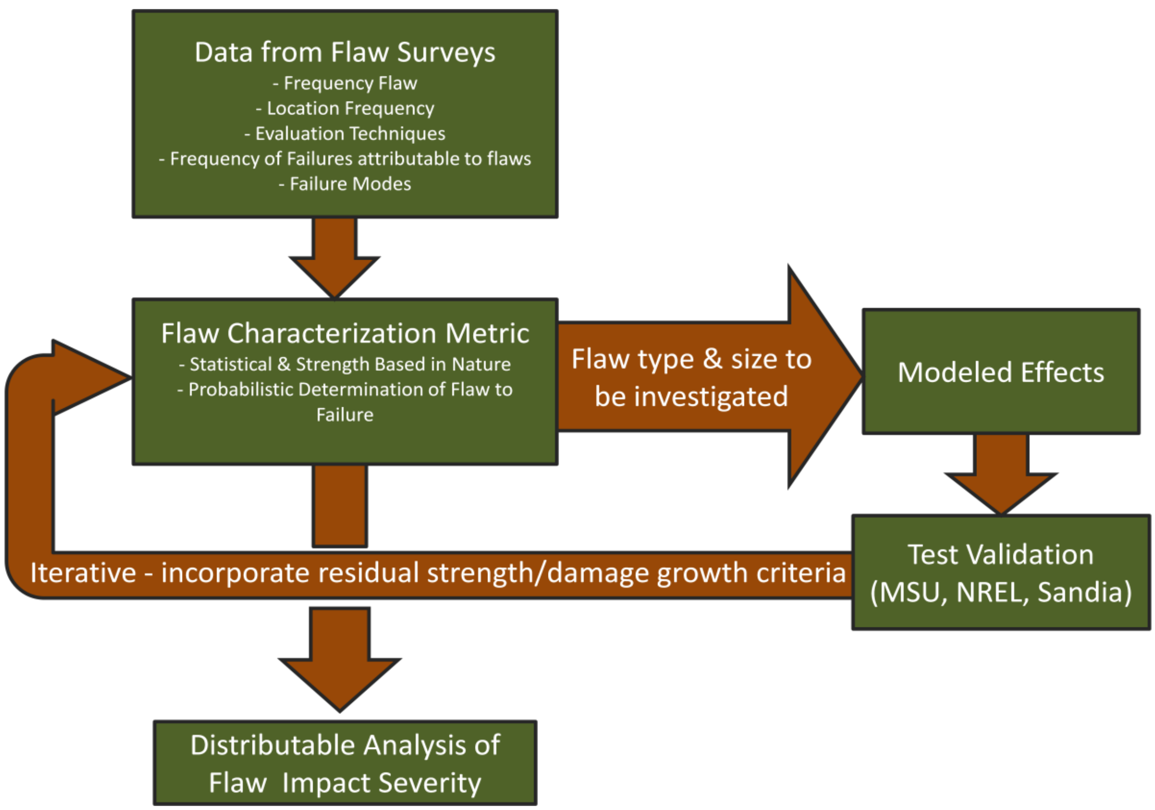


Figure 5: Flow chart describing the general work plan

The preliminary results from a survey of wind turbine blade manufacturers, repair companies, wind farm operators and third party investigators have directed the focus of this investigation on two types of flaws commonly found in wind turbine blades:

waviness and porosity/voids (Figure 6). A variety of flaw geometries as defined by in-field collection of production scale blade data has been investigated and complied. Basic statistical analysis has shown that the data generally follows standard distributions. The preliminary results from this effort and coupon level testing have established a protocol by which a defect in a blade can be characterized quantifiably.

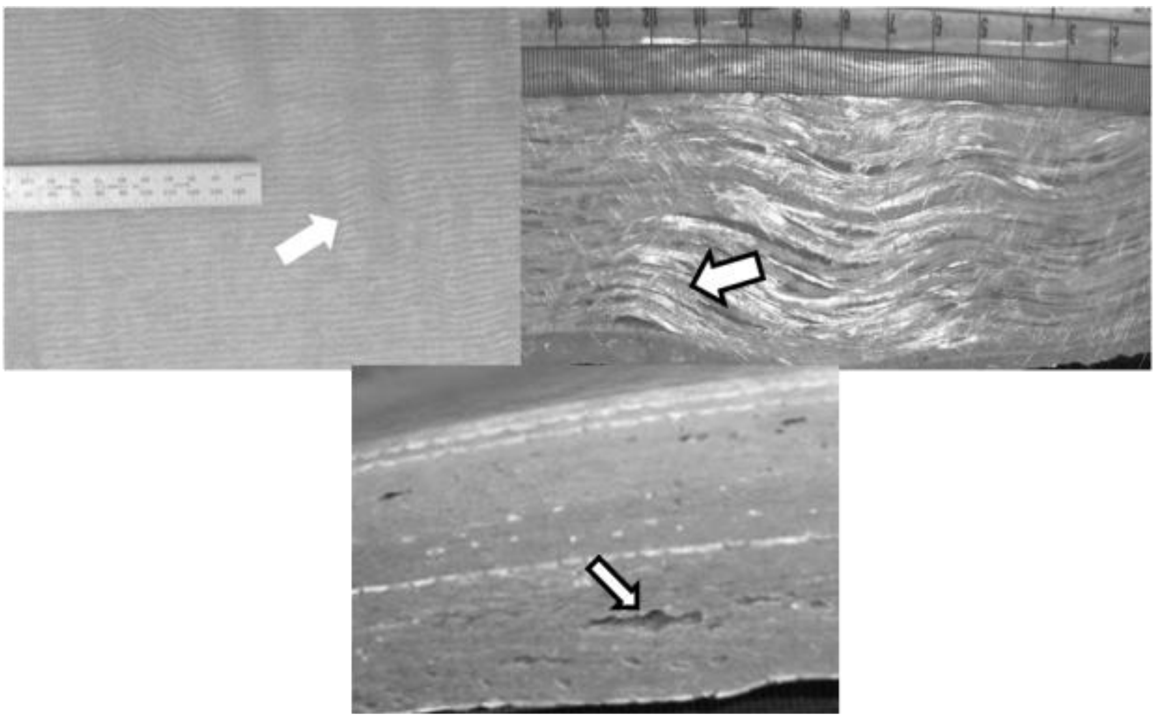

Figure 6: IP Waves seen on the surface (top-left); OP Waves seen through the thickness (top-right); and, Porosity/Voids seen within the laminate (bottom).

## Experimental Overview

Physical testing is necessary to establish damage growth characteristics and to validate tools for prediction of composite wind blade strength and durability in order to contribute toward a reliability infrastructure for the wind industry. The goal of the MSU test program was to characterize the mechanical properties of the critical defect types.

The results were utilized for analytical/experimental correlations, with the purpose of performing laminate analysis with included defects. An understanding of the changes in the material properties associated with characterized flaws was achieved on a coupon level with physical testing performed in several configurations of the different flaw types. The results of the three rounds of testing are presented in Chapter 5.

Generally, laminates were infused utilizing a Vacuum Assisted Resin Transfer Molding process. Coupons were constructed with representative blade materials. This testing program clearly indicated that fiber misalignment and porosity resulted in degraded material properties. While this is not a new development, the testing enabled evaluation of metrics concerning material degradation specific to the wind blade industry.

## Analytical Overview

Variations in the structural behavior of composites cannot be characterized by traditional deterministic methods that utilize safety factors to account for uncertain structural response. While safety factors are often derived from a probabilistic understanding of the inherent uncertainty (and/or variability) in strength or loading, improvements may be made in the design of composites structures with a better understand the system variability.  Sources of variability should be eliminated or assessed in stochastic analysis where possible. Design margins can then be created to consider the rest. Moreover, lightweight composite materials are known to be sensitive to fatigue and defects/damage. Therefore a methodology focused on reliability targets, which incorporates probabilistic modeling, is essential to accurately determine the structural reliability of a composite structure. Typically these methods are used with limit state equations in the design process to describe the reliability or probability of failure a system. [11]

A comprehensive protocol addressing the impact of manufacturing flaws on the reliability of wind turbines has been proposed. The main points of this framework can be summarized in four disciplines; Effects of Defects, Probabilistic Structural Reliability Modeling, Criticality Analysis and In-Field Evaluations. The majority of the work discussed herein is focused on Effects of Defects and Probabilistic Structural Reliability Modeling.

The Probabilistic Structural Reliability Modeling section of this work has incorporated mechanical testing results, developed under the Effects of Defects umbrella, and system (composite laminate structures with flaws) variability/uncertainty, into a novel modeling approach that calculates the probability of failure based on a probabilistic treatment of defects. Consideration was given to structural analysis techniques that include deterministic fatigue life formulation and fracture mechanics based damage progression models. A sensitivity analysis has been performed to correlate model input parameters (e.g. wind loads & defect distributions) to output responses.

To meet the proposed goals of this project, analytical efforts were undertaken in a progressive manner through the various testing programs. Initial rounds of simple uni-directional coupons have utilized relatively simple material degradation models (knockdown factors). However, as test specimen become more complex in future investigations, corresponding models will likely need to become more complex.

## Summary of Results

A consistent framework was established and validated for quantitative categorization and analysis of flaws. With proper characterization, it is possible to establish the structural implication of a flaw. Applying the characterization techniques described in Chapter 4 to incoming data have enabled the generation of a statistically significant and comprehensive flaw database. Understanding the changes in the material properties associated with characterized flaws has been achieved on a coupon level with physical testing being performed with several configurations of several different flaw types. Analysis of the test results show that strength degradation in laminates with waves, tend to correlate slightly better to the average off-axis fiber angle of all layers as opposed to the maximum fiber angle. Compression of OP waves is still under investigation..

Results from this effort have shown that the probability of failure of a wind turbine blade with defects, can be adequately described through the use of stochastic modeling. Comparisons between traditional safety factor analysis and a probabilistic treatment of defects has shown that the inclusion of defects is critical for proper reliability assessment. Moreover, results have shown that safety factors in design can be reduced by including defect centric analysis. It has been concluded, however, that it is necessary to have a comprehensive defect data set with representative distributions. While probabilistic modeling will provide the designer with significant insight, it constitutes only one portion of an effective reliability program. Additional efforts have utilized the results from this analysis to generate a Criticality Assessment protocol, which can be used in-situ to assess as-built composite structure with defects. [12]

# CHAPTER 2

# LITERATURE REVIEW/BACKGROUND

This chapter is intended to provide background on the theory of reliability, probabilistic analysis, existing applications of reliability analysis and a discussion on the state of reliability in the wind industry. It is the synthesis of these elements that has allowed for the development of the Probabilistic Reliability Protocol (PReP) utilizing the computations outlined herein.

## Probabilistic Reliability Analysis

Variations in the structural behavior of composites cannot be adequately characterized by traditional deterministic methods that utilize safety factors to account for uncertain structural behavior. One result of this perspective is that structural reliability cannot be appropriately quantified. A design methodology that incorporates probabilistic modeling is needed to accurately determine the structural reliability of a composite structure [13].

### Fundamental Reliability Analysis/Formulation [14]

Introduction to Reliability Theory. Reliability is simply the probability that the system will perform its stated objective for the specified lifetime. Reliability at the component level can be described by the probabilistic relationship between the applied load and inherent material or structural resistance. This can often be analyzed in engineering terms as an external force and the stress/strain structural response. A common metric for assessing or expressing reliability is the Reliability Index, β.

As depicted in Figure 7, the fundamental concept behind analysis of a engineering problems from a deterministic perspective, where the expected Load (Q) and known Resistance (R) are shown on a number line. In deterministic terms, a safe design is achieved when the load has a value less than the resistance. While Safety Factors are used computationally as deterministic inputs, they are actually designed around the uncertainty of a system. There are two commonly used methods to account for error, or uncertainty, in a deterministic formulation; Factor of Safety and Margin of Safety. Using a Factor of Safety (*FS*) formulation where $FS = R/Q$, a "no failure" state exists where $FS > 1$. With the Margin of Safety (*M*) formulation, $M = R - Q$, a "no failure" state is where $MS > 0$. [14]

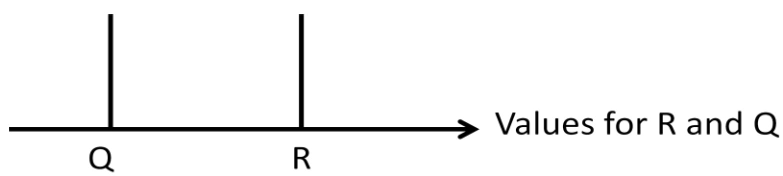


Figure 7: Deterministic view of load ($Q$) versus resistance ($R$).

Uncertainty for both load and resistance can, and does exist. One example of uncertainty in resistance is the simple case of ultimate strength test data for a material (Figure 8). The scatter in the test results inherently depict variability in the material. This scatter or variability, can be described with a probability distribution that mathematically assesses the variation in strength. An example probability distribution  has been applied to the test data presented in Figure 8. The Normal distribution in Figure 9 was generated based on the mean and standard deviation of this same data.

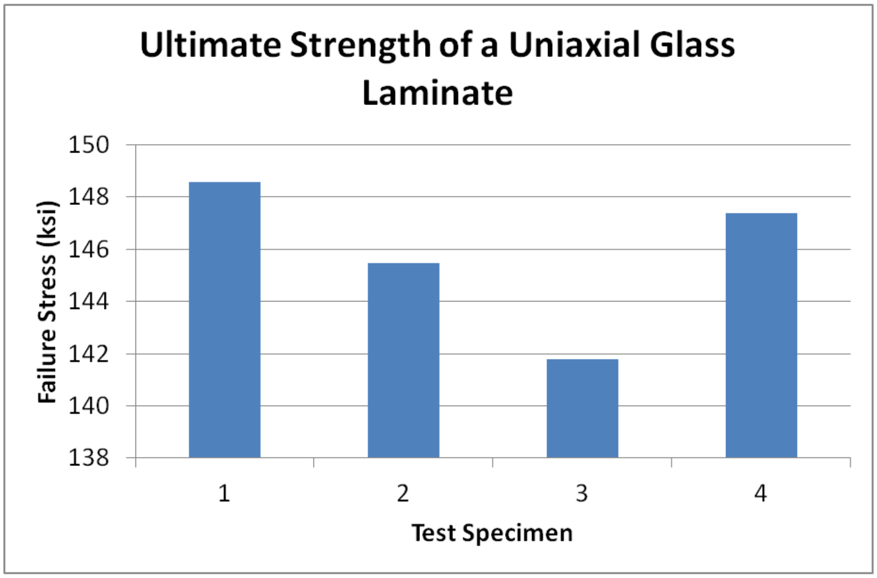


Figure 8: Static Failure Test results of ultimate stress

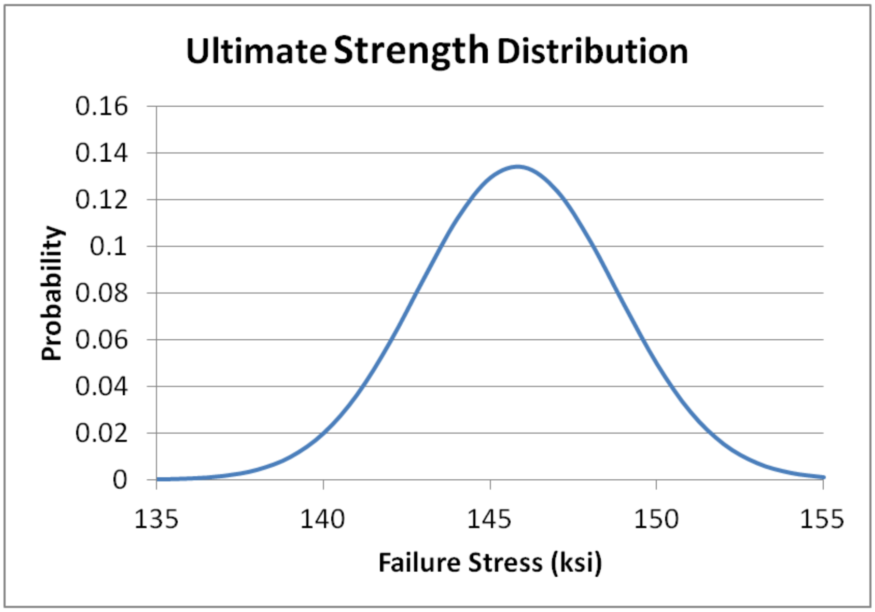


Figure 9: Example of ultimate strength probability distribution

Probability distributions can be generated to describe almost any system with variability, assuming some data is present. In addition to material or structure resistance properties, system loads can also be described with probability distributions. This is quite common in the wind industry as wind speed is inherently variable. When we include the uncertainty of the load and resistance in the analysis (Figure 10), it can be seen that there may exist a region where the load value is higher than the resistance value, and therefore failure can occur.

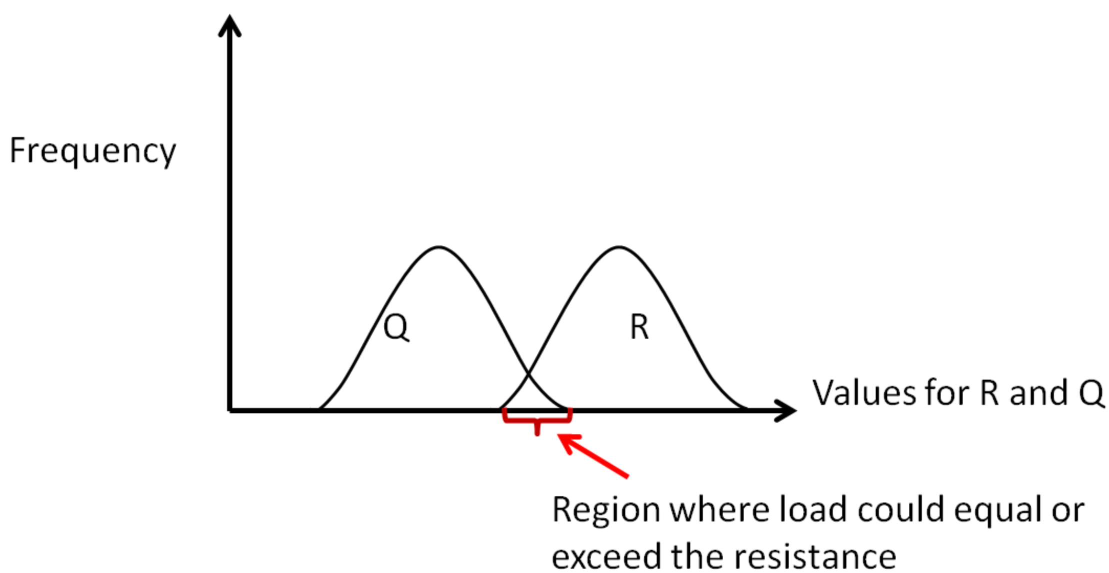


Figure 10: Probabilistic view of load (Q) versus resistance (R).

Using mean values for the load and resistance distributions in a Factor of Safety or Margin of Safety formulation, could result in a "safe" design. However, if there is sufficient uncertainty in the load and/or resistance, then a probability of failure will exist. The fundamental presentation of component reliability can be accomplished using the

Margin of Safety formulation, and assuming that the load and resistance are jointly normal.

$$\mu M = \mu R - \mu Q \tag{1}$$

$$\sigma_M^2 = \sigma_R^2 + \sigma_Q^2 - 2\rho_{RQ}\sigma_R\sigma_Q \tag{2}$$

$$\beta = \mu_M/\sigma_M \tag{3}$$

where $\mu$ is the mean and $\sigma$ is the standard deviation of the load and resistance distributions.

General Reliability Procedure. Most reliability problems require more sophisticated solutions than the one presented in the previous section. This is because the distributions of load and resistance cannot be assumed to be normal (or lognormal) and there are often several uncertainty variables that need to be included in a reliability analysis. There are numerous solution techniques however all of the various solutions follow similar steps;

1.) Determine the equations, formulas, models, etc., that will be used to calculate R and Q. These can be empirical, theoretical, or approximate.

2.) Calculate the first and second moments (mean and coefficient of variation) of R and Q. This is often sufficient, but the full distributions can be used if available.

3.) In many cases the margin of safety formulation is used, $M = R - Q$ so the first and second moments of M are known. Here the uncertainty from R and Q is propagated to M.

4.) Calculate the probability of failure, $P_f$.

5.) Calculate the reliability index, β

Calculation of $P_f$ directly is limited by the assumption of normal or lognormal R and Q and the corresponding failure formulation. The following is a list of common reliability solution techniques that can be used when this assumption is not valid or the formulation is complicated.

• First Order Second Moment (FOSM) applies to any distribution of R and Q, but is only approximate.

• Second Order Second Moment (SOSM) has increased accuracy over FOSM, but is still an approximation.

• First Order Reliability Method (FORM) is the "standard" of reliability analysis and often considered requisite when doing probability of failure calculations.

• Second Order Reliability Method (SORM) is particularly useful as the failure surface becomes more non-linear.

• Monte Carlo Method or Simulations is the brute force approach that provides a robust approximation of the probability of failure. This technique is often used to confirm results found using other methods.

<u>Monte Carlo Method</u>. Additional detail is presented on the Monte Carlo Method (MCM) as it was ultimately chosen to perform the reliability analysis in PReP. The MCM is not one exact methodology, but rather consists of a broad class of computational algorithms. In general, all MCM algorithms rely on repeated random sampling to obtain numerical results, and observing that fraction of the numbers that obey, or yield, a property of interest. Monte Carlo methods are especially useful for simulating systems with many coupled degrees of freedom. They are also particularly useful to model

phenomena with a significant number of uncertainty inputs. Moreover, the MCM can be used to evaluate multidimensional definite integrals with complicated boundary conditions or correlated variables such as those often found in the performance functions used for reliability analysis. [15]

In order to integrate a function over a complicated domain, the MCM sampling procedure picks random discrete points within the domain and solves the function under the specific conditions of the random sample. In other words the algorithm performs a deterministic analysis on a particular set of randomly chosen inputs. The algorithm picks *N* randomly distributed values $x_1$, $x_2$, ..., $x_n$ within the multidimensional volumetric domain *V* and evaluates the function *f*.

The MCM is capable of numerically solving a probabilistic analysis. For this class of problems the sampling procedure selects frequencies of values consistent with the distributions prescribed to the variables. As the simulations are run, the number of evaluations which exceed the limit state (described in following section) are recorded. The probability of exceeding the limit state or in reliability estimation, the probability of failure, is then calculated by dividing the number of exceeded instances by the total number of simulations. This concept is described in the following equation where $P_f$ is the probably of failure, $n_f$ is the number of simulation for which the limit state was exceeded and N is the total number of simulation performed:

$$P_f \approx \frac{n_f}{N} \tag{4}$$

While the exact details of different implementations of the MCM vary, they all tend to follow the same basic steps:

1. Develop the function or model of interest.
2. Define the probability distributions of all uncertain or variable strength and resistance variables.
3. Define a domain of possible inputs.
4. Generate inputs randomly from the probability distribution over the domain of interest.
5. Perform a discrete, deterministic computation of the function/model on the inputs.
6. Aggregate the results and evaluate the probabilities.

Probabilistic Modeling of the Failure State. This methodology is focused on reliability targets, which incorporate probabilistic modeling, is essential to accurately determine the structural reliability of a composite structure. Typically these methods are used with limit state equations in the design process to describe the reliability or probability of system failure. Often the engineer is interested not in outright failure, but some poor performance that would be considered unacceptable. Defining a performance criteria in this manner is often called a limit state. The same mathematics and solution techniques can be used to solve any type of limit state. The margin of safety formulation is generalized to encompass any threshold beyond which an unsatisfactory performance is realized. The limit state function is usually denoted by g and the independent uncertainty variable array as $X$, where.

$$g = X1 - X2 \text{ where } g \leq 0 \text{ is unsatisfactory performance} \tag{5}$$

The limit state is a different way of writing the margin of safety formulation and the solution proceeds by using the same methods previously discussed for the margin of safety. [14] In a time-independent structural reliability analysis this computation usually takes the form of a multi-dimensional integral evaluated over the failure domain of the performance function [16; 17].

$$p_f = P[G \leq 0] = \int_{g(X)\leq 0} f_x(x)dx \qquad \textbf{(6)}$$

where $P_f$ is the probability of failure, X is a vector of random input variables, $f_{\mathbf{x}}$(x) is the joint Probability Density Function (PDF) of X**,** and g is the limit state function [18].

A wind turbine blade is a complicated composite structure where uncertainty exists at many levels. Each random variable (material properties, structural variations, load variability etc.) has a distribution that describes the frequency of occurrence for values of that parameter. The overall system is then a function of the combined Cumulative Distribution Function (CDF), *F*. For the case of more than one random variable, a multivariate distribution is formed as detailed generally by Equation 7.

$$F(x_1, \ldots, x_n) \equiv Pr(X_1 \leq x_1, \ldots X_n \leq x_n) \qquad (7)$$

The PDF describes how the overall system reacts to any one variable and can be found by taking the partial derivative of the joint CDF with respect to each of the variables as shown in Equation 8.

$$f(\boldsymbol{x}) = \left.\frac{\partial^n F}{\partial x_1 \ldots \partial x_n}\right|_x \qquad \textbf{(8)}$$

The joint PDF or the multivariate CDF will depend on the relationship of the variables; i.e. independent or conditionally independent. Methods such as the chain rule of probability, sum (convolution) and ratio (Cauchy) distributions are typically evaluated.

The definition of a joint PDF by law of total probability for a 2-D case is given in Equation 9 and the chain rule in Equation 10.

$$f(x_1, x_2) = f(x_1|x_2)f(x_2) \tag{9}$$

$$f(x_1, \dots, x_n) = f(x_1|x_2 \dots x_n)f(x_2|x_3 \dots x_n)f(x_{n-1}|x_n)f(x_n) \tag{10}$$

The limit state function describes a condition of the structure for which exceedance describes the inability of the structure to fulfill a design requirement. Integrating the joint PDF with respect to the limit state function builds a multidimensional surface wherein combinations of values for the random variables that yield results "below" the surface constitute an unacceptable structural condition. [19; 20]

## Reliability Applications

The following sections individually discuss how reliability analysis is used in several industries. It is important to utilize an understanding of current procedures in other industries when developing a structural reliability infrastructure for wind blades. In short, there is no need to reinvent the wheel, but rather adapt the most relevant prior work to the needs of the wind industry.

Civil. Structural performance in earthquakes and hurricanes exposed the weakness of design procedures and showed the need for new concepts and methodologies for performance evaluation and design. The consideration and proper treatment of the large uncertainty in the loadings and structure capacities, including complex response behavior in the nonlinear range is essential in the evaluation and design process. A reliability-based framework for analysis and design is most suitable for this purpose. [21]

To this end, limit state design has replaced the older concept of permissible stress design in most forms of civil engineering. The design of structural steel in buildings in the United States is principally based on the specifications of the American Institute of Steel Construction (AISC) . Steel bridge design is in accordance with specifications of American Association of State Highway and Transportation Officials 9 (AASHTO).

Load and Resistance Factor Design (LRFD) incorporates state-of the-art analysis and design methodologies with load and resistance factors based on the known variability of applied loads and material properties. These load and resistance factors are calibrated from statistics to provide a uniform level of safety. Beginning in the early 1970's, Load Factor Design (LFD) was introduced into the structural steel specification that reflected the variable predictability of certain load types. This had the effect of varying the factors of safety for different types of loading; however, the load factors were still determined subjectively by the code writers.

$$R_n \geq \sum \gamma_i Q_i \qquad (11)$$

where γi are load factors.

LRFD extends the LFD philosophy by considering the variability in the properties of structural elements in addition to the load variability. In LRFD design, the load and resistance factors are chosen by code writers based upon the theories of probability and reliability. In developing the design specifications, considerable effort was made to keep the probabilistic aspects transparent to the designer. No knowledge of reliability theory is necessary to apply the specifications. The following two major improvements on the LFD methodology result in this conversion into probability-based LRFD:

• Limit states to be considered by the designer are very similar. Some of these are strength-oriented; typically even more are serviceability-oriented, and

• Load and resistance factors are chosen by the code writers based upon the theories of probability and reliability.

The LRFD method of design accounts for variability in both resistance and load, achieves uniform levels of safety for different limit states, and provides a rational and consistent method of design.

$$\Phi_i R_n \geq \eta_i \sum \gamma_i Q_i \tag{12}$$

where $\eta_i$ are load modifiers and $\Phi_i$ are resistance factors.

The Service Limit States within the LRFD Specifications have not been calibrated and therefore some design elements, such as foundations design are still in transition. The remainder of the LRFD Specifications have been calibrated using a reliability index, β. The shift in the load and resistance probabilities to obtain compliance to the Standard Specifications uses a factor equal to 3.5 which equates to a probability of failure of about 1/10,000. When more is known about the load, as in the case for a overload permit, this probability based specification can be adjusted by changing the factor to a lesser value. For conditions where the uncertainty is significantly reduced, a β factor of 2.5 may be appropriate. [22]

Aviation. There is a notable difference between military and civil aviation methods of compliance. For military aircraft, the government defines the requirements with Military Specifications and works with the manufacturer to establish the method of compliance. In civil aviation, the government defines the requirements through regulations (FAR's, JAR's) and accepted means of compliance through Advisory Circulars. Compliance must be demonstrated to the agency and in this instance the government is a neutral third party.

The Federal Aviation Administration (FAA) regulates the safety concerns for the civil aviation industry. Their regulations stretch into the manufacturing and inspection protocols. Federal Aviation Regulation (FAR) 25.571 Damage Tolerance & Fatigue Evaluation of Structure states that "An evaluation of the strength, detail design, and fabrication must show that catastrophic failure due to fatigue, corrosion, manufacturing defects, or accidental damage will be avoided through the operational life of the airplane" [4].

Advisory Circular (AC) 20-107B on Composite Aircraft Structure describes an acceptable means of showing compliance with the provisions of FAR 25.571 for the special case of aircraft structures involving fiber reinforced materials. Guidance information is also presented on design, manufacturing, inspection and maintenance aspects [23]. This process can be described visually in Figure 11. Unfortunately, there are no such regulations in the wind industry because failures in composite wind turbine blades are largely an economic problem, and less of a safety problem [24].

Since the introduction of structural reliability programs in the aviation industry, the safety record has been greatly improved (Figure 12). The technological corollaries between the aviation industry and the wind industry would suggest that similar improvements could be attained by the wind industry. However, the major challenge is to determine the cost/benefit parameter which will achieve the best economic payoff for improved reliability.

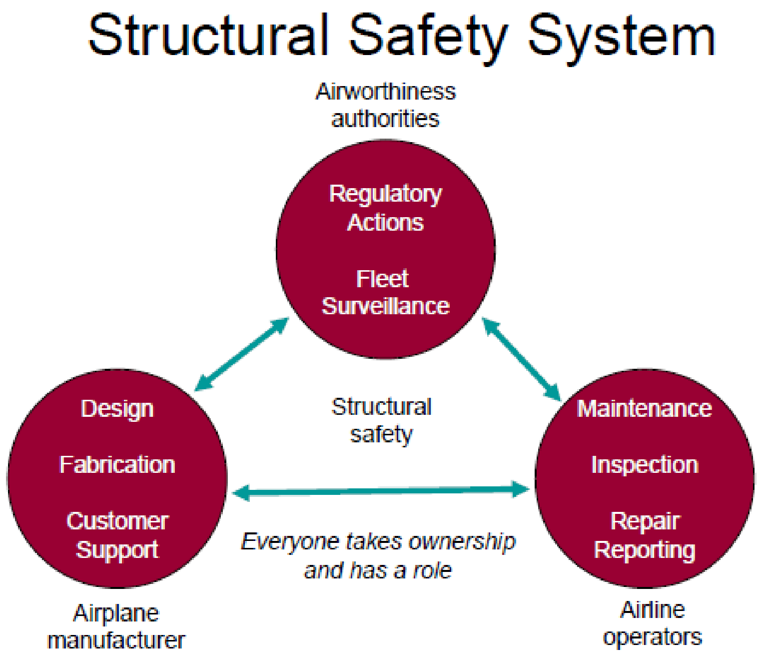


Figure 11: Flow Chart of FAA Safety Program [25].

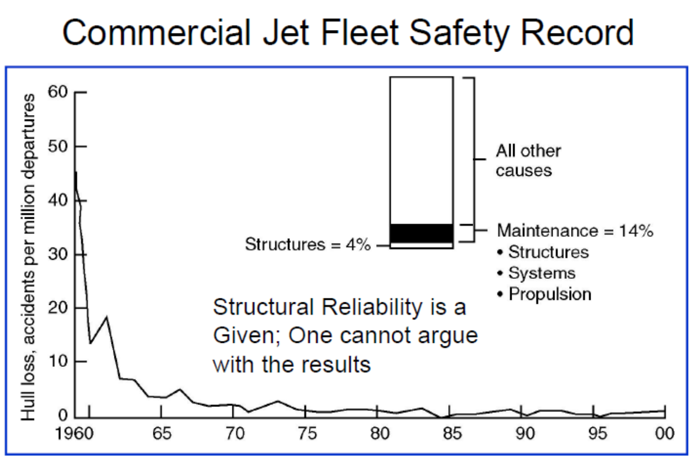


Figure 12: Commercial Jet Safety Record [25].

In order for the wind industry to develop a statistically defensible reliability program, specifications covering materials, material processing, and fabrication procedures must be established to ensure a basis for fabricating consistent and reliable structures. The discrepancies permitted by the specifications should also be substantiated by analysis supported by test evidence; tests at the coupon, element or subcomponent level. Thorough manufacturing records are needed to record part acceptance and allowable discrepancies; e.g. common defects, damage and anomalies. Substantiating data is needed to justify all known defects, damage and anomalies allowed to remain in service without rework or repair. The Composite Materials Handbook 17 offers a process for composite component conformity that has been utilized in military applications. Elements from this process could be applied in the wind industry to achieve these goals.

In order to back up manufacturing records, it must be known what the effects of defects are, so that quality control can determine blade conformance. Thus, the defects must be understood in terms of both residual strength and damage tolerance. The structural static residual strength substantiation of a composite design should consider all critical load cases and associated failure modes. Also included should be effects of environment, material and process variability, non-detectable defects or any defects that are allowed by the quality control, manufacturing acceptance criteria, and service damage allowed in maintenance documents of the end product. The residual strength of the composite design should be demonstrated through a program of coupon to component ultimate load tests to comprehend the effects of defects from flaw to full-blade scale (Figure 13).

In 2008, a preliminary survey of wind turbine farm operators was performed by Sandia National Laboratories. Data collected from five wind farms showed that approximately 7% of all wind turbines blades had to be replaced prematurely. However, based on discussions with a number of major wind turbine OEMs and blade manufacturers this number is probably higher [5]. The operators surveyed in this study reported that the leading causes of repairs and failures where manufacturing defects and lightning strikes [4].

Successful static strength substantiation of composite structures has traditionally depended on proper consideration of stress concentrations (e.g., notch sensitivity of details and impact damage), competing failure modes, and out-of-plane loads. Component tests are needed to provide the final validation accounting for combined loads and complex load paths. When using the building block approach, the critical load cases and associated failure modes would be identified for component tests using the analytical methods, which are supported by test validation.

The following discussion on damage tolerance methodology is particularly relevant to wind blades. While the design criteria vary between wind blades and aircraft, the design procedures are not so different. Moreover, wind blades have been shown to be sensitive to fatigue and in service damage. It is already commonplace in the wind industry to perform regular maintenance inspections of wind blades therefore it is not unreasonable to think that elements of an aviation style damage tolerance methodology could be useful to the wind industry. However, this approach would have to remain economical for the wind industry.

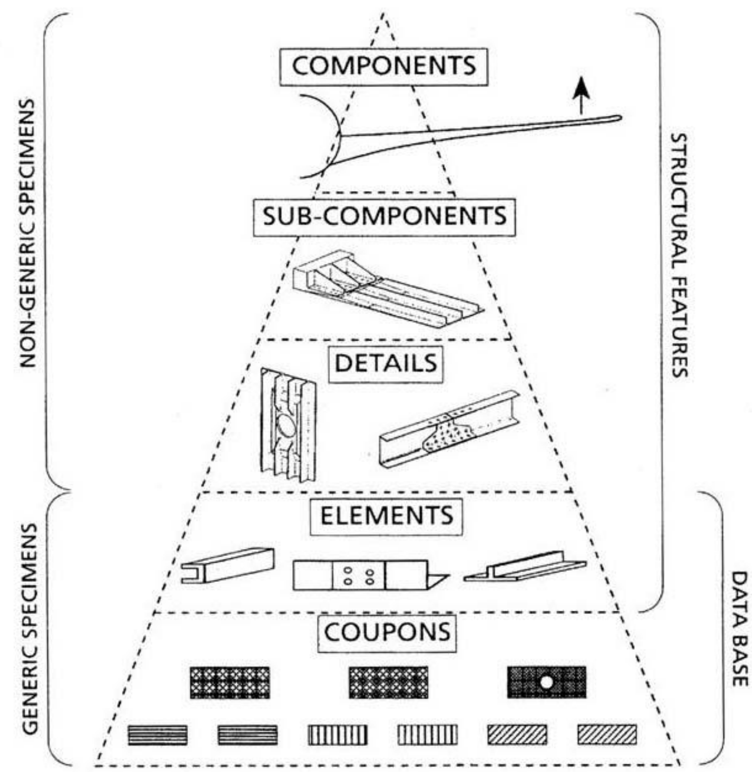


Figure 13: Typical scale steps needed to get from flaw-scale to full-blade scale [26].

In addition, damage tolerance evaluation must show that catastrophic failure due to fatigue, environmental effects, manufacturing defects, or accidental damage will be avoided throughout the operational life of the structure. Commonly, a damage threat assessment must be performed on the structure to determine the effects of locations, types, and sizes of damage, considering fatigue, environmental effects, intrinsic flaws, and foreign object impact or other accidental damage that may occur during manufacture, operation or maintenance. Once a damage threat assessment is completed, various damage types can be classified into five categories of damage. These categories are displayed in Figure 14.

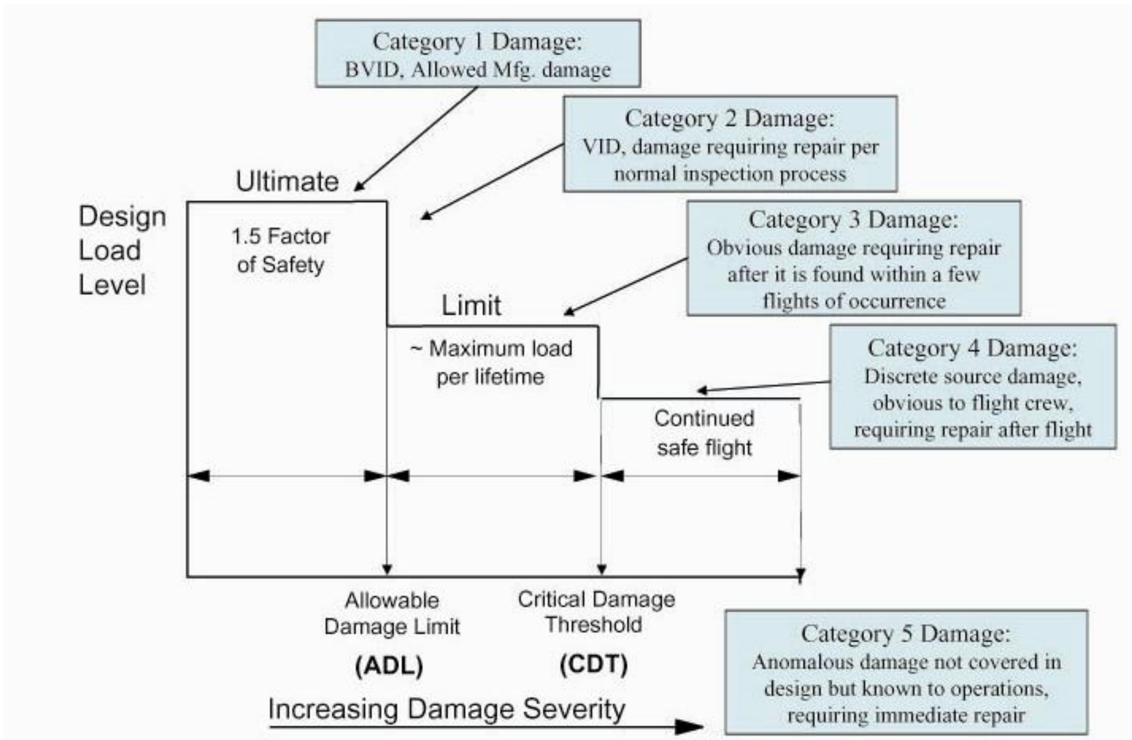


Figure 14: Typical categories resulting from damage threat assessments [27].

Structural details, elements, and subcomponents of critical structural areas should be tested under repeated loads to define the sensitivity of the structure to damage growth. This testing can form the basis for validating a no-growth approach to the damage tolerance requirements as well as determine the effects of defects, thereby establishing the criticality of each type, size and/or location. Once critical rubrics are determined, corrective action can be taken before the blade is put into service or a different in-service protocol may be mandated. Regardless, inspection intervals should consider both the likelihood of a particular type of damage and the residual strength capability associated with this damage. The intent is to ensure that the structure is not exposed to an excessive period of time where the residual strength is less than that which is necessary to guarantee safe operation until the next inspection.

Conservative assumptions for structural safety with large damage sizes that would be detected within a short time of being in-service may be needed when probabilistic data on the likelihood of given damage sizes does not exist. Once the damage is detected, the component is either repaired to restore ultimate load capability or replaced. A schematic showing the relations between damage initiations, residual strength and repair intervals as a function of time are shown in Figure 15 [26]. Two conceptual damage assumptions can be taken: slow-growth and no-growth. For the slow growth case it is assumed that once damage has been initiated there is a time varying reduction in residual strength. Maintenance intervals should designated such that a reduction of residual strength below the expected ultimate loads is caught within in four inspection intervals; at which point the structure should be repaired, retuning it to full design strength. A no-growth approach assumes that once damage has been initiated the residual strength instantly decreases and remains constant. A repair must then be performed close to the time of discovery.

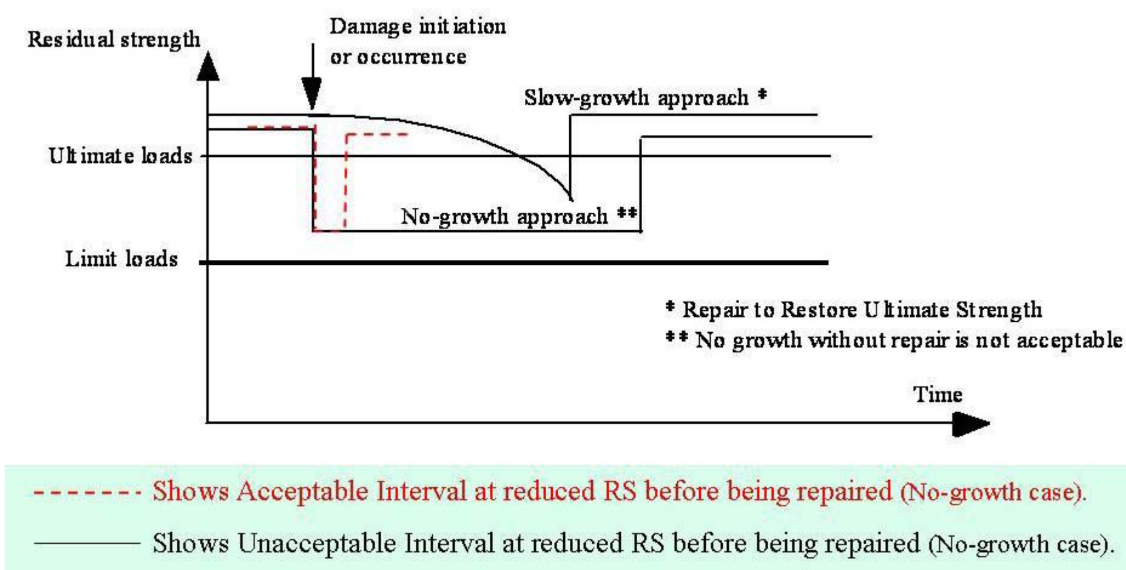


Figure 15: Schematic diagram of residual strength [26].

The extent of initially detectable damage should be established and be consistent with the inspection techniques employed during manufacture and in-service. This information will naturally establish the transition between Category 1 and 2 damage types (i.e., inspection methods used by trained inspectors in scheduled maintenance). Documented procedures used for damage detection must be reliable and capable of detecting degradation in structural integrity below ultimate load capability. This should be substantiated in static strength, environmental resistance, fatigue, and damage tolerance. [26].

Flaw/damage growth data should be obtained by repeated load cycling of intrinsic flaws or mechanically introduced damage. The number of cycles applied to validate both growth and no-growth concepts should be statistically significant, and may be determined by load and/or life considerations and a function of damage size. The growth or no growth evaluation should be performed by analysis based on test results or by tests at the coupon, element, or subcomponent level. The extent of damage for residual strength assessments should be established, including considerations for the probability of detection using selected field inspection procedures. Composite designs should afford the same level of fail-safe, multiple load path structure assurance as conventional metals design. Such is also the expectation in justifying the use of static strength allowable with a statistical basis of 95% probability with 95% confidence.

The ability to detect damage is the cornerstone of any maintenance program employed to ensure the damage tolerance of a specific structure. Inspection procedures can be divided into two main classes. The first, which is most general, includes both destructive and nondestructive methods used for concept development, detailed design, production, and maintenance. The second class includes only those Nondestructive Evaluation (NDE) methods that can be practically used in service to locate and quantify damage. The second class is a subset of the first and depends on a technology database suitable for relating key damage characteristics to structural integrity [27].

After initial process qualification, testing for conformity to design requirements should continue on an appropriate frequency to ensure that the manufacturing process, materials, and associated tooling continue to operate within acceptable boundaries and thereby produce conforming parts. For accepting or rejecting cured structures, NDE equipment and procedures should be used to evaluate specified material defects resulting from fabrication and assembly operations. The NDE technique used for inspection should have the sensitivity to detect maximum allowable discrepancy type and size in the part. Quality control specifications should define allowable limits for each discrepancy such as: adhesive voids, porosity, delaminations, damaged core, core node bond separations, potting cracks, short core, lack of adhesive, etc. [28] The need for this type of specification is a result of the relationship between the size of a flaw and the residual strength of the structure. This relationship is graphically presented in Figure 16.

It follows then that the larger the strength reduction, the sooner the damage should be detected. Furthermore, these methods also consider that the need for inspection cannot disregard the likelihood of damage occurrence. The more likely the damage is, the sooner it should be detected. As a result, these methods depend on service data [27].

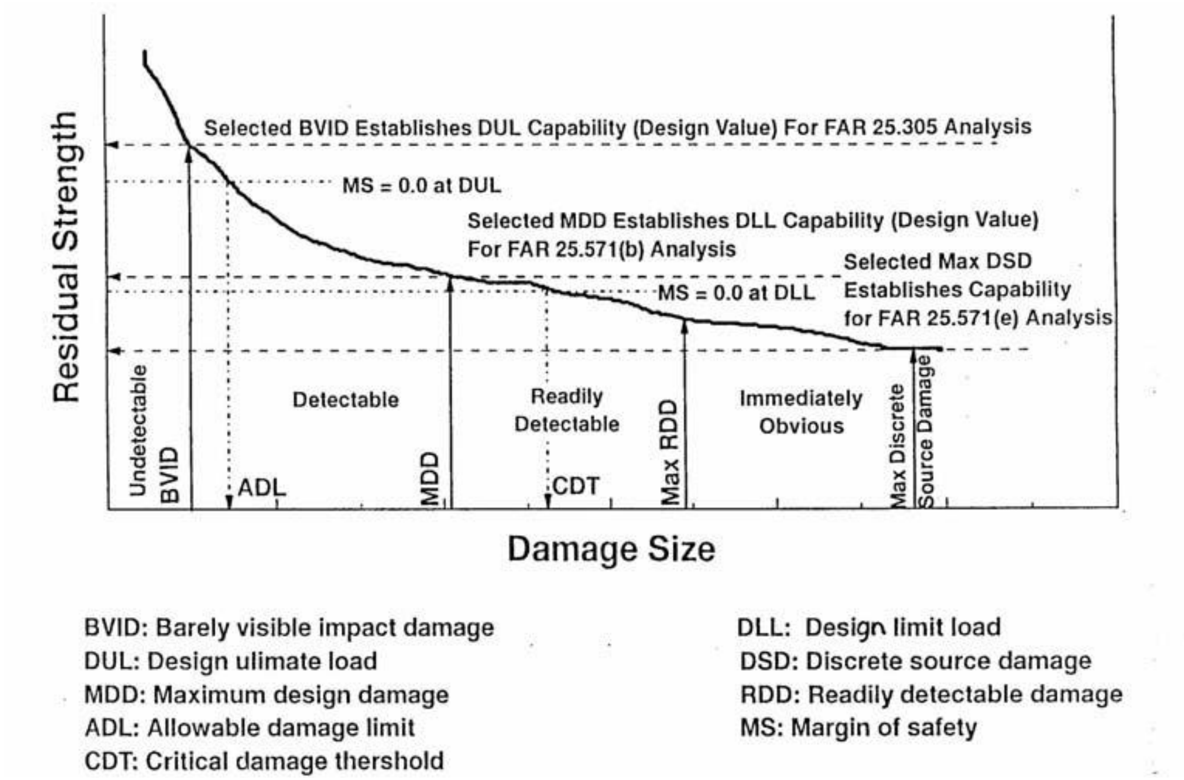

Figure 16: Residual strength requirements versus damage size [27].

Manufacturing defects as well as in service damage can be hard to detect in composite structures, particularly if the flaw is subsurface. The use of non-destructive evaluation is growing throughout the composites industry. There are a variety of NDE technologies used on composites and they all have their pros and cons. Some of the various technologies are listed below [29; 30; 31]:

- **Thermography**: Thermographic NDE methods typically apply heat to a region enabling cameras to 'see' flaws. This is done by analyzing the effect of flaws on the thermal conductivity and emissivity of materials. Thermography is capable of covering large areas in a single frame and does not require coupling. Unfortunately, this method has been found to be unreliable when testing bonded joints with a narrow gap between the unbonded surfaces (kissing bonds). Highly sensitive and effective infrared systems are used to map the cooling or heating profiles. This technique is capable of rapidly indicating flaws.

- **Ultrasonic**: Ultrasonic techniques are the most widely used, versatile and informative NDE methods. All of Ultrasonic techniques function by applying ultrasonic waves to a material and analyzing variations to the speed and shape of the wave pattern. Often times detailed information about flaws can be extracted as well as determination of material properties. To perform rapid inspection, portable scanners have been developed. Charge Coupled Device technology can now be used to form the ultrasonic equivalence of the video cameras. Most often, ultrasonic transducers are used with liquid couplants. The difficultly of applying liquid couplants in field application has led to the development of various fixtures including water filled boots and wheels, bubblers and squirters. Alternative dry coupling methods have also been developed including the use of air-coupled piezoelectric transducers, Electro-Magnetic Transducers (EMAT) and Laser Ultrasonics.

  Leaky Lamb Waves is a particular ultrasonic subset based on obliquely insonified ultrasonic waves. While not used extensively, the analytical and experimental studies are starting to pave the way for their practical application. Leaky Lamb Wave data is acquired in the form of dispersion curves that show the phase velocity as a function of the frequency along various polar angles associated with the fiber direction. Another ultrasonic technique, Polar Backscattering is also based on obliquely insonified ultrasonic waves. Using Polar Backscattering, the fiber orientations can be determined and porosity clusters as well as fatigue cracks can be mapped.

Pulse-echo (or reflection mode) is perhaps the most employed ultrasonic technique. The transducer performs both the sending and the receiving of the pulsed waves. Reflected ultrasound wave characteristics come from an interface, such as the back wall of the object or from an imperfection within the object. The diagnostic machine displays these results in the form of a signal with an amplitude representing the intensity of the reflection and the distance, representing the arrival time of the reflection.

Through-transmission (or attenuation) is another commonly used ultrasonic technique. A transmitter sends ultrasonic waves through one surface, and a separate receiver detects the waves after traveling through the medium. Imperfections or other conditions in the space between the transmitter and receiver reduce the amount of sound transmitted, thus revealing their presence. Using the couplant increases the efficiency of the process by reducing the losses in the ultrasonic wave energy due to separation between the surfaces.

- **Radiography**: Radiography is the generic name for a host of technologies that use X-rays to view a non-uniformly composed material. X-Rays are projected through a material, onto a film or digital collector. Variations in materials can be seen on the resulting images. The development of real time imaging techniques for radiographic visualization helped overcome the time consuming process that was involved with original film recording. Moreover, computer processing of digitized images enabled the enhancement of the images as well as the quantification of the inspection criteria. Several radiographic techniques that deserve attention for composites materials include the Computed Tomography (discussed in Chapter 5) scan, Reverse Geometry X-ray and Microfocus X-ray microscopy.

- **Acoustic Emission**: High tech microphones are mounted to a structure. They pick up sound waves in the material as it undergoes stress (internal change), as a result of an external force. This occurrence is the result of small surface displacement of a material due to stress waves generated when the energy in a material, or on its surface, is released rapidly. One advantage of this technique is that failure or indications of imminent failure can be documented during unattended monitoring.
- **Interferometry (shearography)**: Most Shearography systems use laser diodes and various means such as vacuum changes, thermal flux or vibration to stress the object surface to detect subsurface anomalies This process involves double exposure of the structure at two different stressing levels. The method is very sensitive to the setup vibrations or displacement making it unpractical. A digital Interferometry system is used to detect areas of stress concentration caused by material anomalies. The technique senses

out-of-plane surface displacements in response to an applied load. Data is presented in the form of a fringe pattern produced by comparing two states of the test sample, one before and the other after a load is applied. Electronic Shearography incorporates a Charge Coupled Device camera and frame grabber for image acquisition at video frame rates. Fringe patterns are produced by real time digital subtraction of the deformed object image from the reference object image. Shearography has reasonable immunity to environmental disturbances such as room vibrations and thermal air currents. The capability of Shearography to inspect large areas in real time has significant advantages for many industrial applications including inspection of composite structures and pressure vessels. Experience in testing bonded composites and metallic assemblies at Northrop Grumman Corp. since 1988 showed 75% reduction in inspection time compared to other NDE methods.

Composites in General. In addition to traditional generalized mechanical reliability concepts, four composite specific methods to probabilistic modeling have been investigated for their applicability to wind turbine blades: NASA Integrated Probabilistic Assessment of Composite Structures (IPACS), Level of Safety (LoS), Northup Grumman Commercial Aircraft Division (NGCAD) and Central Aerohydrodynamic Institute (TsAGI).

Visual representations of the elements which need to be incorporated into the model are displayed in Figure 17. The algorithm described by Figure 18 is employed partially in the IPACS method but is in essence a generic procedure for structural assessment.

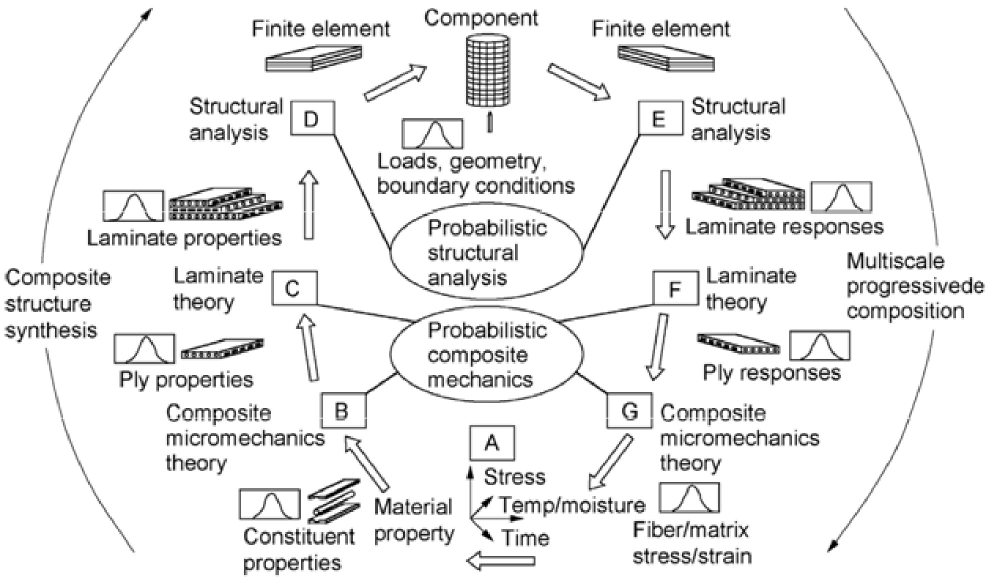


Figure 17: Concept of probabilistic assessment of composite structures [13]

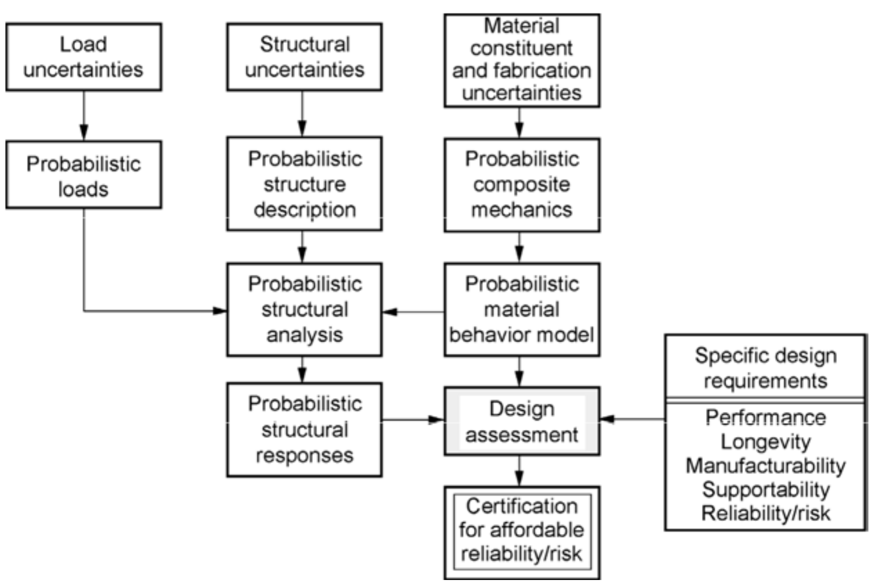


Figure 18: Probabilistic design assessment of composite structures [13]

Wind Industry. The major reliability initiatives within the wind industry are typically related to overall plant performance. Reliability is addressed in terms of availability, which describes how much of the time a wind turbine is available to produce electricity regardless of the wind. Typical reasons for a turbine to be unavailable are scheduled maintenance downtime , malfunctions, and failures. In order to assess the industry as a whole, Sandia National Laboratories began the Wind Plant Reliability Database and Analysis Program (WPDB) to characterize the reliability performance of the US fleet to serve as a basis for improved reliability and increased availability of turbines. The WPDB was designed to fill a need identified by wind plant owners and operators to better understand wind turbine component failures. Thus enabling efforts to be focused on resolving these failures and/or mitigate the consequences, resulting in improved operations and reduced maintenance costs. The goal was to solicit sufficient participation to characterize the industry as a whole. This data would then be able to help prioritize and facilitate R&D efforts to foster component and system design improvements. [32]

This project evolved into developing the Continuous Reliability Enhancement for Wind (CREW) database by Sandia National Laboratories. The CREW database uses both high resolution Supervisory Control and Data Acquisition (SCADA) data from operating plants and Strategic Power Systems' (SPS) ORAPWind® (Operational Reliability Analysis Program for Wind) data. The later consists of downtime, reserve event records and daily summaries of generation, unavailability, and reserve time for each turbine. Together, these data are used as inputs into CREW's reliability modeling. [33]

The CREW effort has produced significant insight concerning the root causes of turbine downtime. In general, twelve categories are used to characterize faults or malfunctions. Data on average number of events and mean down time per event has been complied for each of these categories. The latest reporting of this data is displayed in Figure 19. The data shows that the Wind Turbine Other group, which are uncategorized (miscellaneous events) leads the system for both number of events and duration. The second most frequent cause of unavailability is attributed to the rotor and blades. The data presented for mean downtime suggests that the majority of events are not catastrophic blade failures as such an event would require more than 1 hour to address. These types of issue are usually related to faults associated with the pitch system. However, information discussed previously suggests that blade failures are frequent and that when they occur, the down time is much more significant (i.e. weeks or months instead of hours). Therefore one event which would have a mild impact on the statistics generate in this report would actually have a substantial impact on the availability of a particular turbine or plant.

Even with a large amount of events occurring per year, wind turbines can still be considered a reliable system. Data collected by CREW and reported in Table 1 shows that the vast majority of the time (97%), wind turbines are available. However, the capacity factor of wind plants is significantly lower (36%). The capacity factor describes the yearly percentage of actual production, as compared to the name plate plant rating. This number encompasses both the availability of  the plant and the amount of actual wind supplied to the plant.

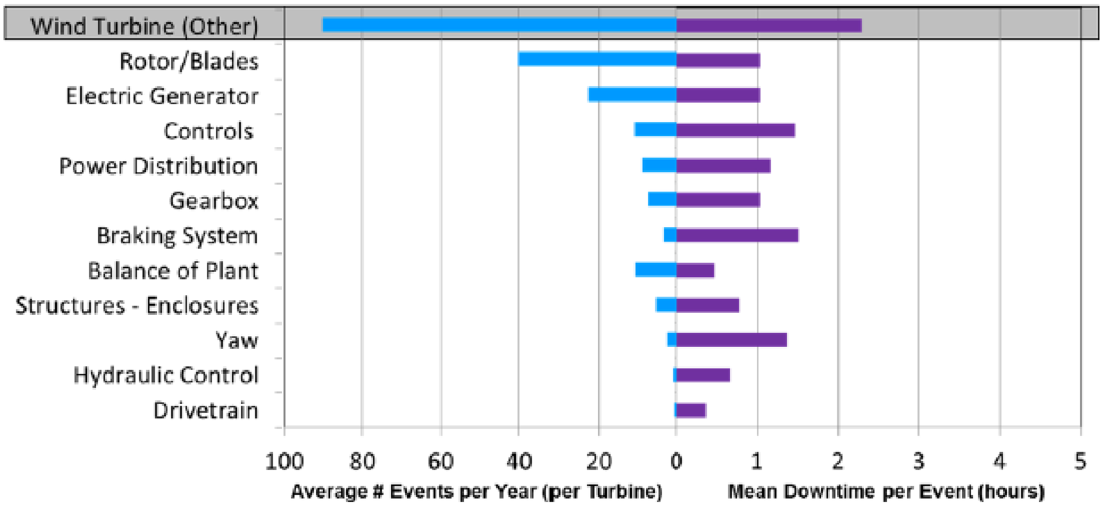


Figure 19: CREW database results [33]

Table 1: Plant metadata statistics

| | 2012 Benchmark | 2011 Benchmark |
|---|---|---|
| **Operational Availability** | 97.0% | 94.8% |
| **Utilization** (Generating Factor) | 82.7% | 78.5% |
| **Capacity Factor** | 36.0% | 33.4% |
| **MTBE** (Mean Time Between Events) | 36 hrs | 28 hrs |
| **Mean Downtime** | 1.6 hrs | 2.5 hrs |

Wind is extremely variable in nature and as such, wind turbines are exposed to variable loading. Subjecting mechanical and structural components to these loads results in fatigue damage. A reliability analysis of these parts must consider the accumulation damage as a result of this fatigue. Several tools have been developed to address fatigue calculations and reliability estimations of wind turbine components. These typically focus on modeling the interaction between the environment, the load response to the environment and the cumulative damage process underlying the lifetime calculation.

In the late 1990s, Sandia National Laboratories distributed FAROW, a computer code that evaluated fatigue and reliability of wind turbine components using standard reliability methods. During this timeframe, design standards for wind turbines and utility scale wind turbines themselves, were still in their infancy and a tool was needed to assess spectrum loading on turbine components. In FAROW, the fatigue life formulation is based on three components; the loading environment, the structural response given the load environment and a failure criterion. The calculated lifetime is compared to targets to assess premature failure. The reliability analysis uses the lifetime calculation as the limit state function in a FORM or SORM protocol. FAROW produces estimates for the probability of premature failure, mean lifetime, variable relative importance, and sensitivity of the results to inputs. [34; 35]

Around this same time, K. Ronold developed two probabilistic models for analysis of the safety of a wind-turbine rotor blades. [36] The first model presented an assessment of fatigue failure in flapwise bending. The model is based on the Miner's rule approach to cumulative damage and capitalizes on a conventional *S–N* curve formulation for fatigue resistance. The model accounts for inherent variability and statistical uncertainty in load and resistance, and model uncertainties are also included. The model was applied to a reliability analysis for a site-specific wind turbine of a prescribed make/model and a 20-year design lifetime was considered. The probability of fatigue failure in flapwise bending of the rotor blade was calculated by means of a first-order reliability method. It was demonstrated that the reliability analysis results may be used to calibrate partial safety factors for load and resistance for use in conventional deterministic fatigue design.

The second probabilistic model analyzed blade failures in ultimate loading where only failure in flapwise bending during the normal operating condition of the wind turbine was considered. The model was based on an extreme-value analysis of the load response process in conjunction with a stochastic representation of the governing tensile strength of the rotor blade material. The probability of failure in flapwise bending of the rotor blade is calculated by means of a first-order reliability method, and contributions to this probability from all local maxima of the load response process over the operational life were integrated. It was demonstrated again, that the reliability analysis results can be used to calibrate partial safety factors for load and resistance for use in conventional deterministic design. [37]

Since that time, at least two agencies, the International Electrotechnical Commission (IEC) and Germanischer Lloyd (GL) have developed design standards addressing the analysis of fatigue life for wind turbines. In wind turbine fatigue design, it is customary to use the partial safety factor approach: loads are inflated by some factor, while material fatigue strength is decreased in calculations. Values for partial factors originally come from civil engineering standards for utility buildings and bridges, and it is not clear that they are optimal for wind turbines. The safety factors are designed to address uncertainties in the engineering calculations. Uncertainty for wind turbine blades analysis can in general, be divided into four groups: Physical Uncertainty, Model Uncertainty, Statistical Uncertainty and Measurement Uncertainty.

The recent surge of interest in offshore wind plants has also required a more in-depth understanding of reliability issues. As one can imagine, the maritime environments provide challenges to turbine access and subject the machines to harsh environmental conditions. Operation and maintenance for offshore wind turbines are expected to contribute a substantial part of the total life cycle costs, and can be expected to increase when wind farms are placed in deeper water and in severe environments. To address these issues, researchers have developed a risk-based life cycle approach formulated for rational and optimal planning of operation (services, inspections, etc.) and maintenance (including repair and exchange) for offshore wind turbines. [38]

Recently (2008), D. Veldkamp of Vestas Wind Systems performed an analysis to ascertain the relevancy of the traditional safety factor approach by comparing it to a stochastic analysis addressing uncertainties. [39] Using a simple cost model, economically optimal failure probabilities and partial factors are derived. The main conclusion of this work was that uncertainties in material fatigue properties and life prediction methods dominate total uncertainty, and hence determine the required partial factors.

Two specific components that have received significant attention in programs aimed at improving reliability are gearboxes and rotor blades. Premature gearbox failures have a significant impact on the cost of wind farm operations. In 2007, the National Renewable Energy Laboratory (NREL) initiated the Gearbox Reliability Collaborative. This comprehensive project combines analysis, field testing, dynamometer testing, condition monitoring, and the development and population of a gearbox failure database. The goal of these efforts is to determine why many wind turbine gearboxes do not achieve their expected design life. [40]

The European Wind Industry has been analyzing the reliability of wind blades since 2009. Two investigators in particular (along with co-authors) have led this effort; T.

P. Philippidis and J. D. Sorensen. [41] Even with known issues for blades, barely a half-dozen papers have been authored on the topic of stochastic reliability for wind blades. Perhaps the most comprehensive effort was performed within the European collaboration UPWIND. UPWIND was led by D. J. Lekou and T. P. Philippidis. The goal of UPWIND was to address the variability in structural performance of wind blades, primarily from a ply level materials perspective.

UPWIND focused on assessing and developing tools for probabilistic strength assessment of rotor blades. Methodologies for probabilistic assessment of laminates under general in-plane loading were integrated into a software package which performed deterministic strength analysis of rotor blades. Reliability analysis was performed at the ply level where composite material properties were treated stochastically. Numerical procedures determined strength while taking into account the stochastic nature of anisotropic material properties as well as the variable loading imposed on the blade. The Edgeworth Expansion Technique and the Response Surface Method were applied for the reliability estimation.

The UPWIND investigators deemed that to accurately predict failure (or non-failure) of a particular blade section, a point to point assessment was necessary. The anisotropic nature of composite materials required the analysis to consider the axial normal stresses (i.e. along the blade length) and complex in-plane stress field in the principal coordinate system of each ply. Failure in the lamina was established using the quadratic failure tensor (Equation 13) developed by Tsai and Wu with stochastic anisotropic material properties.

$$\frac{\sigma_1^2}{X_T X_C} + \frac{\sigma_2^2}{Y_T Y_C} + \frac{\sigma_6^2}{S^2} - \frac{\sigma_1 \sigma_2}{\sqrt{X_T X_C Y_C Y_T}} + \left(\frac{1}{X_T} - \frac{1}{X_C}\right)\sigma_1 + \left(\frac{1}{Y_T} - \frac{1}{Y_C}\right)\sigma_2 - 1 \leq 0 \qquad \textbf{(13)}$$

A laminate can be modeled as a system of many components (layers), each one of them characterized by its own failure function, as described in the previous section. The failure of the laminate may in turn be characterized either by the failure of the first ply (FPF) or by the total failure, that is, the successive failure of all layers in the laminate up to the failure of the last ply (LPF). Since the design was performed based on the FPF methodology, the analysis of a series system will result in the probability of failure for the laminate.

This analysis is implemented in a software routines in the form of pre- and postprocessor that can be used along with current aero-elastic codes. The algorithm for this approach is shown in Figure 20. The reliability estimation for each laminate is conducted with the Edgeworth Expansion technique at the layer level. Not only are the strength properties of the material considered as stochastic parameters of the model, but also the variability of the elastic and thermo-mechanical properties of each layer in the lamination sequence is taken into account. The applied loading is assumed deterministic. The variables used in this analysis (e.g. strength and elasticity properties of the different materials) the mean, standard deviation, coefficient of variation and distribution form are given in

Table 2. Lognormal and Weibull distributions are commonly used to describe variations in composite mechanical properties, however they can often be difficult to implement in complex software routines. This is perhaps the reason why the UPWND program chose to use Normal distributions. The effective properties calculated for each

laminate, together with their statistical properties in a reliability assessment, are fed as input into the main calculation module. [42; 43]

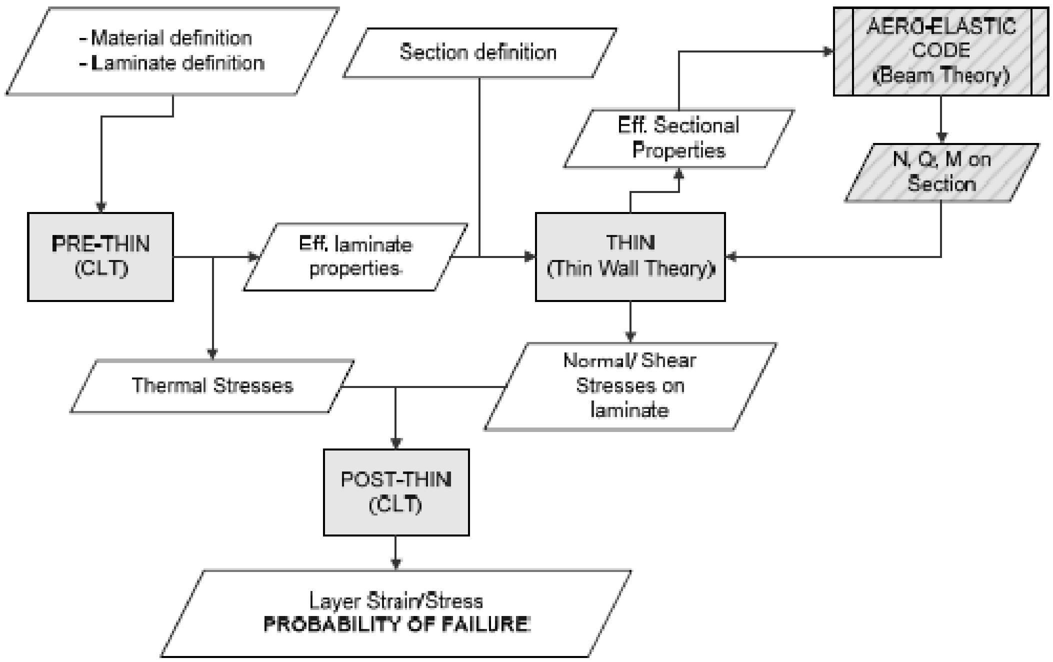


Figure 20: Schematic diagram of the UPWIND software approach [42; 43]

Table 2: Material properties used in the UPWIND program [42; 43]

| Property | Mean Value | St. Deviation | C.O.V. (%) | Distribution |
|---|---|---|---|---|
| | | | | |
| $E_1$ (GPa) | 39.04 | 1.032 | 2.64 | Normal |
| $E_2$ (GPa) | 14.08 | 0.325 | 2.31 | Normal |
| $G_{12}$ (GPa) | 4.24 | 0.099 | 2.34 | Normal |
| $v_{12}$ | 0.291 | 0.0271 | 9.34 | Normal |
| $X_T$ (MPa) | 776.50 | 36.143 | 4.65 | Normal |
| $X_C$ (MPa) | 521.82 | 16.500 | 3.16 | Normal |
| $Y_T$ (MPa) | 53.95 | 2.576 | 4.78 | Normal |
| $Y_C$ (MPa) | 165.00 | 4.849 | 2.94 | Normal |
| S (MPa) | 56.08 | 1.119 | 2.00 | Normal |
| h (mm) | 0.938 | - | - | - |

More recently in 2011, Toft and Sorensen provided a probabilistic framework for design of wind turbine blades. It demonstrated how information from tests can be taken into account using the Maximum-Likelihood method and Bayesian statistics. In this numerical example, the reliability of a wind turbine blade is estimated for a single failure mode in both ultimate and fatigue limit states. In the ultimate limit state, the reliability is evaluated using a Bayesian approach which takes the information from structural testing programs into account. The results show that the reliability is significantly dependent on the number of tests. This dependency is exacerbated especially when the coefficient of variation for material strengths is unknown. Using the test data, the design partial safety factor for material properties is calibrated. Results from this analysis show a significant reduction in the partial safety factor when the number of tests are increased.

In the fatigue limit state, the reliability was estimated for a single failure mode.  The failure criteria took into account statistical variations in the test data using Maximum-Likelihood method. The model uncertainty on Miner's rule is estimated based on variable amplitude fatigue tests with small coupons. The results show that Miner's rule is significantly biased and is associated with high model uncertainty when it is applied to composite materials. A calibration of partial safety factors shows that the existing partial factors in IEC 61400-1 are adequate. [44]

It should be noted that Toft and Sorensens' conclusion that safety factors could be reduced with more material testing is somewhat embodied in IEC 61400-1. In section 7.6.2.2 the standard states: "Partial safety factors for materials shall be determined in relation to the adequacy of the available material properties test data." [45] No further discussion is given in the IEC standard as to types of test or the relevant variation of concern. However, it is well known that variations in standard material properties (e.g. E, Sult, ν, etc) exist for composite materials. The probabilistic modeling approaches discussed thus far, have thoroughly addressed these issues. However there are variations in structural performance that result from the manufacture of the structure as well. Existence of defects in composites structures tend to be related to the industry being evaluated. For instance, the aerospace industry can support high production costs aimed at providing near defect-free parts. However, other industries such as wind energy, must maintain lower manufacturing costs to remain competitive with traditional power generation sources. Defects have been identified as a major cause for premature blade failure. [46] Very little work to understand this problem has been undertaken within the public domain.

The most comprehensive assessment on the reliability of wind blades with defects was performed by Toft and Sorensen in 2011. [47] In this work two stochastic models for the distribution of defects in wind turbine blades were proposed. The first model assumed that the individual defects are completely randomly distributed in the blade. The second model assumes that the defects occur in clusters of different size, based on the assumption that one error in the production process tends to trigger several defects. Both of these models are graphically represented in Figure 21.

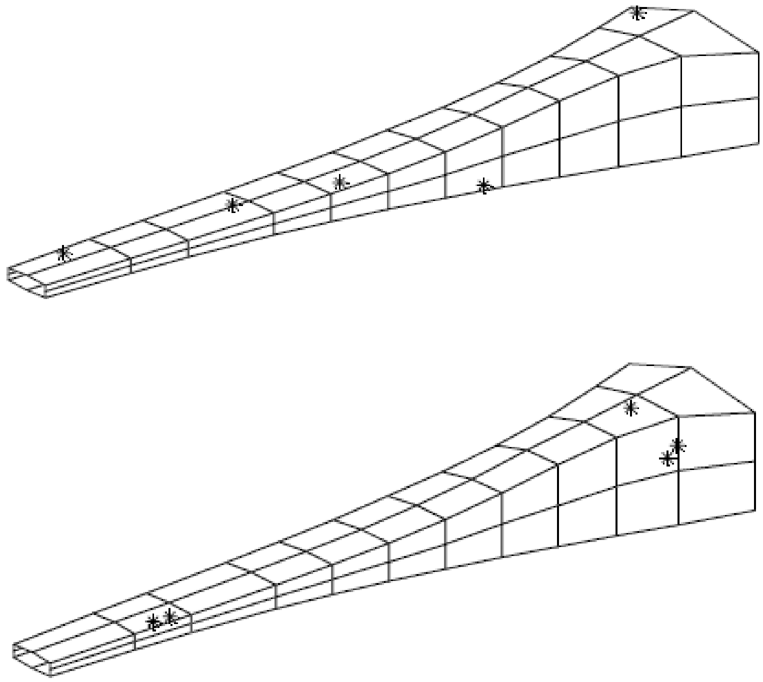

Figure 21: Completely random distributions (top) Cluster distributions (bottom)

For both models, stochastic variables included the number, type, and size of defects. The authors concluded that specific information of defects common to wind turbine blades is in general, impossible to obtain from blade manufacturers. However, in their work a stochastic model template was proposed for the distribution of defects in wind turbine blades. Moreover a reliability based approach to assess the importance of defects was formulated. In their paper only one type of defect (delaminations) was considered. Data on the ultimate load-carrying capacity of delaminations were acquired from another research project, SaNDI. It should be noted that SaNDI focused on sandwich panel structures for ships.

In this study, the maximum-strain criterion was used to predict failure of the lamina. The design equation is written as

$$G = z\frac{1}{\gamma_n}R\left(\frac{\varepsilon_{max,c}}{\gamma_m}, E\right) - \gamma_f L_c \tag{14}$$

where z is a design parameter and $\gamma_m$, $\gamma_n$, $\gamma_f$ are partial safety factors (as defined by IEC).

The load-carrying capacity R depends on εT max = {ε1c , ε1t , ε2c , ε2t , ε6} which is a vector containing the ultimate strain values, and ET = {E1, E2, G12, ν12}, which is a vector containing the elastic properties for the individual lamina. The influence of defects on the load-carrying capacity for a component can be introduced by multiplying the load-carrying capacity by a strength reduction parameter α. The modified limit state function for a component is then written as

$$g(\alpha) = zX_R\alpha R(\varepsilon_{max}, E) - X_L L \tag{15}$$

where εmax and E do not depend on the defects.

The parameter α depends on the type, size, and location of the defects. It is assumed that a wind turbine blade can be represented by a generic blade model which consists of a series system of n parallel systems, each containing m components (Figure 22).

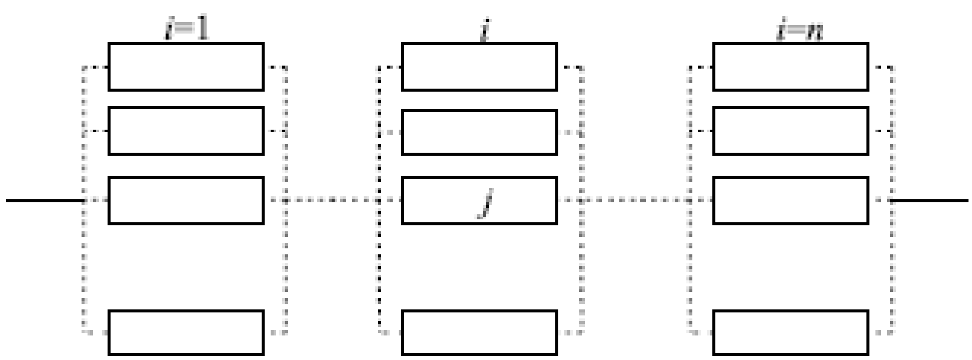


Figure 22: Reliability of a series system of n parallel systems

Each parallel system (1..n) is designated as modeling a section of the blade in the longitudinal direction. The individual components (i..j) model different parts of a cross-section (e.g. shear web, spar cap, etc). Failure of the individual components in the parallel systems is determined by the maximum-strain failure criterion, where the individual components are assumed to experience a brittle failure defined by first ply failure (FPF). Global load sharing (GLS) between the components in the parallel systems is assumed. GLS corresponds to a situation where the load can be redistributed to all components in the cross-section in which failure first occurs. Complete structural failure then ensues when all of the components in that series have failed. Based on this assumption, the probability of failure for the system (including strength reductions factors) is described the following equation.

$$P_f = \sum_{\alpha} P\left(\bigcup_{i=1}^{n} \bigcup_{j=1}^{m} \left(g_{ij}(\alpha) \leq 0\right)\right) P(\alpha) \qquad \textbf{(}16\textbf{)}$$

The reliability of the generic blade model was then numerically determined with Monte Carlo simulation. The authors concluded that treating defects as a completely random distribution, results in significant reduction to reliability. However, an even larger reduction in the reliability is observed when the defects are analyzed as occurring in clusters. [47]

Risoe University (now DTU) in Denmark has also begun an investigation into evaluating the impact of defects in wind turbine blades. Very little of this work is currently accessible in the public domain. A framework for estimating "how much is ok" as it relates to the inclusion of defects was proposed by Bech et al in 2010. The authors proposed a straight-forward routine for the analysis, wherein results NDE is performed and if a defect is found, further Finite Element Analysis is performed. Here again only delaminations were considered. Results from an aeroelastic model for the local region where a flaw was discovered, are used as inputs in a Progressive Damage Model (PDM).

The PDM models the delamination discretely with the use of cohesive zone elements and the traction separation law. More discussion of this approach can be found in ref [10]. Once this analysis is performed, the defect is deemed either critical or non-critical for a 20 year design life. Unfortunately no criteria is given for the evaluation of criticality, nor is there any discussion on fatigue. The protocol proposed by the authors is conceptually displayed in the following figure. [48]

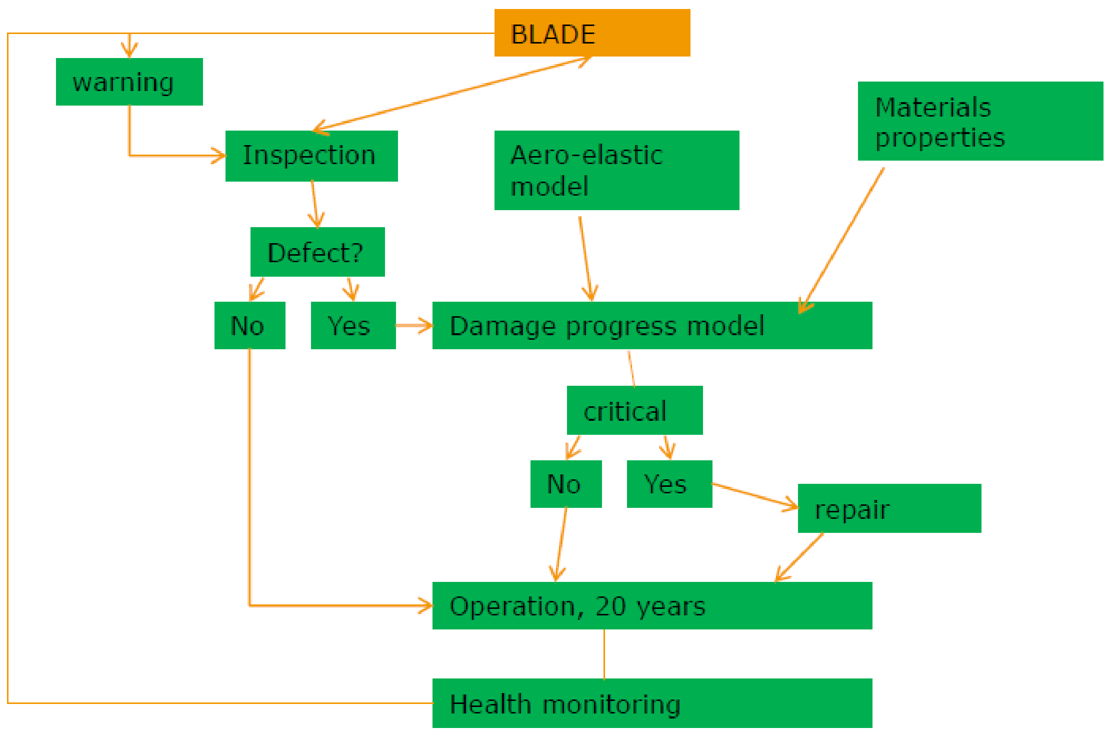


Figure 23: Defect management framework [48]

## Probabilistic Finite Element Analysis

### General Theory

The term probabilistic is used to describe a finite element analysis method wherein uncertainties in the geometry, applied loads or material properties of a structure are accounted for. These uncertainties are usually spatially modeled as random or stochastic fields with the use of probability distributions. Most often this approach is used with a second moment analysis of the response, i.e., computing means, variances, and covariance of the system under uncertainty. This approach provides useful insight into the propagation of structural uncertainties, but it does not provide adequate information for a comprehensive reliability analysis. When designing a structure to have a high level of reliability the analysis should address the tails of the probability distributions. These regions, and the subsequent structural response are poorly defined by the first and second moments. Probabilistic Finite Element methods focused on computing reliability typically use First-Order Reliability Methods in conjunction with Response Surface fitting to estimate the probability distribution of a response quantity.

Implementation of a reliability analysis in a finite element code requires two main algorithmic features. The first is an ability to compute the response of the structure based on a sequence of values (or groups of values) selected from the user defined distributions of the random variables. Each selection requires a single conventional run of the finite element code with the variables determined from the inverse of the probability transformation. The second feature required depends on the reliability methodology chosen. For the case of a first order evaluation there must be a capability to efficiently compute the Jacobian of the mechanical transformation. Whereas in a Monte Carlo simulation, the statistics of the input variables and output responses must be complied and tracked over a huge simulation space. [49]

Applications in ANSYS

General Discussion. ANSYS Inc. has released two tools for use in probabilistic evaluations; the ANSYS Probabilistic Design System (PDS) and the ANSYS DesignXplorer. Both tools can account for randomness in input variables such as material properties, boundary conditions, loads and geometry. The PDS allows users to build a parametric finite element model, solve it, obtain results and extract information on parameters of interest. The PDS can therefore be viewed as a data feeder and logger and is completely independent of the physics captured in a finite element analysis.

The randomness or uncertainty of the input variables is characterized by the probability density functions of the input variables. Mixed moments of order higher than 2 are assumed to be negligible, which means that the joint probability density function can be described by the marginal distribution functions and the correlation structure. Both ANSYS tools provide several statistical distribution functions. The PDS allows the definition of correlation coefficients between random variables to characterize the correlation structure.

Monte Carlo Simulation. The PDS is capable of performing both Monte Carlo simulations as well as utilizing Response Surface methods. The key functionality of Monte Carlo simulation techniques is the generation of random numbers that follow user defined distributions. The PDS uses the L'Ecuyer algorithm for generating these random numbers. Both ANSYS tools use the Latin-Hypercube sampling technique to make the sampling process more efficient and to ensure that the tails of the input variable distributions are well represented.

The interpretation of the results of a Monte Carlo simulation analysis is based on statistical methods. The statistical procedures to calculate mean values, standard deviations, etc. are available ad nauseam in textbooks on statistics and probabilistic methods. For the cumulative distribution function (CDF) the data is sorted in ascending order and the CDF of the ith data point, here denoted with $F_i$, can be derived from:

$$F_i = (i - 0.5)/N \quad \textbf{(}17\textbf{)}$$

where N is the total number of samples.

Monte Carlo simulation methods have only two major inaccuracies. Primarily, the number of samples cannot be infinite, but must be limited. The error due to the limitation of the number of samples can be easily quantified. As described in Ang and Tang [16], confidence intervals from the statistical results of a Monte Carlo simulation can be easily obtained. In the context of finite element analysis another source of error, which is typically overlooked, is the error due to re-meshing the geometry if geometric uncertainties are included in the probabilistic model. The Monte Carlo simulation method does not make any simplification or assumptions in the deterministic or probabilistic model. The only assumption it does in fact make is that the limited number of samples is representative to quantify the randomness of the resulting parameters. With increasing number of samples, the Monte Carlo simulation method converges to the true and correct probabilistic result. The Monte Carlo simulation is therefore widely used as a benchmark to verify the accuracy of other probabilistic methods.

Another advantage is the fact that the required number of simulations is not a function of the number of input variables. The disadvantage of the Monte Carlo simulation method is its computational cost. As a rule of thumb, when addressing low probabilities of failure the number of required simulation loops ($N_{sim}$) is approximately $N_{sim} = 100/P_f$. Where $P_f$ is the targeted failure probability. Hence, if the targeted failure probability is low, then the required number of samples may be prohibitively large, making the Monte Carlo simulation method impractical for real engineering problems.

Response Surface Method. Response surface methods avoid the disadvantages of Monte-Carlo simulation methods by replacing the true input–output relationship by an approximation function. For the approximation function **y,** typically a quadratic polynomial with cross-terms is used. It has the form:

$$\hat{y} = c_0 + \sum_{i=1}^{n} c_i \cdot x_i + \sum_{i=1}^{n} \sum_{j=1}^{n} c_{ij} \cdot x_i \cdot x_j \qquad (18)$$

Here, $c_0$, $c_i$ and $c_{ij}$ with i,j = 1,. . .,n are the regression coefficients and $x_i$, i = 1,. . .,n are the n input variables. This equation is also called the regression model. Response surface methods are based on the assumption that the response surface is an adequate representation of the true input–output relationship. For engineering applications, a quadratic response surface according to Equation 18 is often not sufficient for representing the true input-output relationship. To improve the accuracy of the approximation function, it is necessary to use non-linear transformation functions. The advantage of response surface methods, is their performance. If the response surface is an adequate representation of the true input-output relationship, then the evaluation of the response surface is much faster than a finite element solution. Like Monte Carlo methods, response surface methods are independent of the physics representing the true input-output relationship. All probabilistic methods, other than Monte Carlo simulation methods are based on a set of assumptions with respect to the deterministic or the probabilistic model. One of the disadvantages of the response surface method is that it may be an inadequate representation of the true input–output relationship. This can happen for example, when the true input–output relationship is not continuous. This case is difficult to handle by any probabilistic approach other than Monte Carlo methods.

# CHAPTER 3

# PROPOSED RELIABILTY PROTOCOL

## Framework for Defect Risk Management

Improving and quantifying reliability of wind turbine blades is the primary goal of the BRC. In order to do this, a comprehensive understanding of the causes of blade failures is necessary. This effort begins with classification of known defect types, and then establishes a criticality metric based probabilistic and damage tolerance methodologies. These types of techniques have been successfully utilized to improve airline safety for decades. Implementing this information at the manufacturing level will establish quality guidelines while reducing plant down-time, rework, scrap-rates, and ensuring a successful life-cycle. As noted above and outlined by Nelson (2013), previous research has been performed analyzing the effect of defects in generalized composite laminates. As such, a bridge is necessary to correlate this generalized information to the specific uses of composites in wind turbine blades.

While background research must be performed to acquire and generate quantitative flaw data, this section will primarily focus on the development of a framework which addresses the reliability of wind turbine blades subject to manufacturing defects. This effort can be divided into two major objectives: (1) acquisition of relevant defect statistics and defect laden lamina response and (2) development of a probabilistic model to assess the global structural response, probability of failure, and estimation of time to failure, for wind blades with flaws. Both of these objectives are addressed within the context of a framework called the Probabilistic Reliability Protocol (PReP). A conceptual flow diagram of this PReP is shown in Figure 24. It consists of four major areas which are summarized in the following sections.

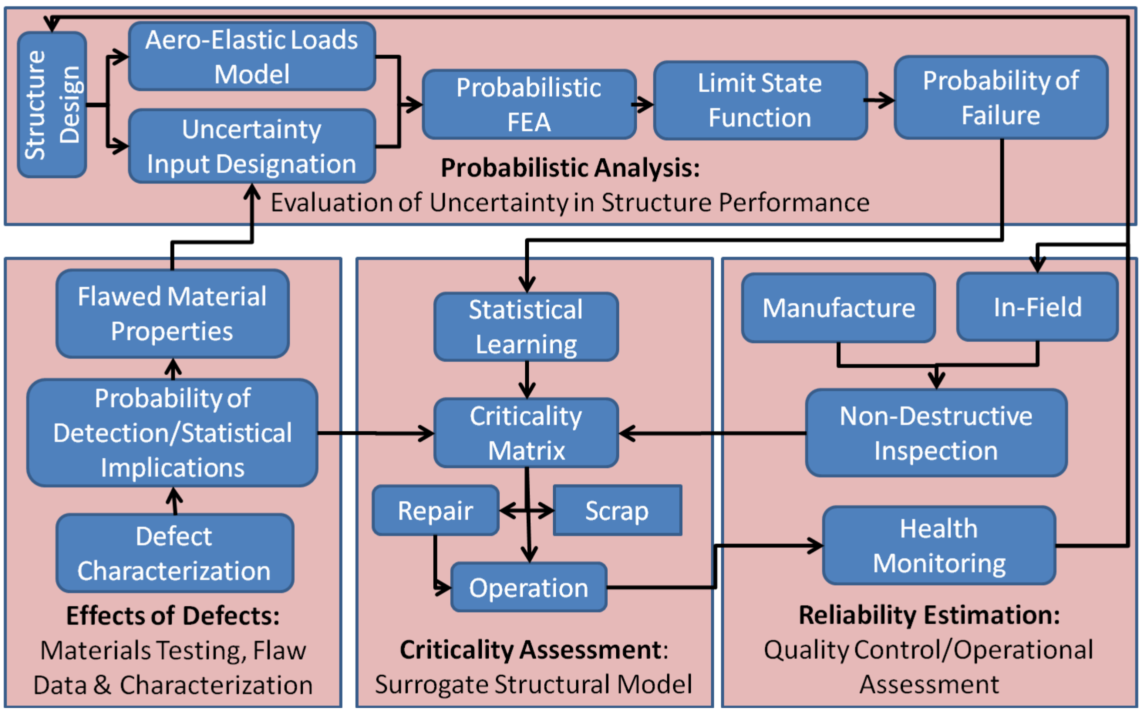

Figure 24: PReP frame work for defect risk management and improved reliability

<u>Effects of Defects</u>

The Effects of Defects block involves the identification, characterization and analysis of defects. Defects and failure data are collected in the field before using the significant geometric properties to develop metrics for characterization of flaws. A statistical analysis is performed to establish distributions relating the frequency and probability of occurrence for various flaw types and sizes. Utilizing these data, laboratory testing may be performed on specimens with representative defects to generate mechanical properties for laminates with flaws (and without flaws) that correlate to defect characterization parameters. The material properties may also then used in subsequent modeling approaches.

Performing a comprehensive assessment of the Effects of Defects in composite materials is not a trivial endeavor. Defect types and sizes can vary between industries, manufacturers, models and even production shifts. Moreover, there are nearly limitless permutations of composite material architecture for which the effect of a defect may vary as well. The investigation on wind blades discussed in Chapters 4 and 5 of the work describes the necessary aspects of such an investigation.

### Probabilistic Analysis

Probabilistic analysis of composites structures is not a new concept as noted in the background section above. However, the majority of the work performed to date has focused on variations in the constitutive material properties and simple manufacturing variations such as ply misalignment. While these properties are deviations from the ideal case and therefore maybe considered as flaws, they are predominantly unavoidable and intrinsic to all composite structures. However, other defects at the ply or laminate level, that result from a specific manufacturing process, such as waves and porosity, may be considered as uncertainty parameters as well. Very little work has been performed to this end in any industry. The Probabilistic Analysis proposed as part of PReP is able to address both levels of uncertainty. Furthermore, the results show that treating defects as random variables can assist in significantly reducing design constraints based on a safety factor approach. A general overview to this approach is given in the last section of this Chapter, Analysis Procedure. This discussion will introduce the reader to the elements required to perform such an analysis enabling a cursory understanding of where the following chapter discussions fit into the overall analysis.

Criticality Assessment

The goal of any quality control program is to meet metrics that are intended to ensure the reliable operation of the product. Much of the time, this effort is performed qualitatively and subjectively by a group of experts. The three proposed Criticality Assessment tools outlined below provide the necessary link between detailed design analysis, NDE, and quality assurance.

- **Surrogate Model**: There are many elements that play a role in failure, some global or macro and some local or micro, most all of which can be captured in a Probabilistic Finite Element Analysis (PFEA). While PFEA will provide the designing engineer with significant insight, the complexity and computational costs render it unusable for case by case in-situ reliability estimation. Instead, a need exists to evaluate the reliability of a structure quickly on the manufacturers’ floor, as a quality control effort or in the field by technicians, that capture more information than a 'not to exceed' specification. This type of assessment needs to be fast, accurate, and interfaced as a 'black box'. Statistical learning algorithms were used to develop a surrogate model from the afore mentioned probabilistic analysis. This enables the engineer to take NDE information on known defects (type, size, location) and rapidly perform an analysis which yields the same information as the complete probabilistic reliability analysis without the time requirements.

- **Criticality Matrix**: A time efficient metric for use by operators, manufacturers and repair technicians, to evaluate the risk of operating a structure with known flaws, and/or damage. Data from as-built structures with flaws are characterized to describe the structure under scrutiny. These inputs are then mapped to criticality/severity space through the criticality analysis algorithm. The structure can be evaluated and a decision is made to operate the structure as is, repair it or scrap it.
- **Criticality Map:** It is not uncommon for a blade designer to specify thresholds for flaw sizes which apply to the entire blade. Often time this results in non-critical flaws being repaired. The criticality map is designed to distribute more information to the technician in the form of a QC schematic (map) of the structure. The Criticality Map details defect sensitive Regions Of Interest (ROI). For each ROI a table is given describing the probability of failure ($P_f$) as a function of flaw type and magnitude. Three risk categories are designated on the map; Low, Moderate, and High.

In-Field Reliability Estimation, Evaluation and Reporting:

The PReP protocol is designed to be a feedback loop. It is imperative for continuous design improvements, that the designer receive information back from manufacturing and in-service technicians. Results from NDE and the Criticality Assessment tools, as well as in-field inspections, confirm the accuracy of the models and the blade reliability implications are incorporated into the design and evaluation procedures. Once the structure has been placed in operation, a health monitoring and inspection procedure should be implemented. The designer can then update probability distributions from NDE data, thereby minimizing uncertainty in the analysis. Also, as structures are monitored in the field operational data can be used to validate damage growth and probability of failure.

## Analytical Procedure

The core of the PReP reliability protocol is Probabilistic Finite Element Analysis and the subsequent probabilistic reliability analysis. A basic overview of these is given here to provide context for the information generated in the following three chapters. Greater detail on the analysis is given in Chapter 6: Structural Reliability. A schematic representation of the components used in this analysis is given in Figure 25. Note the similarities between this analysis flow and the IPACS algorithm presented in Figure 17. The major differences between the two being that PReP analysis is focused on defects and the introduction of defect data. Additionaly, IPACS employs variability in a mulitscale approach that considers micro and macromechics. Whereas, the PReP algorithm only considers a macroscale response.

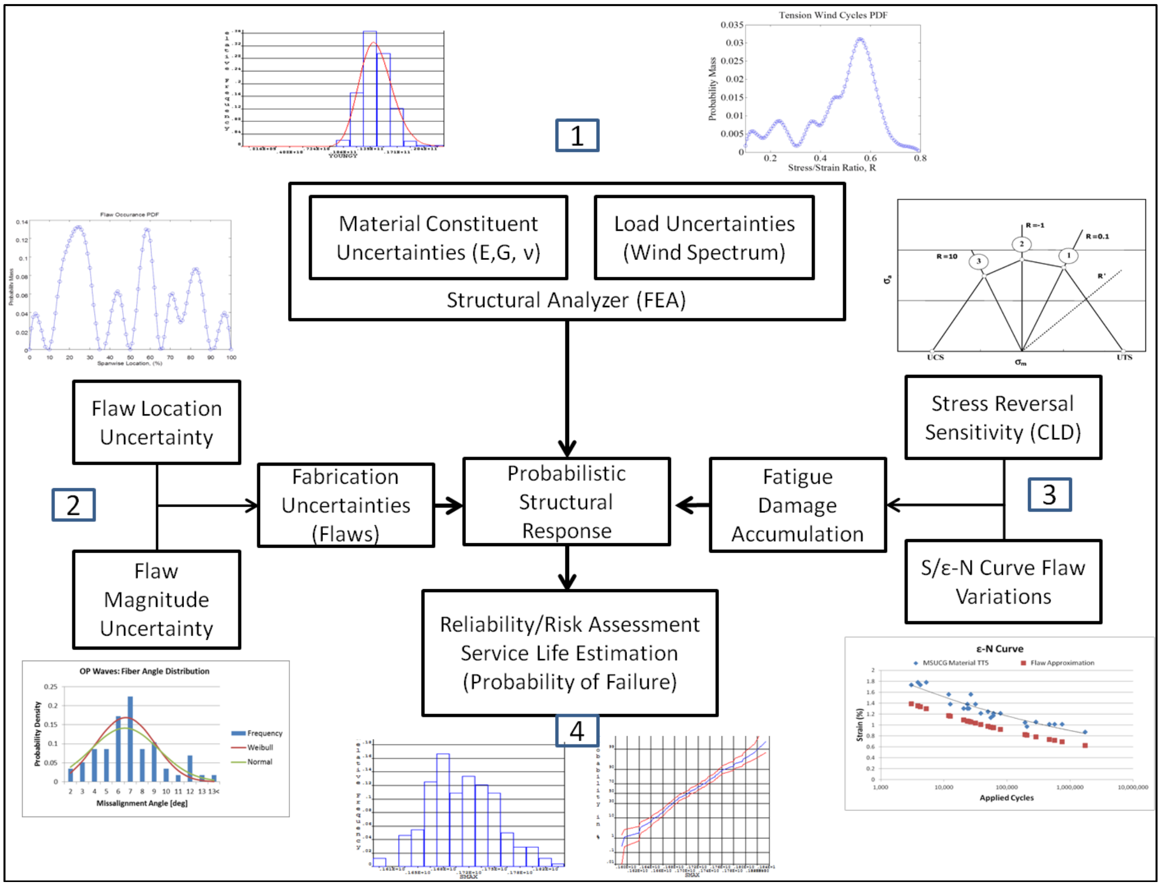

Figure 25: PReP FEA and reliability analysis component flow

Each of these elements must be defined prior to performing the analysis. The steps to this analysis are as follows;

1. Build a parametrically defined finite element model: The model is created in such a way, that key attributes can be described with the use of distributions. These attributes may be any portion of the analysis of interest.
2. Define load scheme and failure criterion: These can be implemented by the structural solver or in a post processing reliability analysis, depending on how the analysis set up. Often times the load is considered a random

variable; therefore, it must be prescribed in the analysis setup in such a way as to allow for variations. In addition, for a probabilistic analysis, the failure criterion is typically dependant on a random variable or multiple variables. For the wind blade analysis, load may be introduced into structural analysis to simulate wind speed effects and a failure criterion may be developed around strain to failure and fatigue.

3. Define Random Variables (RV) and their distributions: In the PReP protocol there are two places for RVs to be evaluated; the structural model (label 1 in Figure 25) and the reliability analysis (label 2 in Figure 25). Variables of interest may vary depending on the application. For a wind blade with defects, example RVs include constitutive properties, load magnitude, flaw type, magnitude and location. Often times these variables are defined based on engineering or expert judgment. Many industries, such as civil infrastructure and steel buildings, have already created standards which detail the variables that need to be considered. It is the hope that research like that presented herein may help define such standards for the wind industry.
4. Define output variables of interest: In a stochastic analysis, the output response will vary according to the input RVs. Output variables should be selected according to needs of the particular analysis. One aspect to be considered, is that if the output variables and input variables are designated appropriately, significant insight into the effect a RV has on the

response can be evaluated through the use of sensitivity analysis. For the wind blade analysis, assessing the probability of failure for a blade with defects is the primary interest. Since failure has been defined by strain in fatigue, the primary output response of interest is strain. Outputs variables of interest are established in much the same way as the inputs. In many cases, standards exist to guide the analysis. The outputs used in this analysis were designed around the IEC standard for fatigue life evaluation. For other cases, it may be necessary to use engineering judgment or expert opinion.

5. Perform structural simulations: In the PReP protocol, two simulation steps are performed. The first is the structural analyzer (FE model) and second is the probabilistic reliability analysis. The Monte Carlo Method has been used with a high degree of success in both analysis portions. Material and load uncertainties may be applied to the analysis and relevant strain data generated.
6. Extract relevant, probabilistic output response data and input data, into reliability analysis: Spatially varying strain data is gathered from the structural simulation and input, into the reliability analysis. For the wind blade analysis, uncertainty related to defects are applied in the reliability analysis. Output of this analysis is probability of failure.

# CHAPTER 4

# DEFECT OVERVIEW

## Blade Survey

Critical to the development of a manufacturing defect-based reliability program is identification of the precise geometric nature of flaws based on statistical commonality in the structures of interest. Several commercial scale wind turbine blades were reviewed to indentify these geometries for the work herein. The data set was limited to four blades which were reviewed for out0if-plane (OP) waves and one for in-plane (IP) waves. However, this data provided a strong foundation for the development of a protocol, by which other blades may be examined and resulting flaw characterization in the future.

The process by which IP wave, OP wave and adhesive joint data were collected were collected from photographs taken of as-built blade sections with visible flaws. The majority of the images were collected of blade sections at NREL's National Wind Technology Center where four utility sized (1-MW to 2.5 MW) blades were examined. Blade specimens had been previously subjected to structural testing at NREL. In the case of OP waves and adhesive bond lines, portions were cut out of blades to provide a cross-section view of the skin and spar cap laminates. A fifth blade located at Sandia National Laboratories was also reviewed and this blade provided data for IP waves only as it had not been tested or sectioned. IP waves were clearly visible under the clear surface gel coat. It is of note that this blade was not a production blade, but rather a one-off experimental design. For all cases, a scale measurement device was placed in the region of interest.

## Flaw Characterization

### Process for Parameterization of Waves

All photographs were taken using the same digital camera and defect parameters were assessed with analysis on the images. The digital images were imported into ImageJ, an open source image processing software package typically used in the medical imaging field. [50] In the ImageJ environment, the photos were converted to 8-bit color, and then the wave features were manually traced with a black line. Examples of this process are shown in Figure 26 for an OP wave and Figure 27 for an IP wave.

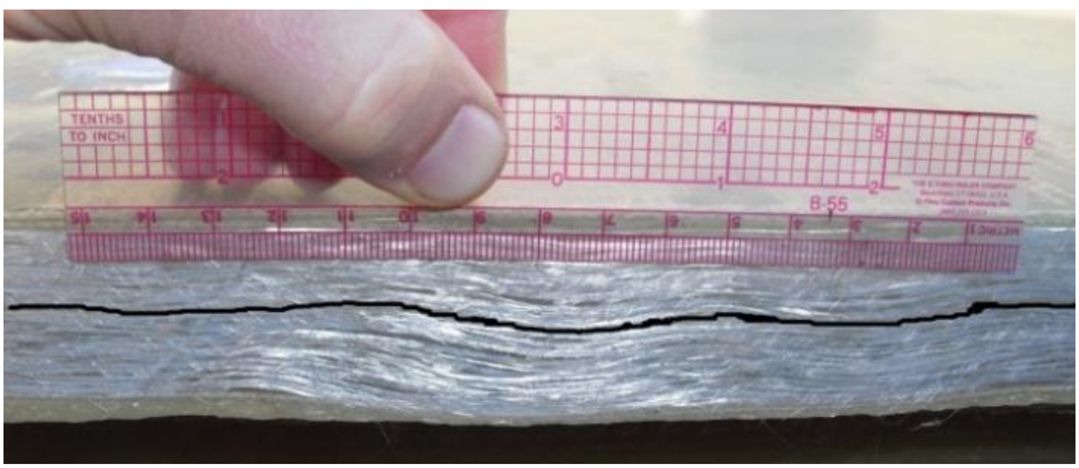


Figure 26: Image of OP wave.

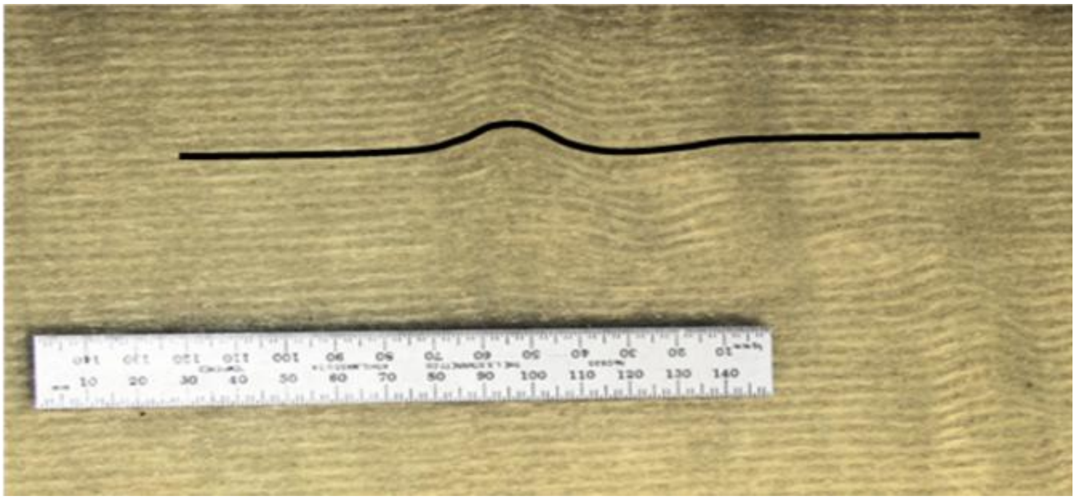


Figure 27: Image of IP wave.

The incorporation of the measurement scale into the photo made it possible to develop a pixel based dimensioning system. In ImageJ, features can be measured in terms of pixels; thus a relationship between the number of pixels in virtual space and the actual physical dimension is determined (mm/pixel) using the imaged ruler increments. Colors in an 8-bit space are represented with a number from 0 (black) to 255 (white), enabling the application of mathematical operations to remove unwanted colors. Manipulating the color depth of each pixel allowed for the removal of the background, leaving only the feature tracing line. This is easily performed by adding a color value of 254 to all pixel designations. What remained were two pixel colors, 254 and 255. The original pixel color for every pixel in the tracing line was 0; therefore, all pixels in the tracing line had a value of 254. Subtracting by a color value of 254 returned the tracing pixels to a value of 0 and all other pixels became 1. Next, all pixel numbers were multiplied by 255. This process created a binary image where the tracing line pixels were black (0) and the background was white (255)  This image was then exported as a binary bitmap to Matlab where a separate processing script was utilized to extract the spatial coordinate data of each pixel.

Tracing a feature with a computer mouse can result in small deviations from the actual feature and often times, a thicker line than is necessary results. This spatial data extraction process began by smoothing the tracing line to a single pixel depth through the use of a moving average scheme. For each horizontal pixel increment, should there be more than one vertical pixel, the pixel locations were combined and averaged. This resulted in single pixel thick tracing line. The pixel planar coordinates were then converted into physical space coordinates by means of the image specific pixel/physical transformation factor. From this data, each complete wave form was discretized into separate individual waveforms at wave peak and through inflection points. This was performed by assessing the change in slope down the length of the waveform. Inflection points were automatically determined by the sign variation of the slope from one pixel to the next. One example of a complete wave, and the resulting waveform discretization locations is shown in Figure 28.

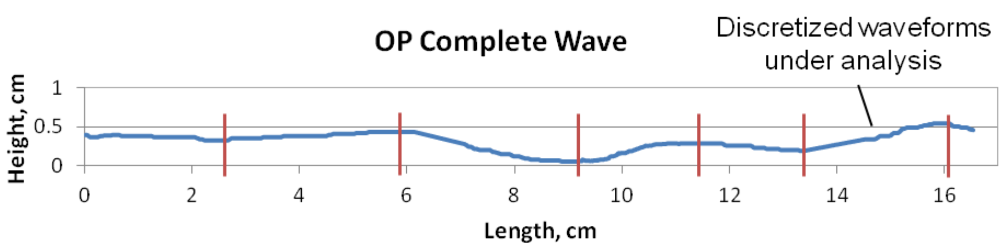


Figure 28: Example OP Wave complete spatial data and discretization positions.

Each discretized wave form's geometry was then mathematically characterized in Excel. Cubic splines (Equation 19) and sinusoidal curve (Equation 30) fits were both evaluated for their applicability to mathematically describe the wave perturbation.

$$Y = Ax^3 + Bx^2 + Cx + D \tag{19}$$

$$Y = E + Fsin(\frac{2\pi}{\omega}x + \phi) \tag{20}$$

where A, B, C, and D are polynomial coefficients. For the sine wave, E is the offset, F is the amplitude, ω is the wavelength and Φ is the phase.

In order to fit the wave spatial data to the mathematical formulations, Excel's add-on Solver function was used to perform an optimization of a user built least squares regression algorithm. The Solver function uses the Generalized Reduced Gradient (GRG) constrained optimization algorithm. In a least-squares data fitting method the most accurate model is established by minimization of the sum of squared residuals. A residual being the difference between an observed value and the fitted value provided by a mathematical model. The GRG algorithm was used to manipulate model values (A, B, C, D, E, F, ω, φ) until the sum of the squares was minimized. [51];

Both models (spline & sinusoidal) yielded similar goodness-of-fit tendencies. The sinusoidal analysis proved to be faster and was chosen for utilization on the bulk data analysis. Moreover, the ability to reference model parameters which also have physical meaning (amplitude, wavelength) was useful in performing statistical characterization of wave parameters. Once a fit was performed, each wave was characterized in terms of wavelength, amplitude and off-axis fiber angle (Figure 29). While, some previous studies have used aspect ratio or wave severity (amplitude/wavelength) instead of fiber angle as a metric for characterization, such quantification may be slightly more challenging in the field. Aspect ratio requires knowing both the amplitude and wavelength whereas the fiber angle can be measured directly. [52; 53; 54]

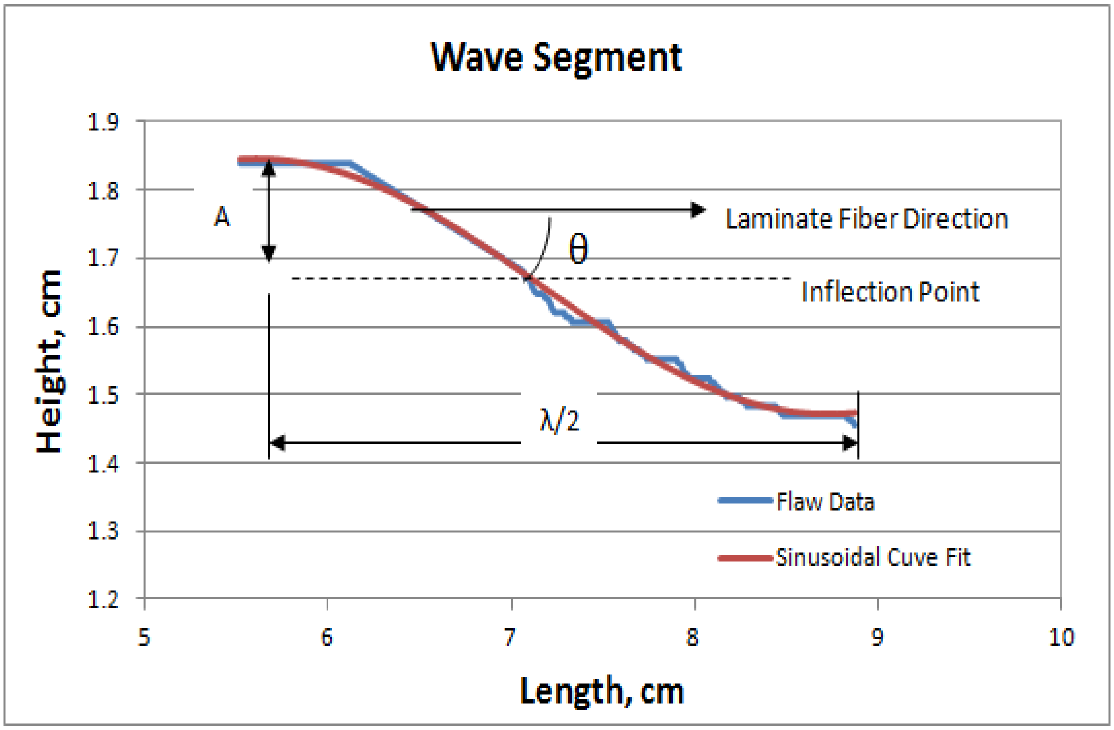


Figure 29: Example of sine wave fit.

<u>Waves Data Summary</u>

Characterization of the various wave flaws found in the field data yielded 63 OP and 48 IP independent, discrete waveforms. Values for amplitude and wavelength of each instance are shown in Figure 30 and Figure 31 for OP and IP waves, respectively. Here it can be seen that there is significant variation within the data. However, the data are well grouped, indicating some consistency in the manufacturing processes. The results of calculated off-axis fiber angles for OP waves and IP waves are shown in Figure 32 and Figure 33, respectively. Specific attention should be paid to the outlying group of angles highlighted by the red circle in Figure 32 because these angles were collected from blade sections which failed at these out-of-plane flaw locations. Wave parameter data for these flaws were collected post-failure. Observing these locations, it was noted that the measured wave misalignment angles were significantly perturbed after the deformation at failure. Therefore, the value for misalignment angle is not considered to be relevant and was not used in any of the subsequent statistical or structural analysis

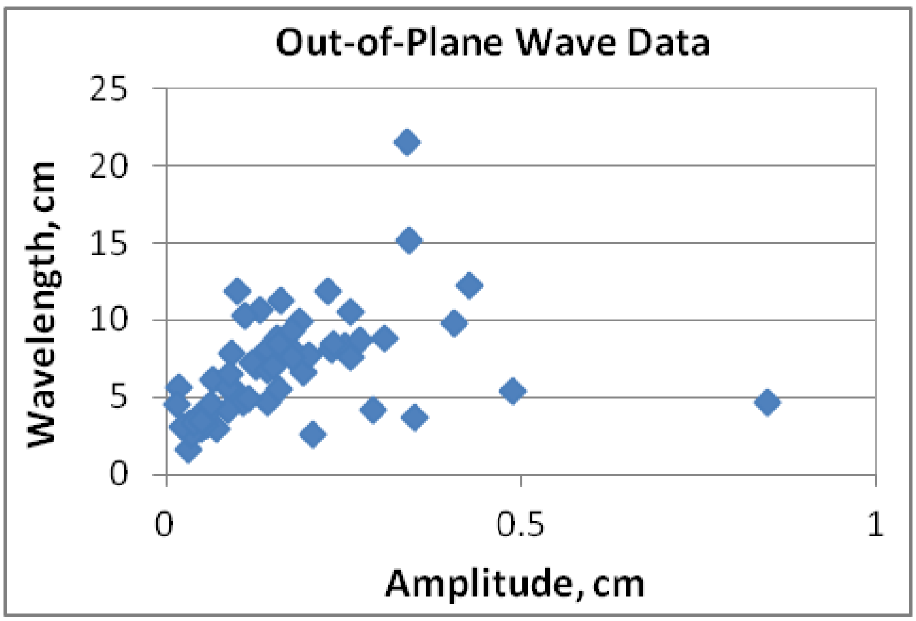


Figure 30: Plot of collected OP wave data.

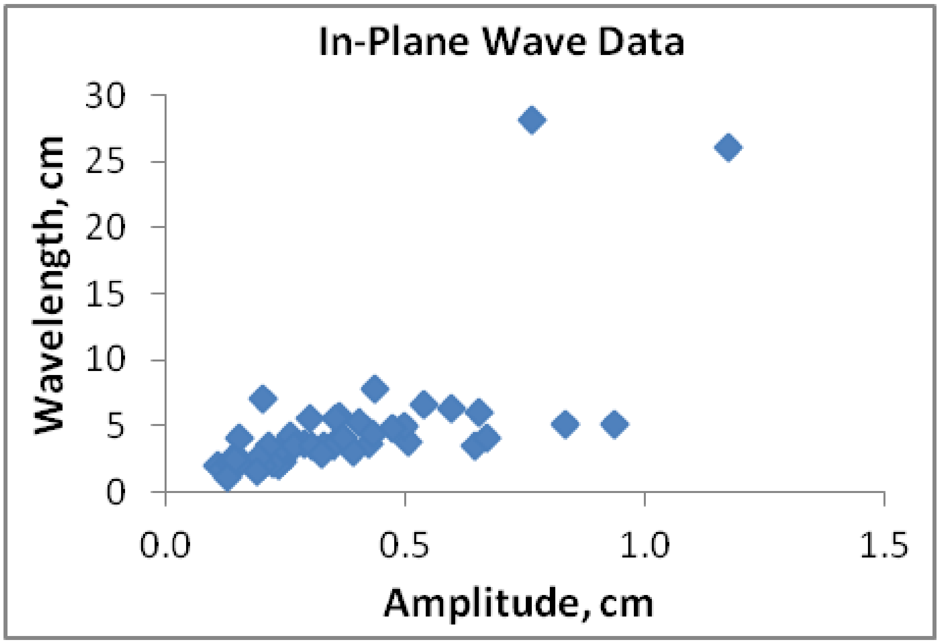


Figure 31: Plot of collected IP wave data.

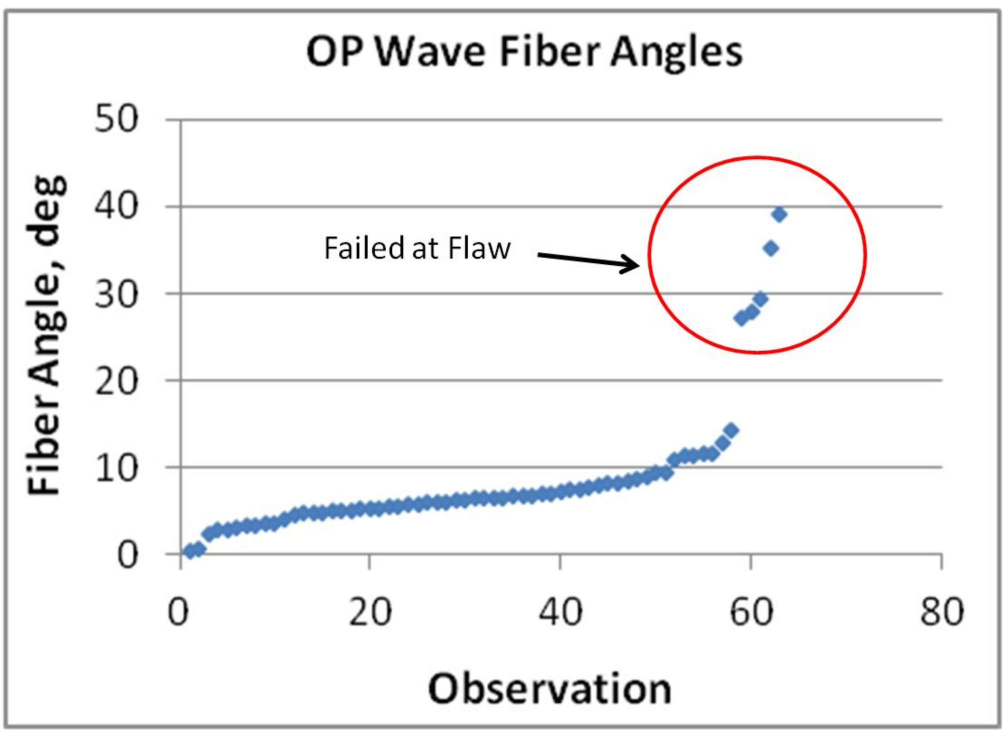


Figure 32:  OP wave off-axis fiber angles.

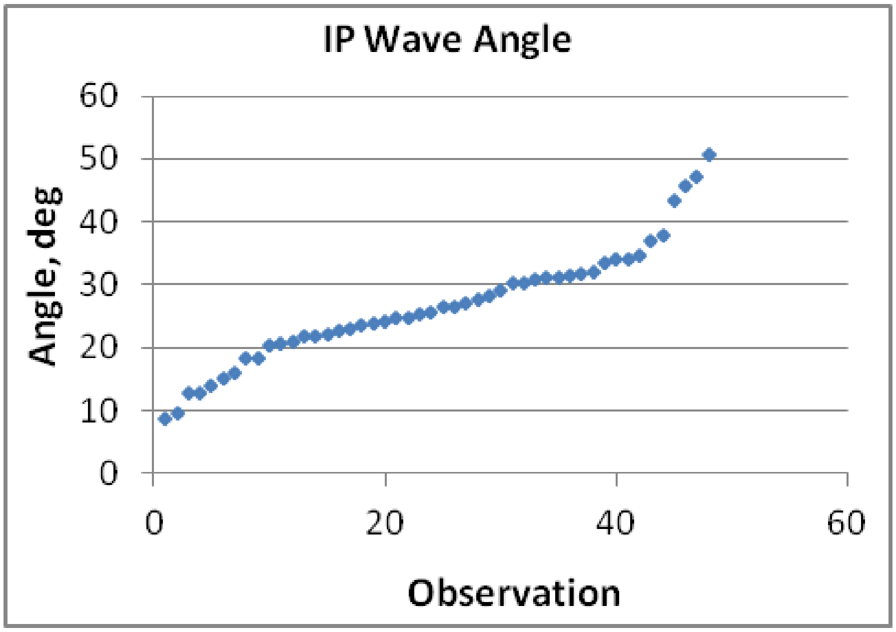


Figure 33: IP Wave off-axis fiber angles.

Mean and standard deviation were used to develop Normal distributions to describe the frequency of flaw magnitude occurrences. Weibull distributions (2 parameter) were generated using Maximum Likelihood Estimation. OP wave fiber angle values shows a strong inclination towards common distributions such as the Weibull and Normal distributions. This can be seen in Figure 34 and Figure 35, where the observed frequency of occurrence is displayed with the distribution curves. The histograms were generated by binning flaw angle data. For the case of out-of-plane waves, angles were binned in one degree increments. In-plane wave angles were grouped in four degree increments.

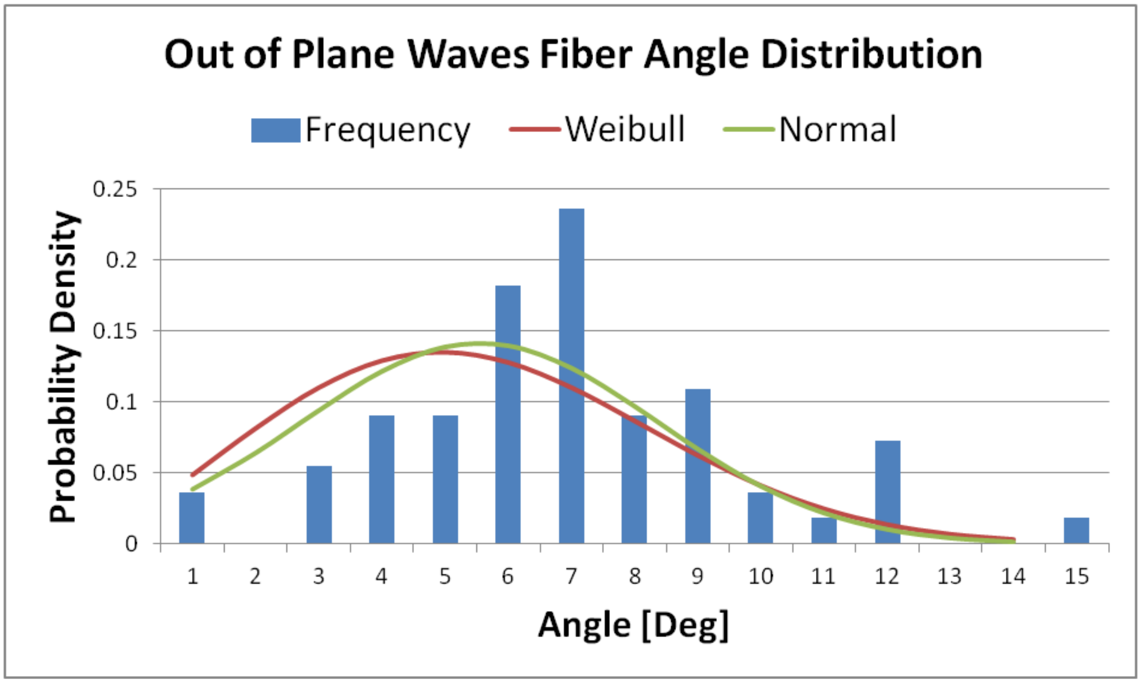


Figure 34: Out-of-Plane fiber angle distributions.

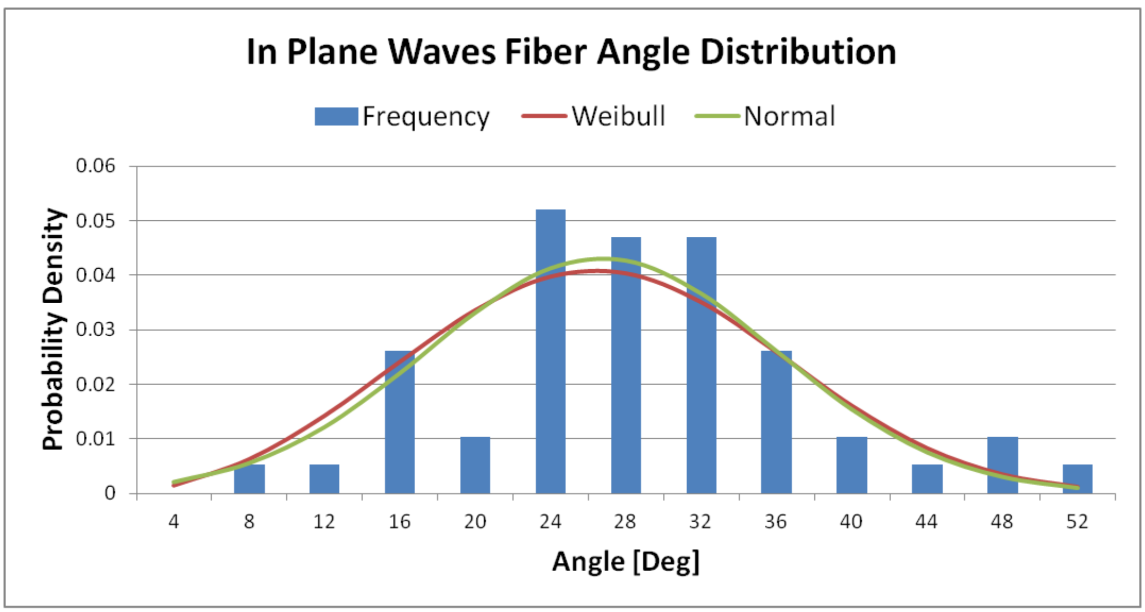


Figure 35: In plane wave fiber angle distribution

Similar binning procedures where applied to amplitude and wavelength data for both wave types. The distributions of this data are displayed in Figures A1.1 – A1.4. In general, the skewed populations with extremal ends lead to a better fit with a Weibull distribution. The data on both in-plane and out-of-plane waves can be summarized in Table 3 below. Parameters displayed for mean and standard deviations were those used to generate the normal distributions.

Table 3: Wave data summary.

| **OP Waves** | **Amplitude, cm** | **Wavelength, cm** | **Fiber Angle, deg** |
|---|---|---|---|
| Min | 0.02 | 1.58 | 0.59 |
| Max | 0.85 | 21.49 | 14.3 |
| Mean | 0.17 | 6.74 | 6.54 |
| Standard Deviation | 0.11 | 3.00 | 2.82 |
| **IP Waves** | **Amplitude, cm** | **Wavelength, cm** | **Fiber Angle, deg** |
| Min | 0.11 | 1.08 | 8.68 |
| Max | 1.18 | 28.12 | 50.66 |
| Mean | 0.37 | 4.75 | 26.73 |
| Standard Deviation | 0.23 | 4.96 | 9.26 |

Porosity

At the onset of the BRC, collaborators directed the MSU team as to which flaws to focus on. In addition to waves, porosity was highlighted as a significant problem. While little information was given concerning waves, the group did give a specific threshold for an acceptable porosity level of 2%. [55] Considering this and the fact that porosity is extremely hard to characterize in the field without expensive NDE equipment, very little data was collected as part of the blade survey. An example of a porosity image collected during the field survey is given in Figure 36. This image illustrates that entrained air can be excessive in wind blades. This brings into question the definition of porosity. Resin-devoid pockets such as some of those found in Figure 36 (label 1) can also be considered voids, dry spots or delamination. However, another variation  exists as a more uniform dispersion of small gas bubbles (Figure 36, label 2). This type of dispersed porosity was the focus of this investigation.

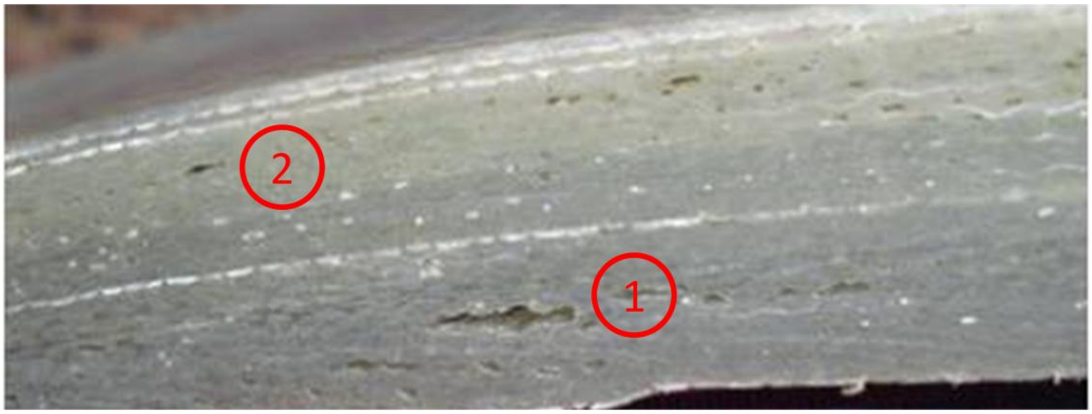

Figure 36: Image of porosity and voids

Adhesive Flaws

After reviewing the same group of blade section images for adhesive bondlines it was inferred that there were two distinct cases where adhesives are used in wind turbine blades. For the purposes of this reporting, the two cases will be referred to as spar, where adhesives are used to bond the spar cap or shear web to the skin of the blade and mold line where adhesives are used to bond the two molded halves of the blade skin together. Representative images of the two cases are shown below in Figure 37.

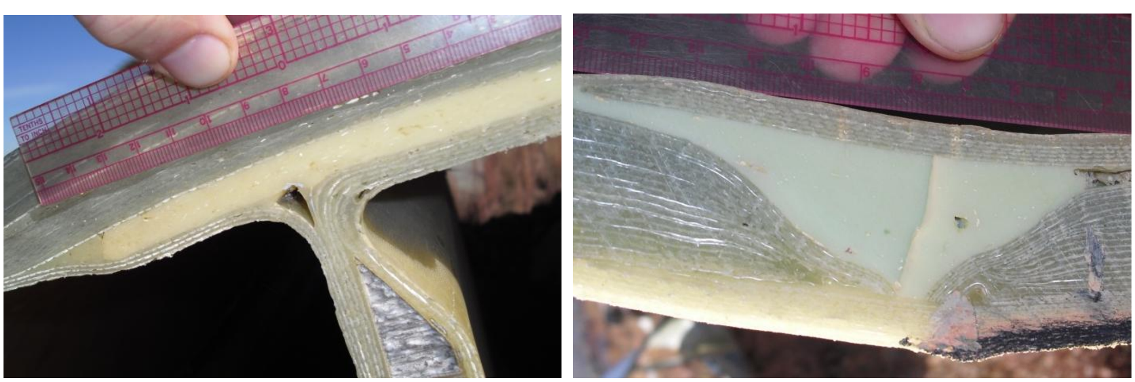
Figure 37: Spar – Shear Web adhesive bondline (Left), Adhesive mold-line (Right)

In both cases, voids were found to be extremely prevalent, nearly ubiquitous. The general shape of voids tended to be elliptical. Moreover, every image showed some porosity (smaller more uniform inclusions) content. Bonding of the spar cap and shear web to the blade skin did not appear to incur a significant amount of defects. Mold lines on the contrary exhibited a variety of negative manufacturing attributes. All mold line cases showed voids, some porosity, ply drops and in many cases extreme out-of-plane waves. Another artifact of the mold joining process was the use of laminate patches on either side of the joint for reinforcement. This design detailed was not considered further.

In addition to identifying the function or type of adhesive application, it is also necessary to define characterizing geometry, such that an application can be quantitatively analyzed. Defining characteristics (Figure 38) of the Spar case include: adhesive thickness, void dimensions and percent porosity.

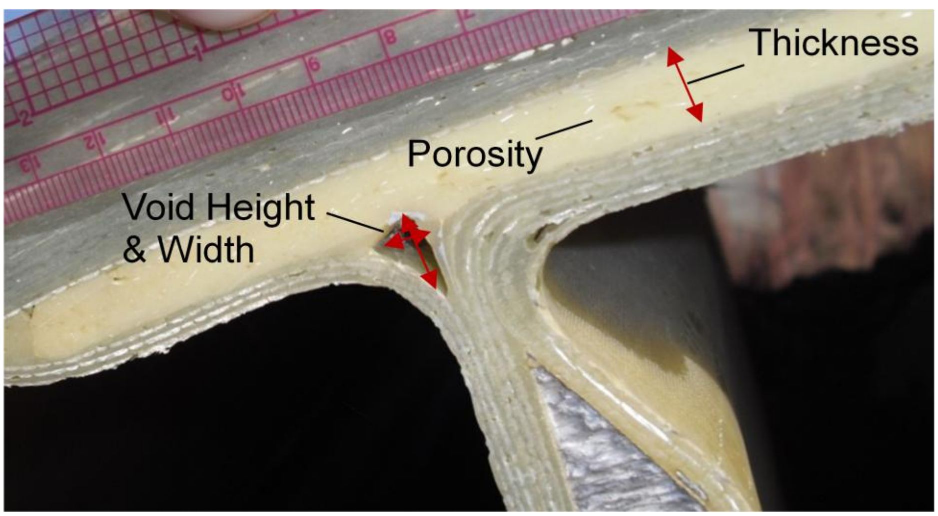

Figure 38: Spar case characterizing geometry

Defining characteristics of the mold line [Figure 39] case include: adhesive height and base, void dimensions (same as spar), number of plies, ply drop height, ply drop length, and ply drop aspect ratio. Based on the images collected, the porosity level proved difficult to obtain.

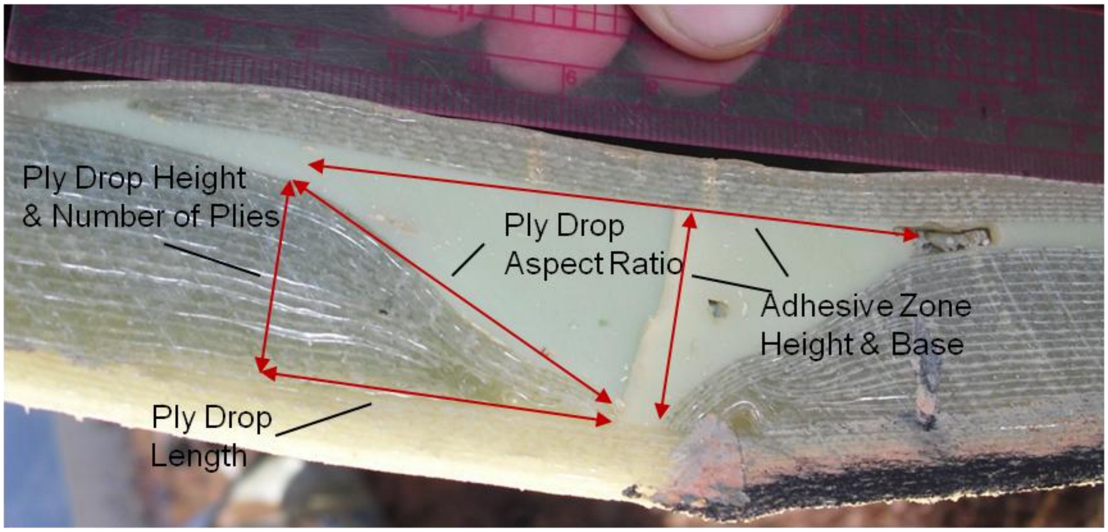

Figure 39: Mold line characterizing geometry

The characteristic data for each case is given in the following tables. This data has also been plotted. It should be noted that this data is most likely specific to the blade design and may only be relevant to those blades that were surveyed. These figures may be found in the Appendix; Figures A.5-7.

Table 4: Summary of spar case parameters

| Spar | Thickness [cm] | Void Width [cm] | Void Height [cm] | Porosity % |
|---|---|---|---|---|
| **Average** | 1.42 | 0.83 | 0.45 | 1.48 |
| **Min** | 0.70 | 0.22 | 0.13 | 0.71 |
| **Max** | 3.05 | 3.12 | 0.89 | 2.57 |

Table 5: Summary of mold mine case parameters

| Mold Line | Height [cm] | Base [cm] | Void Width [cm] | Void Height [cm] | # of Plies | Ply Drop Length [cm] | Ply Drop Height [cm] | Aspect Ratio (L/H) |
|---|---|---|---|---|---|---|---|---|
| **Average** | 1.91 | 6.32 | 0.28 | 0.27 | 16.00 | 3.48 | 1.82 | 1.91 |
| **Min** | 1.43 | 2.63 | 0.12 | 0.18 | 12.00 | 2.16 | 1.13 | 1.73 |
| **Max** | 2.73 | 10.30 | 0.54 | 0.37 | 20.00 | 4.34 | 2.28 | 2.31 |

# CHAPTER 5

# COUPON EXPERIMENTAL WORK

## Introduction

The goal of this work is to understand the effects of defects on composite structures. While characterization of the full-scale structural response is the output of interest, it would be impractical and unrealistic to develop the mechanical relationships with a singular numerical/analytical approach or by only testing full-scale structures. Therefore a laboratory testing program was developed. An understanding of the changes in the material properties associated with characterized flaws was achieved initially on a coupon level. Physical testing was performed on many configurations of the different flaw types with the goal developing criteria to describe the mechanical properties of the defect types on a small scale, then apply those to larger structural analysis. This goal was accomplished with three distinct rounds of coupon scale testing over the course of this project.

### Round 1 Test Program

Three wave forms for each type of flaw were systematically chosen for testing based on geometry characterization and statistical significance [Table 6].

1.) Out-of-Plane Waves: The parameters for waves OP1 & OP2A (Table 6) were chosen because their angles are almost identical however they had statistically significant but varying amplitudes & wavelengths between them. The particular angles chosen to yield two data points around the angular region of interest (data from a failed blade section). The third OP wave (OP4A) had mean values for all three parameters and therefore landed in the center of all of the parameter distributions. These provide excellent data points for describing an OP wave common to the specific wind turbine application. By design, the mean value also delivered baseline values for comparison of the effects of amplitude and wavelength independently with the OP1 and OP2A results.

2.) In-Plane Waves: Similar to the OP test wave designations, in-plane test waves IP2 and IP3 were chosen such that the angles are almost identical. Moreover, these values for off axis fiber angles are in the outer regions of the angle distributions. IP1 also utilized mean values for all of the parameters. Additionally, the amplitude and wavelength match up with IP3 and IP2, respectively allowing for analysis of those parameters independently.

Table 6: Wave forms chosen for first round testing.

| **OP1 Wave** | **As-Built** | **IP1 Wave** | **As-Built** |
|---|---|---|---|
| Max Amplitude, mm | 8.5 | Mean Amplitude, mm | 3.7 |
| Mean Wave Length, mm | 67.4 | Mean Wave Length, mm | 47.5 |
| Angle, deg | 34.9 | Angle, deg | 24.8 |
| **OP2A Wave** | **As-Built** | **IP2 Wave** | **As-Built** |
| Mean Amplitude, mm | 1.9 | 99% Amplitude, mm | 9 |
| Min Wavelength, mm | 15.8 | Mean Wavelength, mm | 47.5 |
| Angle, deg | 35 | Angle, deg | 48.9 |
| **OP4A Wave** | **As-Built** | **IP3 Wave** | **As-Built** |
| Mean Amplitude, mm | 1.9 | Mean Amplitude, mm | 3.7 |
| Mean Wave Length, mm | 67.4 | 10% Wave Length, mm | 20 |
| Angle, deg | 9.7 | Angle, deg | 47.8 |

3.) Scaling Considerations: The first round of mechanical testing was on coupon-sized specimens. Preliminary consideration was given to scaling coupon test specimen flaw geometry to better describe the full-scale response of a laminate flaws. The majority of literature describing scaling effects of composite materials converges to the conclusion that the Weibull approach to size effects and the statistical nature of fracture is valid as a first order treatment. [56; 57; 58; 59; 60] In general, Weibull scaling analysis is based on the so-called weakest link theory which describes a phenomenon where, with increasing material volume, the population of defects increases, and therefore, the probability of a failure from a flaw becomes more likely. This is expressed mechanically by a lowering of fracture strength with increasing material volume. Assuming the same probability of survival between small and large-scale composites, the ratio between fracture strengths can be found with the following expression:

$$\frac{\sigma_1}{\sigma_2} = \left(\frac{V_2}{V_1}\right)^{\frac{1}{m}} \tag{21}$$

where $\sigma_{1,2}$ are the fracture strengths, $V_{1,2}$ are the volumes and m is the Weibull moduli. [61]

Research conducted on glass/epoxy uni-axial laminate test specimen without flaws has shown a typical Weibull modulus of 29.1. [60] It is apparent from this literature investigation that application of results from coupon level testing, to full scale projections, will need to consider scaling effects. The question arises how the flaws found in thick, as-built sections should be scaled for introduction into the smaller coupon level specimen at the onset of a testing program. The theory behind the weakest link phenomenon should still be applicable. Therefore, it was concluded that the flaws themselves would be scaled volumetrically by the same volumetric ratio between the coupons and as-built blade sections.

Review of the blade section images showed that OP wave flaws were found in laminates that had an average thickness of 2.8cm. This is only considering the layup that contained the flaw. Other features which may have contributed to the overall sectional thickness such as gel coats, core material and non-unidirectional plies that capped the uni-axial layers were not considered. The standard deviation of the thickness data set is 0.139cm (~10%), therefore one can conclude the average thickness value is adequate. Comparisons were made between the coupons and as-manufacture sections, utilizing the same length (coupon gauge length) and unit width. The 4-ply laminate test specimen have a thickness of ~3.2mm, which is 8.8 times smaller (volumetrically) than actual as-built blade sections. Using the volume fraction and a modulus of 29.1 in Equation 21, the Weibull scaling expression, it was found that the fracture strength for the larger as-built blade sections was expected to be approximately 7.1% less than the coupons.

In order to scale the as-built flaw waveforms, the mathematical description of each wave was integrated over the half wavelength to calculate the cross-sectional area bounded by each OP flaw curve. This was the only parameter needed as unit width was considered. The volumetric ratio between the full scale blade sections and our test specimen, was then applied to the as-built flaw cross sectional area. Knowing the scaled cross sectional area, the amplitude and wavelength of each wave was solved for. This analysis is appropriate for the out-of-plane waves only. The in-plane waves do not vary with thickness, and therefore, a volumetric scaling approach was not taken. Instead, each was scaled by the same ratio in order to fit within the coupon dimensions. The scaled wave forms are shown in Table 7 it was the scaled waves that were built into the coupons for Round 1 testing.

Table 7: Scaled wave form designations for testing.

| **OP Wave 1**, mm | **As-Built** | **Scaled** | **IP Wave 1**, mm | **As-Built** | **Scaled** |
|---|---|---|---|---|---|
| Max Amplitude | 8.5 | 2.9 | Mean Amplitude | 3.7 | 1.85 |
| Mean Wave Length | 67.4 | 22.8 | Mean Wave Length | 47.5 | 23.75 |
| Angle, deg | 34.9 | 36.8 | Angle , deg | 24.8 | 24.8 |
| **OP Wave 2A,** mm | **As-Built** | **Scaled** | **IP Wave 2**, mm | **As-Built** | **Scaled** |
| Mean Amplitude | 1.9 | 0.7 | 99% Amplitude | 9 | 4.5 |
| Min Wavelength | 15.8 | 5.4 | Mean Wavelength | 47.5 | 23.75 |
| Angle, deg | 34.99 | 34.8 | Angle, deg | 48.9 | 48.9 |
| **OP Wave 4,** mm | **As-Built** | **Scaled** | **IP Wave 3**, mm | **As-Built** | **Scaled** |
| Mean Amplitude | 1.9 | 0.7 | Mean Amplitude | 3.7 | 1.85 |
| Mean Wave Length | 67.4 | 22.8 | 10% Wave Length | 20 | 10 |
| Angle, deg | 9.7 | 9.4 | Angle, deg | 47.8 | 47.8 |

Round 2 Test Program

Review of Round 1 testing exposed gaps in the data, including there were no fiber angles between 0 and 15deg, and porosity values of only <2%. Moreover, some of the results, in particular from the out-of-plane waves were considered to be dubious. Therefore, a more comprehensive testing effort was undertaken and techniques that were developed to characterize the as-built flaw geometry showed that it is possible to completely characterize an as-built defect after manufacturing. With this in mind, Round 2 targeted a wider range of defect variables that are detailed in Table 8

Table 8: Round 2 test matrix

| Flaw Type | Test Type | Flaw Magnitudes | # of Tests |
|---|---|---|---|
| In-Plane Wave | Compression | 11-29 deg | 14 |
| In-Plane Wave | Tension | 11-36 deg | 12 |
| Out-of-Plane Waves | Tension | 4-26 deg | 13 |
| Porosity | Compression | 1-8% | 10 |
| Porosity | Tension | 1-8% | 13 |

Round 3 Test Program

Testing for Rounds 1 and 2 were completed on 4-layer, unidirectional glass laminates only. While this data provided a foundation for defect assessment and model validation, it was necessary to develop a bridge from this data to more complex composite architectures. In particular, the Round 3 test program was designed to address three test groups: more complicated flaw forms, flaws triax laminates and flaws in carbon uni-axial laminates.

## Materials & Methods

Materials and Processing

In all test cases, laminates were infused utilizing a Vacuum Assisted Resin Transfer Molding (VARTM) process with one layer of peel-ply on the top and bottom surfaces. There was one layer of flow medium on the top surface of the laminate, except where noted in the manufacturing procedures above. Mostly uni-directional PPG-Devold 1250 gram-per-square-meter E-glass was used with a Hexion RIM 135 resin system in all cases. Laminates were manufactured with all fibers in the 0° direction with the exception of the Multi-Angle testing which had fiber directions of [0°,+45°,-45°,0°]. [10] The cure profile for each panel was 48 hours at room temperature followed by 8 hours at 70°C. The nominal fiber volume fraction of the panels was 55%, with a nominal thickness of 0.8 mm for each layer.

Test coupons were cut from the panels for use in tension and compression testing. Tensile coupons were cut to approximately 50 mm wide by 200 mm long and were tabbed, which resulted in a gage length of 100 mm. Compression coupons were cut to approximately 25 mm wide by 150 mm, with an anticipated gage length of 25 or 38 mm, where the wavelengths were greater than 25 mm.

In-plane (IP) waves are formed manually, one ply at a time. The first step in the method of forming IP waves is to lay the fabric over a piece of polyethylene tubing, oriented transverse to the 0° fiber angles, in order to form a wave of approximately the desired amplitude and wavelength out-of-plane with the fabric. This is accomplished by pressing the ply gently over the tubing by hand, using only enough force to cause the tows to form around the tube. To ensure fiber integrity, this must be performed slowly due to the stiffness of the tows. Next, steel bars are placed on either side of the tubing to act as an anchor for the fabric when the hose is removed (Figure 40). Holding these steel bars in place by hand, the hose is then unclamped and removed (Figure 41). It is essential that the steel bars remain in place to constrain the wave through the entire process.

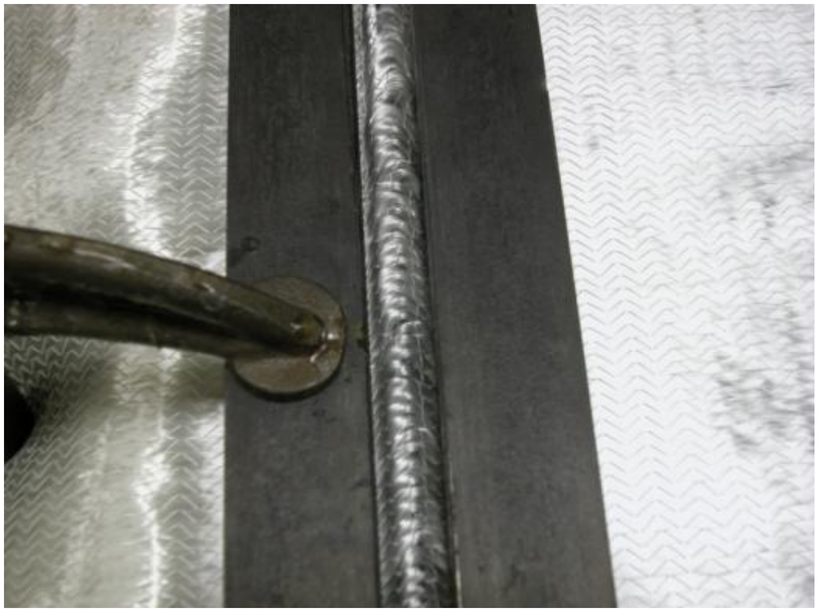
Figure 40: Fabric over polyethylene tubing constrained by steel bars.


Figure 41: After the tubing is removed, the wave is depressed into an in plane wave.

Once the polyethylene tubing is removed, the process of transforming the as-formed out-of-plane wave into an in-plane wave begins. First, the waves are manually pressed over, or essentially rotated to lay at approximately 45° to their initial out of plane orientation. Then the steel bars are removed and placed at a distance apart on the work table, such that the fabric layer is laid between them, so as to use them as end constraints for the tows (Figure 42). The partially formed waves are then manipulated further by hand, with care taken to keep the peaks of the waves aligned transversely to the 0° fiber angle, and to prevent fiber wrinkling. Once the wave form has the approximate desired dimensions, the fabric is covered with glass, while still remaining constrained by the steel bars (Figure 43). The purpose of the glass is twofold: first, the weight added friction between the fabric and the work table so that the wave form will remain as prepared for the time required to allow the tows to relax into the new form. Second, measurements can be made through the glass to get a rough estimate of the off axis fiber angle in the wave. The fabric must rest in this configuration for at least two hours allowing stresses in the fibers to be relieved. Once this is complete, the plies are stacked on the mold for the standard vacuum assisted resin injection process.

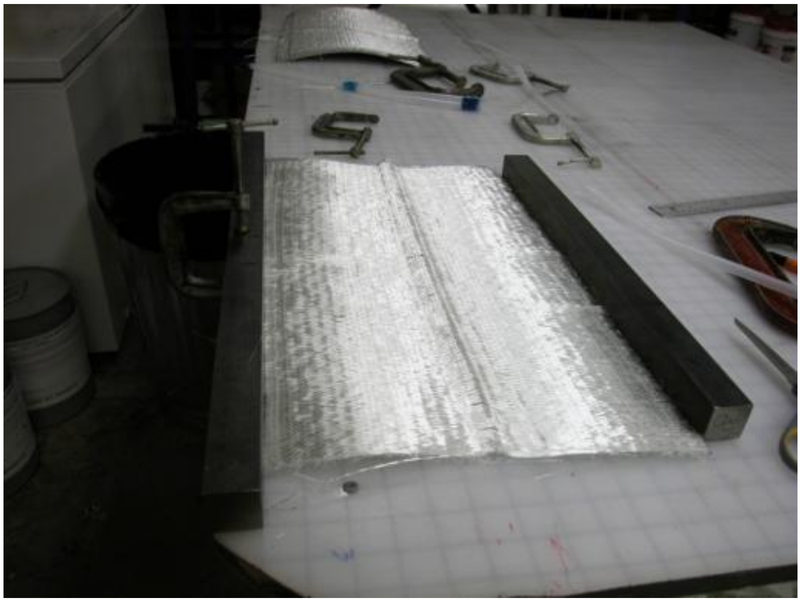

Figure 42: Partially formed wave constrained between steel bars.

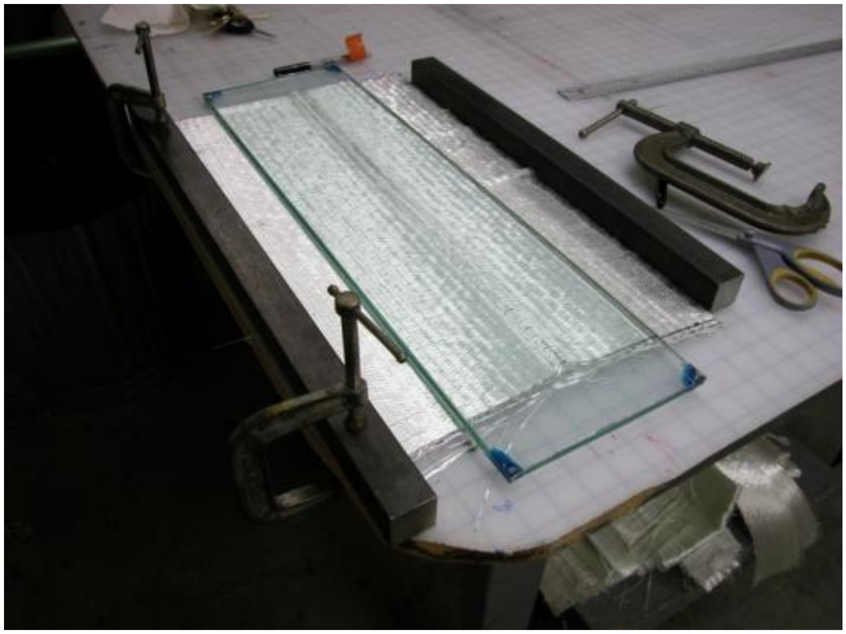

Figure 43: Finished wave relaxing under glass ready to be measured.

The first step in building a plate with OP waves, is to secure the bottom layer of peel ply to the mold tool, to ensure it does not shift during the infusion process. A form for the out-of-plane wave is then constructed using individual fiber tows. The fiber tows used for the wave build-up are cut to the width of the laminate. The wave build-up is created by stacking fiber toes in a pyramid fashion, perpendicular to the zero degree laminate orientation, until the desired amplitude and wave length values are approximately reached (Figure 44). The out-of-plane wave sections are then placed onto the secured peel ply, perpendicular to the direction of resin flow, and to the orientation of the laminate fiber toes.

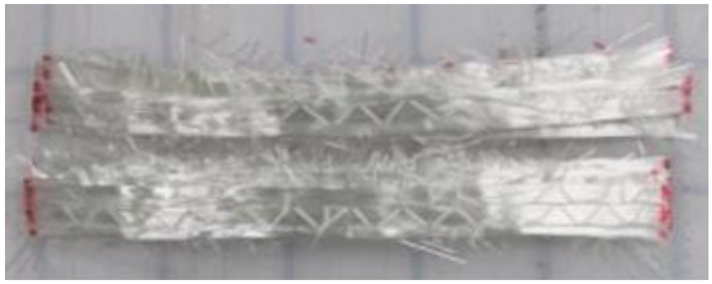

a) Chopped Wave Perturbation Tows

b) Chopped Tows as Implemented for Creation of Out-Of –Plane Waves

Figure 44: Fiber tow sections used to build Out-of-Plane waveforms

Layers of fiberglass sheets are then placed on top of the mold, while ensuring that the out of plane wave build-ups do not shift and remain perpendicular to the fiber direction. The build-up is completed by securing the top layer of peel ply and flow media. Once a vacuum is pulled, the out of plane wave buildups are rolled to ensure no air pockets or voids had formed. Infusion is then completed using a VARTM method (Figure 45).

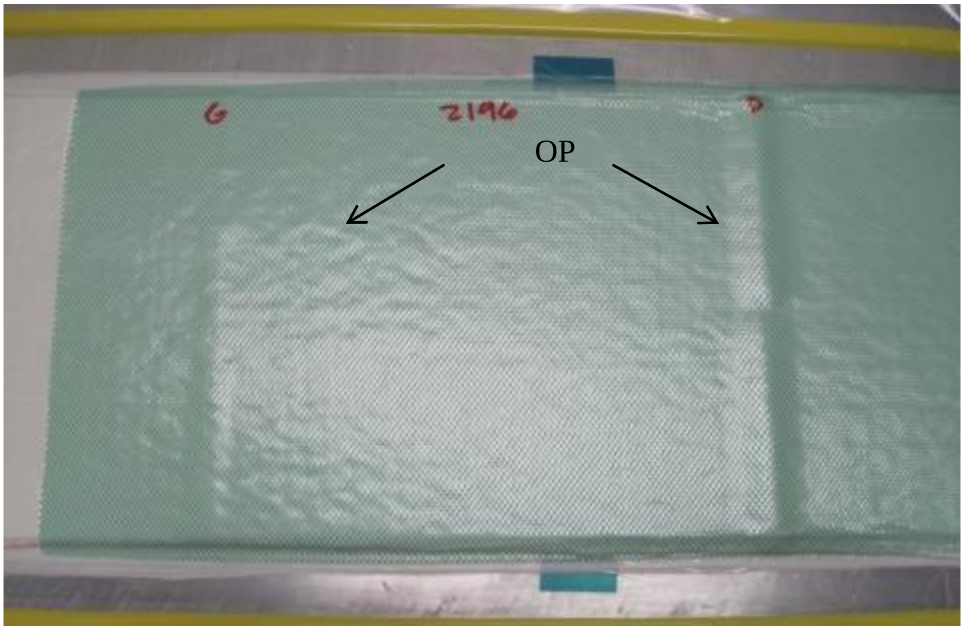


Figure 45: Plate under vacuum with OP waves

A simple, yet effective, manufacturing process was developed for inducing porosity, by introducing air into the plate while injecting resin. This method employs a "double bagging" technique which involves creating a 5.1cm square grid of holes in the first bag and then sealing that with a second bag. As can be seen in Figure 46, the second bag also has an inlet hose for letting air into the bag.

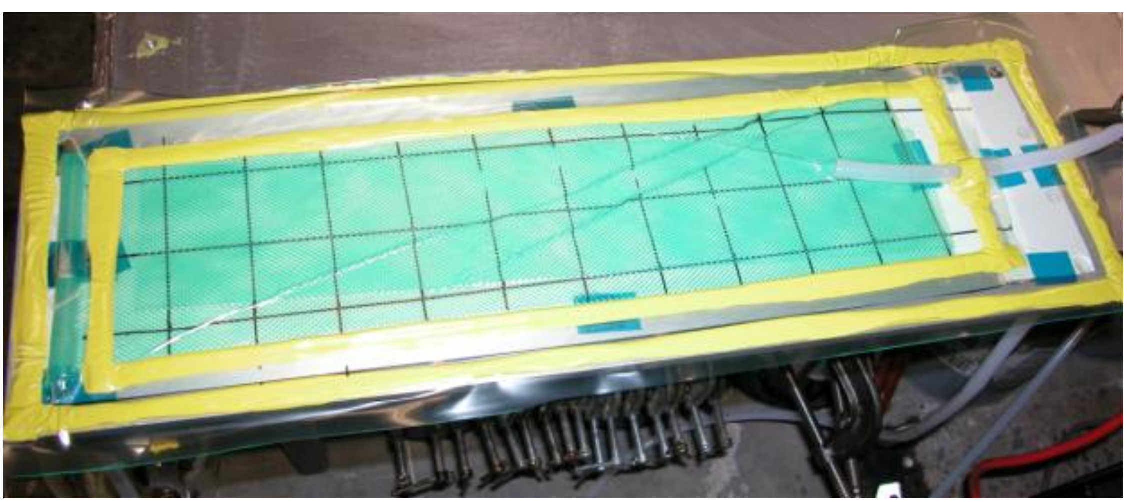

Figure 46: Double bagging with 5.1cm x 5.1cm grid of holes in first bag.

Trials with this approach have found that opening the inlet hose after the plate is infused results in low porosity contents. Higher porosity levels are achieved by allowing air to leak in slowly through the inlet hose during the entire infusion process. In short, when air is introduced during the infusion process, air becomes encapsulated in the laminate resulting in a porous laminate.

### Defect Characterization

Manufacturing defects, as well as in service damage, can be hard to detect in composite structures, particularly if the flaw is subsurface. Destructive inspection procedures have their use in laboratory and forensics studies. However, as the name suggests, the part is no longer useable after the inspection procedure. Therefore, the use of non-destructive evaluation (NDE) is growing throughout the industry. There are several NDE techniques used in detecting defects in composite structures. The most commonly used techniques are visual, audio sonic (coin tapping), radiography, ultrasonics, and mechanical impedance testing. [62; 63] The Blade Reliability Collaborative continues to be engaged in evaluating these and other technologies such as shearography and thermography, for their applicability to wind turbine blades. One technology that can be extremely useful in the laboratory is Computed Tomography (CT) scanning. Unfortunately, CT scanning is not feasible for extremely large-scale objects such as whole wind turbine blades.

In CT a series of x-rays are taken of an object as it, or the scanner revolves 360 degrees. The images are then combined to form a three dimensional radiograph. This technology is predominately employed in the medical field but does have some limited application in industry. A medical imaging CT scanner (Figure 47-Left) was used successfully on the test specimen in this investigation. Three-dimensional renderings of test specimen, allow for precise measurement of the actual flaw geometry introduced into the coupons. Accurate measurement of the introduced flaw is of critical importance in developing analytical/empirical damage correlations.

Figure 47: Image of CT scanner (Left) Coupon with IP wave highlighted (Right)

Figure 47-Right shows an example of a coupon with a manufactured in-plane flaw. This wave can be measured on the surface, but there is no guarantee that the subsurface layers contain a flaw with the same geometry. In this particular case, they did not. Figure 48-Left shows a through thickness, layer-by-layer radiographs which clearly indicate that there were multiple wave forms within the four different laminate layers. The waves can easily be measured with the software interface. The same process can be utilized to measure out-of-plane waves. An example of one of these is shown in Figure 48.

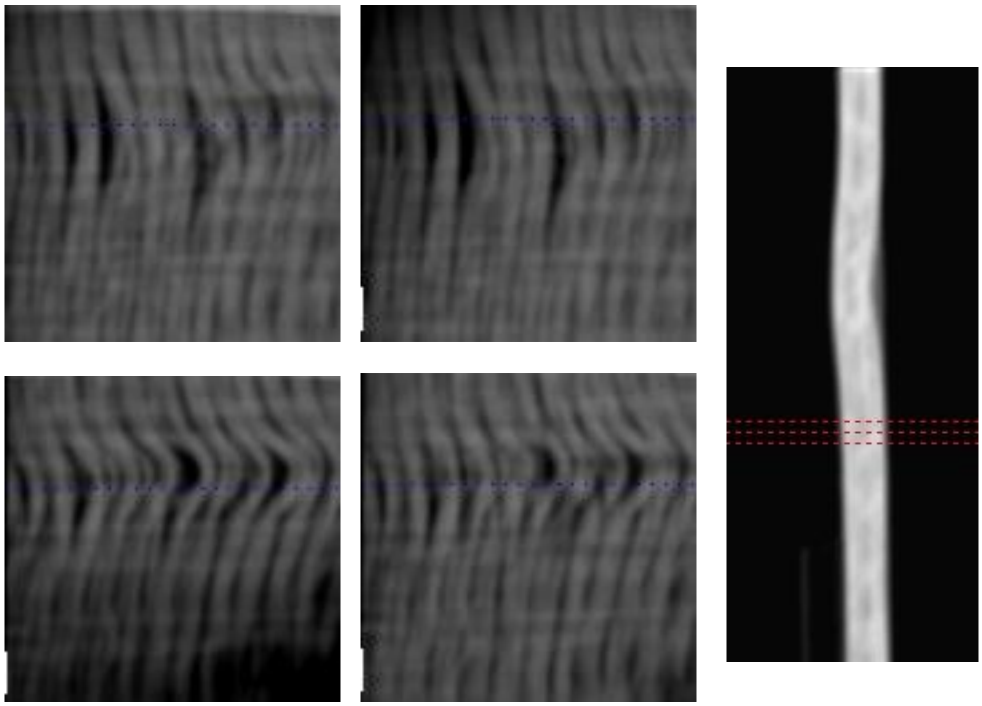

Figure 48: IP wave layer by layer radiograph (Left), OP wave radiograph (Right)

This analysis was carried out on all wave specimen. For the case of IP waves each layers' off axis fiber angle was recorded. An example of the layer by layer variation in fiber angle is given in Figure 49. Once testing of the IP wave samples was completed, the results were reviewed for correlation to the maximum and average, through thickness wave angle. The analysis revealed very similar correlations traits. The average wave angle proved to have a slightly better correlation and was therefore used as the characteristic parameter to describe as-built flaw magnitudes.

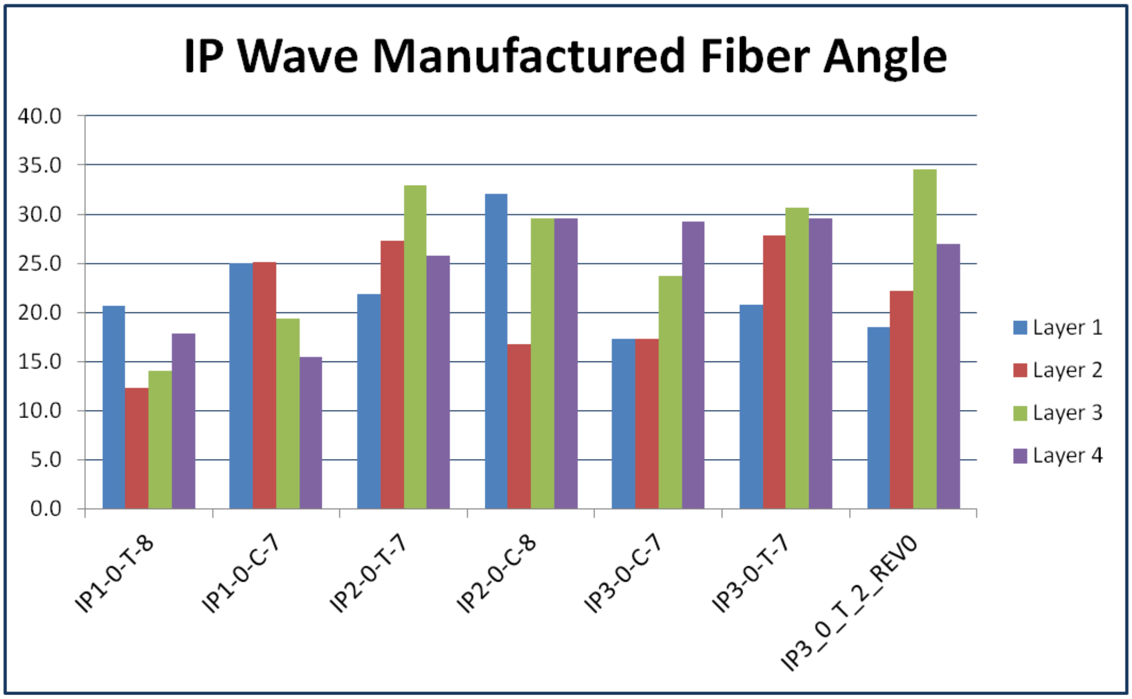


Figure 49: Example of layer by layer characterization

Characterization of porosity content in composites materials is particularly troublesome in large composite parts. It is not uncommon for wind turbine blade manufacturers to be unsure of the porosity content in their blades. Even at the laboratory scale, evaluation of porosity content is labor intensive and time consuming. The method employed by the Montana State University Composites Group with the most success is microscopy. For this process specimen were cut into small pieces, mounted in acrylic resin and then polished. Depending on the size of the voids either an optical or Scanning Electron Microscope (SEM) was used to take digital images of the cut surface plane. Image processing techniques were used to remove the background image such that only the gas inclusions are left. The image is converted to binary which allows for pixel counting of the white porosity areas and the black background. From this image a planar area fraction of porosity content is established. This value is then extrapolated to percent porosity by volume. An image taken by a scanning electron microscope on a specimen with induced porosity is shown in Figure 50.

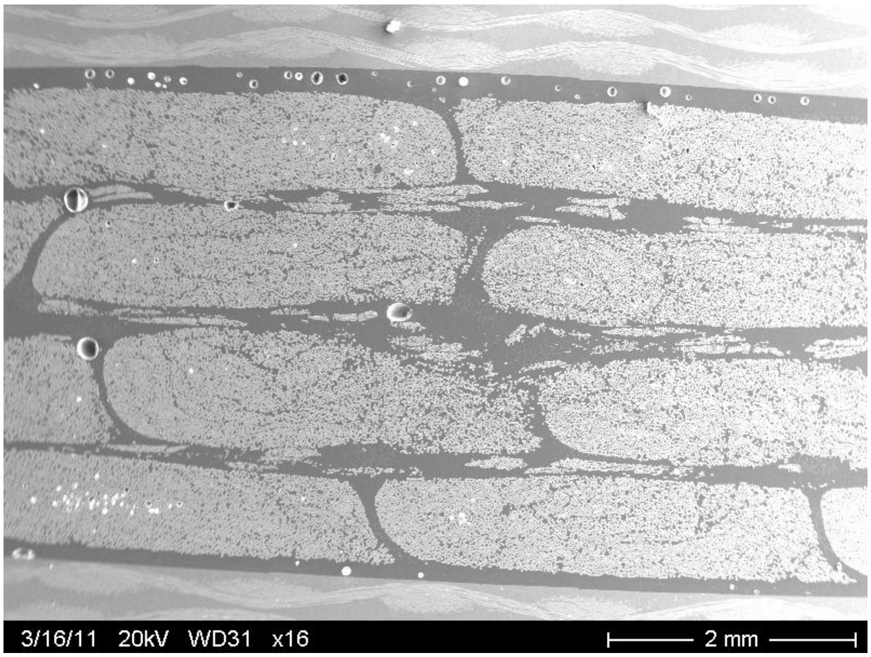


Figure 50: SEM Images of a porosity test specimen.

A novel method for characterizing porosity in composite laminate plates was attempted. Preliminary results showed that there was a good correlation between radiodensity and percent porosity by matrix volume (Figure 51). Radiodensity is a measure of the linear attenuation of X-rays, and is related to both the density and atomic number of a material. Measuring radiodensity is quick and easy with an X-ray machine and as these devices become more portable, this technique may prove to be an inexpensive and efficient way to evaluate porosity in the field and on the manufacturers floor.

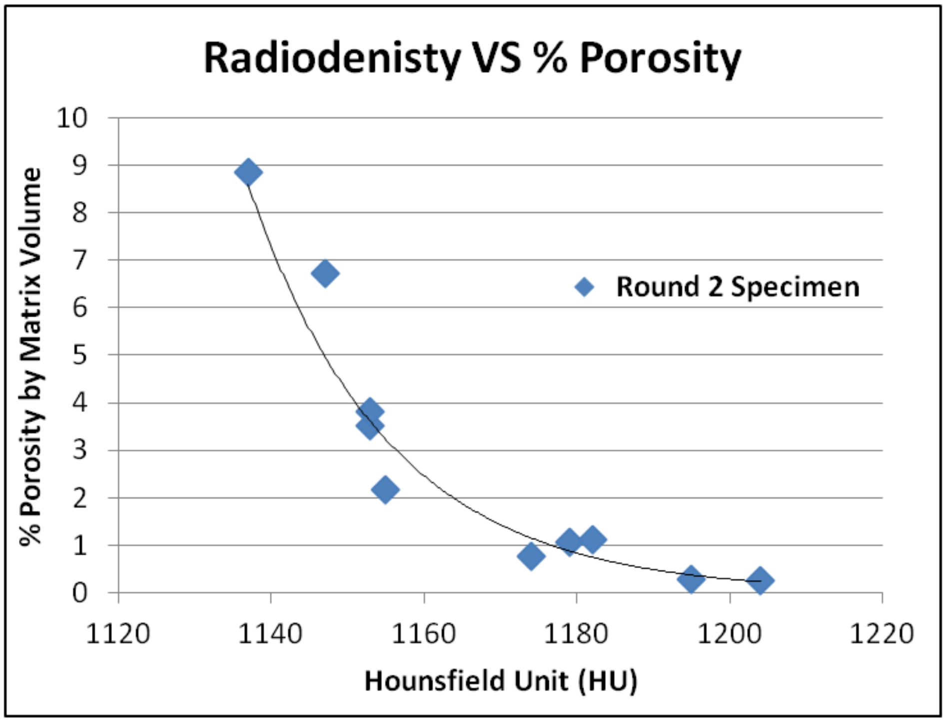


Figure 51: Correlation between porosity and radiodensity

The Hounsfield Scale is a quantitative scale for describing the linear attenuation of X-rays through a material. By definition, distilled water and air at standard atmospheric pressure and temperature have values of 0 and -1000 Hounsfield Units [HU] respectfully. The CT scanner can measure the attenuation of the scanned material and calculate the radiodensity in relationship to air and water using the following equation:

$$HU = \frac{\mu_x - \mu_{water}}{\mu_{water} - \mu_{air}} \times 1000 \qquad \textbf{(22)}$$

where $\mu_x$, $\mu_{water}$ and $\mu_{air}$ are the linear attenuation coefficients for the material under inspection, distilled water and air respectively. This analysis was repeated by another member of the MSUCG team without achieving convincing results. It was concluded that the process is not repeatable and subject to the discretion of the investigator to chose the region being inspected. However, the technique does have promise. For this reason, it was not used to characterize the test specimen used throughout the Effects of Defects investigations. Future efforts should utilize a CT scanner with better resolution such as the micro-CT scanner located in the Montana State University Snow Sciences research laboratory.

In-Plane Static Test Method

Coupons were constructed with representative blade materials and construction processes, though scale was reduced. Scaling was required to achieve compatibility with the Instron 8802 250 kN testing machine and grip capacity (Figure 52). Static ramp tests on the specimens were conducted at a rate of 0.05 mm/s in tension and 0.45 mm/s in compression for all 4-ply coupon and Multi-Angle laminates. Typical of the Montana State University Composites Group (MSUCG), these tensile tests were performed based on the ASTM D 3039 tensile testing of composites standard. [64] This simple test can be used to find the ultimate tensile strength and strain, tensile modulus, Poisson's ratio and transition strain. Likewise, compression testing is more loosely based on ASTM D 3410 and D 6641. [65; 66] Properties that may be derived include ultimate compressive strength and strain, compressive modulus and Poisson's ratio in compression.

Failure within composite materials commonly occurs as the result of delamination. Significant work to understand the strain energy release rates has been performed. Delamination was added to the other defects (IP waves, OP waves and porosity) for testing and analysis in Round 2. With data on delaminations, calculations to determine crack propagation can be performed. This information was predominantly used by J.

Nelson for progressive damage modeling. However, it is also a key aspect in a damage tolerance methodology.

Figure 52: Representative failed coupons in machine grips.

## Results & Discussion

### Uniaxial Tension Compression

It is the goal of this program, to be able to accurately predict the Effects of Defects in thicker laminates, such as those found in wind turbine blades. However testing of thick laminates for model validation is resource intensive; therefore, only a small number of larger scale tests were performed. The purpose of these larger tests was to validate the extrapolation of models developed on thinner laminates to larger ones. The need for generating a comprehensive material properties dataset, coupled with improvements in manufacturing techniques, provided the impetus for continued thin-laminate testing. These provide data at a much wider range of the key variables for each flaw type, allowing for more insightful analyses to be performed. In addition, these data were utilized to provide load-displacement and stress-strain curves. These were of particular use in correlating to analytical models.

Analysis of the results showed that strength degradation in laminates with waves tend to correlate slightly better to the average fiber angle of all layers rather than the maximum fiber angle. Figure 53 and Figure 54 display the results of failure stress verses average fiber angle for IP and OP wave respectively. Results from compression of OP waves is not being presented as they are still under investigation. However, the data on static strength reduction for OP waves in compression was implemented in the reliability analysis as  a place holder. No conclusions have been drawn relating to the reliability of a structure with OP waves specifically. An OP wave embedded in a planar structure under compression is inherently an eccentricity, and is therefore subject to buckling predominately. While buckling is a common mode of failure in a wind turbine blade, buckling is driven in large part by the global structure and local geometry. With this in mind, care must be given to ensure that the failure data, from a material standpoint, is completely understood.

In analysis of the effects of porosity on laminates, it is necessary to consider the variations in the fiber volume ratio. As porosity increases, one of two things must happen as a direct function of encapsulated gases: the volume of the part must grow (typical for vacuum bag manufacturing) or, should the total volume remain the same, (typical of hard/hard mold manufacturing), there must be a reduction of resin content. Either case will cause variations in the fiber volume ratio. Test specimens in the investigation have been manufactured using a vacuum bag technique, therefore it is necessary to include volume effects. A simple method for comparing results in this case is to normalize the failure stresses to 55% fiber volume ratio, $V_f$. Figure 55 shows a comparison between porosity content and the reduced strength.

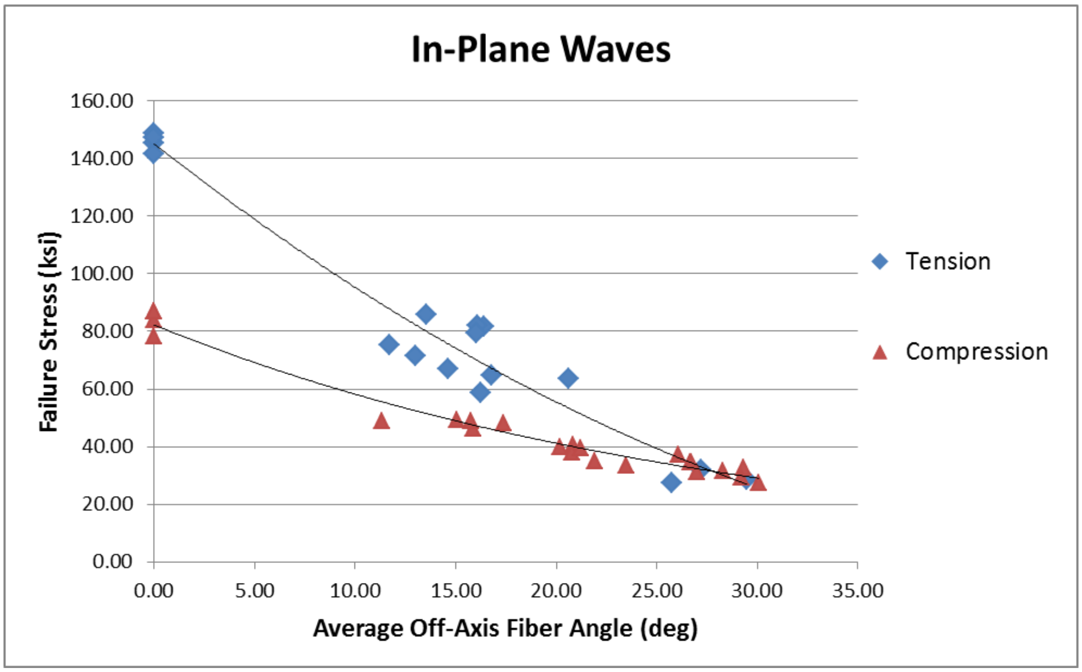


Figure 53: Peak Stress of IP Waves at various fiber angles.

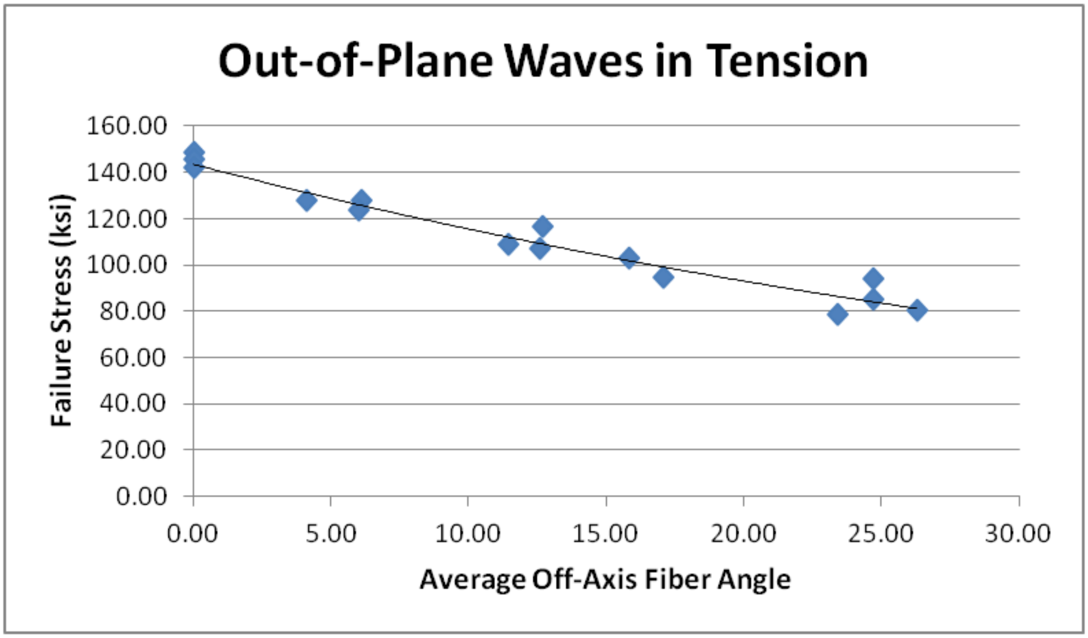


Figure 54: Peak Stress of OP Waves at various fiber angles.

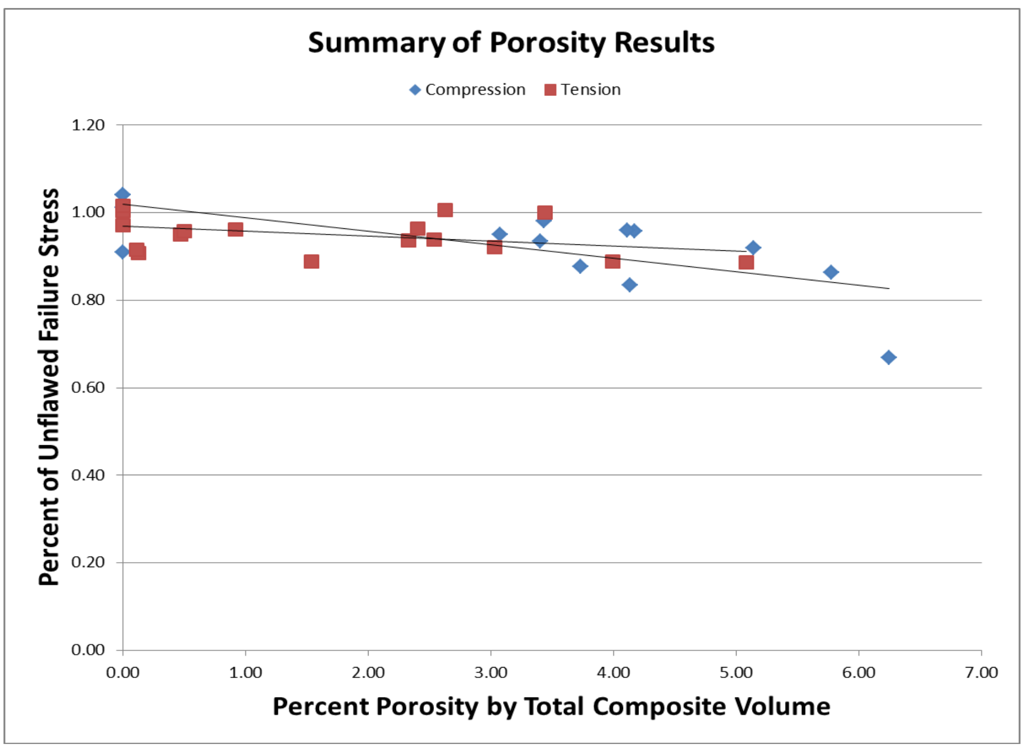


Figure 55: Reduction in Strength due to porosity.

The data in Figure 55 report the as-measured experimental data from mechanical tests. The void content was determined by image analysis of specimens from the same plates which were used for the test coupons. The void data are presented as a function of void content in the composite. Some discussion on the micromechanics of voids in the composite is warranted. The influence of voids on the mechanical properties has the effect of reducing the bulk modulus of the resin. While this does not have as great of an effect in tension, the reduced modulus has a significant effect for compression strength as the reduced modulus does not support the fibers in compression as well as a stiffer matrix.

The first model for resin modulus reduction might be based on the rule of mixtures:

$$E_m' = E_m (1-V_v) \tag{23}$$

where $E_m'$ is the reduced matrix modulus of elasticity, $E_m$ is the modulus of elasticity of the matrix without voids, and $V_v$ is the void volume fraction. However, a void, modeled as a spherical inclusion, reduces the matrix modulus of elasticity to a greater extent, than would be predicted by simple rule of mixtures because of the local strain concentrations from the spherical void geometry. [67; 68; 69] Additional studies, outside the scope of this report, may be necessary to apply these data to other material systems to predict the influence of void content on mechanical properties.

The results of this testing effort have been considered in large part, to be a success. In particular, a comparison was made with a study on compression of fiberglass composites containing porosity, performed by BRC member TPI Composites. [70] Both the TPI and MSUCG data sets are depicted in Figure 56, where strong correlations between the two can been seen. In general, correlation of ultimate strength to flaw characterization parameters, exhibit trends describable through regression with values for coefficient of determination greater than 0.9. Moreover, model predictions of load displacement curves are expected to be accurate to within ±5%.

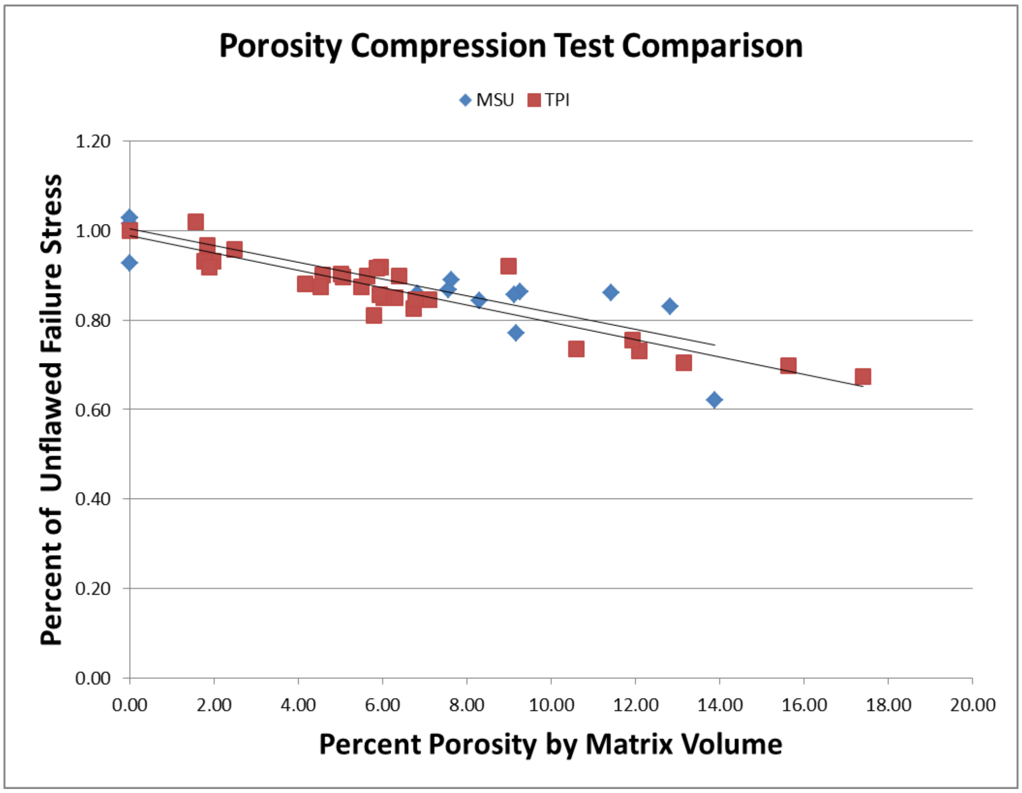


Figure 56: Comparison of porosity testing

The following table lists the empirically derived equations for flaw knockdown factors. Included with equation is an estimate of the models' goodness-of-fit and variability using standard least squares regression.

Table 9: Summary of flaw knockdown equations for uni-axial glass coupons

| Flaw Type | Tension/ Compression | KD Equation (% of unflawed strength) | Goodness of Fit ($R^2$) |
|---|---|---|---|
| IP | Tension | $-0.24 + 177.35e^{-3.46*\alpha} * (\sin\left(\frac{2\pi\alpha}{96.67} + 12.65\right))^2$ | 0.95 |
| | Compression | $0.9782e^{-0.035\alpha}$ | 0.97 |
| OP | Tension | $143.5e^{-0.022\alpha}$ | 0.95 |
| Porosity | Tension | $-0.02394 * P + 0.931$ | 0.3 |
| | Compression | $-0.0309 * P + 1.02$ | 0.5 |

where α is average off axis fiber angel and P is the percent porosity by total volume.

Triax Laminate Tension Compression

A small data set was generated to addresses flaws in more complicated laminates. In order to better address the blade test, coupons were built with the same layup as the Effects Of Defects (EOD) blade test article. A faux triax was built by alternating uni-axial plies with double bias plies. Two new types of flaws were also examined; Chain and Proximity Waves. A Chain Wave is a defect that consists of three contiguous discrete waveforms which is more similar to the defects found in the field. A Proximity Wave consists of three discreet waveforms separated by a specified distance of one wavelength. Both flaw forms are shown in the following figure.

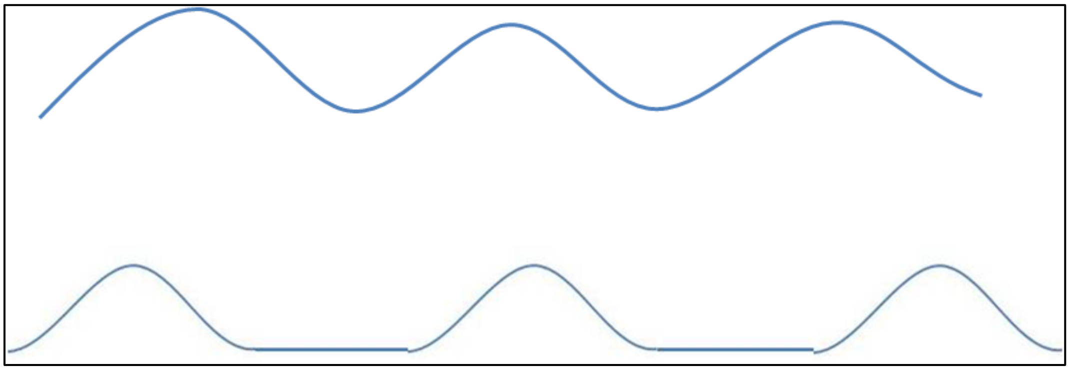

Figure 57: Chain wave (upper), proximity wave (lower)

The results of this testing effort are given in the following two figures. Figure 58 displays the results from all of the OP tensile testing performed with the glass triax layup. It may be seen that OP Proximity wave exhibits significant scatter in the ultimate strength response. Moreover, for a given wave angle it appears that proximity waves have a more severe affect on static strength. This is interesting to note, particularly because a FEA was performed on the coupon geometry predicting that at approximately one wave length of separation between the discrete wave forms, there was no additional strength reduction over one individual waveform. These samples were constructed with this geometry in mind. While the data has significant variation, it does seem clear that in comparison to a single OP wave the proximity case is more deleterious. No testing of these complex waveforms has been performed on uni-axial specimen for comparison.

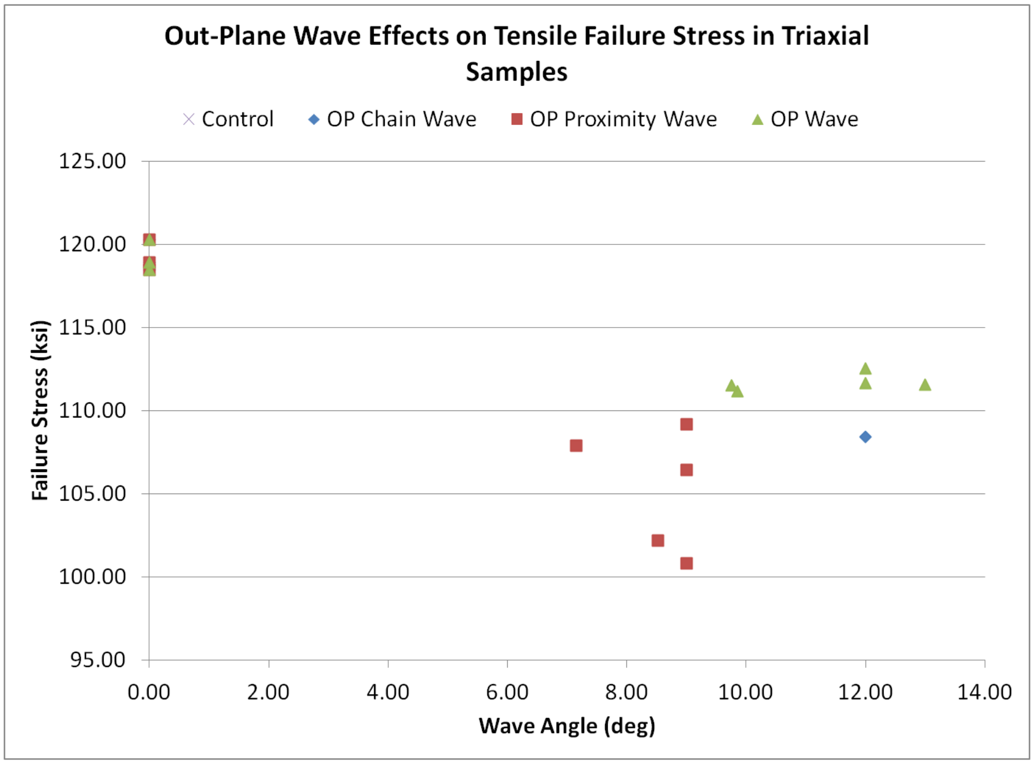


Figure 58: Glass triax tensile testing of Out-of-Plane waves

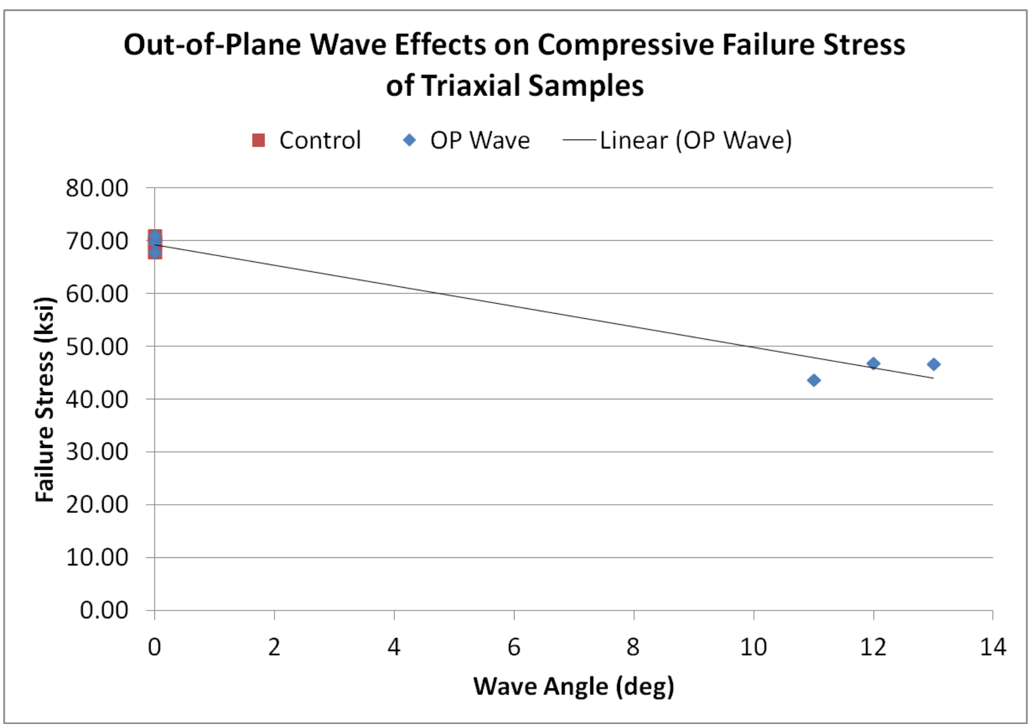


Figure 59: Glass triax compression testing of Out-of-Plane waves

Carbon Laminate Tension Compression

A small data set was generated to address flaws in the carbon spar EOD blade. This hybrid triax was built by alternating uni-axial carbon fiber plies with double bias glass fiber plies. Prior to this testing, it was deemed necessary that uni-axial carbon laminates with flaws, be tested for comparison to glass. Figure 60 displays the test results of uni-axial carbon fiber control and OP Wave specimen. The consistency of these results indicated that the testing was successful and that the results can be trusted. IP waves were not tested at this time, due to concern over the effect of using a pin fixture to create the wave forms.

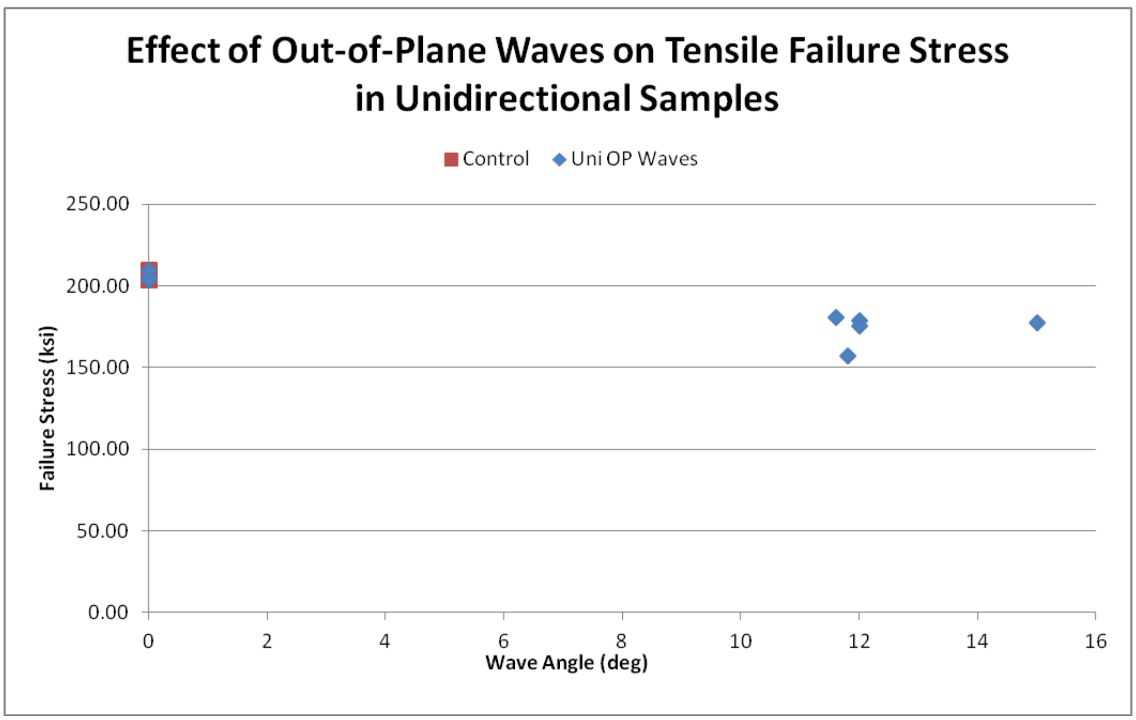


Figure 60: Carbon Uniaxial testing

Figure 61 displays the results of OP waves on the hybrid laminate. At first glance, one would have the impression that the wave type is almost insignificant, and that the effect of a particular wave angle on static strength is similar. However, there is significant scatter in the control data, leading to the conclusion that the results of this test effort are in need of further investigation.

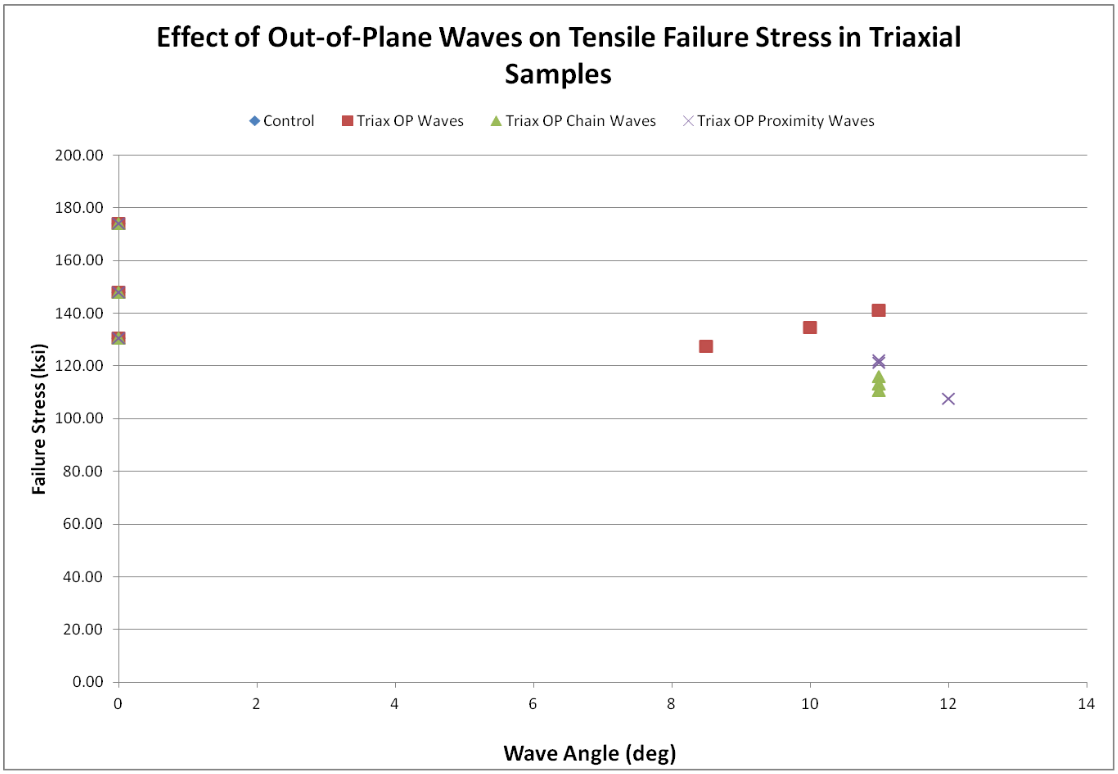

Figure 61: Carbon hybrid triax tensile testing of Out-of-Plane waves

Figure 62 displays the results for compression testing of OP Waves in the hybrid laminate. While limited, the data appears to be well grouped, suggesting consistent correlation between fiber angle and static strength. However, the control compression results, while describing minimum variation, are much lower than would be expected based on manufacture data and simple calculations. Therefore, it is recommended that the compression testing of the hybrid laminate be revisited.

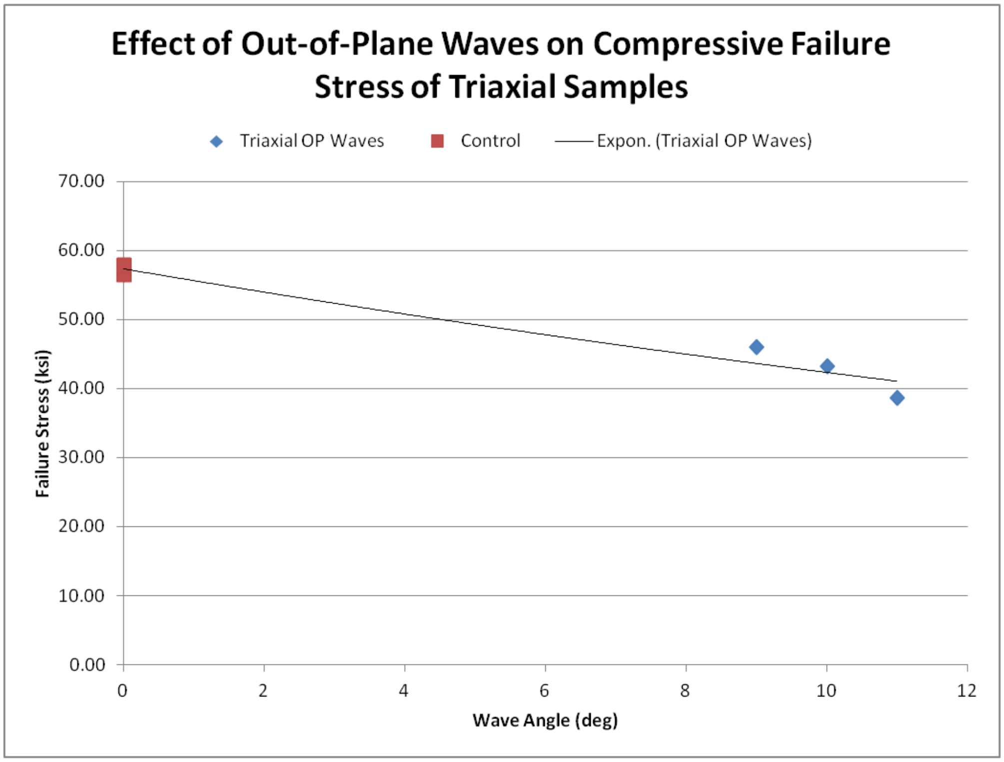


Figure 62: Carbon hybrid triax compression testing of Out-of-Plane waves

# CHAPTER 6

# STRUCTURAL RELIABILITY

## Reliability Analysis Introduction/Setup

The general approach to incorporating finite element analysis into a probabilistic reliability evaluation adheres to the following steps previously described in detail:

1. Build parametrically defined blade model
2. Define Random Variables (RV) and their distributions
3. Define outputs variables of interest
4. Define load scheme
5. Perform simulations
6. Extract relevant probabilistic output response data
7. Input data into reliability analysis

This methodology may be utilized for any application, however the specifics may vary according to the structure and objectives of the analysis. The following table lists in detail, the steps necessary to perform the analysis outlined in PReP for a wind blade application. In this table, a title for each step and task are given as well as a short description of the task. A similar format is used in the following sections to describe the origin of the data used in the analysis; as well as a qualitative designation of any assumptions made while using this data. Following each of the tables (

Table 11 through Table 16) are sections that detail the specific analytical approach for each step.

Table 10: Structural reliability analysis hierarchy

| Step # | Step Name | Description |
|---|---|---|
| **1** | **Analysis Article Set Up** | |
| 1.1 | Article Designation | Establish article of interest |
| 1.2 | Environmental Conditions | Wind speed distribution |
| 1.3 | Governing Article Parameters | Operational Parameters: Tip Speed, RPM, Operating Hours, Design Life |
| **2** | **Structural Analysis** | |
| 2.1 | Finite Element Model | 3-D Shell elements with as-built material properties and layup |
| 2.2 | Flaw Location Discretization | Selection of elements for nodal solution of mechanical response |
| 2.3 | Load Introduction | Uniform pressure distribution applied to HP side of blade |
| **3** | **Development of Failure Criteria** | |
| 3.1 | Fatigue Properties | ε-N Curve for specific R ratios |
| 3.2 | Constant Life Approximation | Piecewise Linear Approximation |
| 3.3 | Designation of Spectrum for Load Reversals | Standardized WISPER reversal spectrum for wind blade loading |
| 3.4 | Derivation of Total Fatigue Cycles | Based on operational parameters |
| **4** | **Flaw Data Implementation** | |
| 4.1 | Development of Flaw Distributions from data | Collected data on waves angles fit to Normal distribution w/non-zero mean. |
| 4.2 | Designation of simulated flaw distributions for comparative analysis | Analyst generated Normal distribution for waves & porosity w/zero mean and for porosity w/non-zero mean |
| 4.3 | Development flaw occurrence distribution | Spatial distribution describing the probably of a flaws existing by location |
| 4.4 | Treatment of flaw structural performance in fatigue | Modification to ε-N Curve single cycle intercept with knockdown factor based on flaw magnitude |
| **5** | **Model verification/tuning** | |
| 5.1 | Model Implementation | Structural model and fatigue failure criteria used on test article |
| 5.2 | Development of Baseline "Design" Case | Load application (pressure) tuned to elicit a blade failure at 20 years (without flaws) |
| **6** | **Probabilistic Analysis** | |
| 6.1 | Probability of Failure | Calculated for all locations for each analysis case. Compared to baseline to how conservatism |
| 6.2 | Time to Failure | Calculated for regions of interest (locations high Pf). |

Figure 63 illustrates the flow of information and interconnections of the various analysis components. Several of the steps identified in the previous table are notated by the corresponding step number on the figure. The following sections detail these steps, as well as the other assumptions necessary to perform the PReP analysis.

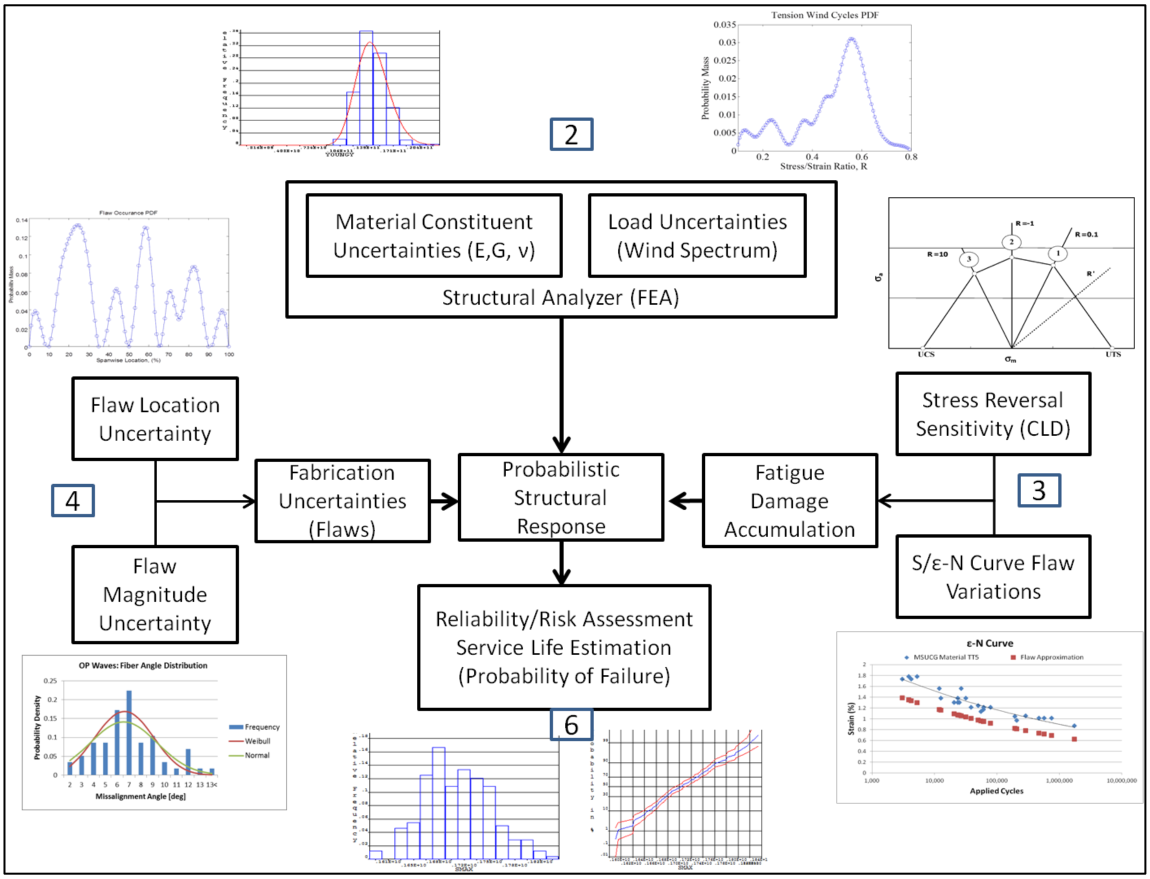

Figure 63: FEA and Risk Analysis Overview

Figure 63 consists of the core analysis necessary in PReP. As a reminder, the PReP framework is displayed again in Figure 64. The analysis elements described by Figure 63 constitute a significant the portion of Probabilistic Analysis block in Figure 64. These elements, which are necessary to estimate the probability of failure, are highlight by a red box.

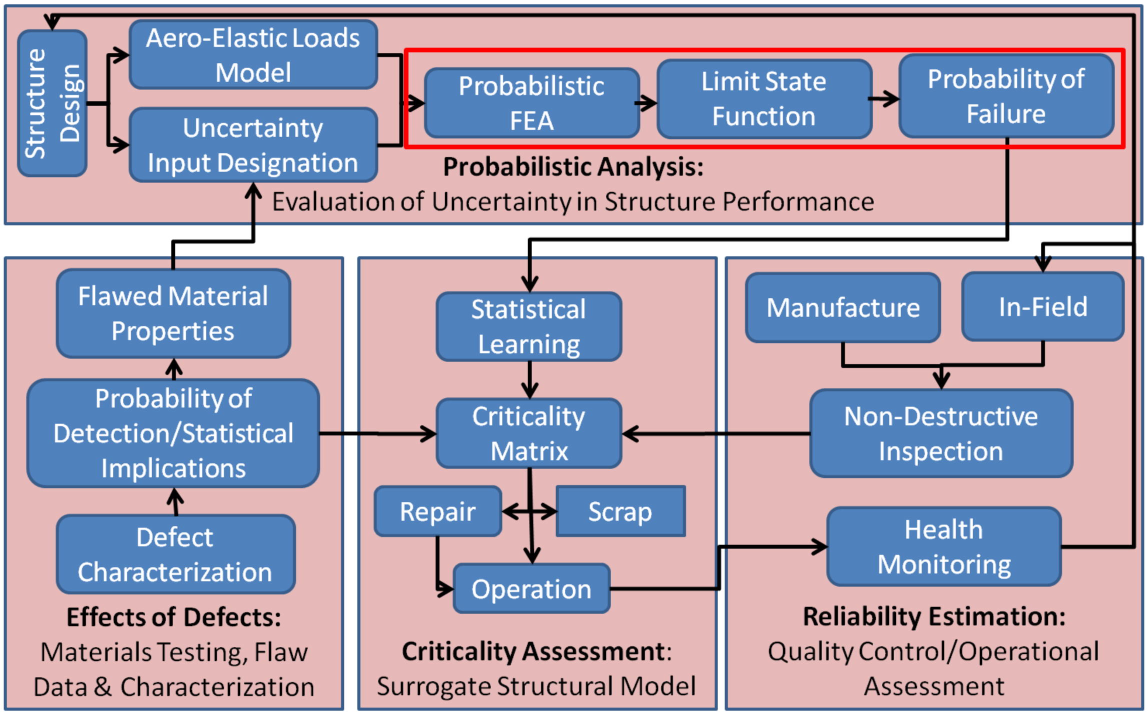


Figure 64: PReP framework for defect risk management and improved reliability

Step 1: Analysis Article Set Up

Table 11: Step 1 Overview

| Step # | Step Name | Origin of Data/Assumptions Used in Analysis | Level of Assumption Integrity |
|---|---|---|---|
| **1** | **Analysis Article Set Up** | | |
| 1.1 | Article Designation | Blade material and structural design provide by Sandia. Consistent with test article used for model implementation. | Very High |
| 1.2 | Environmental Conditions | Usage of Weibull distribution for wind speed, binning of speeds into 1m/s intervals for 18. | High |
| 1.3 | Governing Article Parameters | Values are chosen based on length of blade and generalized analysis | High |

Step 1.1 Article Designation. Since the PReP algorithm has been built so that any composites structure can be evaluated, the first step is to establish an article of interest. For the case of this investigation, the Effects of Defects blade was used. The EOD blade was built off of National Laboratories' 8.3m Blade Systems Design Study (BSDS) blade

platform. [71; 72] More discussion on the design of this blade is given in Chapter 7: Blade Testing.

Assumptions: The article designated for analysis represents the actual article of interest. Considering the fact that the article used in this numerical analysis is consistent with the actual test article of interest, the level of assumption integrity is very high (i.e. little error or discrepancy).

Step 1.2 Environmental Conditions. Wind blade analysis requires an understanding of the environment in which the blade will be placed. One of the most important features of a wind site is the wind speed distribution. Typically these inputs are derived from a standard class of wind sites. For the purpose of understanding the reliability analysis inputs, a custom Weibull distribution for wind speed was fit to a specific site data set. The resulting Weibull shape and scale parameters used in this analysis were; a=1.896, b=5.29. However, any distribution would work within the context of the self-consistent reliability analysis. Wind speeds were binned in eighteen, 1m/s intervals. Further discussion of the wind speed analysis is presented in Appendix B.

Assumptions: Weibull distributions are commonly used to describe wind speed variability. The data used in this analysis fit well with a Weibull distribution. However, the mean wind speed is not as high as a commercial wind site and therefore the level of assumption integrity was given a high rating rather than very high.

Step 1.3 Governing Article Parameters. For the wind blade analysis, the operational parameters necessary to perform a fatigue life calculation are operating hours and design life. Values chosen in this analysis for operating hours and design life are 4,000hrs/year and 20yrs respectively. Any values for these inputs could be chosen and utilized for comparative purposes successfully.

Assumptions: The governing article parameters are consistent with the blades design or expected operation. Specific data for correlating these parameters to the actual blade design were not available. Twenty years is considered a standard design lifetime in the wind blade industry and was used in this analysis. For comparative purposes, these values are adequate within a self-consistent analysis, therefore the level of assumption integrity is considered high.

Step 2 Structural Analysis

Table 12: Step 2 Overview

| Step # | Step Name | Origin of Data/Assumptions Used in Analysis | Level of Assumption Integrity |
|---|---|---|---|
| **2** | **Structural Analysis** | | |
| 2.1 | Finite Element Model | Model Generated in ANSYS from Sandia provided NUMAD code. Model is consistent with test article. | Very High |
| 2.2 | Flaw Location Discretization | Blade is divided into 100 approximately equal segments representing flaws approximately 8.3cm in length the full width of spar cap. For each flaw element group, only the max nodal strain in the material 1 direction (spanwise) is utilized for the failure analysis. | Very High |
| 2.3 | Load Introduction | Not a realistic loading scenario. However provides an adequate metric for comparing the traditional safety factor analysis to probabilistic techniques. | Low |
| 2.4 | Probabilistic Finite Element | Monte Carlo simulation of deterministic calculations has been shown to accurately describe the probabilistic response of a system with random variable inputs | Very High |

Step 2.1 Finite Element Model. Wind turbine blades are complex composite structures and one cannot properly assess the integrity of any portion without considering the global response and load share tendencies. It is well known that 2D shell elements used in 3D Finite Element models are required to capture information such as 3D distortions, stress concentrations and buckling strengths. Other methods such as Beam Property Extraction and 1D classical beam section analysis are widely used for preliminary calculations. [73] These techniques have been used by other investigators for probabilistic analysis of wind turbines. [74; 75] A full 3D finite element blade model was used in this analysis. The blade geometry was initially generated using Sandia's Numerical Manufacturing and Design tool (NuMAD). NuMAD allows the user to select from a library of standard blade airfoils and root geometries to build the global structural elements. Locations and geometry for the spar cap and shear web may also be established. Figure 65 displays an example of the NuMAD design space. Once the general blade shape has been designated, material properties can be applied from a library of commonly used composites laminates. NuMAD is then capable of generating an ANSYS input file. This file is read into ANSYS, generating the finite element model of the blade complete with materials properties (Figure 66). Layered 3-D Shell elements account for different lamina mechanical properties and thickness.

Assumption: The Finite Element Model is a good representation of the actual article of interest. The model was generated based on the EOD blade design, consistent with modeling techniques commonly used (3D, shell elements, etc). Strain values output from the model were nearly identical to as-measured strain on the test article, therefore this assumption integrity is considered very high.

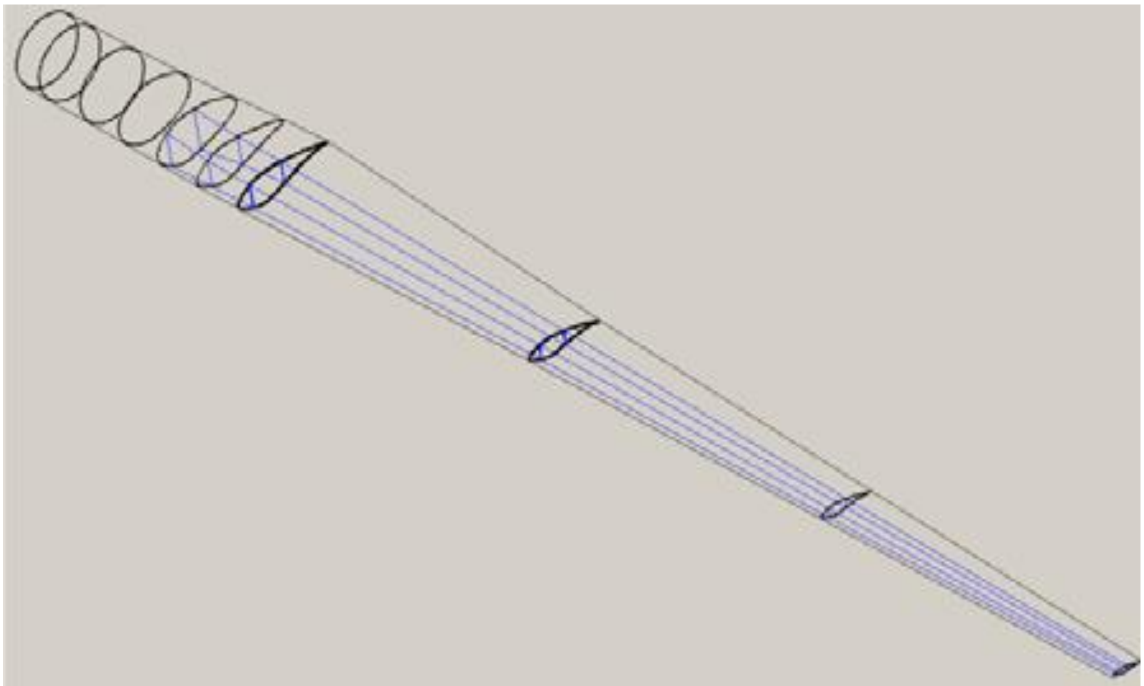

Figure 65: NuMAD feature visualization

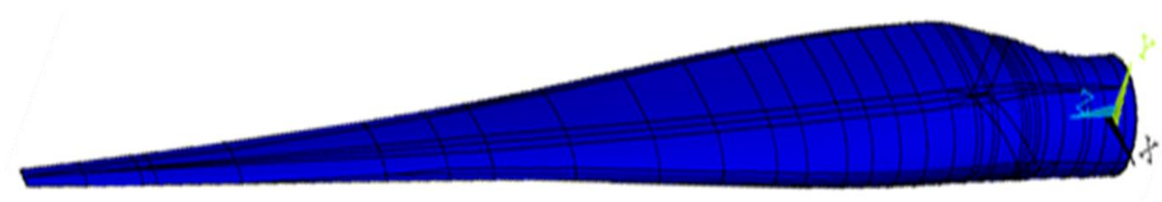

Figure 66: ANSYS FE model of the EOD blade

<u>Step 2.2 Flaw Location Discretization.</u> Flaws are represented in the FE model as a group of elements. For this analysis, the spar cap was the only structural component where flaws were modeled. The spar cap was divided into 100, approximately equal length, spanwise segments. Each segment consists of between 2 and 6 individual elements, depending on location and mesh density. These groups are nominally 8.3cm in

length and the full width of spar cap. A particular set of element groups is displayed in Figure 67. The FE analysis is run based on the load criteria set forth in the following section. For each flaw element group and load case, the maximum nodal strain in the material 1 direction (spanwise)  is fed into the failure analysis (post process). The mechanical response described by this FE solution is consistent with the body of test data concerning coupons with flaws. That is to say that the results describe tension and compression of the flawed region.

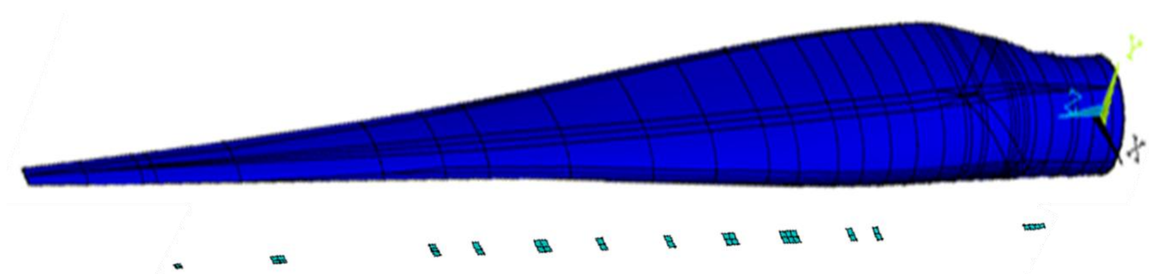

Figure 67: FE blade model and set of element groups which represent flaws

Assumption: Flaw discretization is of adequate fidelity and elements are located appropriately. The 8.3cm modeled flaw length is consistent with the laminate test specimen used in the Effects of Defects laboratory efforts. Modeled flaw widths are consistent with the as-built flaws in the EOD blade test article. Assumption integrity is considered to be very high.

Step 2.3 Load Introduction. In standard blade design, aeroelastic simulations are used to transform wind speeds into internal moment and forces along the blade span for use in the structural analysis. [9] This level of complexity was not necessary in this analysis it's purpose is to addresses the applicability of a reliability framework that focuses on probabilistic defect analysis. Therefore, a simple load case is just as effective as a more complicated analysis. Thus, a uniform pressure distribution was applied to the HP side of the blade. The magnitude of the pressure distribution corresponds to the wind speeds defined by the distribution in Step 1.2. Development of the correlation between wind speed and pressure magnitude will be discussed later in Step 5.2.

Assumption: The load introduced into the model is appropriate for the analysis. While this is not a realistic wind-loading scenario, it is perfectly adequate for comparing the traditional safety factor analysis to probabilistic techniques; therefore the assumption integrity is considered low. However, the PReP algorithm has the capacity to implement high fidelity loading scenarios, as deemed fit by the analyst.

<ins>Step 2.4 Probabilistic Finite Element Analysis.</ins> In addition to the defect specific uncertainty parameters discussed later, several material property variations ($E_{11}$, $E_{22}$, $\nu$) were incorporated into a Probabilistic Finite Element Analysis. These were evaluated in the ANSYS PDS using user defined distributions, and the ANSYS built-in Direct Monte Carlo numerical sampling procedure discussed in Chapter 2. The distributions are consistent with variations found in published data for glass fiber epoxy composites. The distribution inputs for $E_{11}$ (Figure 68) and $E_{22}$ were applied to the entire spar cap. In this figure the redline represents the prescribed lognormal function. Values were sampled continuously from the input distributions (red line in Figure 68). The histogram presented in Figure 68 show sampling frequencies of binned values from the Monte Carlo simulation.

Strain in the material 1 direction was recorded for each discrete analysis case of the MC simulation. Figure 69 shows a histogram of the resulting normalized strain distribution output from the MC solution for a particular flaw location. As each location had different nominal strain values, the data displayed in Figure 69 has been transformed from raw strain (ε), to show change in percent strain around the mean value. This distribution of strain values was relatively consistent down the length of the spar cap. The variation in strain was approximately ±0.03% (300με). Load was not varied for this analysis, the goal being to understand the effect of  material property variations on strain.

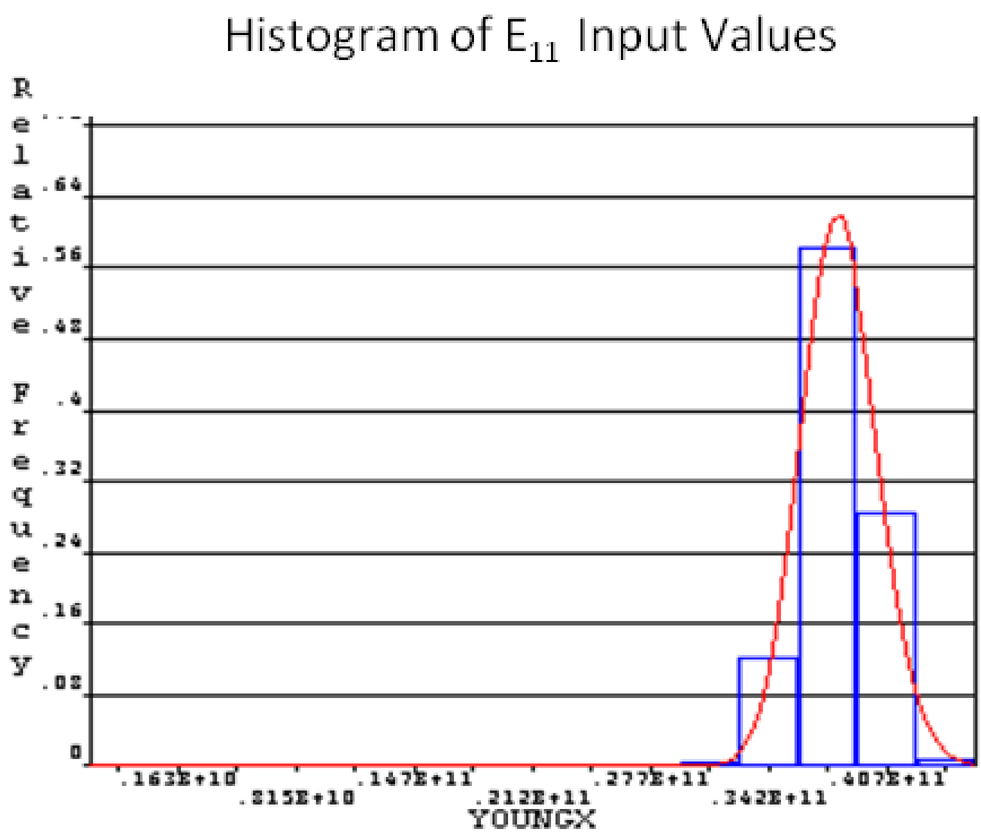


Figure 68: Uncertainty in Modulus of Elasticity Used in Analysis

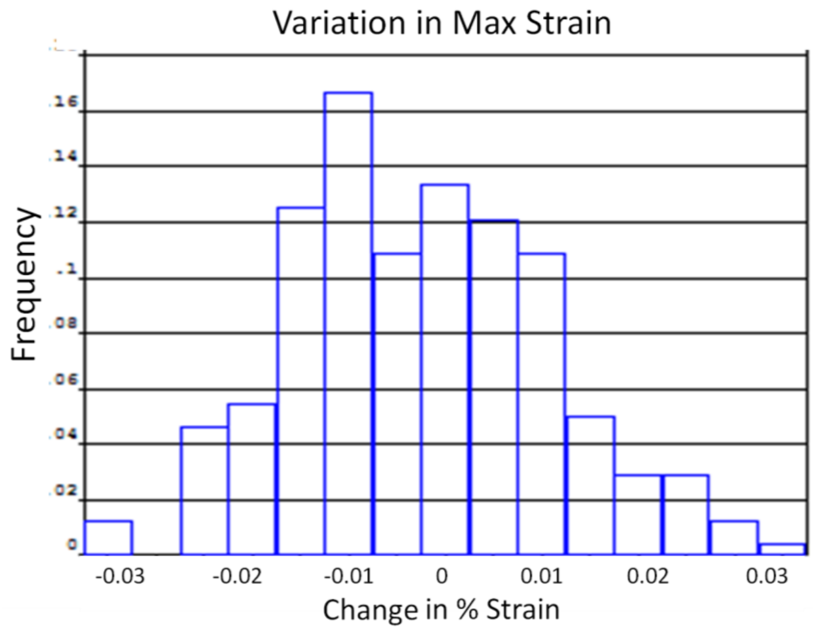

Figure 69: Typical Distribution of Strain Results for one Flaw Location

The focus of the PReP analysis is to evaluate the probability of failure, considering a strain formulation of fatigue life. These results show that varying constitutive properties have little effect on the strain response. Therefore, these variations were not considered throughout the rest of the analysis. There are other failure modes wherein stiffness plays a bigger role, such as tower strikes. However, these are considered outside the scope of the current work. Nevertheless, they could be included in future revisions of the algorithms. It is of note, however, that computational efficiency will become an issue.

Assumption: Probabilistic Finite Element Analysis can be used to understand how material property variability affects a structure. Monte Carlo simulation of deterministic calculations has been used extensively (See Chapter 2) to accurately describe the probabilistic response of a system with random variable inputs. The number of simulations was increased until negligible changes (<1%) in the mean and standard deviation of the resulting strain were observed establishing a very high level of integrity as it pertains to the results.

Step 3 Development of a Failure Criteria

Table 13: Step 3 Overview

| Step # | Step Name | Origin of Data/Assumptions Used in Analysis | Level of Assumption Integrity |
|---|---|---|---|
| **3** | **Development of Failure Criteria** | | |
| 3.1 | Fatigue Properties | Material chosen for this analysis was MUSCG Database TT5. Not exact but very similar to actual material used in test article and model. | High |
| 3.2 | Constant Life Approximation | Utilizes three R-ratio test data sets to interpolate a continuous constant life diagram. Widely accepted but not as accurate as 5 independent R-ratio data sets. | High |
| 3.3 | Designation of Spectrum for Load Reversals | Distribution applied equally to all wind speeds => max ε in R-ratio derivation for CLD approximation | Low |
| 3.4 | Derivation of Total Fatigue Cycles | Assumes 4 cyclic events per revolution. All of which are captured by the chosen spectrum of reversals. | Medium |

Step 3.1 Fatigue Properties. Previous works by Mandell et al. have shown that composites are sensitive to the variations in R-ratio, and therefore, accurate modeling of fatigue damage accumulation requires usage of fatigue life estimations for specific R-ratios values. Constant Life Diagrams (CLD) are used for this purpose, such as the example shown in Figure 70. [76] Use of this data enables generation of ε-N curves for specific R-ratios.

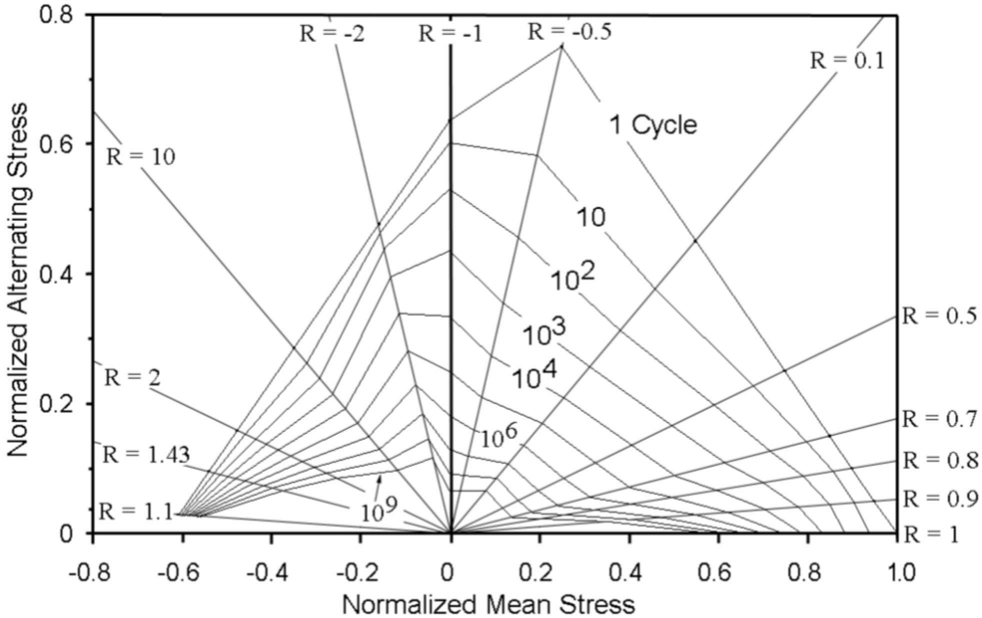

Figure 70: Example GFRP Constant Life Diagram

Assumption: The fatigue properties used in the analysis are representative of the material system used in the article of interest. The material dataset chosen for this analysis was the MUSCG Database material designated as TT5. It is not the exact material, but very similar to the actual material used in EOD fiberglass test blade article and model, therefore a level of assumption integrity of high has been designated.

Step 3.2 Constant Life Approximation. The amount of data necessary to generate a CLD is often prohibitive due to cost and time constraints. Therefore, a number of predictive algorithms have been developed in lieu of copious amounts of testing. Fatigue data for the material systems used in the analysis presented herein, was only available for R=10 and 0.1. The Piecewise Linear methodology (Figure 71) has shown good accuracy with limited amount of test data, and therefore, it was used. This method requires a limited amount of test data and performs linear interpolation between the known data points. This procedure is an acceptable formulation for a CLD. However, accuracy has been shown to improve with 5 independent R-ratio data sets. [77] For this case the known data points from the material testing program are R=10, R=0.1, Ultimate Tension Strain (UTS) and Ultimate Compression Strain (UCS). Ideally the analyst would have values for R=-1 to have a model that can predict fatigue life at all R ratios. However, for the wind blade analysis performed herein, the high pressure side is always considered to be in tension and the low pressure side in compression. While an actual blade in operation will see some cycles in other regimes, this approach was consistent with the EOD blade test used to verify the defect analysis. Therefore, it was only necessary to interpolate between the points designated in Figure 71 as UCS and 3 and between UTS and 1.

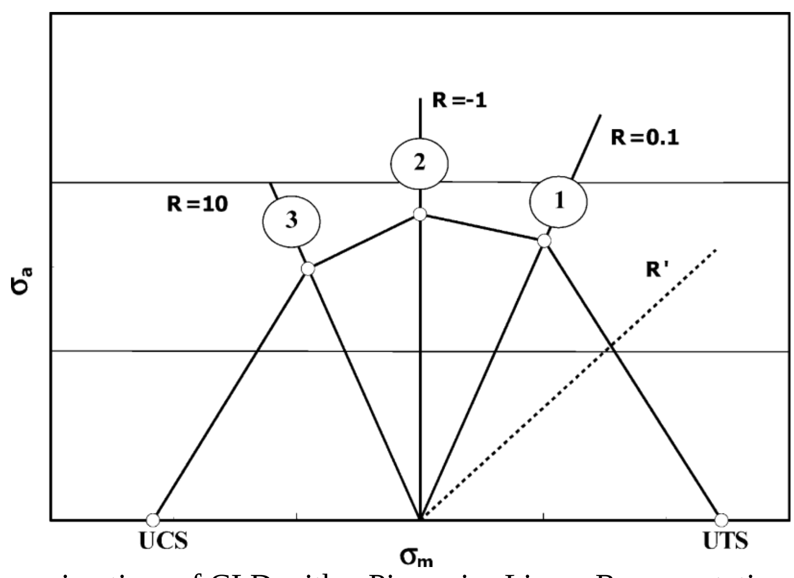


Figure 71: Approximation  of CLD with a Piecewise Linear Representation

The equations for the Piecewise Linear Approximation in compression (Equation 24) and tension (Equation 25) are as follows; [77]

$$\sigma'_a = \frac{UCS}{\frac{UCS}{\sigma_{a3}} - R' + R_3} \tag{24}$$

$$\boldsymbol{\sigma'_a} = \frac{\boldsymbol{UTS}}{\frac{\boldsymbol{UTS}}{\boldsymbol{\sigma_{a1}}} - \boldsymbol{R'} + \boldsymbol{R_1}} \tag{25}$$

where $\sigma'_a$ is the value of alternating stress used in the piecewise formulation, $\sigma_{a3}$ and $\sigma_{a1}$ correspond to the single cycle intercept or power law coefficient for the material system under evaluation for compression and tension respectively, $R_3$ and $R_1$ correspond to the known R ratio data point for compression ($R_3 = 10$) and tension ($R_1 = 0.1$) respectively, R' is the R value for which the piecewise linear interpolation is being performed. These equations have been presented in the notation originally published by Philippidis et al [77]; however, for the analysis presented herein stress was replaced by strain.

Assumption: The Piecewise Linear Approximation accurately represents the fatigue response of the laminate. Additional accuracy could be gained by increasing the number of interpolation points. However, considering that the objective of this analysis is to compare a safety factor design with a probabilistic treatment of defect, and the same Piecewise formulation is used in both cases, the assumption integrity is designated high.

Step 3.3 Designation of Spectrum for Load Reversals. The wind load spectrum utilized for this analysis was derived from the easily accessible and well-known WISPER load reversal sequence. However, it is important to note that any spectrum of load reversals could have been chosen. This spectrum has been used for example purposes, as if it was intended for the design of a turbine. Considering that the objective of this analysis is comparative, the spectrum is not of first order importance. Moreover, for simplicity the spectrum has been applied equally to all wind speeds. That is to say that any one of the 18 wind speeds evaluated from the Weibull distribution had the same shape spectrum (probability distribution of max/min spectrum loading cycles). The WISPER Probability Mass Distribution and complimentary Cumulative Distribution for the High Pressure side are displayed in Figure 72. More information of the usage and derivation of the spectrum can be found in Appendix B.

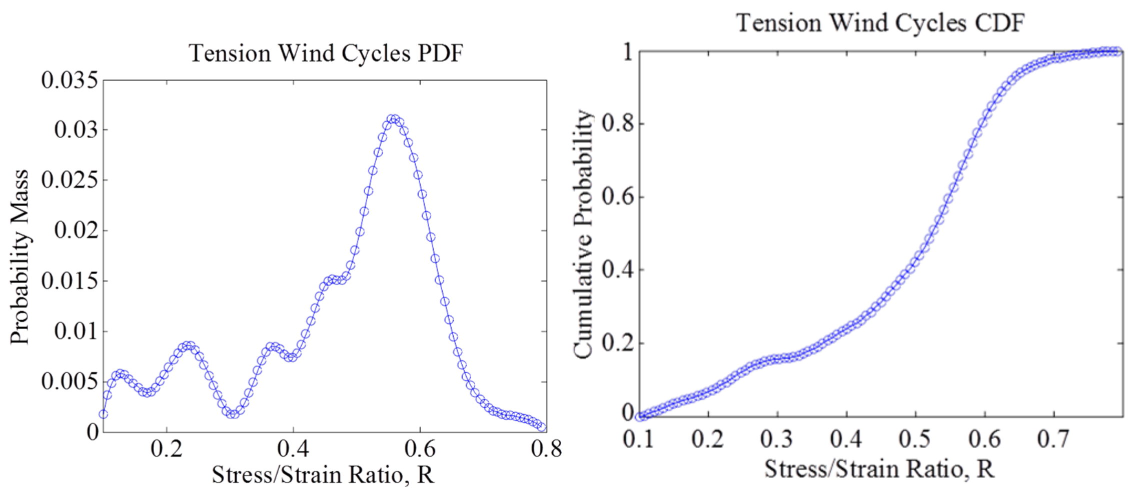

Figure 72: Wind Cycle Distributions

Assumption: The reversal spectrum distribution can be applied equally to all wind speeds. The validity of this assumption is low. The spectrum distribution describes R ratio and therefore needs either max or min strain as an input. As max strain is directly related to wind speeds, the distribution was applied to all wind speeds.

<u>Step 3.4 Derivation of Total Fatigue Cycles.</u> The total number of fatigue cycles was derived from standards defined in "Wind Energy Explained" by James Manwell. [78] This analysis is based on the operational parameters discussed earlier in Step 1, and assumes 4 cyclic events per revolution. All of which are assumed to be captured by the load reversal spectrum. The following equation was used:

$$n_l = 60 k n_{rotor} H_{op} Y \tag{26}$$

where $n_l$ is the total number of cycles, k is the number of events per revolution, $H_{op}$ is the number of hours in operation per year, $n_{rotor}$ is the rotations per minute and Y is the number of years in service. For this analysis, a value of four events per revolution (k) was used. A graphic representation of variable loading is presented in Figure 73.

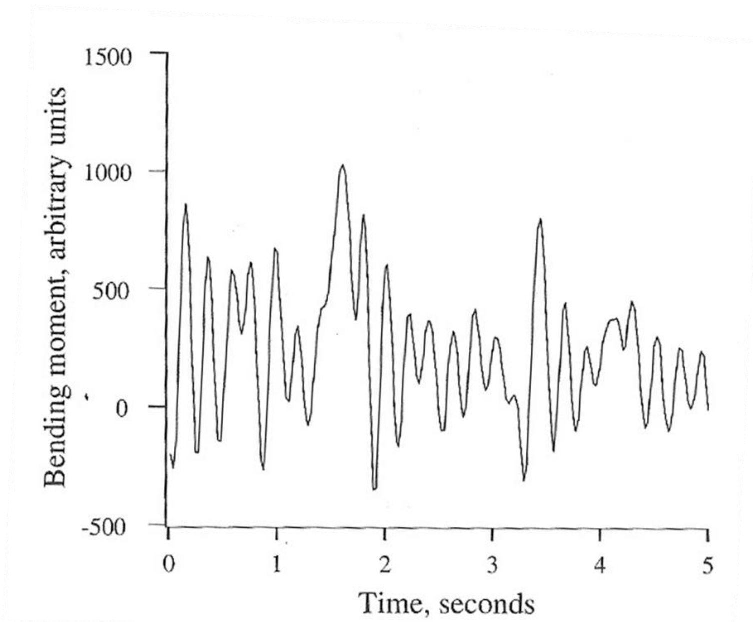


Figure 73: Wind blade fatigue cycle

Assumption: Equations used were from a reputable source, however, some of the inputs were based on the assumptions in Step 1.3 of this chapter. While this approach is not used in commercial blade design, considering the lack of design information and the fact that this analysis is for comparative purpose, this derivation is adequate. Therefore, an integrity level of medium has been designated.

Step 4 Flaw Data Implementation

Table 14: Step 4 Overview

| Step # | Step Name | Origin of Data/Assumptions Used in Analysis | Level of Assumption Integrity |
|---|---|---|---|
| 4 | Flaw Data Implementation | | |
| 4.1 | Development flaw occurrence distribution | Analyst derived from heuristic experiences with test article manufacture. | Low |
| 4.2 | Development of Flaw Distributions from data | Data on OP waves collected from several utility scale blade sections in production. Data collected on IP waves from one utility scale research blade. Data possibly surveyor influenced. | Medium |
| 4.3 | Designation of fictitious flaw distributions for comparative analysis | No data exists for porosity distribution therefore they had to be created. Half Gaussian distributions not represented in the data by heuristically believed to be appropriate for analysis | Medium |
| 4.4 | Treatment of flaw structural performance in fatigue | Knockdown factors developed from regression of quasi-static tension & compression testing performed on defect laden coupons with known flaw magnitudes. | Very High for safe surface; Low for exact response |

Step 4.1 Development of Flaw Occurrence Distributions. Flaw locations and magnitude parameters were treated as stochastic variables. For this analysis, only a 1-D distribution was used to allow for flaws to exist down the length of the spar cap. Two cases for Probability of Flaw Occurrence (PFO) have been assessed, Case 1: Spatially Varying PFO and Case 2: Half Gaussian.

Case 1: Spatially Varying PFO. For this case, the probability of a flaw occurring in a specific location, was described by a spline fit, spatially varying Probability Mass Function (PMF). One novelty of this approach, is the capability for updating procedures that do not rely on the use of traditional, complicated, inference techniques. A user, such as a quality control technician, performing inspections on the composite structure, records the frequency and location of observed flaws. These points are treated as knots in the subsequent piecewise polynomial fitting (cubic spline) procedure, generated through a user defined Matlab algorithm. While the probability mass mapping procedure only utilized 20 user defined locations (knots), the spline formulation allows for smooth interpolation between the points, thus enabling the sampling of all locations between the user defined locations. In this analysis, vertical PMF values per locations were generated for finite widths of 1/100th of the blade length. Conceptually, one might assume that flaws are typically grouped around a region of the mold. This would indicate that they are not inherently found in discrete locations, but rather, hot spots for defects would be regional occurrences. Frequencies can easily be updated as more events are recorded, enabling the regeneration of distributions used in the probabilistic analysis. This data is hard to come by therefore a fictitious set of frequencies was selected by the author.  The chosen frequencies and corresponding PMF is displayed in Figure 74.

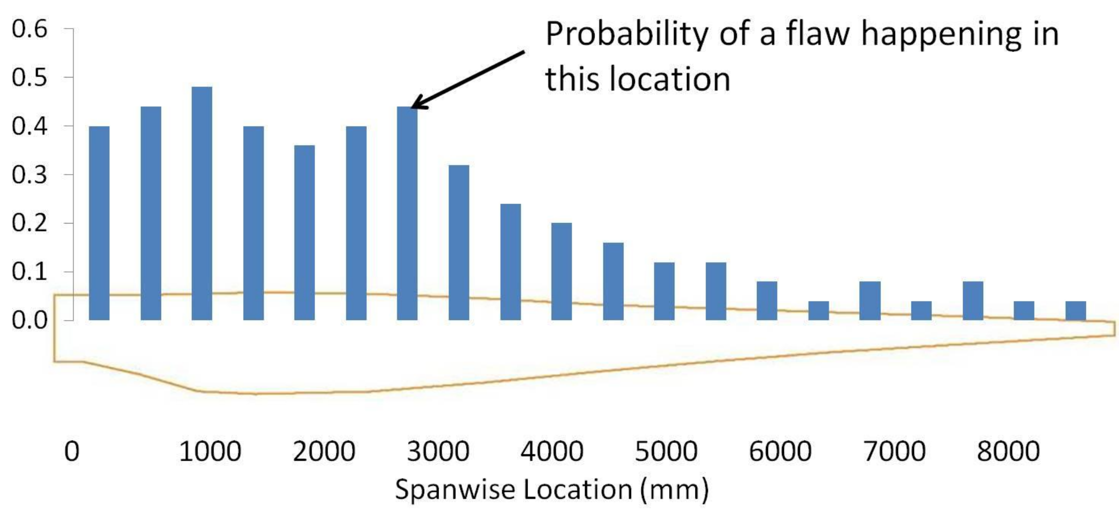


Figure 74: Spatial Distribution for the Probability of Flaw Occurrence

Case 2: Half Gaussian. For this case the probability of a flaw occurring at all locations was assumed to be 100%. However, a user defined Normal distribution for flaw magnitude was generated with a lower limit of zero and an upper limit of 50 degress. This distribution treats a zero degree misalignment as a defect. Figure 75 depicts a visual a representation of the 100% probability of flaw occurrence case. Note that only the same 20 locations are depicted however all 100 locations were used in the analysis.

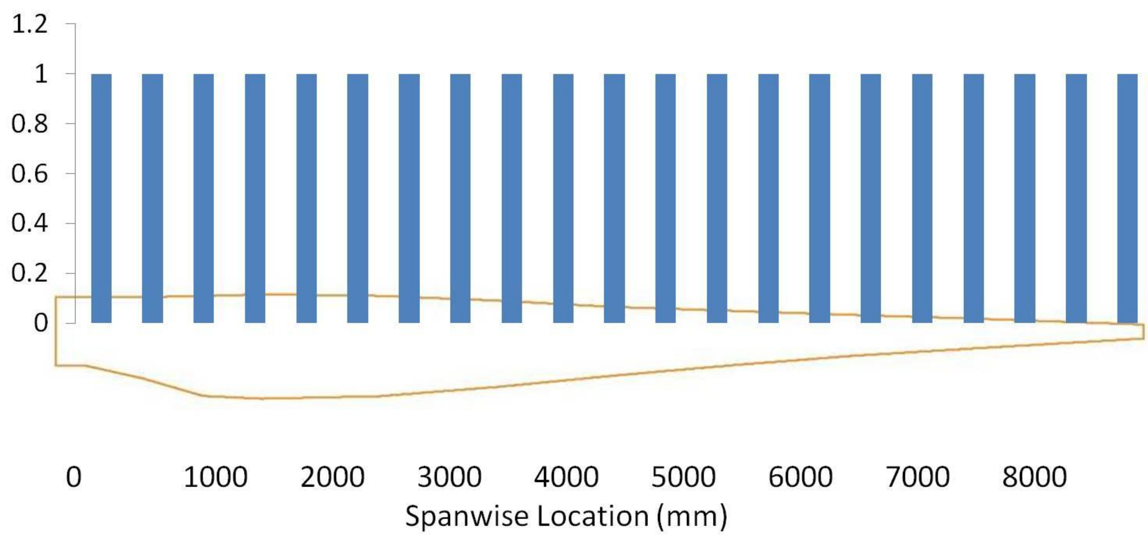


Figure 75: Half Gaussian case, 100% probability of a defect occurring at all locations

Assumption: Probability of occurrence distributions are representative of actual blade manufacture. The Case 1 distribution was derived from heuristic experiences with the blade test article manufacture. The relative probability of one location compared to another seems reasonable, based on the EOD team's experience with a blade build. Unfortunately, no quantitative data exists concerning this. Case 2 is a purely academic formulation, however it stands to reason that if the flaw magnitude distributions are correct, then this approach is meaningful. Considering that no data or prior analysis exist to corroborate these assumptions, the integrity is considered low.  However this approach is still valid for comparing a safety factor design with a probabilistic approach.

Step 4.2 Development of Flaw Distributions. The previous section's approach is used in the probabilistic analysis to ascertain the probability of a flaw occurring in a specific location. When the sampling algorithm identifies the existence of a flaw according to these distributions, a second distribution describes the probability of the flaw's characteristic parameter magnitude. The flaw magnitude distribution is different for each of the two analysis cases.

Case 1: Spatially Varying PFO. Figure 76 displays the data for an example flaw magnitude treated as an uncertainty parameter used in this analysis. All of the other flaw distributions can be found in Chapter 5 and the Appendix. It was found that off-axis fiber angles of waves, collected in a survey of wind turbine blades, follow typical distributions such as Normal and Weibull. Further information on the acquisition and generation of the various flaw distributions and the mechanical response correlating to the characteristic parameter (e.g. wave off-axis fiber angle) can be found in ref [79] and [80].

The PReP code utilized a normal distribution for flaw magnitude. It should be noted that Normal distributions allow for the existence of values less than zero. As defect magnitudes cannot have a value less than zero, a loop is invoked to resample any values less than zero, according the Normal distribution. This same strategy was applied to values greater than 50 degrees, the reason being that no fiber angles were recorded greater than 50 degrees. These loops continued until the predefined number of samples was generated, all with values between 0 and 50 degrees. Figure 77 shows the as-sampled values for misalignment angle according to the defined Normal distribution.

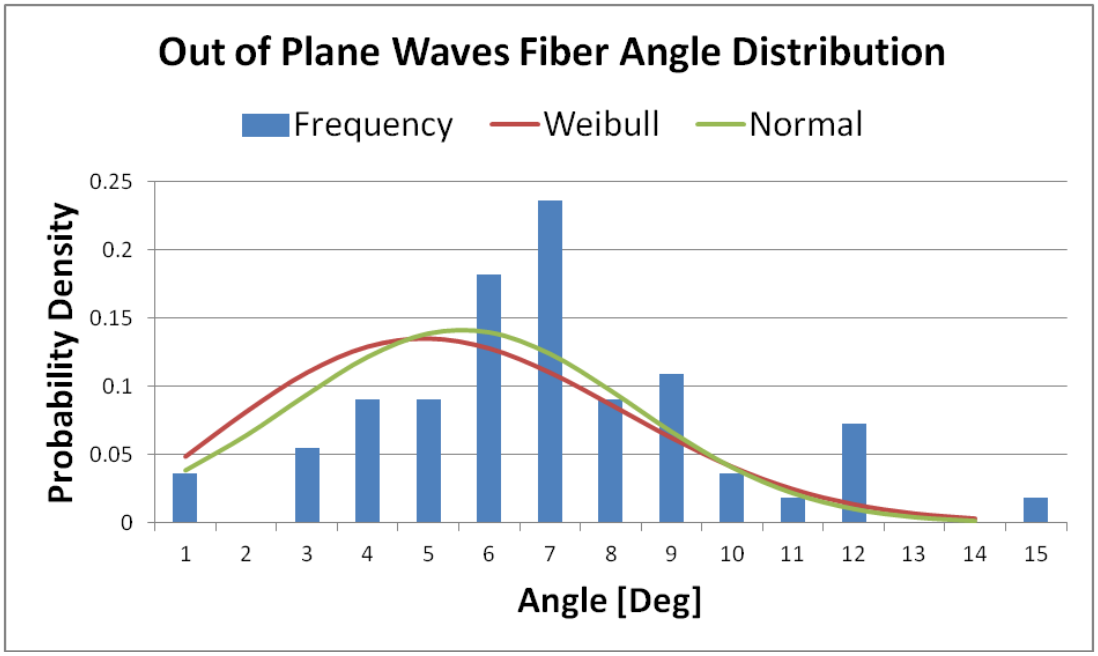


Figure 76: Example of distribution for flaw magnitude

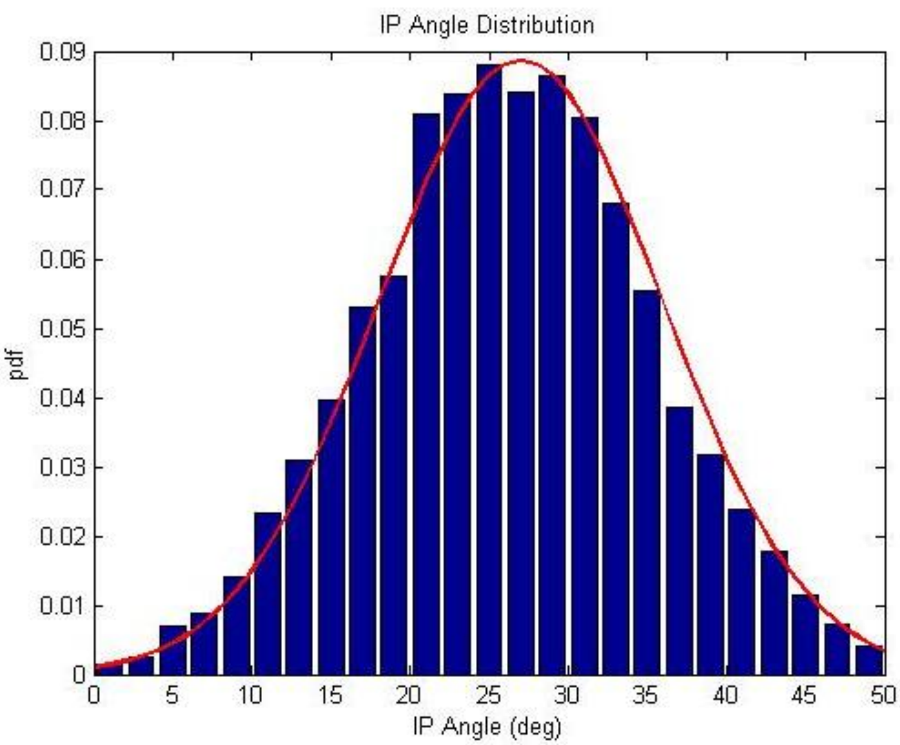


Figure 77: Distribution of sampled (MCM) flaw characteristic parameter magnitude

Case 2: Half Gaussian Flaw Magnitude. In Case 2, every location has a 100% chance of a flaw occurring. It is well known that in commercially manufactured structures, defects do not exist at every location, however it could be conceded the fact that they could. In order to embrace these competing concepts, a user defined Half Gaussian distribution was generated with a mean of zero. This distribution treats a zero degree misalignment as a defect. Since the distribution is "centered" around the value of zero, the zero degree angle is the most likely situation. It stands to reason that this type of distribution is more representative of the actual manufacturing process. Figure 78 displays as-sampled values for misalignment angle, according to the defined Half Gaussian distribution. Once again, a loop was utilize to sample values equal to or greater than zero and less than 50.

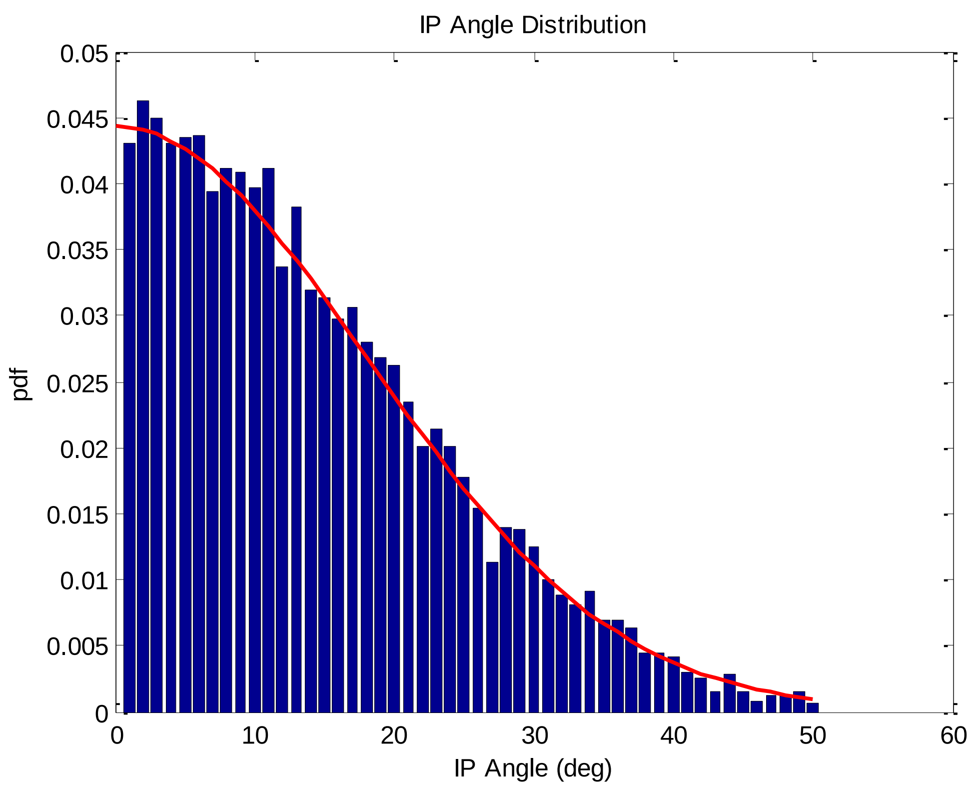

Figure 78: Half Gaussian distribution and MCM sample set for flaw magnitude

Assumptions: Flaw magnitude distributions are representative of actual industry distributions. Articles interrogated as part of the field survey were limited but the data did conform to standard distribution forms and is therefore considered to be of medium integrity.

Step 4.3 Designation of Porosity Distributions. No data presently exists for defining the frequency of occurrence or magnitude for porosity in wind blades. Heuristically, it is well known that porosity is quite common in the wind industry. Accept/reject standards do exist concerning the level of porosity, where in general, anything over 2% is considered unacceptable and in need of rework. Considering this, it stands to reason that a paper trail of work orders for the repair of porous laminates should exist, and therefore a statistical analysis could be performed. However, none were obtained for this body of work. Other investigators in the past have performed stochastic analysis using values for porosity. The origin of this data is not discussed in these publications. The analysis presented herein assumed these same distribution as a place holder, describing porosity variability through a normal distribution with a mean of 1% and standard deviation of 3%. [13; 42; 75]

Assumption: The porosity distribution used is representative of actual blades. No data exists for porosity distribution, therefore they had to be created. The Half Gaussian distribution is not represented in the data, but heuristically believed to be appropriate for this analysis. An assumption integrity level of medium was designated.

Step 4.4 Flaw Performance in Fatigue. At present, very little fatigue data exists on composites containing flaws found in wind turbine blades. A study performed by Mandell, et al. showed significant decreases in fatigue life of a composite in compression, containing in-plane waves. [54] This study will be discussed in more detail in Chapter 9. Other studies on general damaged composites have shown that the fatigue life slope remains largely unchanged with damage. [81] Considering this, an idealized approach has been taken to adjust existing material data S-N (or ε-N) curves, by a shift in the static failure values applied to the single cycle intercept or power law coefficient *A*, The typical power law formulation is given by  Equation 327 [82; 83] The modified equation for flaw fatigue life is given in Equation 28.

$$S = AN^{B} \tag{27}$$

$$S = KAN^{B} \tag{28}$$

where S is the maximum applied stress (or strain) N is the number of fatigue cycles, A is the power lower fit coefficient (often referred to as the single cycle intercept), B is the fit parameter for the power law slope, and K is the flaw knockdown factor.

An illustration of this concept for a flaw that resulted in a 25% reduced static strain to failure, is shown in Figure 79.  Note that the figure includes an extrapolation of fatigue test data out to 10^9 cycles to illustrate the difference in cycles to failure for a given applied strain.

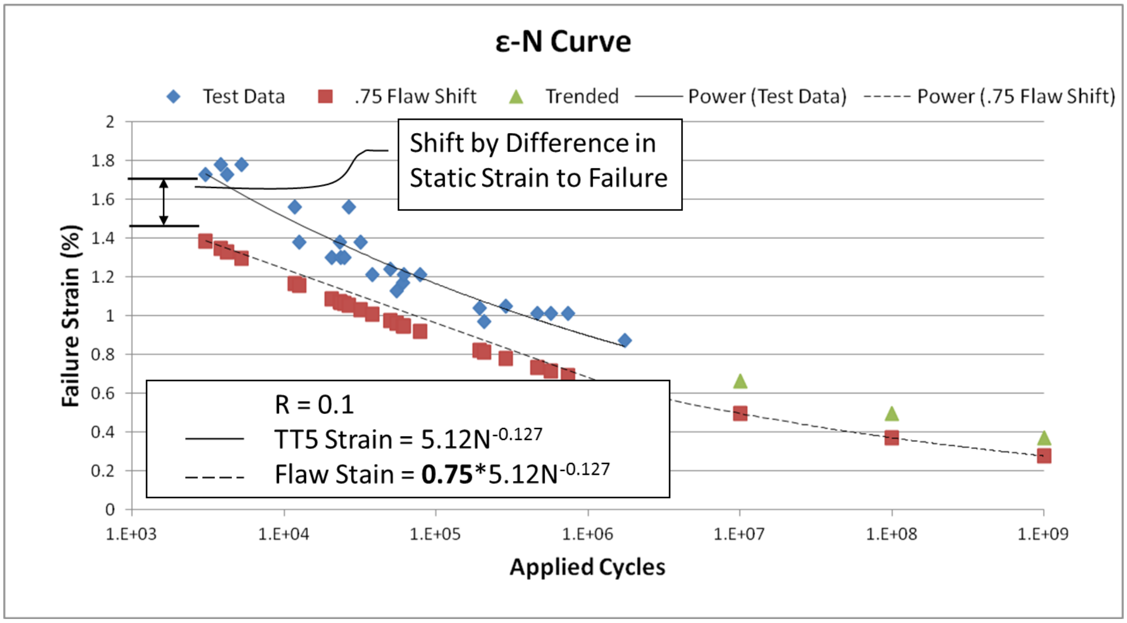


Figure 79: Example of a shifted S-N curve

The failure strengths of composites with defects, were collected by use of quasi-static tension and compression testing. In all cases, these failure strengths/strains were correlated to the characteristic flaw parameter. An example of the knockdown factor data and trend for In-Plane waves is shown in Figure 80. [79] The static strength and knockdown results for other flaws are found in Chapter 5.

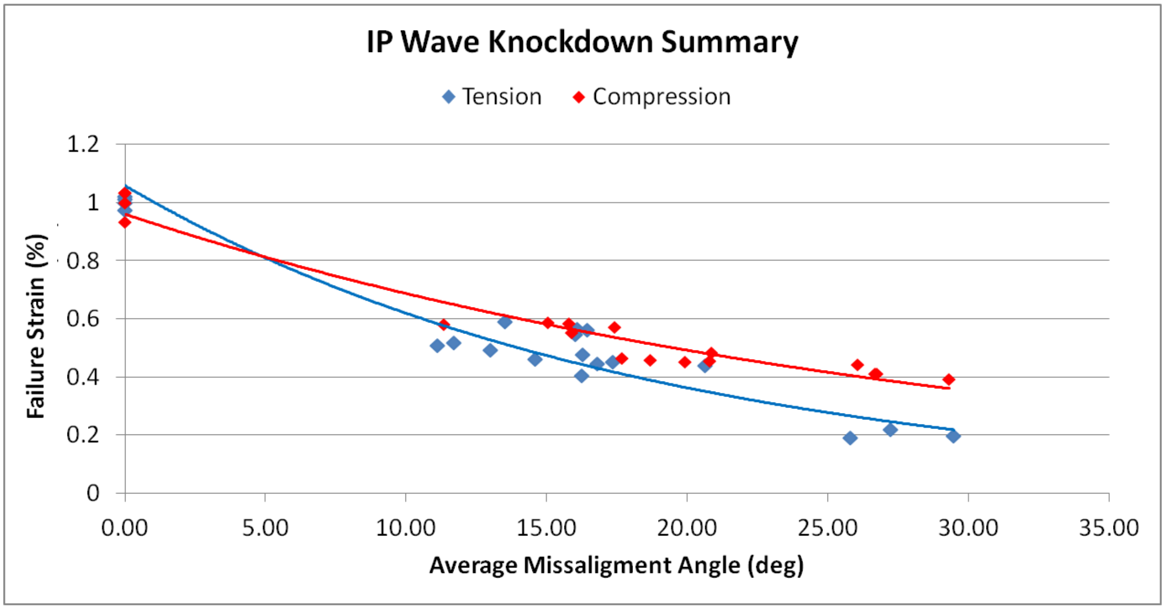


Figure 80: Test data on failure stress for In-Plane waves [79]

The analysis presented herein used the traditional power law formulation described by Equations 27 and 28. For this analysis, where the methodology was verified through a controlled, accelerated blade test, this approach is adequate. However, in practice one would want to consider using the 95/95 confidence limit variations. Usage of this approach takes into account things like environmental effects (temperature, humidity etc). The equations for the 95/95 fatigue life confidence limit is given in the following equations.

$$S_{cl}(N) = 10^{(log_{10}(N)+(b-tol)} \tag{29}$$

and

$$tol = c_{1-\alpha,\gamma}SD \tag{30}$$

where b is the intercept, SD is the standard deviation, $c_{1-\alpha,\gamma}$ is the one sided tolerance limit multiplier with confidence level $1-\alpha$ and probability of survival is γ. [76]

Assumption: Fatigue of flaws can be described by a modification of the power law coefficient. Knockdown factors developed from regression of quasi-static tension & compression testing, performed on defect-laden coupons with known flaw magnitudes are accurate. The level of assumption integrity is considered to be very high for safe surface, conservative analysis but low for describing the exact response. The latter could easily be validated with coupon fatigue test of laminates with defects.

Step 5 Model Verification/Tuning

Table 15: Step 5 Overview

| Step # | Step Name | Origin of Data/Assumptions Used in Analysis | Level of Assumption Integrity |
|---|---|---|---|
| **5** | **Model verification/tuning** | | |
| 5.1 | Model Implementation | Known, built-in flaws used in discrete fatigue analysis. Coupon to structure scaling factored "tuned" based on test results. | Medium - Single data point |
| 5.2 | Development of Baseline "Design" Case | No true design exists for the test article. Therefore a baseline case for which the probabilistic analysis can be compared to had to be developed. This case uses the IEC fatigue standards and assumes a 20 year failure. | In general Low but appropriate for objective |

Step 5.1 Model Implementation. The structural analysis discussed in the preceding section has been validated on a full-scale structural test. As part of the Blade Reliability Collaborative efforts, a subscale (8.3m) version of a multi-megawatt wind turbine blade was manufactured with intentional defects. The article was fatigue tested at the National Wind Technology Center. Forced hydraulic actuation was used at three locations (Figure 81, Figure 82 left), allowing for the assessment of multiple flaw and regional considerations. The test was comparable to three samples of a Monte Carlo simulation, wherein the random variables (flaw type, location & magnitude) were known. This test gave significant insight into the scaling factors for transitioning from laboratory coupons

to full structures and indications that for this type of structure, a local failure constitutes a global structural failure. One failure location at an out-of-plane flaw which was consistent with numerical predictions, is displayed in Figure 82 (right). The detailed testing, analysis and code verification procedures can be found in Chapter 7.

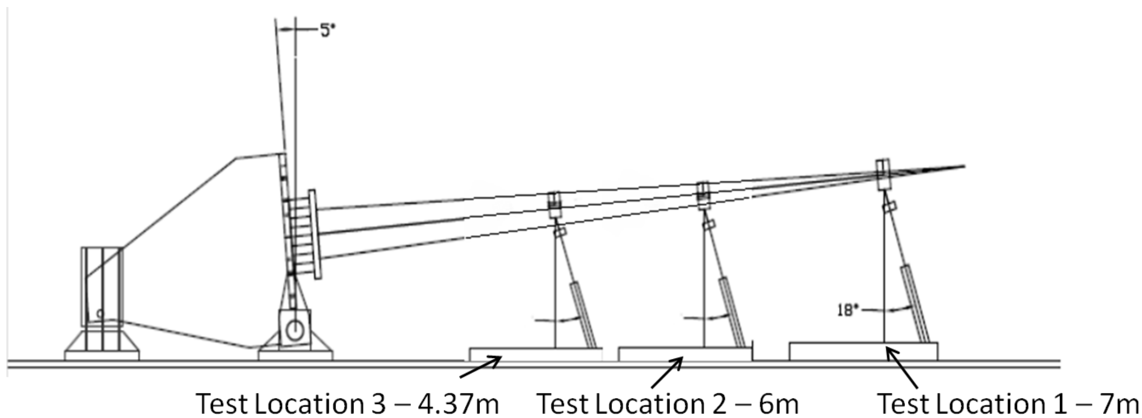


Figure 81: Blade test layout & progression

Figure 82: Blade test (left), Failure at flaw location (right)

Assumption: Scale factor for modifying laminate fatigue response from coupon to a full structure is appropriate. Known, built-in flaws were used in a discrete fatigue analysis. The coupon to structure scaling factored was "tuned" based on one test result. Assumption integrity is considered medium based on the limited data set.

Step 5.2 Development of Baseline, Case 0. Information on the design of the BSDS blade was not readily available; therefore, the blade was reverse engineered to develop a load scenario which results in a fatigue failure after 20 years of operation using the prescribed IEC safety factors, and the same load and spectrum parameters described earlier in this chapter. The pressure load designation was considered arbitrary; it needed only to provide a referencing point to objectively evaluate analysis techniques. For this Baseline Case, the International Electrotechnical Commission (IEC) Safety Factor Fatigue formulation was used. IEC recommends the usage of traditional linear damage accumulation, employing the Palmgren-Miner's rule. Highlights of the IEC fatigue analysis process can be paraphrased as follows: *Fatigue damage shall consider effects of both cyclic range and mean strain, all partial safety factors (load, material and consequences of failure) shall be applied to the cyclic strain (or stress) range for assessing the increment of damage associated with each fatigue cycle.* [84] The three safety factors are further defined by the IEC as follows:

- $\gamma_f$ = 1.25; Safety Factor for loading
- $\gamma_m$ = 1.3; Safety Factor for materials. IEC states that this factor shall be determined in relation to the adequacy of the available material properties test data. Therefore it will be the target of the probabilistic analysis
- $\gamma_n$=1; Component class. Blades are considered class 2 or a "non fail-safe" structural components
- $\gamma$=1.625; Combined Safety Factor

These safety factors or load factors, were applied to the input strain values. Miner's rule for fatigue damage accumulation (Step 6) was used with the afore mentioned spectrum loading distribution and operation parameters. The relationship between wind speed and pressure magnitude was varied until the model indicated that the blade would fail in 20 years. This case did not consider defects and was therefore capable of being used to compare the probabilistic approach to assessing defects.

Assumption: The Baseline case is representative of the actual blade design. No true design exists for the test article. Therefore a baseline case for which the probabilistic analysis can be compared to, had to be developed. This case uses the IEC fatigue standards and assumes a 20 year lifetime, so it seems reasonable. In general the integrity is considered low, but it is entirely appropriate for the objective of comparing a SF approach to a probabilistic one.

Step 6 Probabilistic Analysis

Table 16: Step 6 Overview

| Step # | Step Name | Origin of Data/Assumptions Used in Analysis | Level of Assumption Integrity |
|---|---|---|---|
| **6** | **Probabilistic Analysis** | | |
| 6.1 | Probability of Failure | Each location's Pf is considered statistically independent. | Low |
| 6.2 | Time to Failure | Assumes wind speed and load reversals are not chronologically independent. i.e. at any given time through the year, a particular wind speed and load reversal has the probability. | High for yearly maintenance intervals, Low for shorter intervals |

The Monte Carlo Method was chosen because of ease in adaptation to the PFEA approach and ability to evaluate discrete input values. Moreover, the data generated in the sampling procedure has the capability of being easily transferred to a Statistical Learning method for development of low computational requirement surrogate models that which enable the fast disposition of an as-built structure. [12]

Step 6.1 Probability of Failure. Wind is variable and thus the resulting bending moment that a blade experiences is subsequently variable. Application of these loading scenarios to design and testing is unreasonable therefore rainflow counting is typically used to convert a spectrum of wind speeds (moments) into a set of cycles. The fatigue life can then be used in conjunction with the Palmgren-Miner's rule for linear damage accumulation (Equation 31). [85]

$$D = \sum_{i=1}^{k} \frac{n(S_i)}{N(S_i)} \tag{31}$$

where $D$ is the cumulative damage, $n$ is the number of load cycles at the applied stress $S_i$ and $N$ is the number of cycles to failure at the applied stress $S_i$. Fatigue failure is defined to occur when $D$ exceeds a value of 1. The power law (Equation 27) describing the fatigue life of composites is then used to identify values for the input into Equation 31. The natural extension to this discussion is then to translate a design life of years into cycles. In doing so one can construct the compact limit state function shown in Equation 32.

$$g(X) = 1 - D(X) = 1 - \sum_{i=1}^{k} \frac{\Delta n(S_i)}{N(S_i)} \tag{32}$$

wherein the resulting applied stress ($S_i$ ) is a function of the uncertainty parameter vector $\boldsymbol{X}$. The power of this formulation is it its ability model any fatigue loading spectrum and in its flexibility to predict failure as a function of applied cycles. Typical wind turbine design is based on aeroelastic simulations however this analysis has used a standardized wind loading described through a circannual distribution.

Assumption: Each location's probability of failure is statistically independent. The blade design (geometry) is known to affect flaw occurrence therefore certain regions can have higher concentrations of flaws (geometric transitions e.g. into and out of max chord). Solving the performance function without correlation requires an assumption of statistical independence. This assumption has been applied to both Case 1and Case 2. No data exists concerning the frequency of flaw occurrence therefore some assumptions had to be made. The assumption integrity can be considered to be low.

Step 6.2 Time to Failure. Based on this estimation the performance function (Eq. 36) can be evaluated two ways; assessing the probability of failure for a specific design life (e.g. 20 years) or assessing the time to failure based on an acceptable probability of failure value. In this analysis once a specific probability of failure is designated, the operational in service time can be calculated. This information can then be used to designate maintenance or inspection intervals.

Assumption: Wind speed and load reversals are not chronologically independent; i.e. at any given time through the year, a particular wind speed and load reversal has the same probability. This assumption has High integrity for designated yearly maintenance intervals as the probabilities hold up of the course of a year. However, shorter intervals on the order months could be considered to have a low level of integrity.

## Solution Technique

The majority of the reliability analysis was performed with a post processing script written in Matlab. A routine was written to perform the sampling and necessary MC calculations (all of which are mathematically described in the preceding sections). The structural analyzer (FE model) provided strain data for each potential flaw location under the uniform pressure distribution. It was found early on that the resulting strain scaled linearly with the magnitude of the load. Therefore the wind speed distribution described by Step 1.2 was implemented through scaling the local strain values accordingly. The result was a probabilistic strain distribution as a function of wind speed.

Flaw occurrence and magnitude distributions were sampled using the Matlab built-in function *normrnd*. *Normrnd* generates an array of normally distributed pseudorandom numbers according to the input parameters: mean, standard deviation and array dimensions (number of samples). All of the array values are generated at one time for each distribution using this function. Each value of the array is then called later by the model to perform a discrete evaluation. Every flaw instance calculation is evaluated with the using the previous discussion on fatigue formulation, wherein the damage is accumulated linearly according to the applied load cycle distribution and the power law. In other words the number of applied cycles and cycles to failure, according to the power, are calculated for every array instance at every wind magnitude and R ratio. A Miner's summation is performed to assess the damage index after the application of the load spectrum. All load cycle frequencies are circannual and constitute one year of infield operation. The full twenty year operational lifetime is simply applied linearly.

Probability of failure for every location down the length of the spar cap is then calculated according to Equation 33. Simulations that result in a failure are those where the limit state is exceeded; i.e. the Miner's summation yields a value greater than 1. This formulation allows for assessment of the probability of failure for any particular location down the spar cap. However, a designer is typically interested in the total probability of failure for the blade as a whole. The analysis presented here has focused on the spar cap region only. The assumption has been made that a local failure constitutes a global failure of the wind blade. This formulation is consistent with a reliability assessment of a series system. A series system is one where the entire system fails if any component in the systems fails (i.e., "weak-link-in-the-chain"). The probability of failure of a series system is the joint union of all the failure states of the components which are expressed by the following equation; [14]

$$P_{f,series} = P\left[\cup_{j=1}^{k}(g_j(X) \leq 0\right] \quad \textbf{(}33\textbf{)}$$

For mutually exclusive events, this can be approximated by the sum of all failure states, following the addition rule, if the individual component probabilities of failure are small. The mutual exclusivity clause would assume that only one location can fail at any given time. This is consistent with weakest link concept. Should two locations fail simultaneously in the physical world the result is the same, global failure. If the individual component probabilities of failure are large, then using Equation 33 could result in a probability larger than unity. This is not possible, and the rule breaks down and the compliment of the product of all failure states provides the exact answer. [14] It is this computation (Equation 34) that is used to assess the probability of failure for the entire blade. Either case describes the same set of independent events.

$$P_{f,series} = P\left[1 - \prod_{j=1}^{k}(g_j(X) \leq 0)\right] \tag{34}$$

## Results & Interpretations

In conventional analyses or certifications of structures, the reliability is done with a deterministic analysis. The goal is to provide some conservatism to ensure that minimal failures will occur over the lifetime of the structure. Where available, some parameters receive a statistical treatment (e.g. material strength allowables), while others may not. To account for this, a scalar quantity is applied to the analysis to address that unknown or non-quantified variables. In the wind energy certification, this is called a Safety Factor (SF). The SF will typically have some basis in testing, analysis, or experience and is meant to provide additional conservatism to increase the reliability of a system over its lifetime.

It is difficult to make a one to one comparison to the probabilistic approach presented herein. However, in this section we make some important comparisons to illustrate several points for the advantage of the current analyses. First, if there are manufacturing defects outside of the database used for certification, it will be shown that premature failure can occur, much shorter than the design lifetime, even with a safety factor applied. This implies that the safety factor approach is not conservative, and does not accomplish its intent. It will also be shown that, if a probabilistic approach is taken, safety factors can be decreased resulting in more efficient wind turbine blade structures.

This has the additional advantage in that the reliability can be quantified as opposed to simply assuming the safety factor will accommodate all unknowns.

For this analysis, it was not known what acceptable probability of failure was implied in the IEC safety factors. However, it can be assumed that there was an intended low probability of failure over the 20 year lifetime. A scheme is proposed that compares a baseline analysis that has an assumed low probability of failure, inherent to the Case 0 (Baseline), with the probability that failure is reached within the 20 year lifetime with manufacturing flaws which are not inherent in the certification process (Case 1 and 2). While the results are presented as probabilities of failure they are in fact, the probability of reaching the implied probability of failure as designated but the safety factor approach. In a sense, this is  relative probability of failure which allows for the comparison to the two techniques. Should one know the original design probability of failure, the absolute probability of failure could be tracked as easily through the 20 year life.

Both Case 1 and 2 were evaluated with the use of the prescribed IEC safety factors and with a reduced material safety factor. This treatment allows for comparison of the conservatism in the safety factor approach. In total, 1,000,000 simulations were performed in two stages. 1,000 runs were performed in the structural analyzer (SA) addressing variations in wind loading pressure distributions and material properties.

Case 1: Spatially Varying PFO

Figure 83a displays $P_f$ by location down the length of the blade when applying the IEC safety factors to the FEA simulation output strains and treating defects as random variables. Considering the time dependant formulation of linear fatigue damage accumulation (based on number of cycles), $P_f$ can also be described as a function of time in service. This is graphically depicted by Figure 83b where in can be seen that location 22 essentially has a 100% $P_f$ after 7 years of operation. It can easily inferred by these results that there is a significant chance of failure, demonstrating that when using the SF with a probabilistic simulation of defects the blade will end up being overdesigned to achieve an acceptable probability of failure.

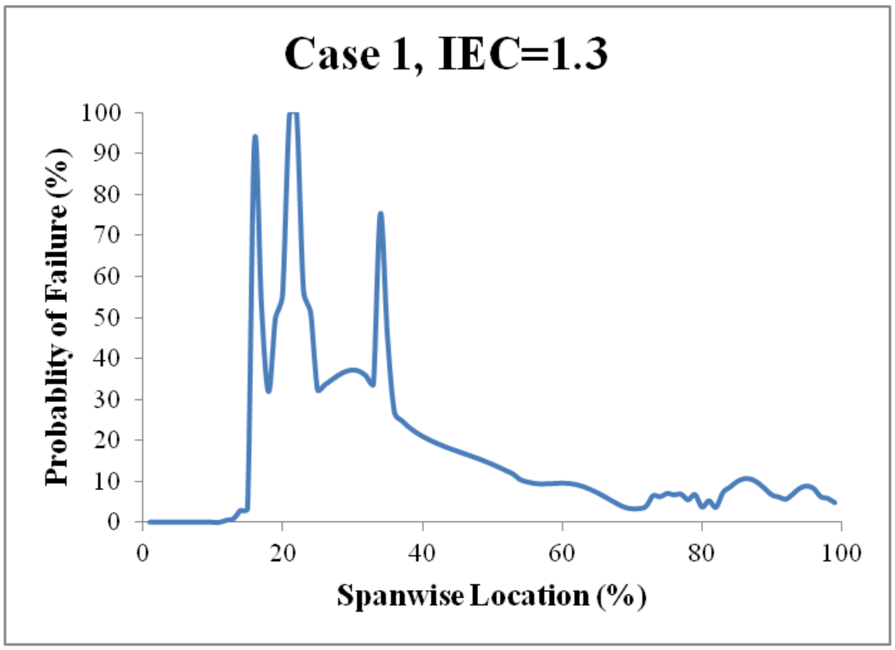


(a)

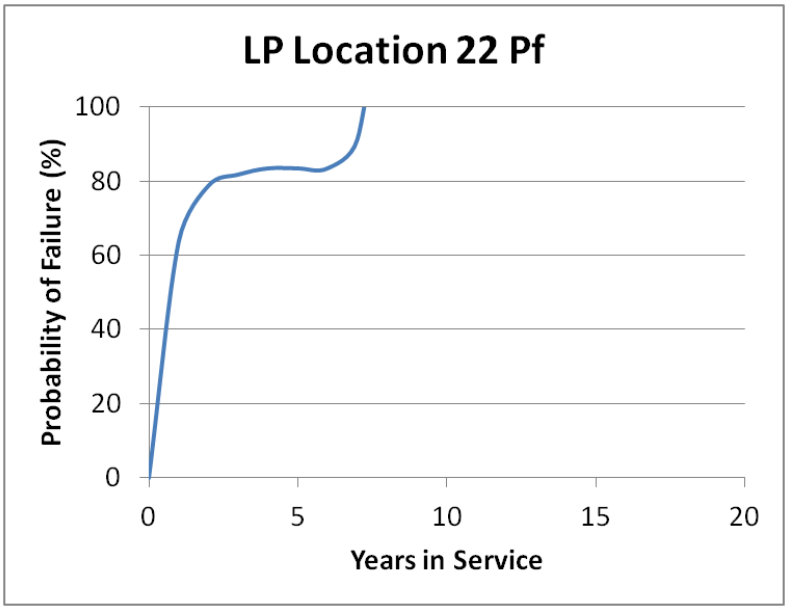


(b)

Figure 83: $P_D$ by location (a), $P_D$ as a function of time for location 22 (b)

The analysis can then be repeated by reducing the IEC Material Safety Factor ($\gamma_m$) to 1.15. The results from this analysis are displayed in Figure 84. With the reduced SF, the $P_f$ is significantly lowered thereby eliminating the need for additional structural reinforcements due to additional uncertainty. This has significant implications for reducing weight and cost while providing quantifiable reliability estimation for wind turbine blades.

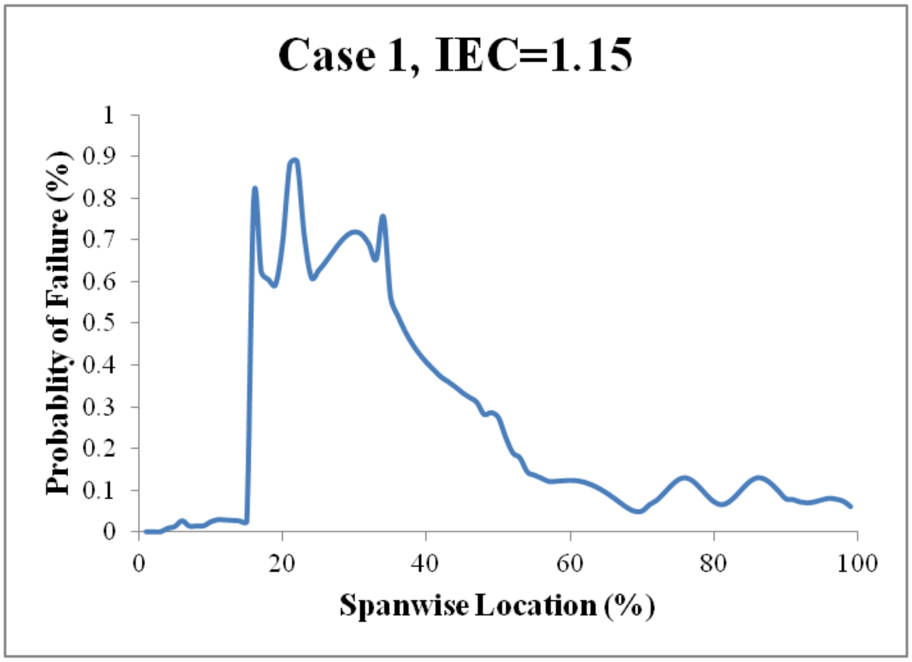


Figure 84: $P_f$ by location with reduced SF

Case 2: Half Gaussian Magnitude Results

The same analysis can be performed using the Half Gaussian approach. The results of the probabilistic analysis both with the standard IEC SF (top) and with the reduced SF (top) are displayed in Figure 85. Once again the conservatism of the IEC SF approach can be interpreted in the same manner as Case 1.

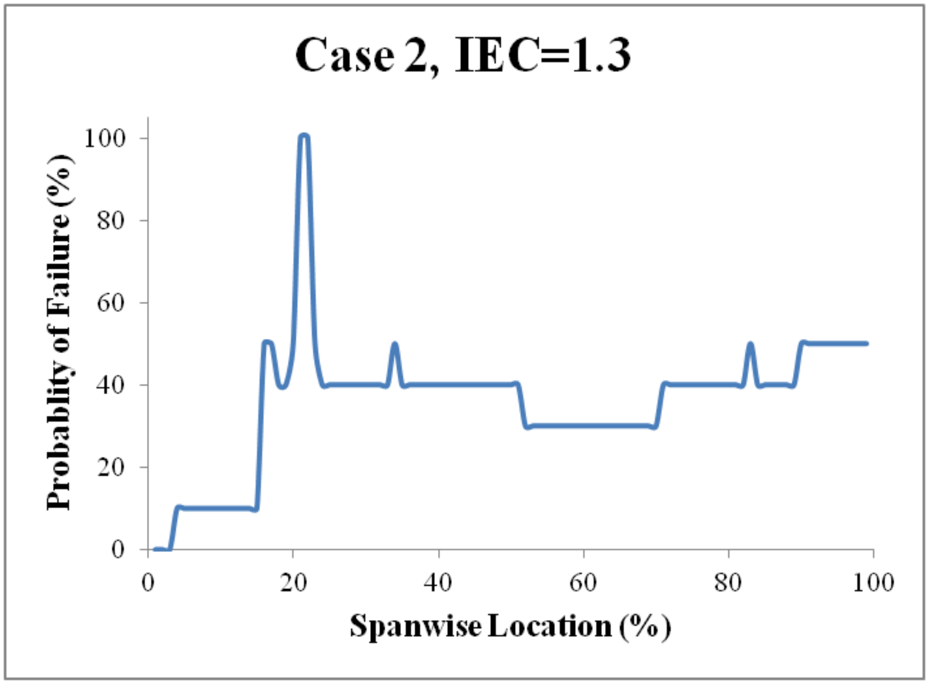


(top)

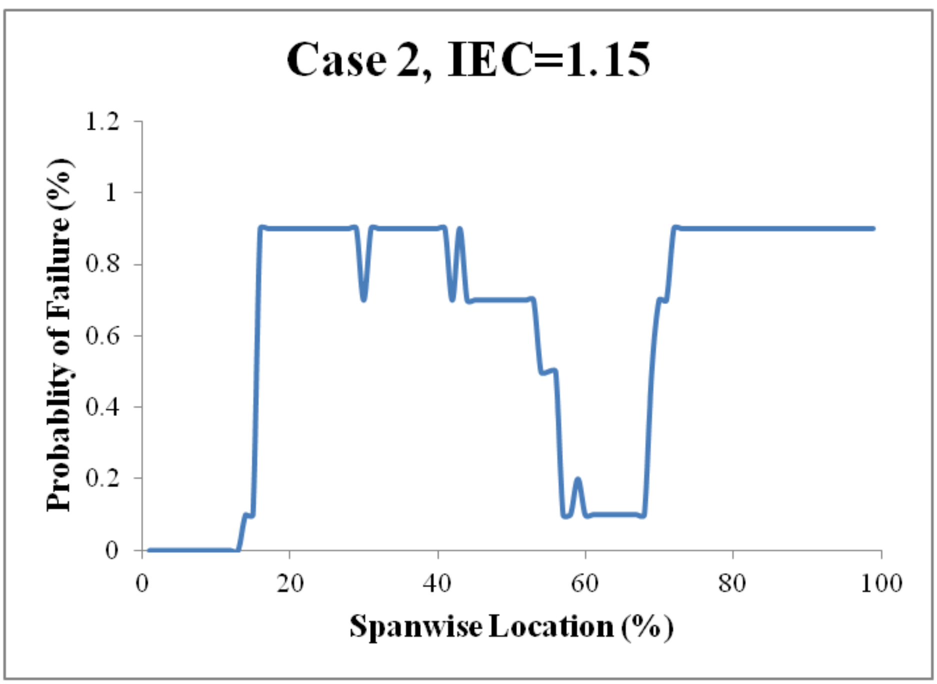


(bottom)

Figure 85: $P_f$ by location with IEC SF (top) and Pf with the reduced SF (bottom)

Discussion of Results

The previous sections reported $P_f$ as a spatial probability mass distribution. This method is extremely useful in understanding the sensitivity of a region to flaws. It provides the designer with information on where changes in the design are needed or regions around which to develop a quality control program. However these detailed results are not useful in the preliminary design stages where a designer may be using a parametric study to evaluate blade design changes. In this case it is more useful to quickly ascertain the $P_f$ for the entire blade. As discussed in the previous section, the probability of failure of a series system can be estimated using Equation 34.

This approach is also relevant to understanding the differences in a pure safety design based on the recommended IEC safety factors discussed in Step 5.2 and a defect focused probabilistic methodology. For this comparison, the first analysis was performed combining the IEC recommended SF of 1.3 with a probabilistic treatment of defects. This scenario would consider the case where information on the variability material and manufacturing system are known but the blade designer is bound by regulations to still use the full safety factor. The second portion of the analysis considers the case wherein the designer reduces the Safety Factor to a value of 1.15. The IEC guidelines require that the Safety Factors be used in essence as load factors applied to the stress/strain analysis outputs. If the Safety Factor can be reduced then the structure can be modified accordingly. The most obvious way to do this would be though reduction of laminate thickness however other structure design components could be altered as well. Regardless, the result should be a leaner, less expensive to manufacture blade.

The series system analysis, for both Safety Factor values was applied to both of the analysis cases described earlier; Case 1: Spatially Varying PFO and Case 2: Half Gaussian. The results of these analyses are given in Table 17. Here it can quickly be seen that utilizing the full Safety Factor and performing the defect reliability analysis results in a near guarantee of premature failure. Thus indicating that the blade design needs to be significantly altered, possibly by adding additional laminate layers and which will ultimately drive up the costs. However, by reducing the Safety Factor value by 15% and applying the defect reliability assessment, the $P_D$ is significantly reduced. This indicates that the current design configuration is acceptable or at least substantially closer to acceptable depending on the target probability of failure for the lifetime of the blade.

Table 17: Probability of failure for a series system analysis

| | **Case 1** | | **Case 2** | |
|---|---|---|---|---|
| | W/SF = 1.3 | W/SF = 1.15 | W/SF = 1.3 | W/SF = 1.15 |
| **$P_f$** | 100% | 22% | 100% | 46% |

# CHAPTER 7

# BLADE TESTING

## Motivation

The Blade Reliability Collaborative initiative manufactured two Blade System Design Study (BSDS) blades as validation test pieces to examine effects of defects (EOD) and non-destructive inspection (NDI) at a scale larger than coupon level and an as-built wind blade. The BSDS blade was chosen due to a wealth of previous test data, proportional geometric similarity to modern blade designs, and proven structural efficiency of the design. Both glass and carbon spar versions of the blades were produced to examine the difference in response of the two material systems.

The EOD validation blades were fabricated by TPI Composites in Warren, RI and tested at the National Renewable Energy Laboratory's National Wind Technology Center. The Montana State University team was primarily responsible for the blade analysis. This effort provided for verification of the PReP algorithm.

## Blade Design

### Introduction

The BSDS blade [71; 72] was selected as the test bed for the Effects of Defects and Inspection Validation blades. The SNL BSDS blade design consists of three distinct sub-components, a low-pressure (LP) skin, a high-pressure (HP) skin and a shear web (SW). The LP and HP skins and shear web are fabricated separately with each consisting of several layers of composite materials. Within each skin (LP and HP) there is a spar cap, which itself consists of several layers. The spar cap in each skin starts at the blade root and terminates close to the blade tip. The three subcomponents are then assembled and bonded together into a blade. In the first blade assembly step, the shear web is bonded to the HP skin, and then the LP skin is bonded to the cured assembly of shear web and HP skin. The illustration in Figure 86 show key areas in one skin of a BSDS blade. The laminates in the other skin are symmetrically very similar. [86]

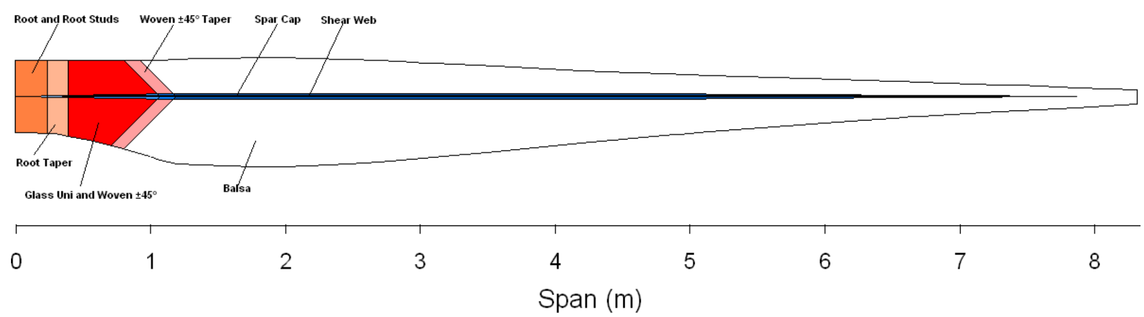


Figure 86: Diagram of key areas in a BSDS blade.

## Effects of Defects Validation Blades

Two Effects of Defects Validation Blades were built by the team. The first Effects of Defects Validation blade followed the standard BSDS blade design, which is fabricated with a carbon spar cap in the LP and HP skins. The second blade was built with a fiberglass spar cap in the LP and HP skins. The standard BSDS blade design was modified by Josh Paquette of SNL to incorporate a fiberglass spar cap in the LP and HP skins. TPI Composite, Inc., engineers generated the two sets of blade layup drawings. The MSU and SNL teams then added additional information to certain pages in these layup drawing for the implementation of each flaw during the blade manufacturing. TPI Composite, Inc., engineers also created the drawings for the carbon and fiberglass spar caps, which are shown in the Appendix. [86]

The purpose of this test was to produce significant insight into the effect defects have on wind turbine blade structures and to help in the design of future programs. To this end, flaw types, sizes and locations were designated such that post-testing analysis would be tractable. Flaws were introduced into the blade to mimic coupon testing and existing models as closely as possible. For instance, flaws in the spar region traversed the entire width of the spar. This situation more closely resembled previous laboratory testing to help reduce the number of variables in correlating from coupons to a full-scale blade.

Knockdown factors were applied to the regions where defects were located as reduced strength multipliers found during testing of thin coupons. Results from these tests were most applicable to the glass spar. A reduced testing set on carbon and hybrid laminates with flaws was also performed. In general, flaws were originally designated so that they increase in severity with increasing distance from the root. Conceptually, this would allow for multiple failures starting from the tip and moving inward. Allowing for more insight to be gained by having several failures at different locations and varying flaw types. This is visually shown by the preliminary reduced strength targets described in Figure 87. A subset of flaws were placed in the panel regions purely for NDI purposes. A preliminary structural analysis provided two pieces of conclusive information; avoid the triangular region and focus on the spar cap.

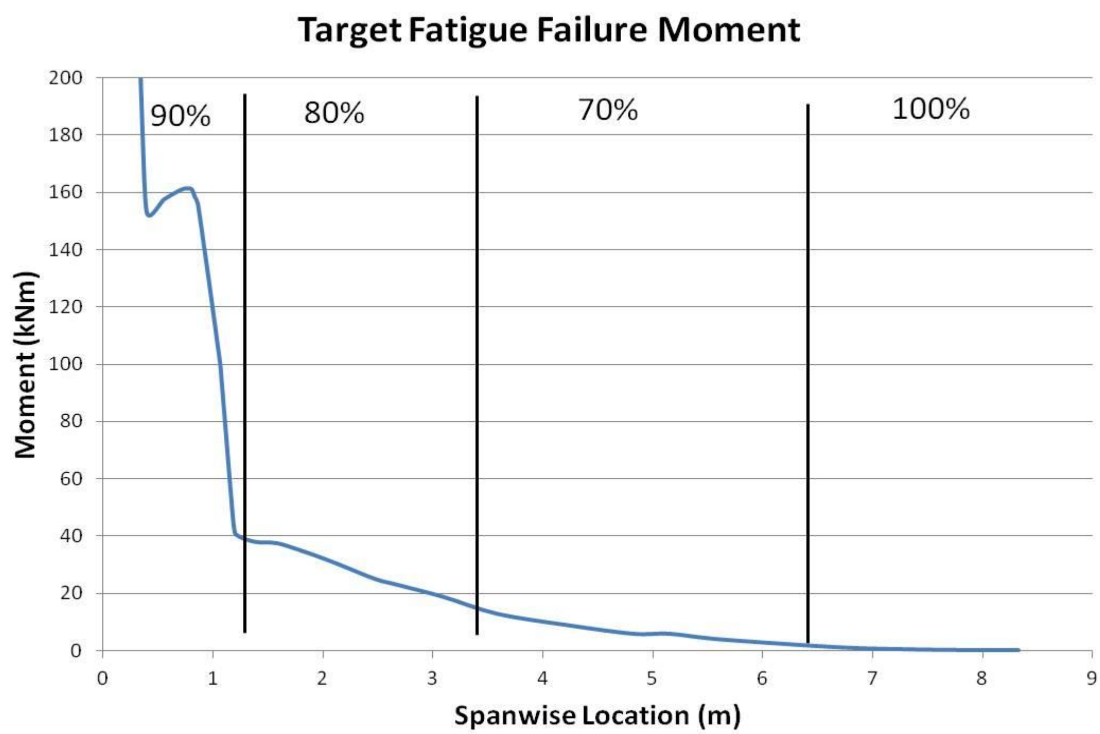


Figure 87: Target reduced strength down the length of blade

A description of the impetus for the chosen flaws follows;

Adhesives. Data obtained on adhesive flaws from the field show that some flaws, such as ply drops, are predominantly driven by geometry effects. Voids are extremely prevalent in bondlines. Discussions with manufacturers, indicate that voids are caused predominately in the manufacturing process when blade halves must be repositioned after the adhesive has come in contact with the part.  Based on the data collected to date, voids in the spar cap to shear web connection tend to be larger than voids in the leading and trailing edge bondlines.

Waves in General. An attempt was made to use three different angles for each of the wave types. Initially, one value was designed to embody the highest frequency, the other two filling out the tails of the distribution or providing extremal event data. At a minimum, two different angle ranges were introduced. In addition, analytical testing was performed to optimize the distance between proximity waves so that peak stresses would not overlap as they do in chain waves. It was found that this optimal length was equal to one wavelength between waves.

Out-Of-Plane Waves. The midpoint of the surveyed OP wave distribution was 7°, typical high angle values are in the 12-13° range and max angles were observed over 40°. An attempt was made to introduce the 5-7° and 12-13° values. Strength data on the low end of the distribution for OP waves in tension showed mild effects.

In-Plane Waves. The surveyed distribution is centered on 28°, with a significant amount of the cumulative probability happening between 22° and 38°. However, these data were from a limited source and believed to be extreme. Waves of approximately 15° were established as the high-end extreme for blade testing. For the lower end of the distribution an angle around 7° was chosen.

Porosity. Little data exists to develop a distribution of percentages; however, in general 2% is considered unacceptable in industry. Data showed minimal effects on strength for porosity levels up to ~8-10% range. Larger values, such as 12-14%, are interesting from an academic standpoint; however, it does not seem that this is a relevant number. Anecdotal information suggests that porosity levels in the 2-5% range are statistically significant and may prove to have an impact in combined flaws.

Preliminary Structural Analysis

A first pass structural analysis was performed to ensure that the chosen flaw placement and magnitude were reasonable from a testing perspective. In doing so, two efforts were performed; standard closed form beam bending and 3D finite element analysis. The equations describing a beam in fatigue bending are as follows:

$$M = \frac{(1-k)*\varepsilon_f*N^B EI}{y},\ P = M * x \tag{35}$$

where $k$ is the percent reduction as a function of a flaw in ultimate static strength or strain, $\varepsilon_f$ is fatigue life coefficient or cycle failure intercept, $N$ the number of applied fatigue cycles, $B$ is the fatigue slope exponent, $EI$ is the flexural stiffness of the blade by location, and $y$ is the distance from the bending neutral axis.

Loads were then evaluated through an optimization approach where three $P$ and $x$ combinations vary within constraints to minimize difference between target and actual moment. The local strain was then corroborated with a FEA model. The process for the FEA analysis was as follows:

1) Build model, choose flaw locations by creating components.

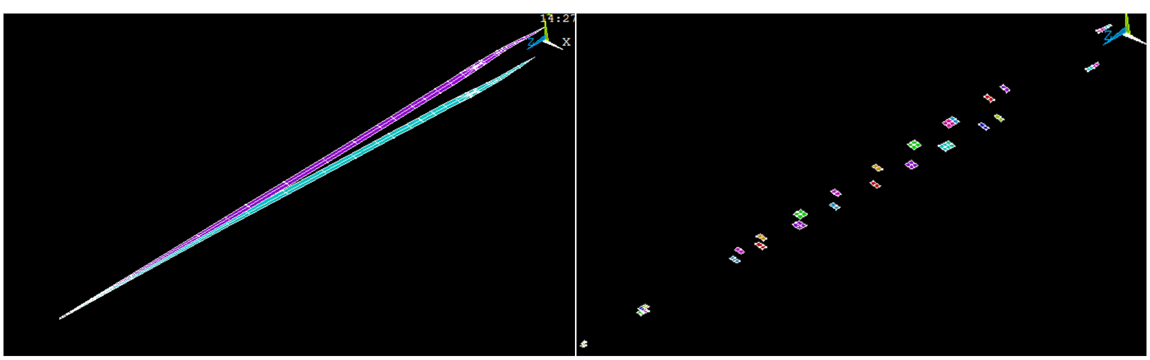

Figure 88: Finite Element Model, Blade Spar Cap (left), Flaw elements (right)

2) Use $P$ and $x$ from beam bending analysis as inputs.

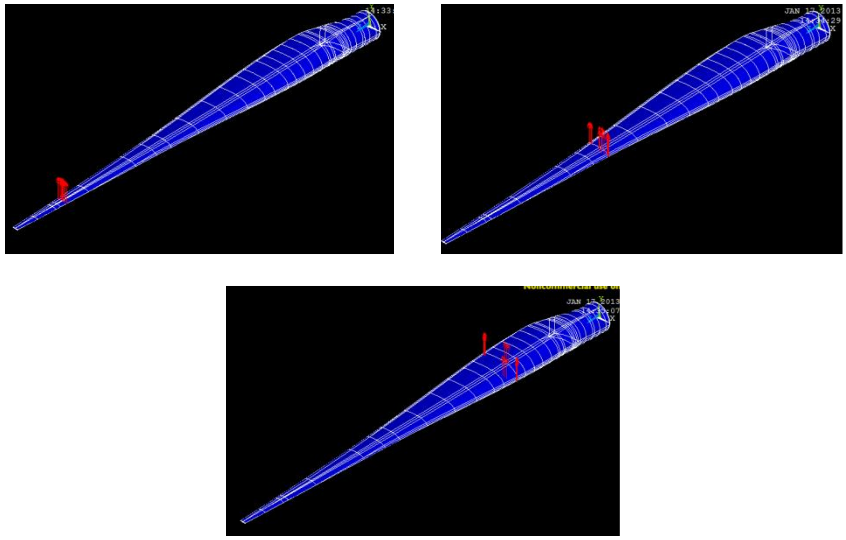

Figure 89: Applying static load cases at three test locations

3) Run all three fatigue load cases independently in a static analysis.

The nodal results were output for strain and stress in the material 1 direction (tension & compression) for all components and run in fatigue analysis. The fatigue life can then be used in conjunction with the Palmgren-Miner's rule for linear damage accumulation. [85] Miner's rule was used in combination with the power law for fatigue life as described in Chapter 6. In general, flaws were chosen so that they increase in severity with increasing distance from the root. Some flaws were placed in the panel regions purely for NDI purposes. The preceding FE analysis offered two pieces of conclusive information; avoid the triangular region and focus on the spar.

The idealized approach of adjusting material data S-N (or ε-N) curves by a shift in the static failure values applied to the single cycle intercept *A*, as described by Equation 28, was used in this analysis. An illustration of this concept for a flaw that resulted in a 25% reduced static strain to failure was shown earlier in Figure 79. The failure strength of composites laminates with defects were collected by use of quasi-static tension and compression testing. In all cases, these failure strengths/strains were correlated to the characteristic flaw parameter. An example of these results for In-Plane waves is shown in Figure 90. [79]

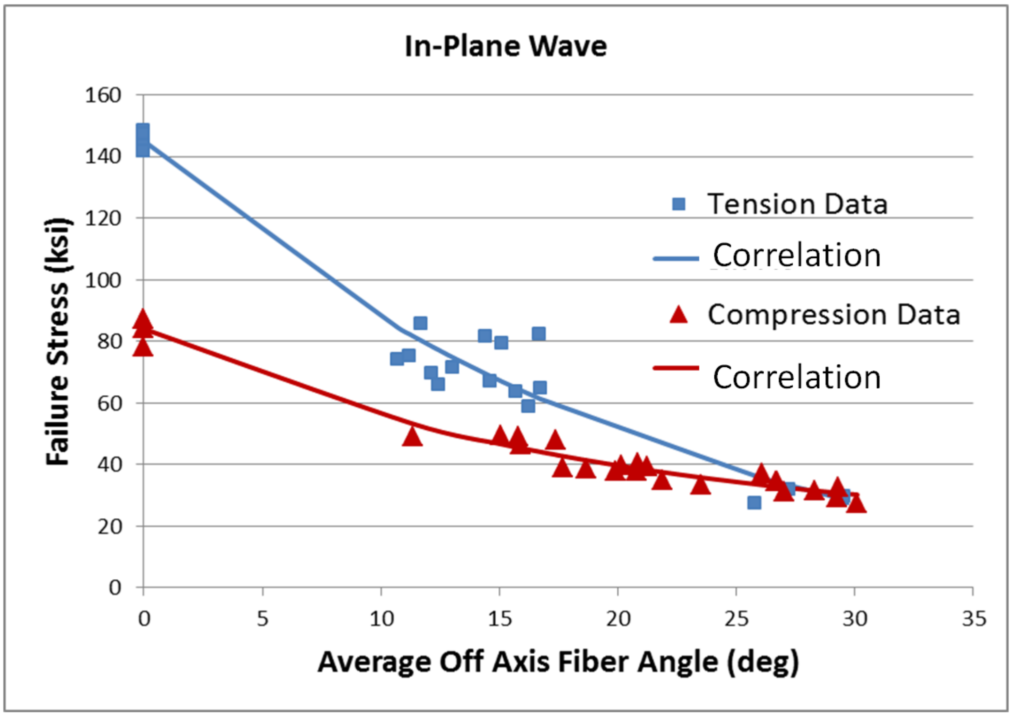


Figure 90: Test data on failure stress for In-Plane waves

## Blade Manufacture [86]

The test articles were manufactured by TPI Composites at the Warren, RI facility. The blades were fabricated with a clear gel coat on the outside blade surface. The BRC Effects of Defects Validation blades, subsequently referred to as simply BRC blades, are based on the SNL BSDS design. Two BRC blades were delivered, one with a glass spar and another with a carbon spar. A list of the defects and locations are given in the following two tables.

Table 18: Location of Bondline Flaws in EOD Blades.

| *Region* | *Flaw ID* | *Flaw Type* | *Flaw Size* | *In-Joint Flaw Location* | *Flaw Station (mm)* |
|---|---|---|---|---|---|
| **Shear Web - HP** | SW1 (AANC 8) | Pillow Insert | 0.5" (12.7 mm) | SC surface (Interface 1) | 2100 |
| | SW2 | Bubble/PTFE Void | 1.0" (25.4 mm) | SW surface (Interface 2) | 4100 |
| | SW3 (AANC 9) | Microballoon | 0.75" (19.0 mm) | SW surface (Interface 2) | 5400 |
| | SW4 (AANC 12) | Pillow Insert | 0.5" (12.7 mm) | SW surface (Interface 2) | 6750 |
| **Shear Web – LP** | SW6 | PTFE Strip | 1.0” (25.4 mm) | SW surface (Interface 2) | 4000 |
| **Leading Edge** | LE1 | PTFE Strip | 0.5” (12.7 mm) | LP surface | 750 |
| | LE2 | PTFE Strip | 0.5” (12.7 mm) | LP surface | 3000 |
| | LE3 | PTFE Strip | 1.0” (25.4 mm) | LP surface | 7500 |
| **Trailing Edge** | TE1 (AANC 10) | Pillow Insert | 0.5" (19.0 mm) | HP surface | 4500 |
| | TE2 (AANC 13) | Pillow Insert | 0.5" (19.0 mm) | LP surface | 5500 |
| | TE3 (AANC 11) | Microballoon | 0.75" (19.0 mm) | LP surface | 6000 |
| | TE5 | PTFE | 1.0” (25.4 mm) | HP surface | 7500 |

Table 19: Location of Laminate Flaws in Carbon Blade

| ***Bond Region*** | ***Flaw ID*** | ***Flaw Type*** | ***Flaw Magnitude*** | ***Surface of Blade*** | ***Depth of Flaw*** | ***Flaw Spanwise Station (mm)*** |
|---|---|---|---|---|---|---|
| Root Section | AANC 7 | Pillow Insert | 0.5" (12.7 mm) | HP surface | Layer 39 | 320 |
| | AANC 5 | Pillow Insert | 0.5" (12.7 mm) | HP surface | Layer 28 | 350 |
| | AANC 2 | Pillow Insert | 0.5" (12.7 mm) | HP surface | Layer 15 | 305 |
| | CH1 | Porosity | TBD | HP surface | All | 400 |
| | CH2 | OP | 6.5 | HP surface | Approx Layer 38 | 165 |
| | CL1 | Porosity | TBD | LP surface | All | 400 |
| | CL2 | OP | 4 | LP surface | Approx Layer 38 | ?? |
| Spar Cap - HP | | Pillow Insert | 0.5" (12.7 mm) | HP surface | Layer 10 | 5750 |
| | | Pillow Insert | 0.5" (12.7 mm) | HP surface | Layer 26 | 3000 |
| | | Pillow Insert | 0.5" (12.7 mm) | HP surface | Layer 18 | 5500 |
| | CH3 | IP | 4.95 | HP surface | Layers 7, 11, 15, 19, 23, 27, 31 | 1600 |
| | CH4 | Porosity | TBD | HP surface | All | 1800 |
| | CH5 | OP-Prox | 5.7 | HP surface | Layers 10-31 | 2250 |
| | CH6 | OP-Prox | 5.77 | HP surface | Layers 10-31 | 2300 |
| | CH7 | OP | 5.5 | HP surface | Layers 10-31 | 2750 |
| | CH8 | Porosity | TBD | HP surface | All | 3200 |
| | CH9 | OP | 9.95 | HP surface | Layers 10-31 | 3750 |
| | CH10 | IP | 6.89 | HP surface | Layers 7, 11, 15, 19, 23, 27, 31 | 4215 |
| | CH11 | OP-chain | 6.04 | HP surface | Layers 10-31 | 4700 |
| | CH12 | IP-chain | 7.62 | HP surface | Layers 7, 11, 15, 19, 23, 27, 31 | 5017 |
| | CH13 | IP-Prox | 5.63 | HP surface | Layers 7, 11, 15, 19, 23, 27, 31 | 6220 |
| | CH14 | IP-Prox | 5.59 | HP surface | Layers 7, 11, 15, 19, 23, 27, 31 | 6270 |
| | CH15 | Porosity | TBD | HP surface | All | 7000 |
| Spar Cap - LP | CL3 | IP | 5.01 | LP surface | Layers 7, 11, 15, 19, 23, 27, 31 | 1600 |
| | CL4 | Porosity | TBD | LP surface | All | 1800 |
| | CL5 | IP-Prox | 4.72 | LP surface | Layers 7, 11, 15, 19, 23, 27, 31 | 2240 |
| | CL6 | IP-Prox | 4.92 | LP surface | Layers 7, 11, 15, 19, 23, 27, 31 | 2300 |
| | CL7 | OP | 2.9 | LP surface | Layers 10-31 | 2750 |
| | CL8 | Porosity | TBD | LP surface | All | 3200 |
| | CL9 | OP | 4.68 | LP surface | Layers 10-31 | 3750 |
| | CL10 | IP | 7.69 | LP surface | Layers 7, 11, 15, 19, 23, 27, 31 | 4200 |
| | CL11 | OP-chain | 2.6 deg | LP surface | Layers 10-31 | 4700 |
| | CL12 | IP-chain | 7.72 | LP surface | Layers 7, 11, 15, 19, 23, 27, 31 | 5000 |
| | CL13 | OP-Prox | 3.12 | LP surface | Layers 10-31 | 6200 |
| | CL14 | OP-Prox | 3.63 | LP surface | Layers 10-31 | 6250 |
| | CL15 | Porosity | TBD | LP surface | All | 7000 |

In-Plane Wave Manufacture

In-plane waves were created in a laminate using the jig shown in Figure 91. The jig, designed and built by undergraduate assistant Julie Workman, was made up of 19 bars with a linear row of pins in each bar. Each bar (with pins) was free to move in-plane. At the location of each in-plane wave, the fabric of the spar cap laminate was pressed down on to the pins, as is shown in Figure 92. When the bar was shifted, in-plane it forced the spar cap laminate at that location, to be displaced or shifted in the plane of the skin. Masking tape temporarily held the bars in place and the setup was left untouched for at least 15 minutes so the fibers making up the in-plane wave would stabilize in place.

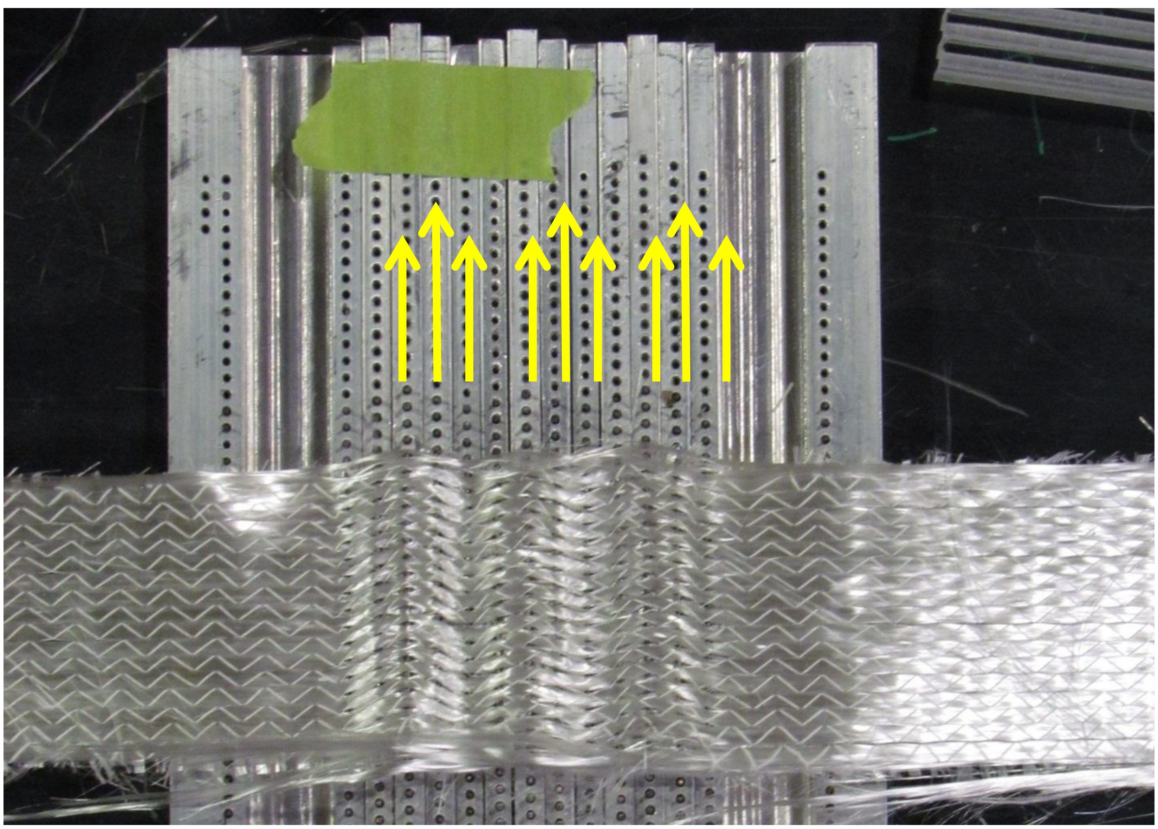

Figure 91: Photo of MSU jig creating three IP waves in one fiberglass laminate

Figure 92: Photo showing IP waves formed into one carbon laminate of the spar cap

After each in-plane wave was created, the geometry of the in-plane wave was measured, as is shown in Figure 93, to determine the Fiber Angle Misalignment. To verify the geometry of each in-plane wave had not changed in the handling process, the Fiber Angle Misalignment was checked and rechecked several times until the laminate was covered up in the layup process. It turned out the in-plane wave geometry was very stable and did not change.

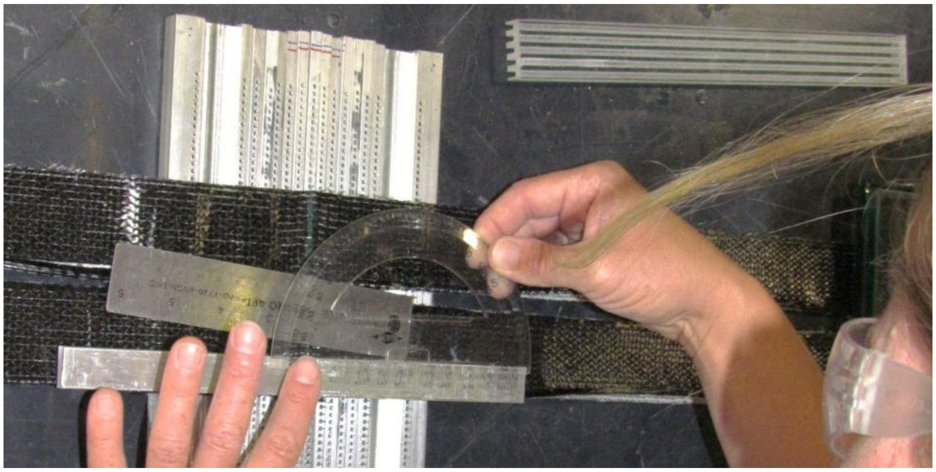

Figure 93: Photo showing an IP wave Fiber Angle Misalignment being measured.

In-plane waves were created in a spar cap by creating in-plane waves at the same point in each of the seven laminates that made up the spar cap. The MSU team constructed the in-plane waves, and the TPI blade fabrication shop floor staff worked with the teams from MSU and SNL to carefully and accurately install and align the flaws in the Effects of Defects validation blades. Each in-plane flaw in and along the spar cap laminate was carefully aligned and stacked onto the underlying in-plane flaw, as is shown in Figure 94.

Figure 94: Photo showing a group effort to align the IP waves in the carbon spar cap.

Out-of-Plane Wave Flaw Manufacture

Out-of-plane waves were created by stacking a defined number of precut layers of PPG 1250-2026 glass fabric onto the spar cap. Figure 95 shows several precut layers being cut from a strip of fiberglass fabric.

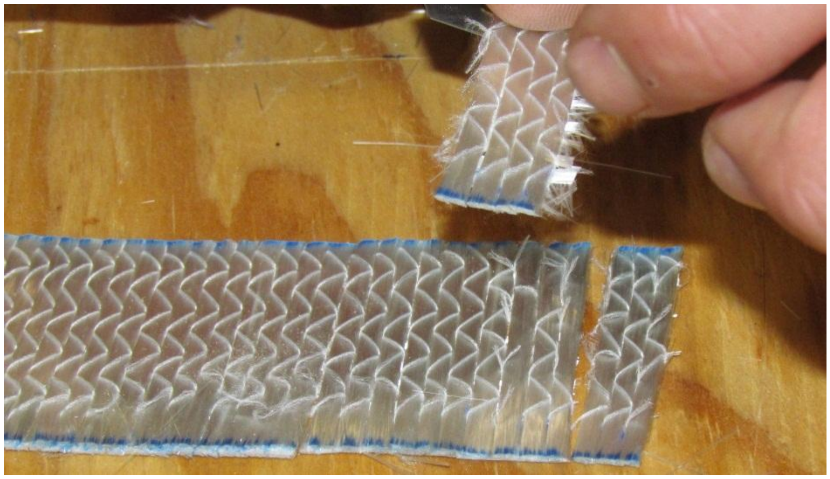

Figure 95: Photo of OP layers being cut from a sheet of fiberglass fabric.

The following process developed by Dan Guest describes the details for constructing OP waves in composite laminates using glass fiber tow bundle build-ups. All waves forming build-ups, were constructed using PPG 1250-2026 fabric architecture. The critical element in manufacturing OP Waves is the stacking sequence. The following list outlines a few of the stacking sequences which were most useful during the BRC EOD Blade construction process. In this list, stacking sequence is always labeled such that left to right corresponds to from bottom to top of the wave form.

For the carbon (hybrid) laminates:

3-5$^{o}$ OP wave - 2 (# of tow bundles in first row)
6-7$^{o}$ OP wave - 3/1
12-15$^{o}$ OP wave - 5/4/3/2

For the glass laminates:

3-5$^{o}$ OP wave - 2 (# of tow bundles in first row)
6-7$^{o}$ OP wave - 4/3
13-15$^{o}$ OP wave - 5/4/4/3

See Figure 96 for an example cross section detail, as to how the stacking sequence works for the 13-15$^{o}$ wave build-up

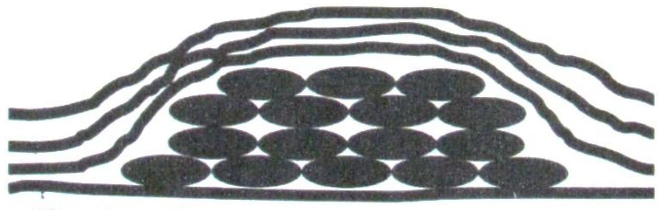

Figure 96: Stacking sequence for the wave build-up 5/4/4/3.

The first step in constructing OP waves, is to prepare the tow bundles in the appropriate lengths. If a specific wave is to be more than 10" in length cut the bundles down to lengths no longer than 10" to facilitate completed saturation. Cut the tows per the stacking sequence outlined and set them carefully to the side until all necessary tows have been cut.

Figure 97 displays one OP wave and Figure 98 shows the start of five OP waves in the BRC EOD blade with a carbon spar cap.

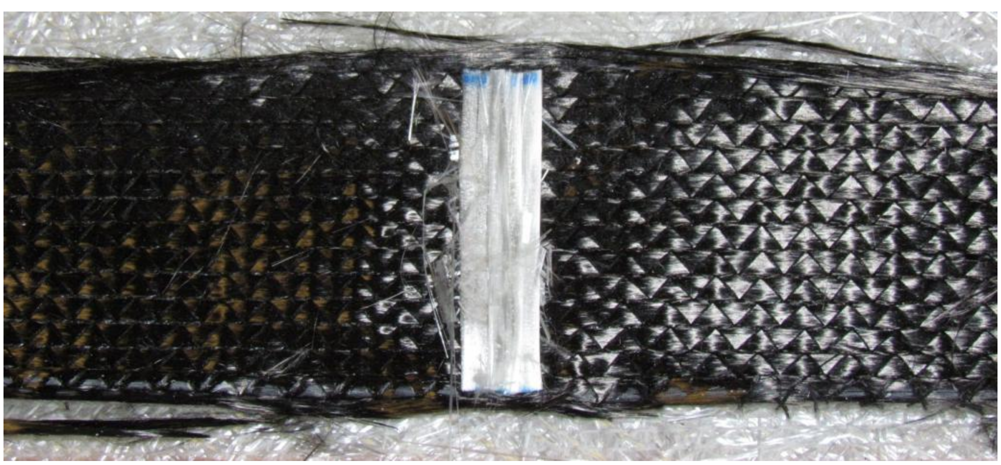

Figure 97: Photo showing a stack of glass fibers that will create one OP wave.

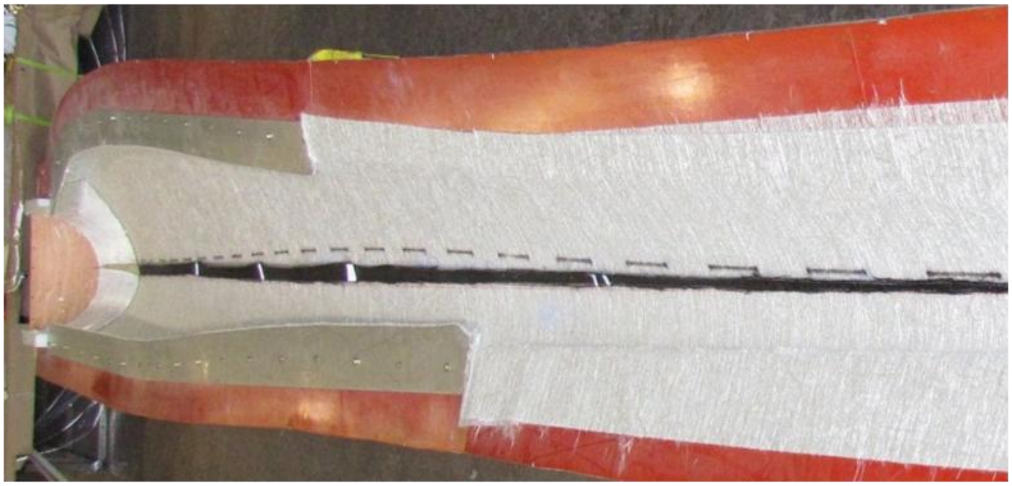

Figure 98: Photo showing the start of five OP waves in the carbon spar cap.

Implementation of Laminate and Adhesive Voids

In addition to flaws placed in the laminate by the MSU team voids were also introduced by Sandia National Laboratories Air Worthiness Assurance Center into bonds and laminates. No analysis was performed by the MSU team on these flaws. A description of these flaws can be found in Ref. [86].

Implementation of Porosity Flaws

Several areas down the length of the spar and in the root section were chosen for placement of dispersed porosity defects. These flaws were formed by using a syringe to inject a specific volume of air into the laminate (Figure 99). After the skins had cured for 180 minutes, air was injected into the root build-up, and into panel sections of the blade to induce areas of porosity in the skin.

Figure 99: Injection of air to generate porosity in a partially cured skin.

## Blade Testing

The target test loads were chosen based on the MSU finite element analysis described in the preceding sections, as well as a preliminary beam analysis performed by Joshua Paquette of  Sandia National Laboratories.  All test loads were initially designed to induce a fatigue failure at 100,000 cycles. Three loading locations were chosen, consistent with the earlier discussion. All stations were loaded through the use of hydraulic cylinders connected to saddles on the blade (Figure 100). Table 20 provides the test loads and loading schedule for the test.  Displacement values were generated with the finite element model to describe the displacement at the actuator location. Strain values presented were also generated from the finite element analysis. Values given are for the flaw locations where failure was expected. Figure 101 provides the resulting moment distributions (generated through closed-form beam analysis) down the length of the blade. Figure 102 provides estimated strain distributions for each load block as calculated by the finite element model.


Figure 100: Fatigue test at the 7m station

Table 20: Initial Test Loads and Fatigue Loading Sequence

| Load Block | Orientation | Location (m) | Applied Load (kN) | Max Target Root Moment (kN-m) | Predicted Displacement (m) | Predicted Strain (ue) |
|---|---|---|---|---|---|---|
| 1 | Flap | 7 | 3.23 | 22.60 | 0.584 | 4006 |
| 2 | Flap | 6.17 | 7.22 | 44.55 | 0.497 | 4252 |
| 3 | Flap | 4.37 | 16.66 | 72.83 | 0.172 | 6270 |

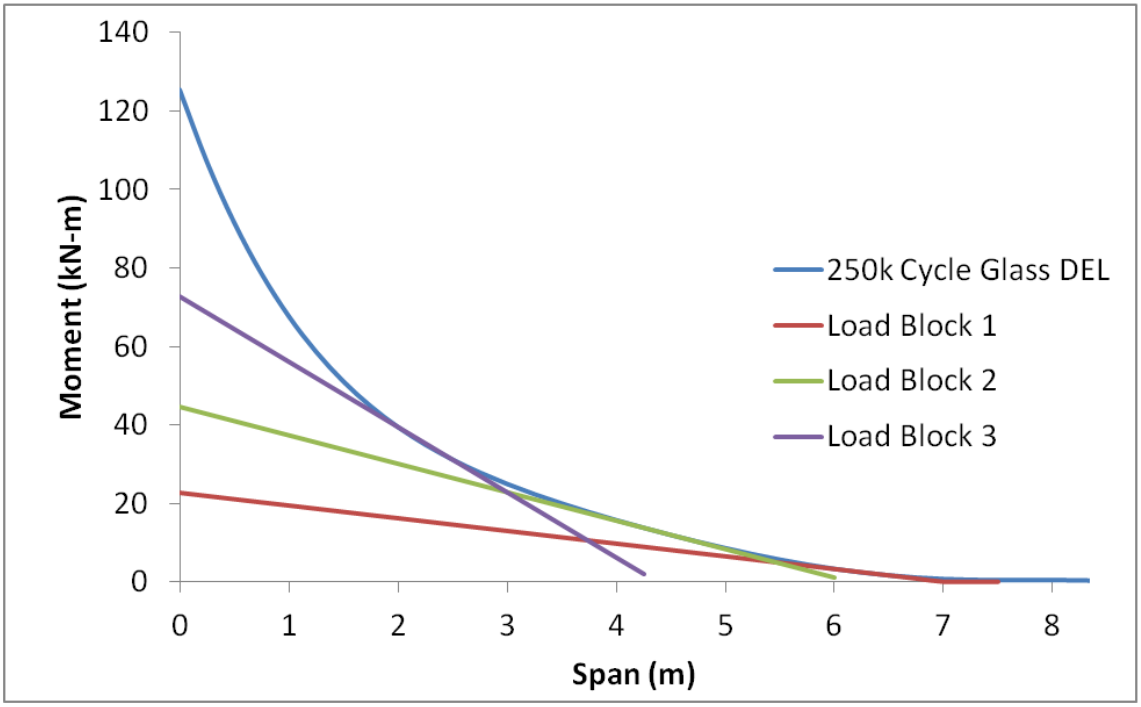


Figure 101: Test Moment Distributions

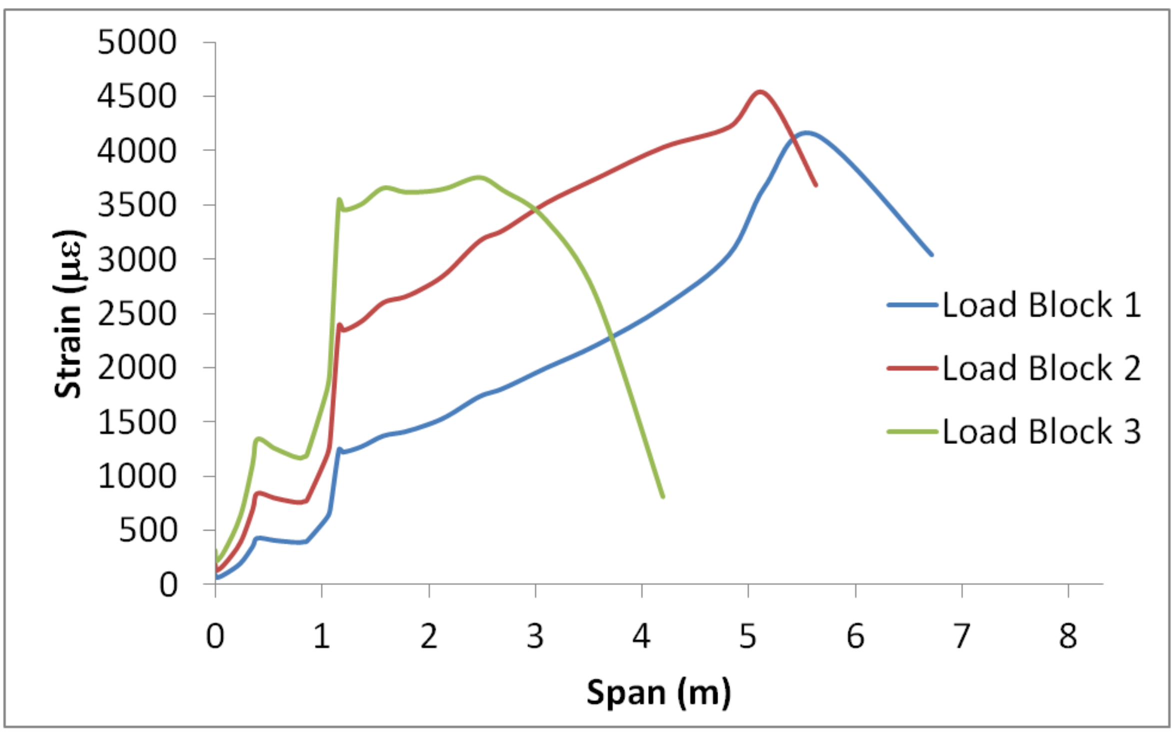


Figure 102: Predicted Strains Profiles

The strain data displayed in Figure 102, were used to validate the finite element model. Sixteen flaw locations were chosen for Aramis Digital Image Correlation (DIC). These locations were all speckled with the necessary DIC imaging pattern. All locations were initially imaged to provide correlation to the models. However, once the testing began, only 3 to 4 defect locations were imaged for each test locations. These flaws were those deemed most critical by the earlier fatigue analysis.

## Results & Discussion

DIC provides data describing the full strain field within the imaging location. In all cases, strain values measured by the DIC system were within 5% of the predicted values, indicating that the finite element model was quite accurate. While the DIC provided strain values consistent with the finite element blade model, it was regrettably unable to detect any specific flaw induced damage for correlations to defect geometry. While the correlation to the progressive damage modeling performed by Jared Nelson suffered as a result, useful data was still generated to verify the PReP analysis and algorithms for the glass blade. These correlations are presented in Chapter 9: Results and Discussion. The final fatigue test loads and locations for the glass blade are given in the following table.

Table 21: Glass blade fatigue test summary

| Test Block | Load Application Location (m) | Max Load (lb) | Max Load (kN) | Loading Cycles |
|---|---|---|---|---|
| 1 | 7.0 | 850 | 3781 | 120557 |
| 2 | 7.0 | 900 | 4003 | 16381 |
| 3* | 7.0 | 500 | 2224 | 7523 |
| 4* | 7.0 | 900 | 4003 | 6635 |
| 5* | 7.0 | 1200 | 5338 | 36292 |
| 6* | 7.0 | 1450 | 6450 | 4062 |
| 7 | 6.0 | 1500 | 6672 | 1279 |
| 8 | 6.0 | 1800 | 8006 | 3641 |
| 9 | 6.0 | 2200 | 9786 | 55593 |
| 10 | 6.0 | 2780 | 12365 | 103801 |
| 11 | 6.0 | 2890 | 12855 | 238936 |

* Clamped at 6m location

The blade failed catastrophically at two locations. The third test sequence was stopped after the most inboard failure location exhibited a significant loss in stiffness. However, a catastrophic failure was not observed. The first failure occurred at the Low Pressure 6.2 m station where a 4deg OP Proximity Wave was located while loading at the 7m station. The failure is displayed in Figure 103. The second failure occurred at the High Pressure 3.75m station where a 10deg OP Wave was located while loading at the 6m station. The failure is displayed in Figure 104. The third failure did not occur at flaw location. It did however occur at the triangular region previously identified as a potential failure location. This failure locations is displayed in Figure 105.

Figure 103: OP Proximity Wave failure at the 6.2m LP location

Figure 104: OP Wave failure at the 3.75m HP location


Figure 105: Failure at the 1.2 m location

# CHAPTER 8

# SURROGATE MODEL FOR CRITICALITY

## Machine Learning

There are many elements that play a role in failure, some global or macro and some local or micro most all of which can be captured in a PFEA. While this type of analysis will provide the designing engineer with significant insight, the complexity and computational costs render it unusable for case-by-case in-situ reliability estimation. There exists a need to evaluate the reliability of a structure quickly on the manufacturers' floor as a quality control effort or in the field by technicians, that capture more information than a 'not to exceed' specification. This type of an assessment needs to be fast, accurate and interfaced in a stand-alone fashion, transparent to the user.

One approach that has been taken in recent years has been to use SL techniques to produce a surrogate model of the finite element solver that provides the value of the performance function g(x). These applications generally follow a regression approach. However, the reliability problem can be regarded as a classification task. Defining the safe and failure classes as $g(x)>0$ and $g(x)<0$ respectively, a classification function can be used for the disposition of new samples in the training data based solely on sign (Equation 36). [87] Both techniques were assessed in this body of work.

$$c(x) = sgn(g(x)) \tag{36}$$

The fundamental approach to supervised statistical leaning consists of 3 elements: a random vector generator function, a supervisor, and a learning machine. The vector generator produces random vectors x, consisting of the random variables sampled from the joint distributions. The supervisor yields the correct class label (c) which corresponds to a vector of sampled variables, x. The supervisor in this case is the PFEA. There are many classical and modern classification methods which can be used for the learning machine. Methods evaluated for this analysis include Fisher Discrimination, Bayesian Classification, Classification Trees, Probabilistic Neural Networks, Multi- Layer Perceptrons and Support Vector Machines. Models that have shown the most success for these types of problems and were therefore compared in this investigation are; Multi-Layer Perceptrons (MLP) and Support Vector Machines (SVM). In classification analysis, the MLP models is described as follows: [88]

$$g(x) = \bar{h}(\sum_{k=0}^{m} w_k h(\sum_{j=0}^{d} w_{kj} x_j)) \qquad (37)$$

where a problem has number of dimensions d and m number of hidden layer neurons. Sigmoid functions are typically used for the h functions. The weights, w, can be optimized by minimization of the square error function sum (Equation 38). [88]

$$R_c = \frac{1}{2} \sum_{j=1}^{l} (c_j(x) - \hat{c_j}(x))^2 \qquad (38)$$

The SVM has model of form described by Equation 39 where $\alpha_i$ are Langragian multipliers, b is a threshold and s the number of support vectors.. Particular emphasis is placed on the kernel function, K. Several functions were evaluated: polynomial, Fourier, sigmoidal, and inverse multiquadric. The Radial Basis Function (Equation 40), was chosen for this analysis. [87]

$$g(x) = \sum_{i=1}^{s} \alpha_i c(x_i)(K(x_i, x) + b) \qquad (39)$$

$$K(x, y) = \exp(-\zeta \|x - y\|^2) \qquad (40)$$

Data on flaw location, magnitude, strain response and probability of failure was generated in the Monte Carlo simulations and used for training the SL algorithms. Both techniques, regression and classification were successful at predicting the PFEA response given an input set of data. The regression technique was used to generate localized strain and damage accumulation response which can be of use to the designer assessing sensitivities and performing optimization on a structure.

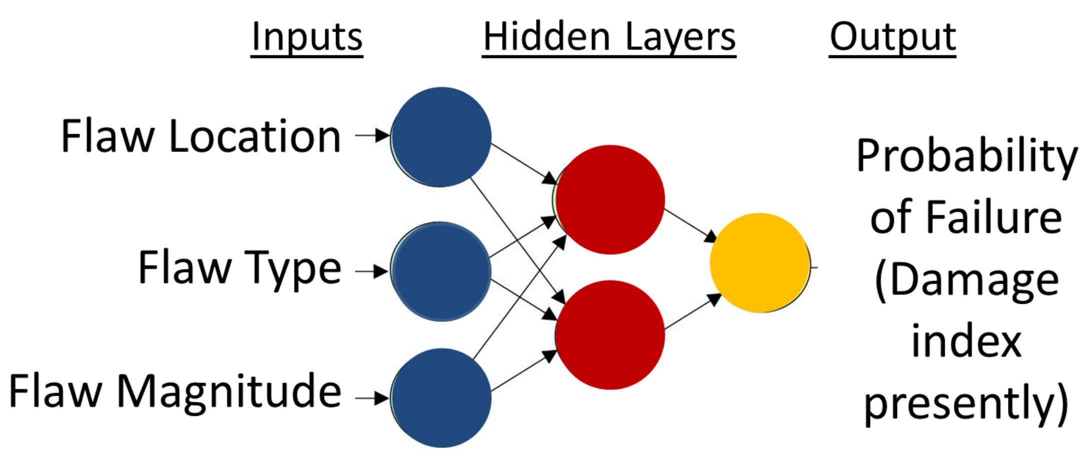


Figure 106: Conceptual representation of SL algorithms

## Surrogate Model Interface and Preliminary Results

As described in the preceding section the original direction of this investigation was to look at performing classification tasks (i.e. fail or does not fail). However, it was concluded that a functional approximation would be more useful. By employing this technique, the algorithm was expected to produce the actual probability of failure given the specific inputs. The training data inputs were made up of many data sets each of which represented a discrete Monte Carlo simulation. Each training data set was structured such that it contained results for 100 positions down the spar cap of each side

(200 location strings total). Each string contains identifiers describing the inputs (flaw type and magnitude) and the model output (probability of failure ).

Various algorithms were then used to correlate the inputs to a continuous output. This approach allows for approximation of the exact probability of failure given the inputs. Probability of failure was defined from 0 to 1 where 0 represents 0% chance of probability of failure and 1 represents 100% probability of failure. Two different algorithms were used with varying success. They can be summarized as follows;

- Multilayer Perceptron = 70% error
- Support Vector Machine = 70% error

These results were less than ideal, so a second round of analysis was performed. It was hypothesized that reducing the possible output values would also reduce the model error. For the second attempt the output data was binned into 11 bins of 0.1 increments. In other words if the Monte Carlo simulation predicted a Pf of 0.37 for a particular discrete analysis the output training value for this data set was rounded to 0.4. Due to the computational time associate with the statistical learning algorithms only Multilayer Perceptron were used in this second case. By binning the data it was found that the error was reduced by more than half to 30%. The increase in accuracy is encouraging, however still unacceptable.

Should this investigation continue the original approach to a classification task seems reasonable. It stands to reason that significant reductions in error would be achieved by minimizing the potential output response even further. Such is the approach to a classification task, wherein the data would effectively be binned into to the output responses. The previous discussion considered two classes: safe and failed. However, in light of the research developments made by this body of work, a reformulation of the class states could be performed to better address the reliability of a structure with flaws. Similar to the Time-to-Failure formulation presented in Chapter 6, the analysis or decision maker could specify an acceptable value for probability of failure. For instance, should $P_f = 0.15$ be chosen, then the output response would be divided into two sets greater than and less than 0.15. The two states would then designate un-safe or repair and safe or operational ready.

## Criticality Estimation

Use of these models have yielded success as a surrogate model for predicting the probability of failure and detailed structural response. However, this information may be inadequate or unintuitive for performing an in-situ risk analysis concerned with disposition of flaws in composite structures. The next step is to incorporate the results of PReP into a Criticality Assessment (CA).

Failure Modes and Effects Criticality Analysis (FMECA) was originally developed by the US Military in the late 1940s. It was later further developed and applied by NASA in the 1960's to improve and verify the reliability of space program hardware. Used as a reliability evaluation technique to determine the effect of system and equipment failures, failures were classified according to their impact on mission success and personnel/equipment safety. Over the years the analysis has been fine tuned and transcribed by military standards and technical memorandums. [89; 90]

FMECA is an analysis technique that facilitates the identification of potential problems in the design or manufacturing process by examining the effects of failures. Recommended actions or compensating provisions are made to reduce the likelihood of the problem occurring and/or mitigate risk of a failure. The FMECA has been adopted herein and is under modification to better address the issue of reliability for wind turbine blades. There are two general parameters that define a space in which reliability issues are evaluated; criticality and severity. The Military Standard 1629A defines these parameters as follows:

*Criticality:* A measure of the frequency of occurrence of an effect. This value may be based on qualitative judgment or on failure rate data.

*Severity:* Considers the worst possible consequence of a failure classified by the degree of injury, property damage, system damage and mission loss that could occur.

In general, this analysis was developed to assess components in a system rather than a particular structure. However, the approach could be modified to view various structural details as components in a large structure. This view point is consistent with the recently popular systems engineering approach. A variation of this concept is employed in PReP for developing the Criticality Assessment. In order to facilitate this transition the definitions for criticality and severity have been modified for evaluations of wind turbine blades as follows;

*Criticality:* Quantitative designation of the sensitivity of a structural region to a flaw. Established through comprehensive structural analysis.

*Severity:* Quantitative description of the effect a flaw has on the material under consideration. Established through comprehensive Effects of Defects testing.

Similar to the surrogate model, the primary objective of this effort, is to establish a tool for reliability evaluations of flaws in-situ by manufacturers, turbine installers and maintenance technicians. This procedure combines flaw geometry data, mechanical response models, and blade information. The proposed Criticality Matrix is an efficient procedure for evaluating the reliable operation (or risk) of an as-built composite structure with known defects.

An example of the current revision criticality analysis has been performed on the flaws placed into the low pressure side of the BRC EOD blade test article. For this case, the severity number is tantamount to the reduction in ultimate strength of a laminate with flaws as found in the Effects of Defects testing program. For instance, an IP wave with a 6 degree misalignment angle may have a reduced static strength of 25%. Therefore, it's severity number is 0.25. The Criticality Number was generated from the PFEA described in Chapter 6. EOD Blade location 21 exhibited the highest region of strain concentration in the structural analysis. Strain data as a function of location, was normalized to the max strain found at this area. This concept is illustrated in Figure 107. Here it can be seen that Location 21 has a criticality number of 1 and all other locations have a criticality number less than 1.

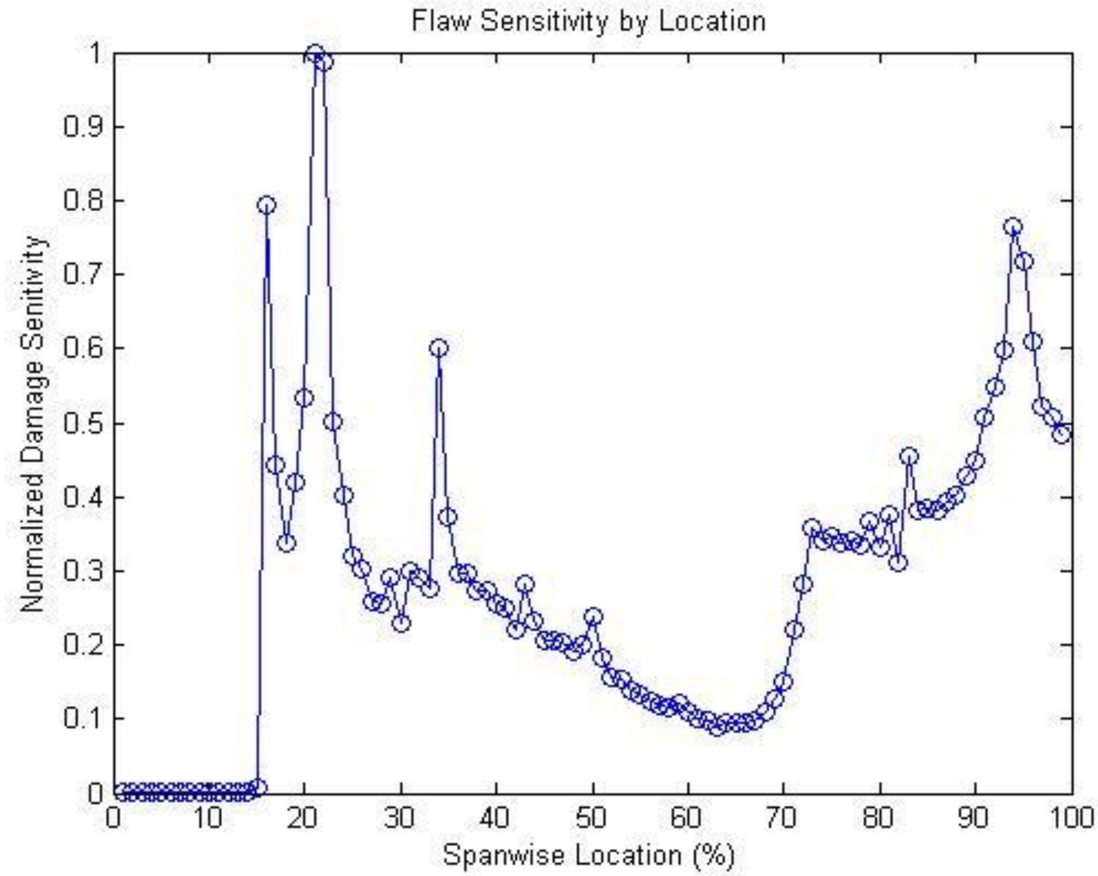


Figure 107: Criticality number by location

The graphed results of the example Criticality Analysis are displayed by the Criticality Matrix (CM) in Figure 108. This example illustrates how criticality and severity are mapped and quadrants are established describing the risk of a specific flaw instance. At present, the risk quadrants and severity designations are place holders. Further analysis and input from manufacturers will help define the quadrant space. The original Critically Matrix concept was developed arbitrarily, with a generic flaw base and location sensitivity, to define the approach. Figure 108 was the example generated to illustrate how a very severe flaw may not be critical at the evaluation time. However, a less severe flaw considering other parameters has a high risk. For instance, flaws 101 and

104 have almost identical characterization parameters and, therefore, have significant structural implication to the local region. However, flaw 101 is not located in a high strain region, and therefore, may be consider non-critical. These flaws, and the others notated in the graph do not hold any significant meaning, but rather are just intended as visual cues.

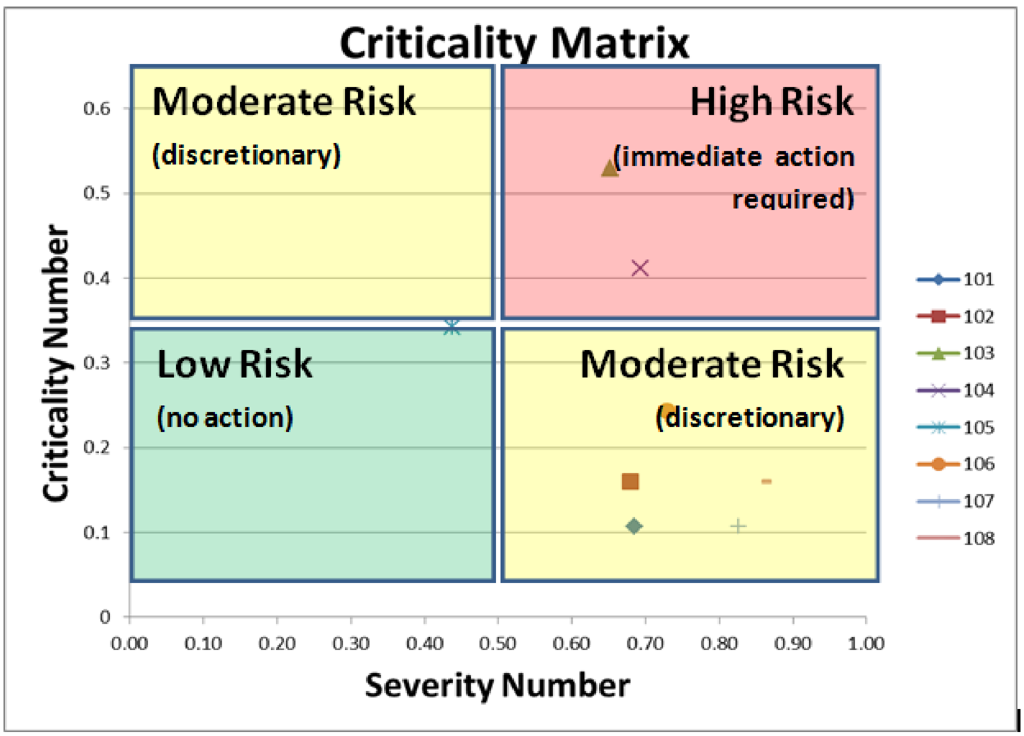


Figure 108: Criticality Matrix

While the previous discussion was conceptual, a Criticality Matrix was built for the EOD Blades. In doing so all of the flaws introduced into the two blades were plotted. The compliment of the knockdown factor for each flaw were input on the X-axis as the severity designation. Each blade test was actually a series of three fatigue tests, wherein three different locations were actuated. Each load location had a different strain response in the blade and therefore a CM had to be built for each test. The strain response of the flaw locations were normalized as described earlier by Figure 107. The corresponding normalized sensitivity value for each flaw location was then entered in the CM for the Y-axis criticality value.

Figure 109 displays two Criticality Matrices; (a) is for the first load station of the blade test, (b) is for the second load station, and (c) describes the final test. The outliners are circled by the black oval were porosity flaws. The value of porosity was never confirmed, therefore these flaws were never actually considered critical. Therefore, they are indicated here as outliers and not included in the matrix risk blocks. For each of the two images, red diamonds indicate the flaw which failured during that test. The other black markers indicate flaws that failed in subsequent tests. Descriptions for each of the flaws are given in Chapter 7.

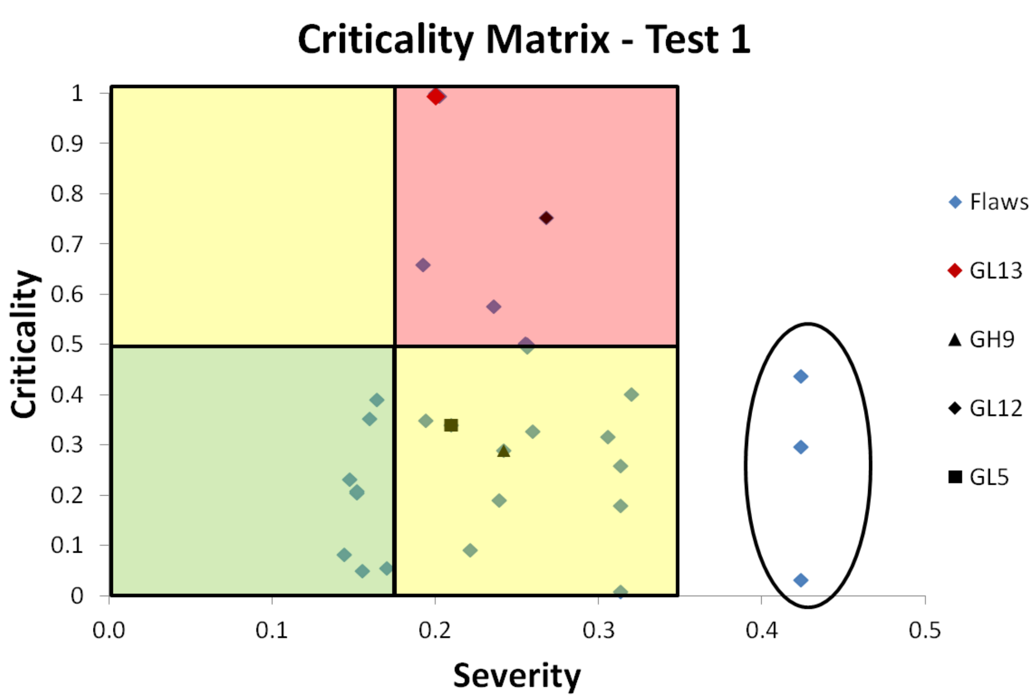


**(a)**

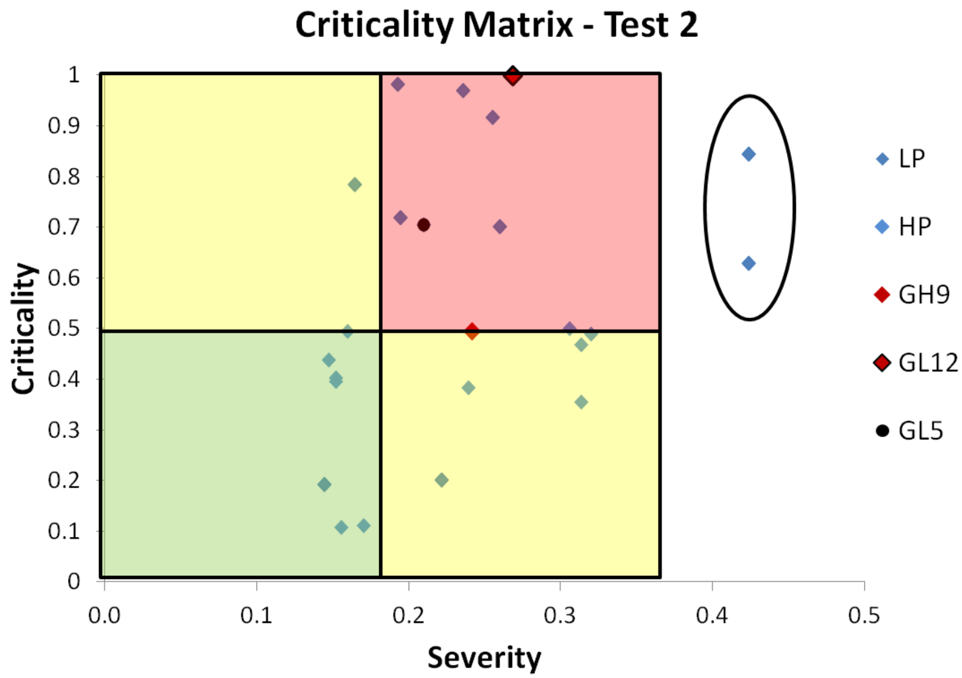


**(b)**

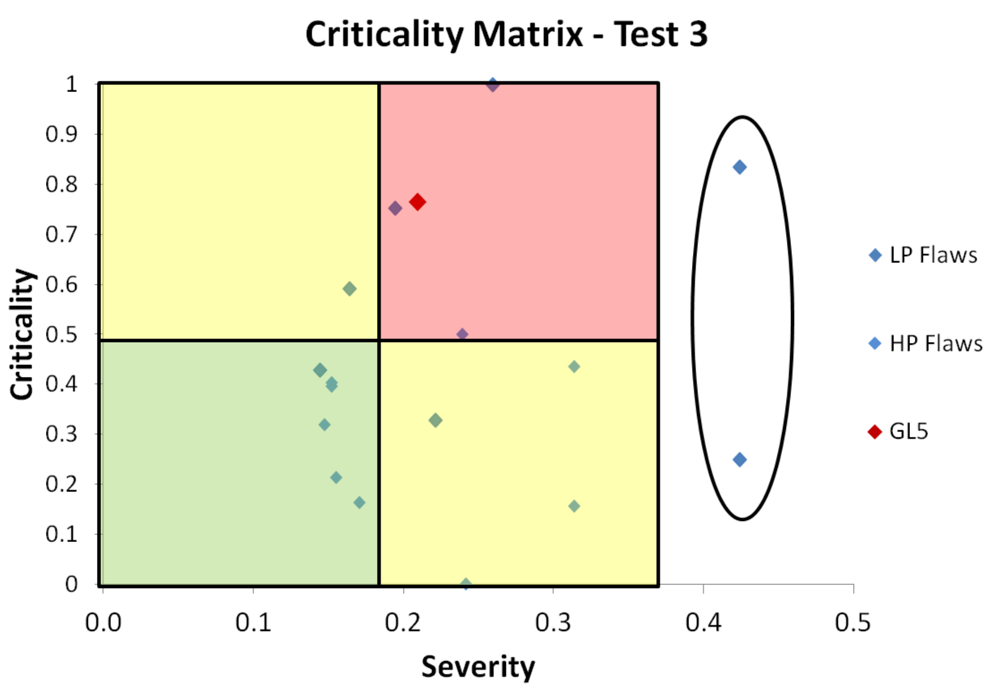


**(c)**

Figure 109: Criticality Matrix Blade Test 1(a) Test 2 (b) and Test 3 (c)

A Criticality Matrix which would store data for all locations and inspections of every location is probably not realistic. A second approach to performing a Criticality Assessment that conveys useful information of particular locations which may be problematic has been developed. This variation is called the Criticality Map. The Criticality Map is a visual quality control tool that the designing engineer can easily generate, to express the need of focusing QC efforts in certain areas, referred to as Regions of Interests (ROI).

As an example, this approach has been applied to the EOD Blade. The resulting Criticality Map is displayed in Figure 110. For this example 4 ROIs have been identified as particularly sensitive to defects based on the structural analysis of blade described in Chapter 6. For each ROI a table is given detailing three risk categories. The risk categories are based on defect knockdown factors, or the probability of failure for teat location. For this illustration, defects that have less than a 5% knockdown or probability of failure are considered low risk. In between 5 and 15% is considered moderate risk which could possibly require further analysis by an engineer to assess the disposition of the ROI. Greater than 15% is suggested as high risk and would require a repair.

| ROI | Flaw | Low Risk | Moderate Risk | High Risk |
|---|---|---|---|---|
| 1 | Porosity | % < 2% | 2% < % < 5% | % > 5% |
| | IP Wave | Angle < $7^{o}$ | $7^{o}$ < Angle < $12^{o}$ | Angle > $12^{o}$ |
| | OP Wave | Angle < $5^{o}$ | $5^{o}$ < Angle < $10^{o}$ | Angle > $10^{o}$ |

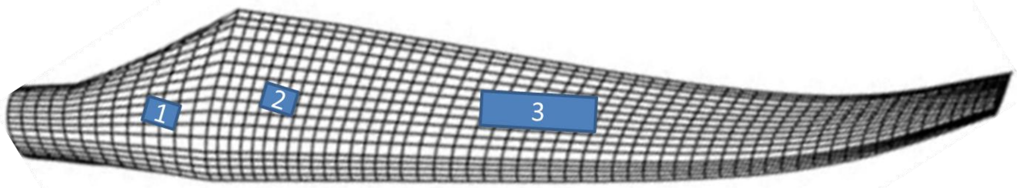


| | | |
|---|---|---|
| **Low Risk**<br>**$P_f$ > 0.05%**<br>**(no action)** | **Moderate Risk**<br>**0.05 < $P_f$ < 0.15**<br>**(discretionary)** | **High Risk**<br>**$P_f$ > 0.15%**<br>**(immediate action required)** |

Figure 110: Criticality map

# CHAPTER 9

# RESULTS AND DISCUSSION

## Experimental

### Coupon Testing

The laboratory testing program described in Chapter 5, has shown that, with proper characterization, it is possible to establish the structural implication of a flaw. Preliminary statistics have been reported which show that flaws generally occur with frequencies predominantly described by the Normal and two parameter Weibull distribution. Results of this investigation are based on a relatively small data set. Applying the characterization techniques described herein to incoming data will enable the generation of a statistically significant and comprehensive flaw database.

Flaw distributions were defined from observations in the field, which were focused on specific cut sections of several blades. These sections were cut after testing, because either the blade exhibited a visible anomaly at the surface or instrumentation at those locations showed a heightened strain response. Therefore, these locations were chosen for further post failure forensic evaluations. While the amount of viewed area was not quantified, it represented a very small portion of the total blade. Moreover, it was the observers objective to focus on acquiring data on flaws specifically. While analysis of the images was performed objectively, systematically and in a mathematical manner, this level of rigorousness was questionably not applied to the image collection process. Therefore, one could conclude that the data generated is biased.

Images were taken at will of flawed regions. The larger the flaw, the higher the chance the observer focused on it. No images were taken of unflawed regions by comparison. Initially, it was thought that enough data could be generated to properly assess both the probability of occurrence of a flaw and the flaw magnitude probability distribution. However, in hindsight one could almost say that the field survey was performed subjectively. While this process gave significant insight into the size, type and shape of wind blade flaws in general, the overall statistics could be called into question. This should in no way detract from the models proposed herein, as they stand-alone as numerically and functionally correct. It was this concern that led to Case 2 of the probabilistic analysis.

All testing of thin laminates with and without flaws showed appropriate mechanical responses and repeatable results. This coupled with the comprehensive nature of the testing has enabled the generation of database for which high levels of confidence exists. Data from the thin laminate testing has shown that these more consistent manufacturing processes have improved the range, and in some cases the consistency, of the test data. In particular, the new OP wave specimens showed failure modes more representative of what one would expect to see in the field.

A fairly comprehensive test program has shown that strength degradation in uni-directional laminates with waves tend to correlate well to the average fiber misalignment angle of all layers. Based on the success of these results a smaller test set was developed for more complicated layups (triax) and carbon laminates. The hypothesis was that trending of the reduced strength would remain relatively the same between the uni, multidirectional and carbon laminates. Therefore, only a minimal data set needed to be collected to verify this. Results from these testing efforts indicated that the In Plane waves were less severe in the multi-axial layups. Upon further thought one should expect this as the waves were only introduced in the uni-axial layer of the triax layup. Early testing showed that inducing IP waves in $\pm 45^0$ laminates yielded varied results some of which improved strength as the waves actually aligned the fibers better in the orientation of the applied load.

Compression of Out of Plane waves in the triax laminates suffered the same inconsistencies as Out of Plane waves in the uni laminates. It does appear that there again, the flaw has a somewhat diminished effect on strength as compared to the unidirectional specimen however no strong conclusions can be drawn. Tension of OP waves in both uni-axial and triax layups was successful. A small amount of testing was performed on the triax laminates to see if there was a correlation to the uni-axial response. However, it can be inferred by the knockdown factor displayed in Figure 111 that this is not readily apparent. The results indicate that that OP waves in a triax laminate are not as deleterious as in uni-axial laminate, however more testing is needed to confirm this.

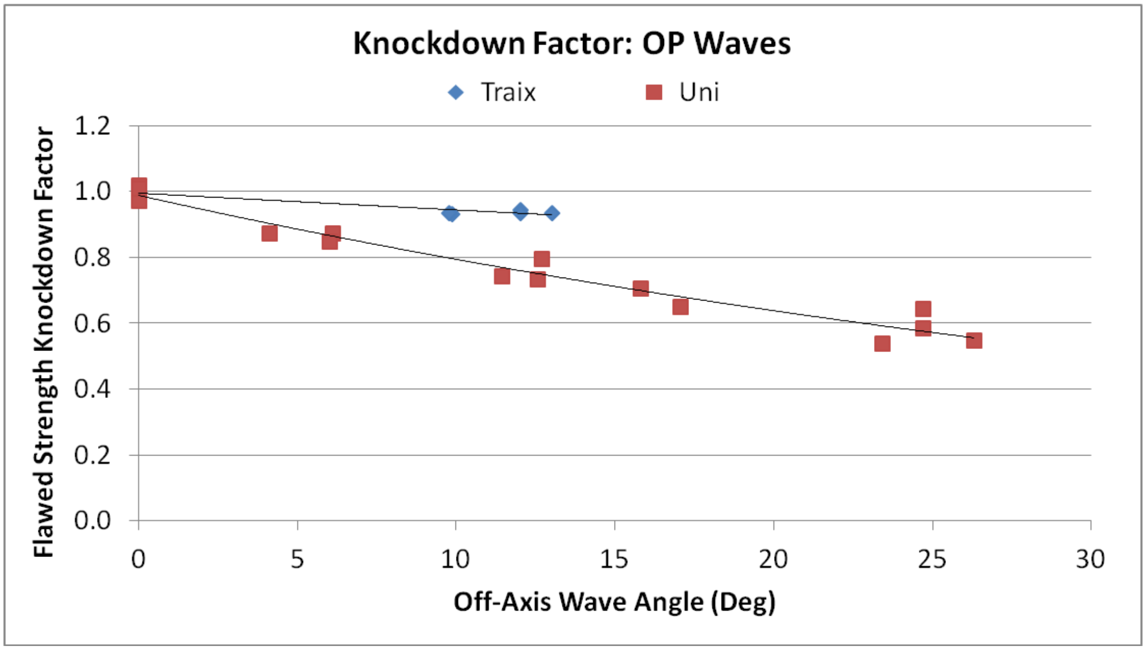


Figure 111: Comparison of OP wave strength reduction in tension

Due to scheduling conflicts, testing of uni-axial carbon samples with IP waves was not completed. Compression of OP waves in carbon uni-directional laminates once again was unsuccessful. Tension testing of OP waves in carbon were completed. A comparison between knockdown factors for OP waves in glass and carbon uni-direction laminates is shown in Figure 112. The carbon data set is limited but the results indicate that that OP waves are not as harmful to carbon laminates however more testing is needed. The hybrid laminate showed significant scatter in the control data. Due to this result comparison of strength reductions may not be considered accurate.

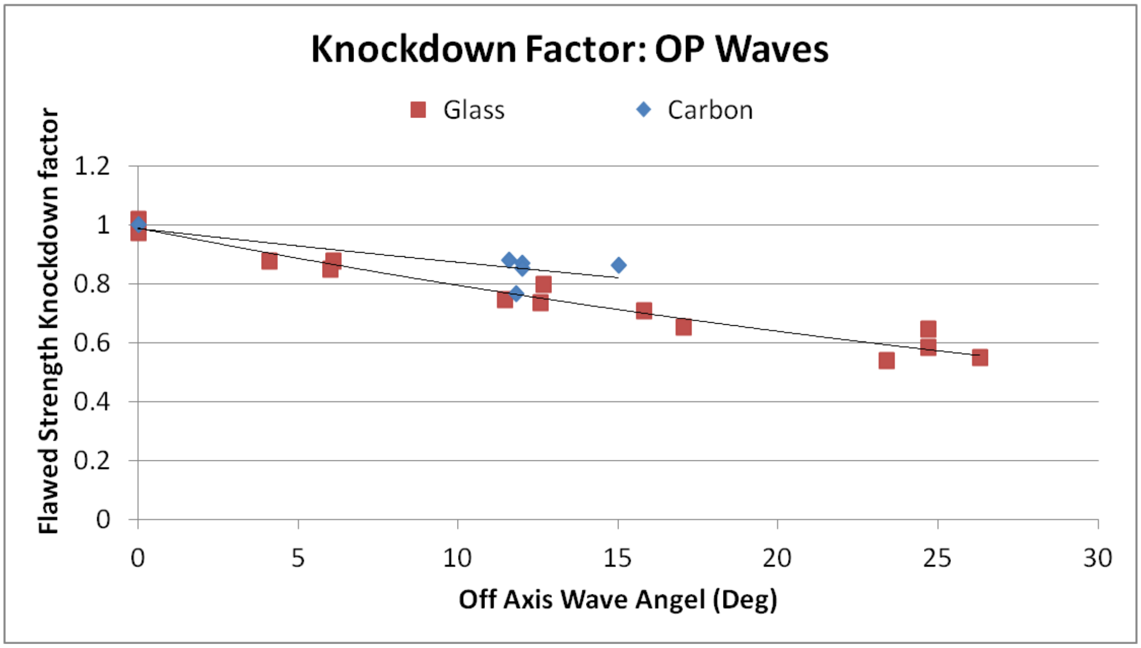


Figure 112: Comparison of OP wave strength reduction in tension

<u>Blade Testing Program</u>

The objective of the EOD blade testing program was twofold: to provide a test article for investigations of the capability of NDI technologies to "see" defects, and as mechanism to understand effect flaws have on a composite structure. The first objective of assessing NDI technologies was not under the purview of the MSU team. However, the flaws built into the blade by the MSU team were used by Sandia National Laboratories to evaluated NDI. The second objective can be considered in general, to be a success as the blade did fail at two flaw locations, and these failures allowed for the PReP algorithm to be verified.

During the design of the EOD blade program, the analysis described in the Chapter 7 was used as a starting place to define the flaws. The target test duration was 100k cycles for each of the three load introduction locations. At the onset of the testing each location was analyzed by using the PReP damage accumulation computation described in Chapter 6. In addition to the PReP approach, it was suggested by Sandia and NREL staff that a 30% scaling factor be applied to the fatigue life in the same manner as the knockdown factors. A critical flaw was found for each of the loading locations. The fatigue test load was then designated, by back solving for a failure in 100k cycles using the critical flaw and the fatigue life knockdown formulation (Equation 28).

Failure at the first load location (7m) was not achieved during the 100k cycles. Therefore the load level increased as reported in Table 21. Once failure was achieved the damage accumulation calculation was revisited. It was found that by reducing the coupon to full structure scaling factor to 18% an accurate prediction was achieved. The second fatigue test was then designed around this parameter. The prediction was found to be conservative, though it is not known exactly how conservative. During the first test the blade was clamped at the 6m station. This allowed for higher frequencies and larger loads to be applied. However, due to the pivot introduced at the 6m location the moment distribution was reversed inboard of the saddle. Therefore, the 2nd failure location was in compression during the second half of the first fatigue test block. The FEA blade model was updated with a boundary conditions similar to that of the 6m saddle however this configuration was never validated with the actual blade. Considering the fact that the prediction was conservative, it is assumed that the limited number of cycle with this change in R ratio had a negligible effect.

## Analytical

### Analysis Inputs

The blade modeled in this body of work was designed from a structural perspective, to be a scaled down version of a multi-megawatt design. While structural considerations were preserved, aerodynamic considerations were not. Therefore, an attempt at reverse engineering the blade, through an aeroelastic simulation, would have yielded unrealistic results. For proving the feasibility of this analysis, a simplistic load scenario is just as useful as a complicated one. Therefore, a generic pressure distribution was defined, and a linear correlation between wind speed and pressure magnitude was developed. Variations to the loading, based on angle of attack were not considered. Though this is not a typical approach to developing blade loading scenarios, it is important to realize that it suffices to address the usefulness of the PReP model algorithms.

Flaw frequency data is implemented at two levels in this analysis: probability of occurrence and probability of flaw magnitude. Data used in this analysis was predominately acquired through destructive inspection. The ideal situation would be to build these distributions with Nondestructive Evaluations techniques. These technologies bring into question the probability of detection. Unfortunately, at present the probability of detection for the flaws used in this analysis is near zero, even though the probability of defects existing is not insignificant.

While the probabilistic analysis has proved useful in addressing the uncertainty of manufacturing defects it must be performed with detailed and accurate information. For instance, this analysis has shown the significance of flaw magnitude distributions.

Previous discussion in Chapter 5, detailed the exponential decrease in the strength of laminates with waves. Figure 113 displays histograms of the strength reduction sample sets used in the Monte Carlo simulation for each of the two approaches. Here one can see the dramatic shift in laminate strength as a function of the flaw magnitude distributions. For reference, an image of the two sample approaches, Case 1 and Case 2 are given in Figure 114.

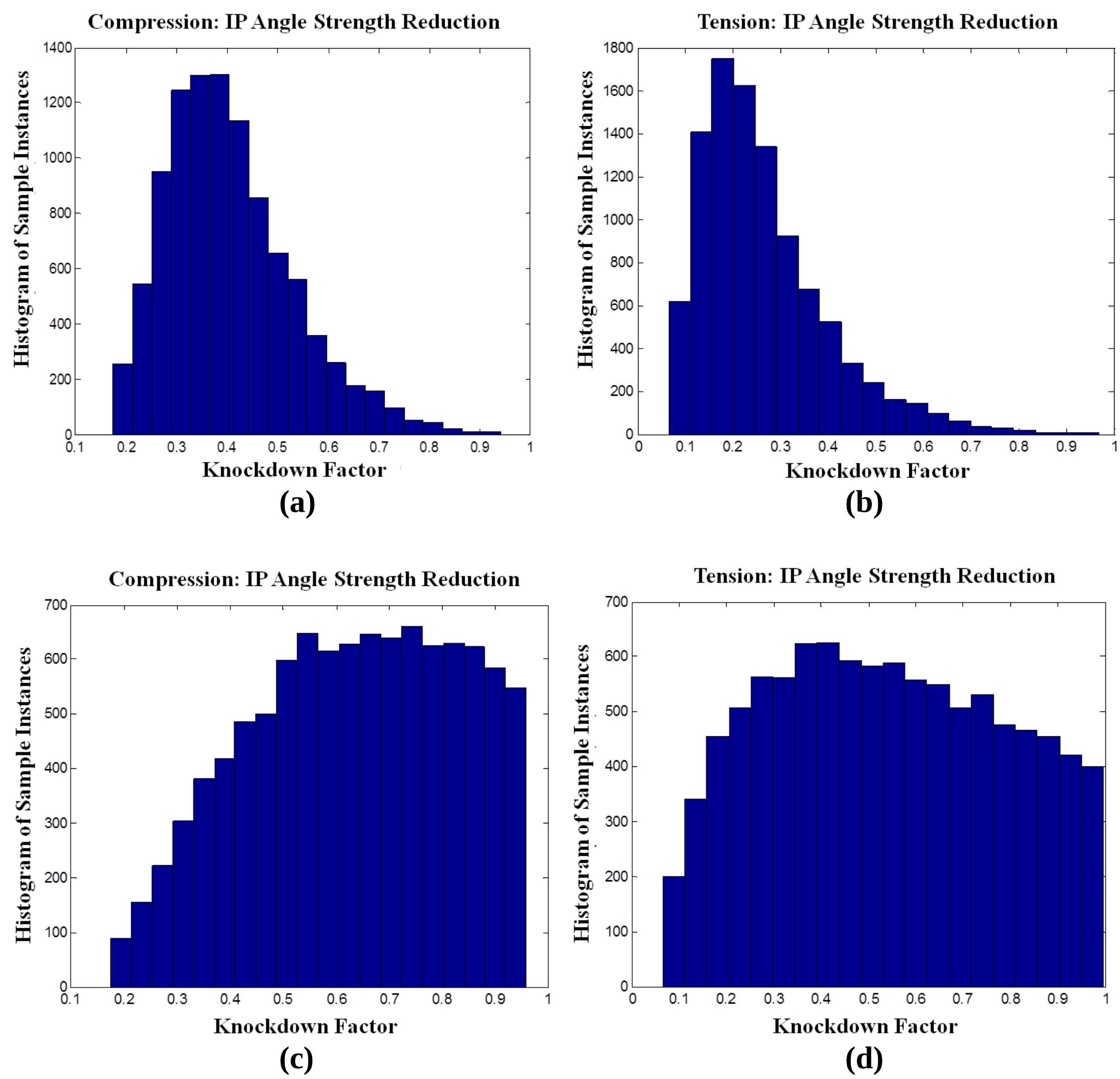


Figure 113: Knockdown factor as a function of the flaw magnitude distributions (a) Case 1 Compressive, (b) Case 1 Tensile, (c) Case 2 Compressive, (d) Case 2 Tensile

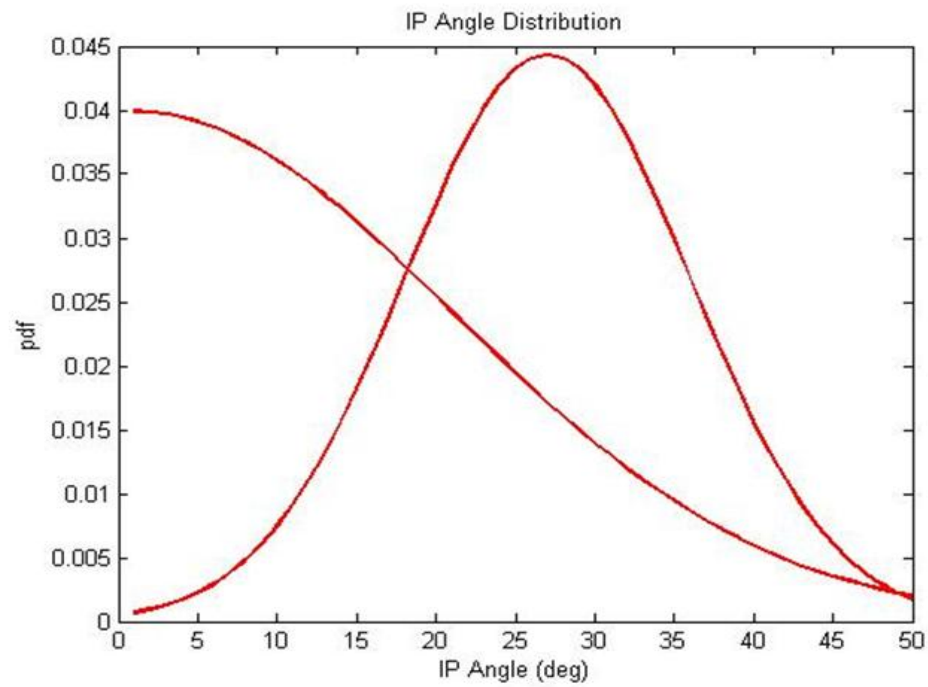


Figure 114: Comparison of Case 1 and Case 2 sample distributions

Both the mean and the standard deviation play a role in this phenomenon. For instance, when the algorithm samples from a flaw distribution with a mean of 27 the resulting knockdown factor means for the IP wave case are ~0.35 in compression and ~0.2 in tension. By comparison, when the algorithm samples from a one sided flaw distribution with a minimum of 0 (Half Gaussian), the resulting knockdown factor means for the IP wave case, are ~0.65 in compression and ~0.5 in tension. As the static strength reduction has a direct impact on the fatigue life under the PReP formulation, this effect shows the need for accurate distribution data.

<u>Analysis Sensitivity</u>

The results of the reliability estimation presented in Chapter 6 assumes that increased knowledge of the material system, particularly in relation to defects, can be used to reduce Safety Factor magnitudes. While the reasoning for this assumption is valid, the utility of the PReP algorithm is not contingent on the integrity of this assumption. Significant insight can be gained into reliability issues by examining the sensitivity of the results to the material system, specific fatigue response, and input distributions of random variables. To illustrate this point, the probabilistic reliability analysis described in Chapter 6, has been repeated with varying input distributions in this section. A cursory analysis of laminates with flaws in fatigue is presented is the following section.

The mean and standard deviations of flaw magnitudes were targeted for this sensitivity study. In doing so, one may gain insight into the role that defect data plays on the results on the reliability analysis. Only Case 1: Spatially Varying PFO with the reduced Safety Factor (1.15) has been used to provide insight into this issue. The results from this study are tabulated in Table 22.

Table 22: Results from Sensitivity Analysis ($P_f$)

| | Standard Deviation | | |
|---|---|---|---|
| | 5 | 9 | 13 |
| $P_f$ | 100% | 26% | 8% |

| | Mean Flaw Magnitude | | |
|---|---|---|---|
| | 15deg | 27deg | 32deg |
| $P_f$ | 11% | 22% | 36% |

Varying the standard deviation for flaw magnitude, has a dramatic effect on the results. It is interesting to note that reducing the standard deviation increases the probability of failure, whereas increasing the  standard deviation reduces the probability of failure. The results from varying the mean flaw magnitude are more intuitive. As the mean flaw magnitude decreases so does the probability of failure, while increases in mean conversely increase $P_f$. To get a better sense of effect of mean variations the three data point have been plotted indicating there is an exponential response.

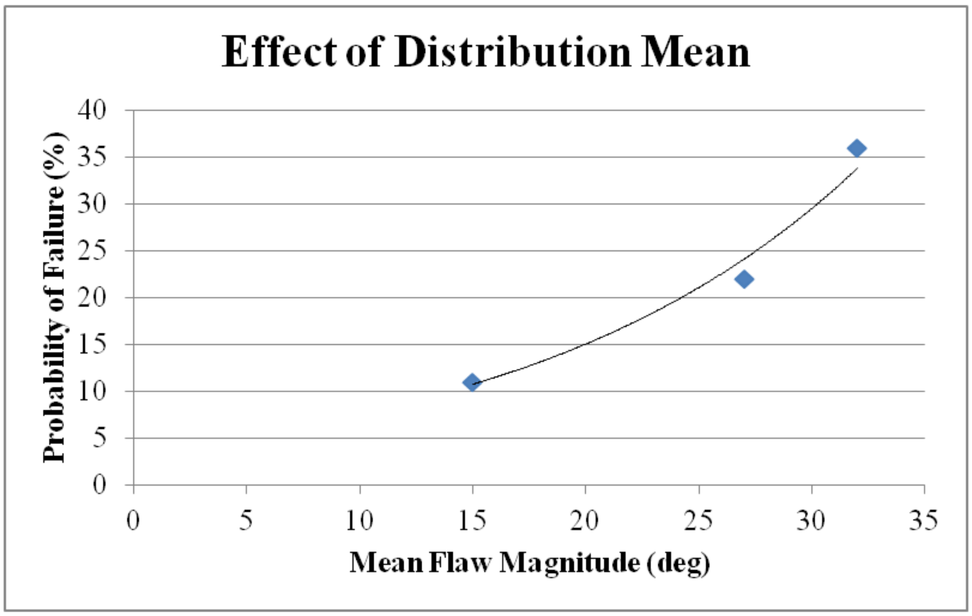


Figure 115: Effect of mean flaw magnitude on probability of failure.

These results indicate that flaws do not have to be removed from the system but reductions in flaw distribution means can significantly improve a design. This is particularly convenient since it is unreasonable to think that a manufacturer can eliminate defects altogether.

<u>Reliability Analysis Interpretation</u>

The analysis presented herein has shown that a better understanding of safety factors is necessary. It can be interpreted by the IEC standards that the safety factor approach is meant to "overbuild" the structure so that, should defects exist, the structure will not be significantly impacted. The analysis presented herein, postulates that one should assess defects as a design parameter in a parametric probabilistic analysis. In doing so it was shown that reducing uncertainty related to defects is quantifiable, and can have a direct impact on the design of a blade.

To illustrate this point, the blade finite element model was modified by varying the thickness of the spar cap. The PReP analysis was run utilizing a Case 1 with the full 1.3 IEC Safety Factor. The spar cap thickness was then increased until the probability of failure approximately matched that of the original model with a 1.15 Safety factor. The thickness had to be increased by ~100%, doubling the amount of material in the spar cap. This indicates that a modification of the original design based on the defect analysis would have required 7 additional layers. While this analysis did not considered stiffness effects or other design constraints, does show that blade design can be modified with a probabilistic treatment of defects.

The IEC standard allows for reductions in safety factor magnitudes if the designer has more in depth data on the material response. It is then natural to assume that if the design team has additional information on the frequency and effect of defects, they could reduce the safety factor magnitudes accordingly. The results presented in Chapter 6 addressed this issue by presenting an analysis focused on reducing safety factors and adding a probabilistic defect analysis. If one assumes that defects account for some of the uncertainty in the blade design and these defects are analyzed with application specific data, then it follows that safety factors can be reduced.

In a probabilistic analysis, the limit state is the failure state. Visually this can be represented by a surface in the random variable/output design space. The limited test data, acquired to date and presented herein, on laminates with defects in fatigue and full scale structures with defects suggest that the PReP analysis is not exact. However, verification of the PReP algorithm through the blade test shows that the analysis is conservative. This conservatism can be interpreted as safe boundary surface, rather than a failure surface. The actual failure state surface would then be encompassed by the unsafe region. This concept is graphically represented by Figure 116.

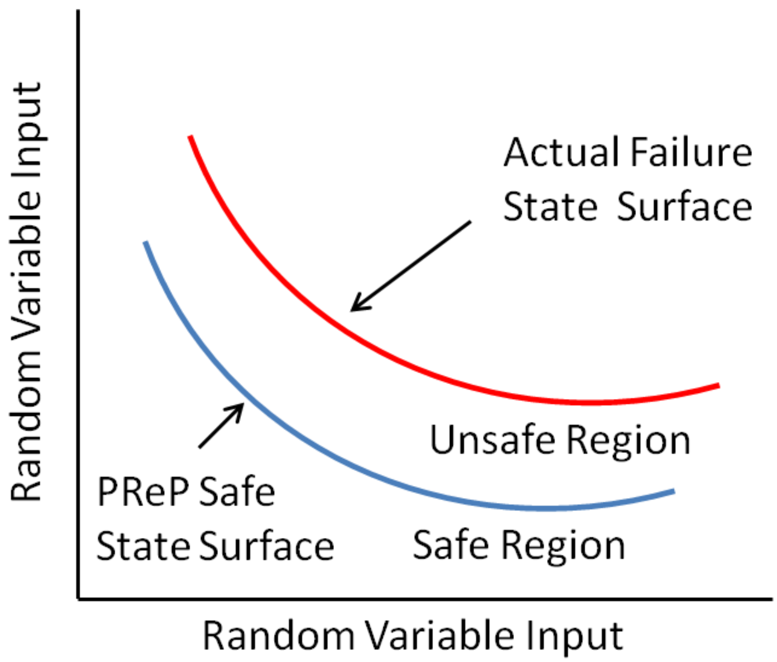


Figure 116: PReP algorithm limit state VS the structure failure state

It is also important to note that all data should be verified through testing of the particular material system and defects of interest. This is illustrated through examining the failed laminate fatigue data presented by Mandell et al. [54] The authors of this study examined several geometries, and the results presented in the publication related to glass/polyester laminates in the configuration [0/±45/0]s. In-plane waves were introduced to all 0° layers at the same location. The fatigue response of control coupons (unflawed laminate) is presented in Figure 117, for comparison to a laminate with an In-Plane wave and the PReP predicted responses using the knockdown formulation. This analysis showed that perhaps the approach to analyzing fatigue life, while conservative in the EOD blade experiments, may not always be conservative. Therefore, another technique is also compared, wherein the laminate fatigue response is shifted by the reduction in static strength as a result of the defect. This effectively results in parallel S-N curves. However, this approach is not ideal as it would suggest that even with a max compressive stress of 0Mpa, there is a finite life. The approach does generate an interesting failure envelope created between the two models, around the empirical response.

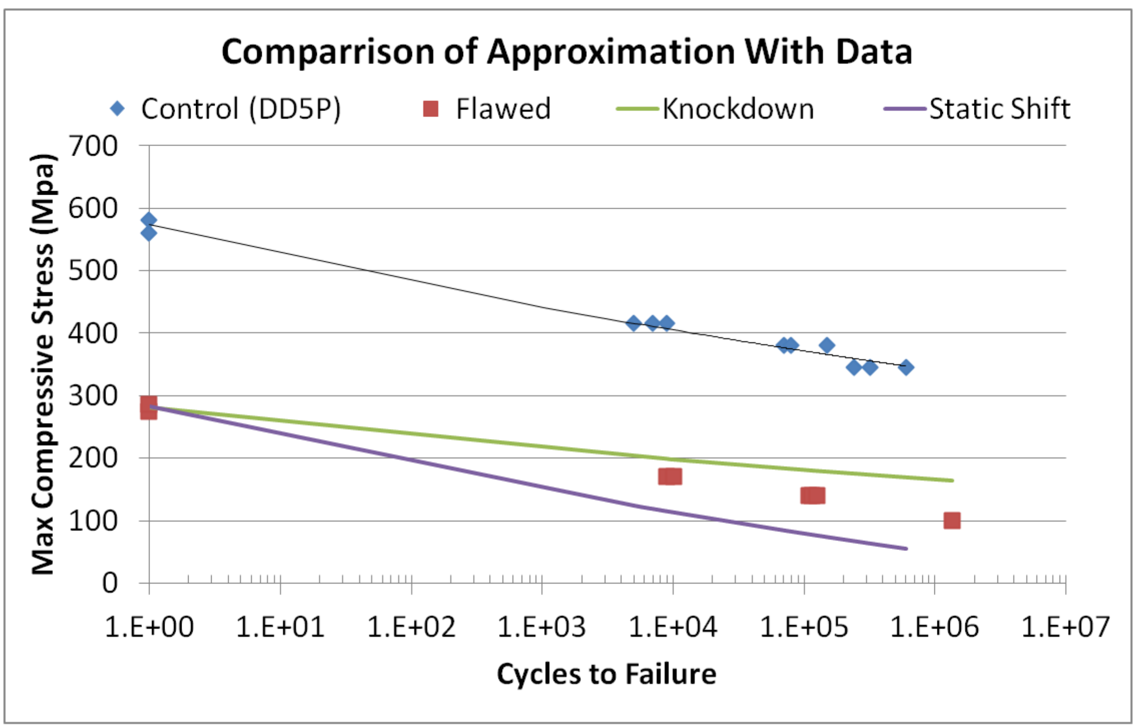

Figure 117: Fatigue life approximation techniques

The failure criteria used in this analysis was a fatigue life estimation based on max strain; however, the algorithm is not limited to this criterion. The analysis could be used with any number of criteria; any strain or stress based approach (e.g. Tsai-Wu, Tsai-Hill etc) could be seamlessly incorporated. Other failure modes where the structure design/geometry plays a large role (e.g. buckling) would be harder to address but not impossible. This particular application would require an iterative method which reruns the FE model based on the degraded material properties as a function of a region of laminate containing a flaw.

# CHAPTER 10

# CONCLUSIONS AND FUTURE WORK

## Conclusions

The work presented herein has established that characterization of defects common to wind turbine blades is possible. A consistent framework has been established and validated for quantitative categorization and analysis of flaws. However, it relies on accurate and multiple source data collection, with consistent scientific procedures. Understanding the changes in the material properties associated with characterized flaws has been achieved on a coupon level with physical testing being performed with several configurations of several different flaw types.  Analysis of the test results show that strength degradation in laminates with waves tend to correlate slightly better to the average off-axis fiber angle of all layers as opposed to the maximum fiber angle.

The analysis presented in this thesis postulates that one should assess defects as a design parameter in a parametric probabilistic analysis.  Results from this effort have shown that the probability of failure of a wind turbine blade with defects, can be adequately described through the use of probabilistic modeling. The two approaches detailed in this analysis have shown that by treating defects as random variables one can reduce the design conservatism of a wind blade in fatigue. Reduction in the safe operating lifetime of a blade with defects, compared to one without has shown that the inclusion of defects is critical for proper reliability assessment. If one assumes that defects account for some of the uncertainty in the blade design and these defects are analyzed with application specific data, then safety factors can be reduced.

This analysis has shown that the probability of failure is sensitive to the flaw magnitude distributions. Therefore, care must be taken to collect data specific to the structure and material system under scrutiny. The probabilistic analysis should be incorporated into a full reliability program that starts with an effort to investigate the Effects of Defects, then employ these results in a stochastic simulation process which aides the design process by establishing $P_f$, and finally utilize these results as a mechanism to evaluate defects during manufacturing and service life.

The completion of this work has been considered a success. The models converge adequately and predict results consistent with the verification blade test. While probabilistic modeling will provide the designer with significant insight, it constitutes only one portion of an effective reliability program. Additional efforts have utilized the results from this analysis to generate a Criticality Assessment matrix that can be used in-situ to assess as-built composite structure with defects.

Should PReP be accepted by industry, it's usage may be a merger of three design concepts: safe life probabilistic and damage tolerance. Obviously, the PReP procedure produces probabilities of failure and can therefore be considered a probabilistic approach. However the probabilities are generated based on a designated operational life (e.g. 20 years), with an acceptable value for the probability of failure chosen by the risk assessment of decision makers. The concept of basing a design around an operational life is more akin to a safe life approach. In addition there is ability to analysis the probability of failure as a function of time in service. This allows for maintenance or inspection intervals to be designed around this analysis. This perspective could be tailored to address a corollary to the aviation damage tolerance approach.

As with any business, the deployment of wind turbines is an economic consideration. In order for the wind industry to remain financially attractive and meet clean energy production goals, it is imperative that reliability be improved. While data has been collected on wind turbines, the framework for analysis and protocols described herein are applicable to the evaluation of any composite structure where preventing failures is critical to safety, performance or economic issues.

The effort completed herein fostered collaboration between all members of the BRC, and led to insight into the role of defects and reliably on wind blades. These results and techniques, if adopted by the wind industry, could result in reduced failures and increased availability of wind plants. Ultimately, this would result in reducing long-term wind energy costs which will make wind energy an even more viable power resource. At a minimum, further research has been identified which can continue to improve blade design as well as manufacturing, to improve reliability and reduce costs.

## Future Work

The inadequacy of linear damage accumulation techniques to the formulation of fatigue life for composite materials is well known. Other future work will evaluate the use of progressive damage modeling for assessment of fatigue damage accumulation. The foundation for the progressive damage modeling of composite laminate defects, has already been performed by Nelson. [91] The next step in the evolution of this work is to combine the methodology described herein with the progressive damage models into a closed loop structural analysis procedure. It is expected this approach will be computationally expensive and require the use of a high performance computing center, but yield significant insight into modeling damage propagation and load redistribution tendencies.

The following list describes other items where this work may have been deficient, or where next steps should be taken.

1. Coupon Scale Testing: Some results were obtained for the static glass triaxial testing however OP Proximity and Chain Waves need further testing. Also no glass IP waves were tested. The carbon uni-axial control and OP waves in tension were successful. Carbon uni-directional IP wave need to be tested as well. All hybrid laminate tension results are dubious considering the significant scatter in data. It is recommended that the hybrid testing program be performed again with the inclusion of IP waves. It is recommended that no compression testing be performed for this data set. A small effort should be undertaken to address the effect of combined flaws (e.g. porosity and IP waves). Lastly, it is recommended that fatigue testing of coupon with flaws be performed. Considering the difficulty of testing OP Waves in compression these should only be tested in tension. IP waves and porosity should consider up to three R values, 10, .1 and 1.
2. Subscale Test Fixture: The subscale testing facility is scheduled to be online in the near future. It is recommended that the remaining compression testing

of flaws in laminates be performed in bending using a beam structure. If this is not reasonable, then at least the OP waves should be tested on the fixture.

3. Load Sequence Effects: At present, the analysis does not consider the effect load sequencing has on the fatigue life of a composite laminate. The limited data available in the public domain relating to these issues should be surveyed for applicability. It is expected that some testing at either the coupon or subscale level would need to be performed to really understand these issues.
4. Probabilistic Analysis: The analysis does not currently address variability in the ultimate strength of laminates, laminates with flaws or in the fatigue life approximation. Future work should consider assessing this additional variability. However it should be noted that much of this variation is captured in a 95/95 confidence fatigue life formulation. At present the analysis utilizes a 1D flaw distribution sampling procedure. The analysis should be extended to use 2D flaw occurrence distributions as well. Adhesive or bondline flaws could also be included. Once the testing of the hybrid laminates is completed, another probabilistic analysis of the carbon EOD blade should be performed. The Case 0 or Baseline case which the two probabilistic approaches were compared to was developed in a reverse engineering approach. Ideally the original design parameters used by Mike Zutek would be incorporated into the Baseline case. In addition, if the implied probability of failure were known then, the absolute probability of

failure could be tracked throughout the analysis. A preliminary sensitivity analysis showed that the probability of failure for a blade is sensitive to the standard deviation of the input distributions. This phenomenon should be thoroughly investigated to understand it's implications. Similarly, the time to failure formulation could provide significant insight into design and maintenance practices. The formulation should be further investigated.

5. Analysis Extensions: Several options exist for extending this analysis into a tool which could be of more use to the wind industry. NuMAD, the Sandia distributed code for design of wind blades, is written in Matlab. A subroutine could be written in NuMAD to modify the ANSYS input code in support of probabilistic modeling. NuMAD could also be modified to perform the fatigue and probabilistic calculations developed in the PReP algorithm. Additional work could be performed to address improved accuracy of the surrogate model. This would require many more runs of the reliability analysis to generate additional input to the SL algorithm and parametric variations to the SL algorithms.
6. Protocol Implementation: Considering the dependence of the analysis on the material system and particular defect geometries, it would be difficult to define distributions and knockdowns, which could be used by all manufacturers for all blade models. Moreover, the lack of transparency in the industry as it relates to defects would make it difficult to develop cross-platform distributions. Therefore it may be necessary that the entire PReP

(as currently defined) be implemented on an individual manufacturer basis. Standards could be designed around the analysis objectives and procedures to ensure that the appropriate steps are being taken. The amount of testing necessary in this situation may be cost prohibitive. One aspect that could help reduce the cost is the incorporation of numerical modeling techniques (i.e. progressive damage modeling) which could used in lieu of copious amounts of testing.

# REFERENCES CITED

1. **AWEA.** *2012 U.S. Wind Industry Annual Market Report.* s.l. : AWEA, 2013.

2. —. *AWEA Annual Report for the 2008 Year Ending.* 2009.

3. **Department of Energy.** *20% wind Energy by 2030: Increasing Wind Energy's Contribution to US Electricity Supply.* July 2008. DOE/GO-102008-2567.

4. *Sandia Blade Workshop.* **Veers, P. & Hill, R.** s.l. : Sandia National Labratory, May 2008.

5. **Cairns, D.** *Personal correspondance with wind turbine OEMs & blade manufactures.*

6. **Staff.** Suzlon Blade Recall: Retrofit Program to Address Cracking. *Composites World.* Feburary 2010.

7. **Freeman, S.** Boeing Hits a Hitch in 'Dreamliner' Fuselage. *Washington Post.* August 2009.

8. **Mandell, John F, et al.** *Analysis of SNL/MSU/DOE Fatigue Database Trends for Wind Turbine Blade Materials.* Bozeman, MT : Montana State University, 2009. SAND2009-XXXX.

9. *Alternative Composite Materials for Megawatt-Scale Wind Turbine Blades.* **Griffin, A. & Ashwill, T.** 0696, s.l. : American Institute of Aeronautics, 2003.

10. **Nelson, Jared W.** *Doctoral thesis: A COMPARISON OF CONTINUUM AND DISCRETE MODELING TECHNIQUES.* Bozeman : Montana State Univerity, 2013.

11. **Ditlevsen, O., Madse, H.** *Structural Reliabilty Methods.* Chishester : John Wiler & Sons Ltd, 1996.

12. *Use of Statistical Learning in a Reliabilty Program for Risk Assessment of Composite Structures with Defects.* **Riddle, T., Donnelly, P., Cairns, D., Nelson, J.** Boston : AIAA SDM, 2013.

13. **Chamis, C.** *Probabilistic design of Composite Structures.* s.l. : NASA/TM, 2006. 2006-214660.

14. **Moss, Robb.** Lectures notes for ECIV 491. *Engineering Risk Anlaysis.* Bozeman : Montana State University, 2012.

15. **Hubbard.** 2009.

16. *Structural Reliability Under Combined Load.* **Rackwitz, R., and B. Fiessler.** s.l. : Computers and Structures, 1978, Vol. 9.

17. **Ditlevsen, O. and Madsen, H.** *Structual Reliability Methods.* Chichester : John Wiley & Sons Ltd, 1996.

18. *Reliability Analysis of Solid Rocket Motor under Bayesian Framework.* **Kim, W., Gang, J., Kim, K.** Honolulu : AIAA SDM, 2012.

19. **Foregger, T., Drummond, A., Jao, D., McLeman, C.** probability distribution function. *PlanetMath.org.* [Online] Version 8. http://planetmath.org/Distribution.html.

20. **Weisstein, E.** Joint Distribution Function. *MathWorld--A Wolfram Web Resource.* [Online] http://mathworld.wolfram.com/JointDistributionFunction.html.

21. **Wen, Y., K.** RELIABILITY IN STRUCTURAL PERFORMANCE EVALUATION AND DESIGN. [book auth.] A. Haldar. *Recent Developments In Reliability-Based Civil Engineering.* 2006.

22. **Transportation, Kansas Department of.** *KDOT Bridge Design Manual.* 2008.

23. **Billington, R. & Allan, R.** *Reliability Evaluation of Engineering Systems.* New York : Plenum Press, 1992.

24. *Low Cost Inspection for Improved Blade Reliability.* **Cairns, D.** s.l. : Sandia Blade Workshop, 2008.

25. **Cairns, D. & Mohaghegh, M.** Aircraft Structures. s.l. : MSU/Boeing ME458 Course , 2009.

26. **Administration, Federal Aviation.** *Composite Aircraft Structure.* s.l. : U.S. Department of Transportation, Septemeber 8, 2009. AC: 20-107B.

27. **Defense, Department Of.** *COMPOSITE MATERIALS HANDBOOK.* s.l. : DOD. MIL-HDBK-17-3F.

28. **Administration, Federal Aviation.** *Advisory Circular: Quality Control for the Manufacture of Composite Structures.* s.l. : Department of Transportation, 1989. AC21-26.

29. *Non-destructive Evaluation (NDE) Methods for Inspecting the Integrity of Composuite Structures in the Offshore Oil Industry.* **Ochoa, O.** s.l. : NDE Composites Workshop, 2002.

30. Ultrasonic testing. *Wikipedia.* [Online] http://en.wikipedia.org/wiki/Ultrasonic_testing.

31. *Emerging NDE Technology and Challenges at the beginning of the 3rd Millennium.* **Bar-Cohen, Y.** 2, s.l. : NDT.net, 2000, Vol. 5.

32. **Hill, R., Peters, V., Stinebaugh, J., Veers, P.** *Wind Turbine Reliability Database Update.* s.l. : DOE, Sandia National Labratories, 2009. SAND2009-1171.

33. **Peters, V., Ogilvie, A., Bond, C.** *Continuous Reliabilty Enhancement for Wind (CREW) Database: Wind Plant Reliability Benchmark.* s.l. : DOE - Sandia National Labroatories, 2012. SAND2012-7328.

34. *FAROW: A tool for fatigue and relinilty of wind turbines.* **Veers, P., Lange, C., Winterstein, S.** San Francisco : American Wind Energy Society, 1993.

35. **Winterstein, S., Veers, P.** *Theory Manual for FAROW Version 1.1.* s.l. : DOE - Sandia National Labratories, 2000. SAND94-2459.

36. *Reliability-based fatigue design of wind-turbine rotor blades.* **Ronold, K., Wedel-Heinen, J., Christensen, C.** s.l. : Engineering Structures, 1999, Vol. 21.

37. *Reliability-based design of wind-turbine rotor blades against failure in ultimate loading.* **Ronold, K., Larsen, G.** s.l. : Engineering Structures, 2000, Vol. 22.

38. *Framework for Risk-based Planning of Operation and Maintenance for Offshore Wind Turbines.* **Sorensen.** s.l. : Wind Energy, 2009, Vols. 12:493-506.

39. *A Probabilistic Evaluation of Wind Turbine Fatigue Design Rules.* **Veldkamp, D.** s.l. : Wind Energy, 2008, Vols. 11:655-672.

40. Gearbox Reliability Collaborative. *NREL.* [Online] April 2012. http://www.nrel.gov/wind/grc/.

41. **Tsai, S. Hahn, H.** Introduction to Composite Materials. Westport : Technomic Publishing Co, 1980.

42. *PRE- and POST-THIN: A Tool for the Probabilistic Design and Analysis of Composite Rotor Blade Strength.* **Lekou, D., Philippidis, T.** 2009, Vols. 12:676-691.

43. **Lekou, D., Philippidis, T., Bacharoudis, K.** *UPWIND: Probabilistic Strength Assesment of Rotor Blades.* s.l. : European Commission, 2011.

44. *Reliability-based design of wind turbine blades.* **Toft, H., Sorensen, J.** s.l. : Structural Safety, 2011, Vol. 33.

45. **Commission, International Electrotechnical.** Wind Turbines - Part 1: Design Requiremnts. s.l. : IEC, 2005. IEC-61400-1.

46. **members, BRC.** *Collaborative dicsussions with BRC industry partners.* Albuquerque, August 2011.

47. *Defect distribution and relinilty assesment of wind turbine blades.* **Toft, H., Branner, K., Berring, P., Sorensen, J.** s.l. : Engineering Structures, 2011, Vol. 33.

48. *Manufacturing defects in wind turbine blades "how much is ok?".* **Bech, J., McGugan, M., Andersen, T., Sorensen, B.** 2010.

49. *The stochastic finite element method in structural reliabilty.* **Kiureghian, A., Ke, J.** 2, s.l. : Probabilistic Engineering Mechanics, 1988, Vol. 3.

50. **Health, National Institute of.** Image J: Image processing analysis in JAVA. [Online] http://rsbweb.nih.gov/ij/.

51. **Biegler, L., T.** Nonlinear Programming: Concepts and Algorithms for Process Optimization. Pittsburgh : Carnegie Mellon: CAPD Center, 2011.

52. *Compression strength reductions in composite laminates due to multiple-layer waviness.* **Adams, D., & Bell, S.** s.l. : Composites science and technology, 1995, Vol. 53.

53. *Effects of layer waviness on the compression strength of thermoplastic composite.* **Adams, D. & Hyer M.** s.l. : Journal of reinforced plastics and composites, 1993, Vol. 12.

54. *NEW FATIGUE DATA FOR WIND TURBINE BLADE MATERIALS.* **Mandell, J., Samborsky, D., Wang, L., Wahl, N.** s.l. : AIAA, 2003.

55. **Riddle, T.** Personal correspondance with BRC members. Albuquerque : s.n., 2010.

56. *Statistical aspects of fracture.* **Argon, A. S.** s.l. : Composiste Materials, 1974, Vol. 5.

57. *Statistical concepts in the study of frature properties of fibers and composites.* **Wagner, H. D.** s.l. : Application of fracture to mechanics of composite materials, 1989.

58. *Is there a size effect in composites.* **Zweben, C.** s.l. : Composites, 1994, Vol. 25.

59. **Wisnom, M. R.** *Size effects in tensile, compressive and inter-laminar failure of unidirectional composites.* s.l. : ASME, 1997. AD-Vol 55.

60. *Size effects in the testing of fibre-composite materials.* **Wisnom, M. R.** s.l. : Composite science and technology, 1999, Vol. 59.

61. *A statistical distribution function of wide applicability.* **Weibull, W.** s.l. : Journal of applied mechanics, 1951, Vol. 18.

62. *Emerging NDE Technology and Challenges at the beginning of the 3rd Millennium.* **Bar-Cohen, Y.** s.l. : Material Evaluation, 2008, Vol. 58.

63. *Non-destructive Evaluation (NDE) Methods for Inspecting the Integrity of Composite Structures in the.* **Ochoa, O.** s.l. : NDE Composites Workshop, 2002.

64. *Standard test method for tensile properties of polymer matrix composite materials.* ASTM D3039.

65. *Test Method for Compressive Properties of Unidirectional or Cross-ply Fiber Resin Composites.* s.l. : American Society for Testing and Material. ASTM D3410.

66. *Standard Test Method for Compressive Properties of Polymer Matrix Composite Materials Using a Combined Loading Compression (CLC) Test Fixture.* ASTM D6640.

67. **Nielsen, L. E.** s.l. : Journal of Applied Polymer Science , 1966, Vol. 10.

68. **Nielsen, L.** s.l. : Journal of Composite Materials, 1967, Vol. 1.

69. **Nielsen, L. E. and Landel, R. F.** Mechanical Properties of Polymers and Composites. s.l. : Marcel Dekker.

70. **TPI-RI Materials Testing Lab.** *Compressive Testing of Specimens with Artifically High Void Content.* 2010. Doc. No. 10022.

71. **Berry, D., Berg, D.** *Blade System Design Studies Phase II: Final Project Report.* s.l. : Sandia National Labratories, 2008. SAND08-4648.

72. **Griffin, D., Ashwill, T.** *Blade System Design Study Part II: Final Project Report (GEC).* s.l. : Sandia National Labratories, 2009. SAND09-0686.

73. **Veers P.S., Ashwill T.D., Sutherland H.J., Laird D.L., Lobitz D.W., Griffin D.A., Mandell J.F., Musial W.D., Jackson K., Zuteck M., Miravete A., Tsai S.W., Richmond J.L.** Trends in the design, manufacture and evaluation of wind turbine blades. *Wind Energy*. 2033, Vol. 6.

74. *Farrow: A tool for fatigue and reliability of wind turbines.* **Veers, P., Lange, C., Winterstein, S.** San Francisco, CA : Windpower, 1993.

75. **Lekou, D., Philippidis, T.** PRE- and POST-THIN: A Tool for the Probabilistic Design and Analysis of Composite Rotor Blade Strength. *Wind Energy,*. 2009, Vol. 12.

76. **Mandell, J., Samborsky, D., Pancasatya, A., Sears, A., Wilson, T.** *Analysis of SNL/MSU/DOE Fatigue Database Trends for Wind Turbine Blade Materials.* s.l. : DOE, 2010. SAND2010-7052.

77. *Life prediction methodology for GFRP laminates under spectrum loading.* **Philippidis, T. P., Vassilopoulos, A. P.** s.l. : Composites Part A, 2004, Vol. 35.

78. **Manwell, J.** *Wind Energy Explained.* West Sussex : John Wiley & Sons Ltd, 2002.

79. *Effects of Defects: Part A - Development of a Protocol for Defect Risk Management & Improved Reliability of Composite Structures.* **Riddle, T. W., Cairns, D. S., Nelson, J. W., Workman, J.** Honolulu : American Instiute of Aeronautics and Astronautics, 2012.

80. *Effects of Defects: Part B—Progressive Damage Modeling of Fiberglass/Epoxy Composite Structures with Manufacturing Induced Flaws.* **Nelson, J.W., Riddle, T.W., & Cairns D.S.,.** Honolulu : 53nd AIAA/ASME/ASCE/AHS/ASC Structures, Structural Dynamics and Materials Conference, 2012.

81. **FAA.** *Determining the Fatigue Life of Composite Aircraft Structures Using Life and Load-Enhancement Factors.* s.l. : DOT, 2011. DOT/FAA/AR-10/6.

82. **Nijssen.** *Fatigue life prediction and strength degredation of wind turbine rotor blade composistes.* s.l. : Sandia National Labratories, 2007. SAND2006-7810P.

83. *The SNL/MSU/DOE Fatigue of Composite Materials Database: Recent Trends.* **Samborsky, D., Mandell, J., Miller, D.,.** Honolulu : 53nd AIAA/ASME/ASCE/AHS/ASC Structures, Structural Dynamics and Materials Conference, 2012.

84. **Commission, International Electrotechical.** *IEC 61400-1 Ed.3: Wind turbines - Part 1: Design requirements.* s.l. : IEC, 2005.

85. **Dowling, N. E.** *Mechanical Behavior of Materials.* s.l. : Prentice-Hall, 1999.

86. **Rumsey, M., Nelson, J., Riddle, T.** *Report on the Blade Manufacturing Process of the Effects of Defects Validation Blades.* s.l. : Sandia National Labratories, 2013. SANDXX-XXXX.

87. **Hurtado, J. E.** An examination of methods for approximating implicit limit state functions from the viewpoint of statistical learning theory. *Structual Safety.* 2004, Vol. 26.

88. **Hurtado, J.E., Alverez, D. A.** Neural network-based reliability analysis: a comparative study. *Computer Methods in Applied Mechanics and Engineering.* 2011, Vol. 191.

89. *Procedures for performing a failure mode, effects and criticality analysis.* 1980. MIL-STD-1629A.

90. *Failure modes, effects and criticality analysis (FMECA) for command, control, communications, computer, intelligence,.* s.l. : Department of Army, 2006. TM 5-698-4.

91. *Effects of Defects: Part B - Progressive Damage Modeling of Fiberglass/Epoxy Compsite Structures with Manufacturing Induced Flaws Utilizing Cohesive Zone Elements.* **Woo, K., Nelson, J., Cairns, D., Riddle, T.** Boston : AIAA SDM, 2013.

92. **Red, C.** Wind turbine blades: Big and getting bigger. *Composites World.* 2008.

93. **Kan, H.** *Assessment of probaabilistic certification methodlogy for composistes materials.* s.l. : DOT, 2011. DOT/FAA/AR-00/74.

94. *Damage prognosis framework for monitored structural systems with multi-site fatiuge-driven damage growth.* **Gobbato, M., Conte, J., Kosmatka, J.** Denver : AIAA, 2011.

95. *Probabilistic approach to damage tolerance design of aircraft composite structures.* **Lim, K., Styuart, A.** 4, s.l. : Journal of Aircraft , 2077, Vol. 44.

96. **Standard, Military.** *Procedures for performing a failure mode, effects and criticality analysis.* 1980. MIL-STD-1629A.

97. **Army, Department of.** *Failure modes, effects and criticality analysis (FMECA) for command, control, communications, computer, intelligence, surveillance, and reconnaissance (C4ISR) facilities.* 2006. TM 5-698-4.

98. **Weisstein, E.** Monte Carlo Integration. *Mathworld--A Wolfram Web Resource.* [Online] http://mathworld.wolfram.com/MonteCarloIntegration.html.

99. **Press, W. H., et al.** Simple Monte Carlo Integration and Adaptive and Recursive Monte Carlo Methods. *Numerical Recipes in FORTRAN: The Art of Scientific Computing.* Cambridge : Cambridge University Press, 1992.

# APPENDICES

# APPENDIX A:

## ADDITIONAL FLAW DATA GRAPHS

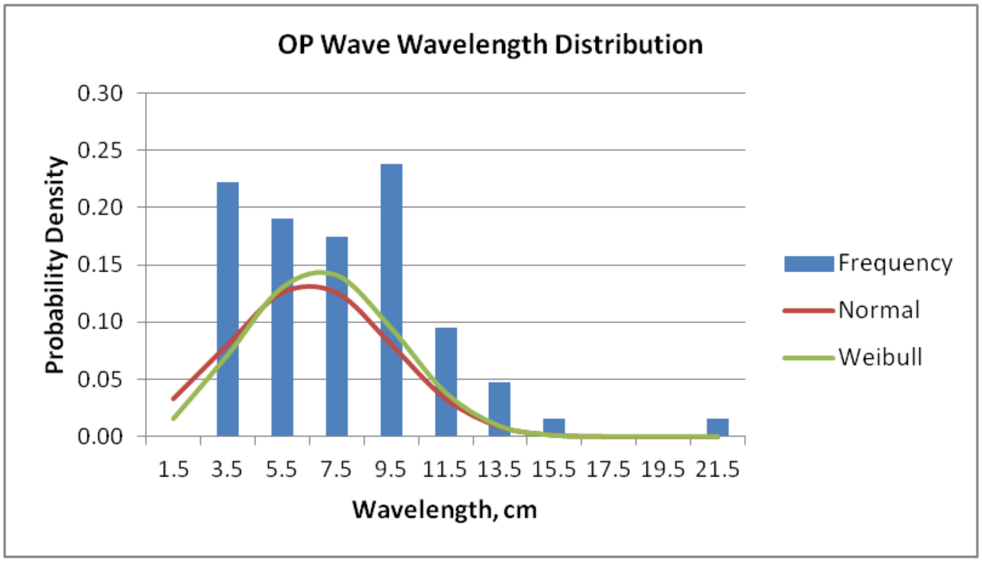


Figure A. 1: Out-of-Plane wavelength distributions.

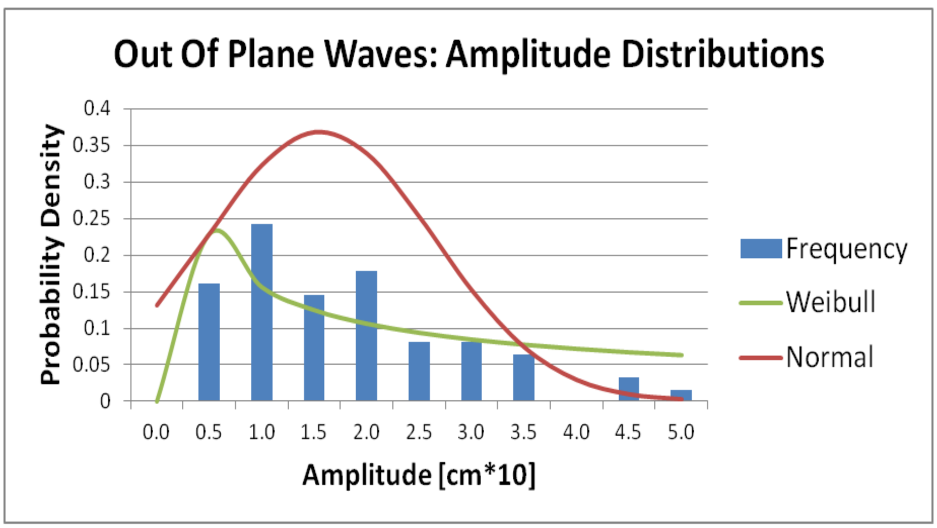


Figure A. 2: Out-of-Plane amplitude distributions

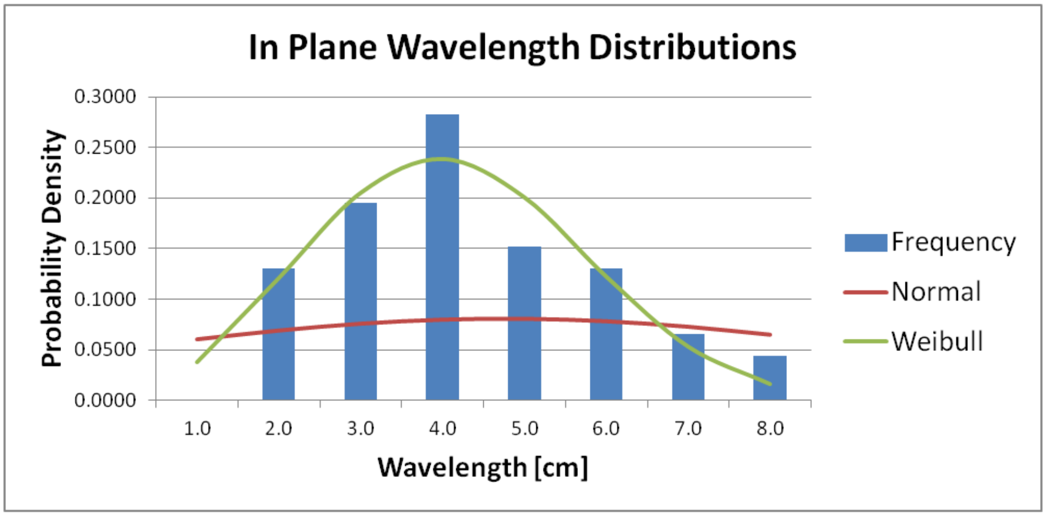


Figure A. 3: In-Plane wavelength distributions.

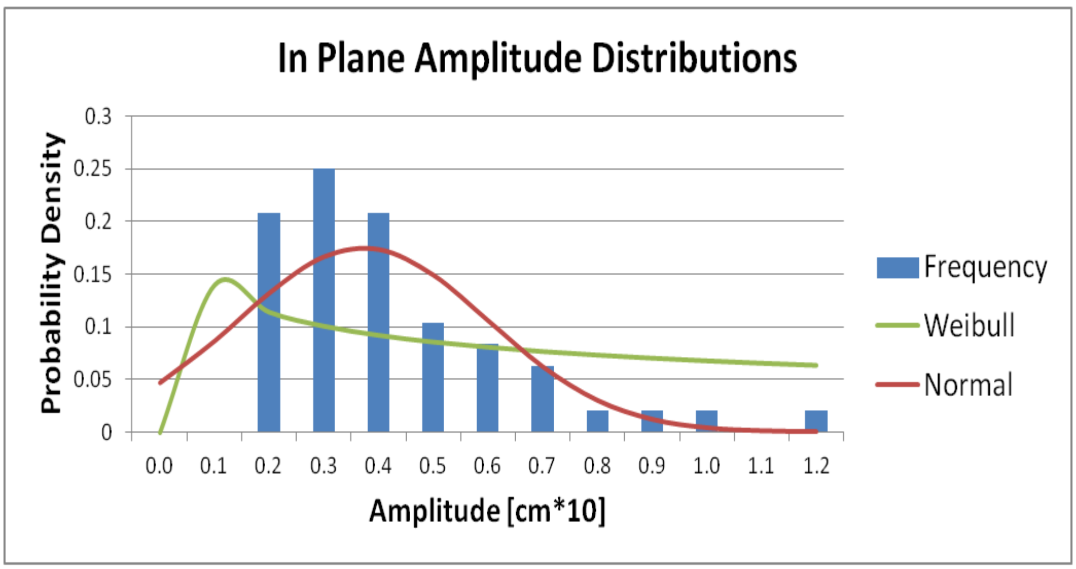


Figure A. 4: In-Plane amplitude distributions

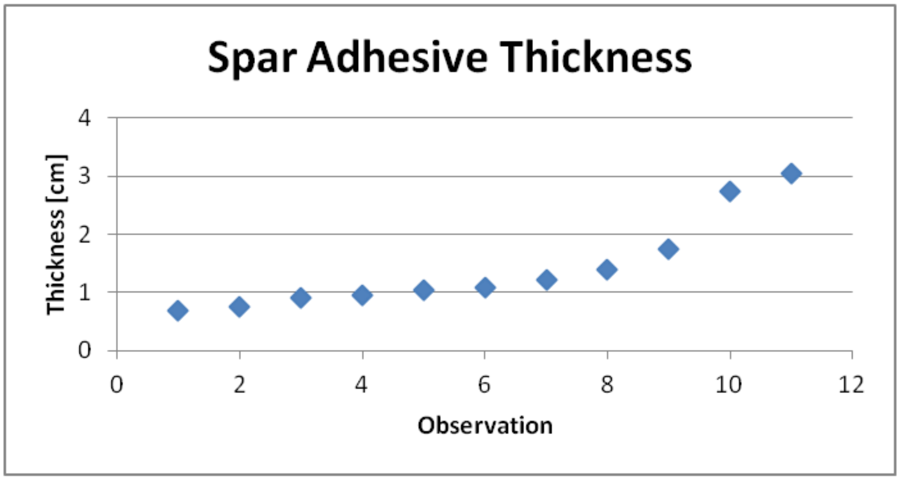


Figure A. 5: Plot of Spar bond thickness

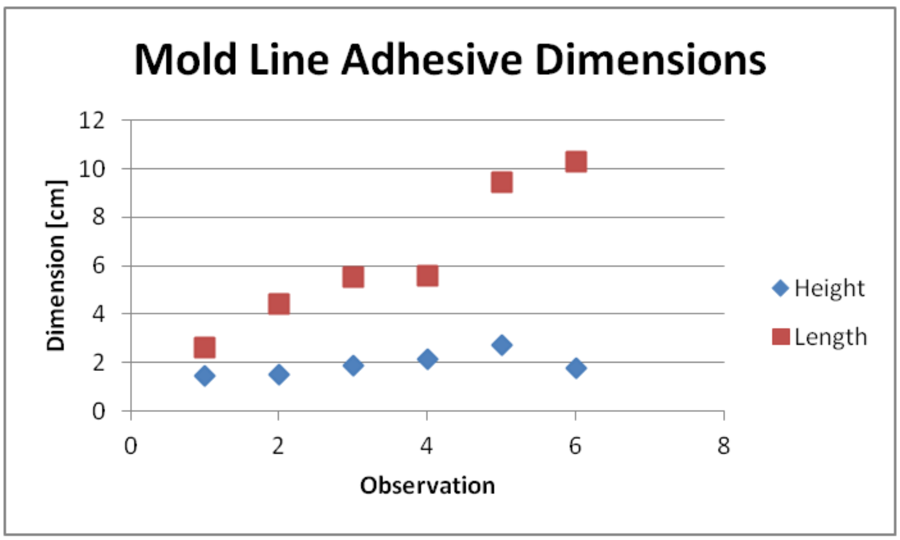


Figure A. 6: Plot of Mold Line adhesive thickness

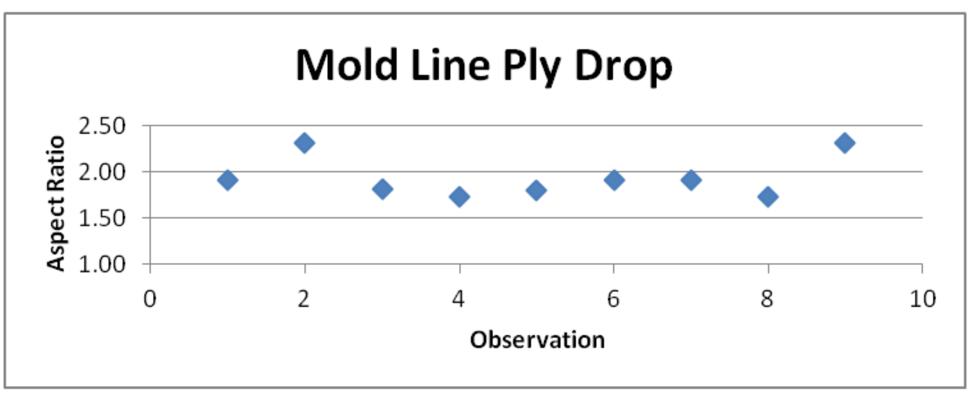


Figure A. 7: Plot of ply drop aspect ratio found in Mold Line bonds

# APPENDIX B:

## WIND ANALYSIS

Step 1.2: Environmental Conditions. For this analysis, wind speed data was gathered from a Montana Department of Transportation weather center located on a ridge top just east of Bozeman, MT. This data was fit to the standard Weibull distribution (Figure A. 8), often used in wind speed characterization. The resulting Weibull parameters were; a=1.896, b=5.29.

Assumptions: The environmental conditions chosen for the analysis are representative of what the blade might see in service. Weibull distributions are commonly used to describe wind speed variability. The data used in this analysis fit well with a Weibull distribution. However, the mean wind speed is not as high as a commercial wind site and therefore the level of assumption was given a High rating rather than Very High.

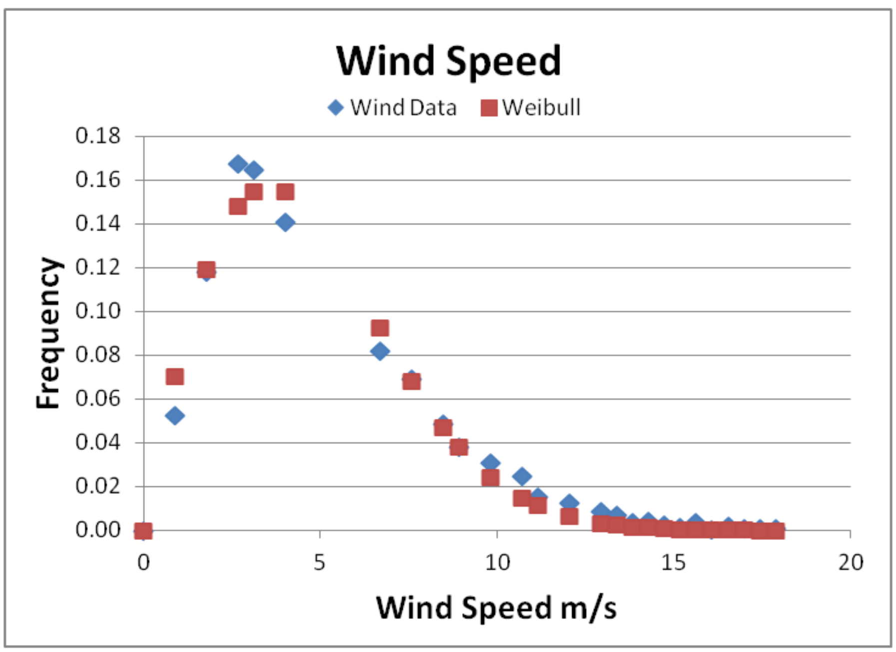


Figure A. 8: Wind speed distribution used in analysis

**Step 1.3 Governing Article Parameters**

For the wind blade analysis, the operational parameters necessary to perform a fatigue life calculation are operating hours and design life. The following values were chosen for this analysis:

- Mean Tip Speed: 77m/s
- Mean RPM: 82
- Yearly operating hours: 4000
- Design life: 20 years

Assumptions: The governing article parameters are consistent with the blades design or expected operation. Specific data for correlating these parameters to the actual blade design were not available. Twenty years is considered a standard design lifetime in the wind blade industry and used in this analysis. Four thousand hours per year of operation is based on operating 45.6% of the year. Tip speed was calculated based on an optimal tip speed ratio of 7 as discussed by Manwell [78] and applied to a mean wind speed of 5.57m/s as calculated from the wind speed data. While the calculations are sound, it is not known what the design intentions were, therefore the level of assumption integrity is considered High.

Step 3.3 Designation of Spectrum for Load Reversals. Two Probability Mass Functions (PMF) were developed from the WISPER data to assess the High and Low Pressure sides of the blades independently. The High Pressure side was assumed to be in tension at all times thus the PMF R ratio values varied from 0.1 to 0.8. Conversely, the Low Pressure side was assumed to be in compression, thus R ratio values varied from 1.25 to 10. Based on the WISPER data and these modifications, probability values were generated for 100 discrete load reversal bins. The Probability Mass Distribution and complimentary Cumulative Distribution for the High Pressure side are displayed in Figure 72.

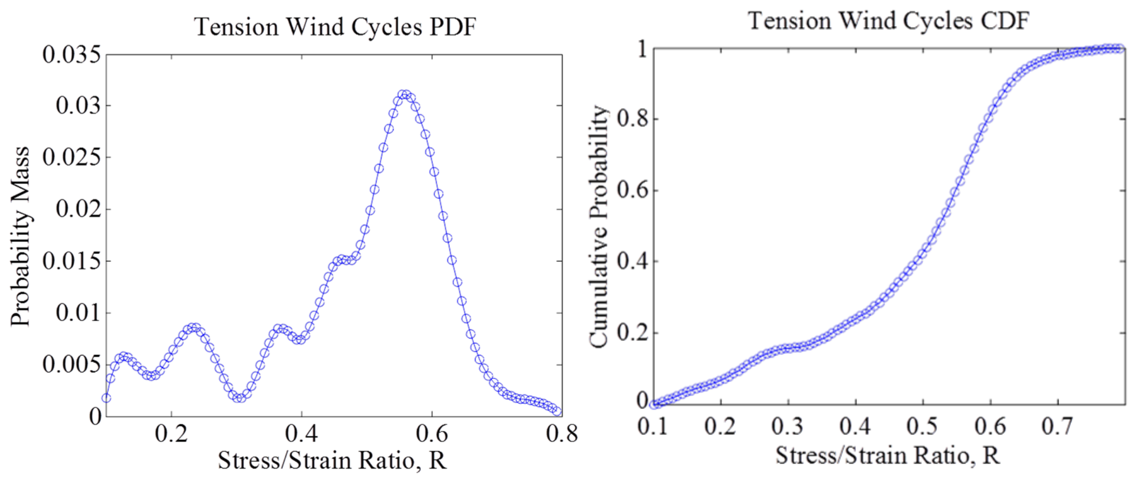


Figure 118: Wind Cycle Distributions

The R ratio is defined for any given fatigue cycle as maximum applied stress (or strain), divided by the minimum applied stress (strain). The WISPER spectrum was developed more as a material qualification tool, rather than a wind blade design tool. In performing material property evaluations, one can set the max applied stress as necessary, to fill out the S-N curve. Very little information is found in the literature as to how to apply these spectrum loads to blade fatigue life design.  For this analysis the distribution was applied equally to all wind speeds. That is to say that any one of the 18 wind speeds evaluated from the Weibull distribution had the same shape spectrum (probability distribution of max/min spectrum loading cycles). This formulation was able then to effectively transform probabilities into proportions, such that should a particular wind speed see 1000 total events, and the probability mass of a particular R ratio be 0.04, then the total number of events at that wind speed and R ratio contributing to the overall spectrum count, is 40.

Assumption: The WISPER distribution can be applied equally to all wind speeds. The validity of this assumption is unknown. The WISPER distribution describes R ratio and therefore needs either max or min strain as an input. As max strain is directly related to wind speeds, the distribution was applied to all wind speeds.

# APPENDIX C:

## MATLAB CODE

```
clear all;
close all;
winddist;
FlawDist;
importdata;
probfail;
```

**Wind Distribution**

Program Name: winddist.m

```
% Wind cycle PDFs Based on WISPER Distribution


Rt = [0.1,0.14,0.17,0.24,0.31,0.37,0.4,0.46,0.48,0.55,0.65,0.7,0.8];

TFreq=[0.001748499,0.005439774,0.003885553,0.008548217,0.001748499,...
0.008548217,0.007382551,0.015153658,0.015153658,0.03069587,0.010102438,...
0.002914165,0];

bins=100;
int=(max(Rt)-min(Rt))/bins;
minR=min(Rt);
maxR=max(Rt)-int;

% Build Tension Distributions

wt=spline(Rt,TFreq);
tinergral=diff(fnval(fnint(wt),[.1 .8]));

figure;
tt=minR:int:maxR; % R value in tension
Twinddist = spline(Rt,TFreq,tt);
plot(tt,ppval(wt,tt),'b-o');
title('Tension Wind Cycles PDF');
xlabel('Stress/Strain Ratio, R');
ylabel('Probability Mass');

figure;
Twindcdf=fnint(wt);
Twindcdf.coefs=Twindcdf.coefs/ppval(Twindcdf,Twindcdf.breaks(end));
plot(tt,ppval(Twindcdf,tt),'b-o');
title('Tension Wind Cycles CDF');
```

```
xlabel('Stress/Strain Ratio, R');
ylabel('Cumulative Probability');

% Build Compression Distributions

Rc=[10,7.14,5.88,4.17,3.23,2.70,2.50,2.17,2.08,1.82,1.54,1.43,1.25];

CFreq=[0.001748499,0.005439774,0.003885553,0.008548217,0.001748499,...
    0.008548217,0.007382551,0.015153658,0.015153658,0.03069587,...
    0.010102438,0.002914165,0];

inc=(max(Rc)-min(Rc))/bins;
minRc=min(Rc);
maxRc=max(Rc)-inc;

wc=spline(Rc,CFreq);
diff(fnval(fnint(wc),[0 1]));

figure;
cc=minRc:inc:maxRc; % R values in compression
Cwinddist = spline(Rc,CFreq,cc);
Cwinddist = Cwinddist*1.245424;

plot(cc,ppval(wc,cc),'b-o');
title('Compression Wind Cycles PDF');
xlabel('Stress/Strain Ratio, R');
ylabel('Probability Mass');

figure;
Cwindcdf=fnint(wc);
Cwindcdf.coefs=Cwindcdf.coefs/ppval(Cwindcdf,Cwindcdf.breaks(end));
plot(cc,ppval(Cwindcdf,cc),'b-o');
title('Compression Wind Cycles CDF');
xlabel('Stress/Strain Ratio, R');
ylabel('Cumulative Probability');
```

**<u>Flaw Distributions</u>**

Program Name: FlawDist.m

```
% Build Flaw Distributiuons

%Spline - for flaw occurance --------
```

```
loc = [0,0.05,0.1,0.15,0.2,0.25,0.3,0.35,0.4,0.45,0.5,0.55,...
    0.6,0.65,0.7,0.75,0.8,0.85,0.9,0.95,1];

% %IPFreq=[0,0.029411765,0,0.073529412,0.117647059,0.132352941,0.088235294,...
%    0,0.029411765,0.058823529,0,0.088235294,0.117647059,0,0.058823529,...
%    0.029411765,0.073529412,0.073529412,0,0.029411765,0];

IPFreq=[0.4,0.44,0.48,0.4,0.36,0.4,0.44,0.32,0.24,0.2,0.16,0.12,0.12,0.08,...
    0.04,0.08,0.04,0.08,0.04,0.04,0];


x=0:1:100;
xx=0:.01:1;
FlawLocDist=spline(loc,IPFreq,xx);
figure;
plot(x,FlawLocDist,'b-o')
title('Flaw Occurance PDF');
xlabel('Spanwise Location (%)');
ylabel('Probability Mass Distribution');
% yy=ppval(y,xx);


%
% plot(xx,y,'b-o');
% title('Flaw Occurance PDF');
% ylabel('Probability Mass')
% xlabel('Spanwise Location, (%)')

figure;
y=FlawLocDist;
T=SplineDistGen(y,1,10000,'plot');

% ----------- IP Waves -------------------------

IPmean = 0;
IPstd = 18;

% Sample IP angles ------------

IPangle = normrnd(IPmean,IPstd,1,10000);
%IPangle = round(IPangle);
for r = 1:100;
    for i= 1:10000;
```

```
    if IPangle(i)<.6;
      IPangle(i)=normrnd(IPmean,IPstd);
    end

    if IPangle(i)>50;
      IPangle(i)=normrnd(IPmean,IPstd);
    end
  end
end

IPx = 1:1:50;
nhist=hist(IPangle,50);
nhist=nhist./10000;
figure;
bar(IPx,nhist);

hold on;
IPx = 0:50;
IPdist = normpdf(IPx,IPmean,IPstd);
p=plot(IPx,2*IPdist);
title('IP Angle Distribution');
xlabel('IP Angle (deg)'); ylabel('pdf');
set(p,'Color','red','LineWidth',2)
hold off;

% OP Waves -------------------------

OPmean = 6.5;
OPstd = 2.8;

% Sample OP angles

OPangle = normrnd(OPmean,OPstd,1,10000);
for i= 1:10000;
  if OPangle(i)<0;
    OPangle(i)=0;
  end
end
for i= 1:10000;
  if OPangle(i)>14;
    OPangle(i)=0;
  end
end
```

```
figure;
OPx = 0:14;
nhistop=hist(OPangle,15);
nhistop=nhistop/10000;
bar(OPx,nhistop);


hold on;
OPx = 0:14;
OPdist = normpdf(OPx,OPmean,OPstd);
p=plot(OPx,OPdist);
title('OP Angle Distribution');
xlabel('OP Angle (deg)'); ylabel('pdf');
set(p,'Color','red','LineWidth',2)
hold off;

% IP Waves KDs ---------

IPrad = degtorad(IPangle);
IPkdComp = .978232.*exp(-.034605*IPangle); % Converts angles to Compression
knockdowns
IPkdTen = 1.0301*exp(-0.055*IPangle);

IPkdTen=transpose(IPkdTen);
IPkdComp=transpose(IPkdComp);

% IPkdX=0.025:.025:1;
% IPkdTenHist=hist(IPkdTen,40);
% IPkdTenHist=IPkdTenHist/10000;
% bar(IPkdX,IPkdTenHist);
% title('IP Angle Strength');
% xlabel('Reduced Static Strength (0.01%)'); ylabel('Samped Instances (PDF)');

figure;
hist(IPkdTen,20);
title('Tension: IP Angle Strength');
xlabel('Reduced Static Strength (0.01%)'); ylabel('Samped Instances (PDF)');

figure;
hist(IPkdComp,20);
title('Compression: IP Angle Strength');
xlabel('Reduced Static Strength (0.01%)'); ylabel('Samped Instances (PDF)');
```

**Spline Distribution**

```
function T = SplineDistGen(P,N,M,varargin)

%check for input errors
for i=1:numel(P);
    if P(i)<0;
P(i)=0;
    end
end
if and(nargin~=3,nargin~=4)
    error('Error:  Invalid number of input arguments.')
end

if min(P)<0
    error('Error:  All elements of first argument, P, must be positive.')
end

if size(P,1)>1
    P=P';
end

if or(N<1,M<1)
    error('Error:  Output matrix dimensions must be greater than or equal to one.')
end

%normalize P
Pnorm=[0 P]/sum(P);

%create cumlative distribution
Pcum=cumsum(Pnorm);

%create random matrix
N=round(N);
M=round(M);
R=rand(1,N*M);

%calculate T output matrix
V=0:1:100;
[~,inds] = histc(R,Pcum);
T = V(inds);

%shape into output matrix
T=reshape(T,N,M);
```

```
for i=1:N*M
   if T(i)<0
   T(i)=0
   end
end

xx=0:1:100;

%if desired, output plot
if nargin==4
   if strcmp(varargin{1},'plot')
      Pfreq=N*M*P/sum(P);
      hold on
      hist(T(T>0),length(P))
      plot(xx,Pfreq,'r-o')
      title('Flaw Occurance PDF');
      ylabel('Probability Mass')
      xlabel('Spanwise Location, (%)')
      axis tight
      box on
      hold off
   end
end

% figure;
% Tx = 1:100;
% Thist=hist(T,100);
% Thist=Thist/10000;
% bar(Tx,Thist);
%
```

**Import Strain Data**

Program Name" FlawDist.m

```
%% Import data from text file.
% Script for importing data from the following text file:
%
%    C:\Users\Riddle.Home\SkyDrive\Spring
%    2013\Rev1\REV1_LP_STRAIN_Results.txt
%
% To extend the code to different selected data or a different text file,
% generate a function instead of a script.
```

```
% Auto-generated by MATLAB on 2013/03/24 20:20:01

%% Initialize variables.

% Home ----
filename = 'C:\Users\Riddle.Home\SkyDrive\Fall 2012\EoD
Blade\BRC_BSDS_Glass\REV1_LP_STRAIN_Results.txt';

% Work ----
%filename = 'C:\Users\trey.riddle\SkyDrive\Fall 2012\EoD
Blade\BRC_BSDS_Glass\REV1_LP_STRAIN_Results.txt';

%Laptop ----
%filename = 'C:\Users\SENSE\SkyDrive\Fall 2012\EoD
Blade\BRC_BSDS_Glass\REV1_LP_STRAIN_Results.txt';

delimiter = '';

%% Format string for each line of text:
%   column1: double (%f)
% For more information, see the TEXTSCAN documentation.
formatSpec = '%f%[^\n\r]';

%% Open the text file.
fileID = fopen(filename,'r');

%% Read columns of data according to format string.
% This call is based on the structure of the file used to generate this
% code. If an error occurs for a different file, try regenerating the code
% from the Import Tool.
dataArray = textscan(fileID, formatSpec, 'Delimiter', delimiter,  'ReturnOnError', false);

%% Close the text file.
fclose(fileID);

%% Post processing for unimportable data.
% No unimportable data rules were applied during the import, so no post
% processing code is included. To generate code which works for
% unimportable data, select unimportable cells in a file and regenerate the
% script.

%% Allocate imported array to column variable names
LPStrain = dataArray{:, 1};
```

```
LPStrain = 100*LPStrain;

%% Clear temporary variables
clearvars filename delimiter formatSpec fileID dataArray ans;

%-----Import HP Strain results-----------------------

% Home
filename = 'C:\Users\Riddle.Home\SkyDrive\Fall 2012\EoD
Blade\BRC_BSDS_Glass\REV1_HP_STRAIN_Results.txt';

% Work ----
%filename = 'C:\Users\trey.riddle\SkyDrive\Fall 2012\EoD
Blade\BRC_BSDS_Glass\REV1_HP_STRAIN_Results.txt';

%LAptop
%filename = 'C:\Users\SENSE\SkyDrive\Fall 2012\EoD
Blade\BRC_BSDS_Glass\REV1_HP_STRAIN_Results.txt';

delimiter = '';

formatSpec = '%f%[^\n\r]';
fileID = fopen(filename,'r');
dataArray = textscan(fileID, formatSpec, 'Delimiter', delimiter,  'ReturnOnError', false);
fclose(fileID);
HPStrain = dataArray{:, 1};
HPStrain = 100*HPStrain;

clearvars filename delimiter formatSpec fileID dataArray ans;
```

**Example LP Strain Data File**

Program Name: REV1_LP_STRAIN_Results.txt

-0.001094318078
-0.001312814616
-0.001714327481
-0.002463618975
-0.002787487916
-0.003023662496
-0.002775567055
-0.002808839907

-0.002732623322
-0.002949618739
-0.003011623257
-0.003145949431
-0.003499206407
-0.004347297409
-0.004714071794
-0.006555721131
-0.006289823135
-0.006169006631
-0.006264707008
-0.006371325485
-0.006664178114
-0.006658053398
-0.006345110893
-0.006243666296
-0.006142633091
-0.006121502813
-0.006051526978
-0.006045023896
-0.006104375046
-0.005998320387
-0.006113702999
-0.006103849792
-0.006078400789
-0.006427101972
-0.006212105678
-0.006112557534
-0.006111953180
-0.006077325942
-0.006075005270
-0.006045569662
-0.006035067745
-0.005984966863
-0.006087172336
-0.006004417263
-0.005956985447
-0.005957062360
-0.005950168590

-0.005922800466
-0.005944329167
-0.006015698245
-0.005906604989
-0.005836109540
-0.005830805613
-0.005790690060
-0.005772684624
-0.005741157499
-0.005727624087
-0.005715866677
-0.005736192105
-0.005688708554
-0.005655128481
-0.005650711453
-0.005606234544
-0.005638523800
-0.005636444877
-0.005629407232
-0.005652490381
-0.005690441707
-0.005754580903
-0.005823442934
-0.005986236539
-0.006087640347
-0.006195652973
-0.006173055513
-0.006177410980
-0.006167032337
-0.006170795087
-0.006164458172
-0.006203718361
-0.006160355831
-0.006215454155
-0.006133209227
-0.006300057949
-0.006222603346
-0.006225262935
-0.006223405872

-0.006235194842
-0.006244619809
-0.006273961064
-0.006294573650
-0.006348352459
-0.006385628078
-0.006424609788
-0.006537333488
-0.006507781289
-0.006432844623
-0.006363618455
-0.006350635266
-0.006327632974

**Example HP Strain Data File**

Program Name: REV1_HP_STRAIN_Results.txt

0.001180771770
0.001396114536
0.001797192544
0.002507987740
0.002968120063
0.003279070811
0.002913193028
0.002979872687
0.002899073381
0.003123629027
0.003231144059
0.003298576532
0.003685704450
0.004567256418
0.004923502187
0.007441253661
0.007146099649
0.006853725944
0.006673364879
0.006661616495
0.006726509941

0.006634648959
0.006354272203
0.006307041865
0.006300550024
0.006340590068
0.006276385893
0.006271282089
0.006322279978
0.006238417801
0.006323027099
0.006312997936
0.006235618813
0.006633507979
0.006395942945
0.006295135369
0.006298910567
0.006273186709
0.006255732322
0.006222724150
0.006222226025
0.006189491376
0.006191738766
0.006152697651
0.006125154695
0.006076464327
0.006053726587
0.006016141761
0.005996978595
0.006028266549
0.005925362369
0.005866444459
0.005819776583
0.005732178710
0.005700839547
0.005638135427
0.005609453282
0.005574035447
0.005553693110
0.005501903003

0.005430330621
0.005406159989
0.005347659535
0.005359568973
0.005283455928
0.005322470977
0.005286332907
0.005376644156
0.005379964539
0.005446544097
0.005515021706
0.005698201765
0.005844774651
0.005631701436
0.005639518724
0.005587839685
0.005583178895
0.005574491981
0.005582447891
0.005578378805
0.005482233067
0.005576532133
0.005574297655
0.005526062644
0.005500410795
0.005488167538
0.005458632249
0.005446844015
0.005427005731
0.005418844861
0.005412673100
0.005406958245
0.005407040259
0.005467055923
0.005533569791
0.005354573584
0.005251516270
0.005202885019
0.005100354850

**Failure of Probability Analysis**

Program Name: probfail.m

```
% Find probabality of failure based on flaw occurance and magintude
% distributions

Tflaw = zeros (10001,10000);
for i = 1:10000
   Tflaw(1,i)=T(i);
end


% Solve for failure -----------------------------------------------

% Alternating Strain - Piecwise Linear CLD Formulation
% Life prediction mtheodology for GFRP laminates under spectrum loading
% Theodore P. Philippidis*, Anastasios P. Vassilopoulos

%----------- LP ----------------
scale=.835;  % modify for scaling coupon to structure

UTS=3.3; % R of 0.1
UCS=2.5;

% Tension: R=0.1
ealtT=scale*5.12; % -- CBB --
ealtprimeT=UTS./((UTS./ealtT)+(1+tt)./(1-tt)-(1+.1)./(1-.1));

% Compression: R=10
ealtC=scale*2.138; % -- CBB --
ealtprimeC=UCS./((UCS./ealtC)-(1+cc)./(1-cc)+(1+10)./(1-10));

% Fatigue Parameters, Modifed single cycle intercept
% Convert alternating strain to max strain

At=(2*ealtprimeT)./(1-tt);
Bt=-.127;

Ac=abs((2*ealtprimeC)./(1-cc));
Bc=-.0713;

% wind speed m/s
```

```
windpseedbins = [1.00,2.00,3.00,4.00,5.00,6.00,7.00,8.00,9.00,10.00,...
    11.00,12.00,13.00,14.00,15.00,16.00,17.00,18.00];

% max speed based on Weibull Dsirtibution a=1.896446, b=5.290971
% for windspeedbins

%windspeedcycles = [77154,127944,153263,154880,138760,112746,84126,...
    %58090,37314,22379,12566,6621,3278,1528,671,278,109,40];

windspeedcycles = [1.2147E+08,2.0144E+08,2.4130E+08,2.4384E+08,2.1846E+08,...
    1.7751E+08,1.3245E+08,9.1458E+07,5.8748E+07,3.5234E+07,1.9784E+07,...

1.0423E+07,5.1611E+06,2.4051E+06,1.0561E+06,4.3736E+05,1.7098E+05,6.3142E+04
];

% ------------ Actual in service life ------------

usefullife = windspeedcycles*1; %------------EDIT--------------
usefullife = transpose(usefullife);

% ----------------------------------------------

windspeedfreq=windspeedcycles/sum(windspeedcycles);

importdata; % Import strain data file p=13000
pressure = 13000; % for 1e6  failure
critialspeed = 11.575; % m/s
escale = 409; % Sclaing strain based on applied pressure

strainscalefactor = (escale.*windpseedbins)./pressure;
Lpstrainscaled = zeros(99,18);
Hpstrainscaled = zeros(99,18);

for i= 1:18;
    for j = 1:99;
        Lpstrainscaled(j,i)=(abs(LPStrain(j)))*strainscalefactor(i);
        Hpstrainscaled(j,i)=(abs(HPStrain(j)))*strainscalefactor(i);
    end;
end;

% Applied Cycles
%life=20;
%Nyr = 15246*3; % Total cycles in a year
Nlife = 1574400000; % cycles for 20 year with safety factor
```

```
NperRt=Nlife*Twinddist;
NperRc=Nlife*Cwinddist;

% Number of cycles to failure using adjusted power law S-N

index = 0;

LPcount = zeros(99,1);
HPcount = zeros(99,1);

NfT = zeros(99,18);
NfC = zeros(99,18);

DindexT = zeros(99,18);
DindexC = zeros(99,18);

LowPdamage = zeros(99,1);
HighPdamage = zeros(99,1);

PfLP = zeros(99,1);
PfHP = zeros(99,1);

gf = 1.25; % Loads SF IEC: 1.25
gm = 1.15;  % Material SF IEC: 1.3

anglenum = 1000; %------------EDIT--------------

   for i= 1:99;
      for h = 1:anglenum;
         for j = 1:18;
            for k = 1:100

%NfT(i,j)=NfT(i,j)+Twinddist(k).*(((Hpstrainscaled(i,j))./(IPkdTen(h,1).*At(k))).^(1/Bt)
);

%NfC(i,j)=NfC(i,j)+Cwinddist(k).*(((Lpstrainscaled(i,j))./(IPkdComp(h,1).*Ac(k))).^(1/
Bc));

NfT(i,j)=NfT(i,j)+Twinddist(k).*(((gf*gm*Hpstrainscaled(i,j))/(IPkdTen(h,1).*At(k))).^(
1/Bt));

NfC(i,j)=NfC(i,j)+Cwinddist(k).*(((gf*gm*Lpstrainscaled(i,j))/(IPkdComp(h,1).*Ac(k)))
.^(1/Bc));
```

```
            end
          end;

          for j = 1:18;
            DindexT(i,j)=(windspeedcycles(j)/NfT(i,j));
            DindexC(i,j)=(windspeedcycles(j)/NfC(i,j));
          end

          LowPdamage(i,1) = 0;
          HighPdamage(i,1) = 0;

          for j = 1:18;

            LowPdamage(i,1) = LowPdamage(i,1)+DindexC(i,j);
            HighPdamage(i,1) = HighPdamage(i,1)+DindexT(i,j);
          end

          if LowPdamage(i,1)>1;
            LPcount(i,1) = LPcount(i,1) + 1; % number of failed instances
          end

          if HighPdamage(i,1)>1;
            HPcount(i,1) = HPcount(i,1) + 1; % number of failed instances
          end

        end

    PfLP(i) = 100*(LPcount(i)/anglenum);
    PfHP(i) = 100*(HPcount(i)/anglenum);

    end;

%     for i= 1:99;
%         PfLP(i) = 100*(LPcount(i)/anglenum);
%         PfHP(i) = 100*(HPcount(i)/anglenum);
%     end


figure;
plot(PfLP);
title('LP Probability of Failure');
xlabel('Spanwise Location (%)');
ylabel('Probability of Faliure (%)');
```

```
figure;
plot(PfHP);
title('HP Probability of Failure');
xlabel('Spanwise Location (%)');
ylabel('Probability of Faliure (%)');

for i = 1:99
    CompPf(i) = FlawLocDist(i)*PfLP(i);
end

figure;
plot(CompPf);
title('Compression Probability of Failure');
xlabel('Spanwise Location (%)');
ylabel('Probability of Faliure (%)');

for i = 1:99
    TenPf(i) = FlawLocDist(i)*PfHP(i);
end

figure;
plot(TenPf);
title('Tension Probability of Failure');
xlabel('Spanwise Location (%)');
ylabel('Probability of Faliure (%)');

% -- Devloping Results fro one Location ----



CumPfLP = cumsum(CompPf);
figure;
plot(CumPfLP);
title('LP Cumlative Probability of Failure');
```

# APPENDIX D:

## FEA ANSYS CODE

```
  et,11,shell99,,0
  keyopt,11,8,1

  et,12,shell99,,0
  keyopt,12,8,1
  keyopt,12,11,1

  et,14,shell99,,0
  keyopt,14,8,1
  keyopt,14,11,2
.
.
.
et,21,mass21,,,0
  r,999,0.0,0.0,0.00001,0.0,0.0,0.0

  et,31,shell281
  keyopt,31,8,2

  et,32,shell181
  keyopt,32,8,2

! WRITE MATERIAL PROPERTIES ===========================

  ! 075oz_Mat
  mp,ex,1,7.58e+009
  mp,ey,1,7.58e+009
  mp,ez,1,7.58e+009
  mp,prxy,1,0.3
  mp,pryz,1,0.3
  mp,prxz,1,0.3
  mp,gxy,1,4e+009
  mp,gyz,1,4e+009
  mp,gxz,1,4e+009
  mp,dens,1,1687
.
.
.
!!!! Begin Parametric Material Designation ========

  YoungX=4.14e+010
  YoungY=1.63e+010
```

```
  ! PPG_Devold_L1200_G50_E07
  mp,ex,12,YoungX            !!! Probabilistic Material Definition ====
  mp,ey,12,YoungY            !!! Probabilistic Material Definition ====
  mp,ez,12,YoungY            !!! Probabilistic Material Definition ====
  mp,prxy,12,0.23
  mp,pryz,12,0.3
  mp,prxz,12,0.23
  mp,gxy,12,1.68e+010
  mp,gyz,12,6.27e+009
  mp,gxz,12,1.68e+010
  mp,dens,12,1900
.
.
.
  ! SteelA36
  mp,ex,13,2e+011
  mp,dens,13,7850
  mp,nuxy,13,0.3

! WRITE THE COMPOSITES =================================

  ! BSDS_2_Strip
  sectype,1,shell
    secdata,0.000508,11,0,,Gel_Coat
    secdata,0.000305,1,0,,075oz_Mat
    secdata,0.002946,9,0,,DBM1708
  secoffset,bot
.
.
.
/title,BRC_BSDS_Glass
ZrCount=1

! DEFINE KEYPOINTS FOR SECTIONS AND CONNECT KEYPOINTS WITH
LINES

local,1000,CART,0,0,0, -90,0,-90

csys,0
  ksel,none
    k,1,-0.254251,0.0826111,0
    k,2,-0.263361,0.0459203,0
    k,3,-0.265317,0.0327489,0
.
```

```
.
.
   zAirfoil
   csys,1000
   clocal,1035,CART,8.325,0,0, 0,0,-0

local,12,CART,0,0,8.325, 0,0,0

   csys,0
ksel,all

allsel

! GENERATE SPANWISE LINES FOR LATER AREA CREATION ======

*get,z_lines_after_splining,line,,num,max

*dim,z_HP_line,,35
*dim,z_LP_line,,35
*dim,z_HP_area,,34
*dim,z_LP_area,,34
*dim,z_TE_line,,34
*dim,z_LE_line,,34
*dim,z_LP_knee_line,,34
*dim,z_HP_knee_line,,34

! Generate HP and LP lines at each station ============

   ksel,s,kp,,1,62
      lslk,s,1
      lcomb,all,,1
      *get,z_HP_line(1),line,,num,max
.
.
.
! Generate TE and LE spanwise lines from station to station

csys,0
allsel
   l,1,1001
   *get,z_TE_line(1),line,,num,max
   l,62,1062
   *get,z_LE_line(1),line,,num,max
.
```

```
.
.
! Generate areas needed for later LAREA commands =======

csys,0
allsel
   al,z_HP_line(1),z_LE_line(1),z_HP_line(2),z_TE_line(1)
   *get,z_HP_area(1),area,,num,max
   al,z_LP_line(1),z_TE_line(1),z_LP_line(2),z_LE_line(1)
   *get,z_LP_area(1),area,,num,max
.
.
.
! Generate spanwise area-bounding lines with LAREA command

  larea,3,1003,z_HP_area(1)
  larea,30,1030,z_HP_area(1)
  larea,58,1058,z_HP_area(1)
  larea,62,1062,z_HP_area(1)
  larea,66,1066,z_LP_area(1)
  larea,94,1094,z_LP_area(1)
  larea,121,1121,z_LP_area(1)
.
.
.
! Cleanup entities generated exclusively to facilitate LAREA command

   adel,z_HP_area(1)
   adel,z_LP_area(1)
   ldel,z_HP_line(1)
   ldel,z_LP_line(1)
   ldel,z_LE_line(1)
.
.
.
! COMBINE LINES IN EACH CROSS SECTION INTO LONGER (COMPLEX)
LINES

  lsel,none
  cm,tip_station_lines,line
   lsel,s,line,,1,2
   lcomb,all
   lsel,s,line,,3,29
   lcomb,all
```

```
   lsel,s,line,,30,57
   lcomb,all
   lsel,s,line,,58,61
   lcomb,all
   lsel,s,line,,62,65
   lcomb,all
   lsel,s,line,,66,93
   lcomb,all
   lsel,s,line,,94,120
   lcomb,all
   lsel,s,line,,121,122
   lcomb,all
.
.
.
llsel
!   numcmp,kp
!   numcmp,line

! GENERATE SKIN AREAS ==================================

   asel,none
   lsel,all
   csys,0
   a,1,3,1003,1001
     aatt,,,32,1001,23
   asel,none
   lsel,all
   csys,0
   a,3,30,1030,1003
     aatt,,,32,1001,23
.
.
.
allsel
!   numcmp,kp
!   numcmp,line
! CREATE AREAS FOR SHEAR WEBS ===========================

   asel,none
   lsel,all
   csys,0

   l,30092,30034
```

```
  l,31033,31092
  a,30092,30034,31033,31092
    aatt,,,32,1031,1020
.
.
.
! MESH THE AREAS ==========================================

allsel
  areverse,all
  local,11,CART,0,0,0,90,0,-90
  esys,11
  mshape,0,2d
  aesize,all,0.050000
  amesh,all
  csys,0

  csys,12
  nsel,none
  n,,0.0,0.0,0.0
  *get,z_master_node_number,node,,num,max
  type,21
  real,999
  e,z_master_node_number
  nsel,all
  csys,0
  allsel

  cmsel,s,tip_station_lines
  nsll,s,1
  nsel,a,node,,z_master_node_number
  cerig,z_master_node_number,all

! APPLY BOUNDARY CONDITIONS ==================

  nsel,s,loc,z,0
  d,all,all
  nsel,all

  FK,33001,FY,1000
  FK,33020,FY,1000
  FK,33031,FY,1000
  FK,33037,FY,1000
  FK,33060,FY,1000
```

```
  FK,33088,FY,1000
  FK,33099,FY,1000

allsel
!   nummrg,all
!   numcmp,node
csys,0

!!! SOLVE =============

/SOLU

   ANTYPE,STATIC
   SOLVE

!!! RETREIVE RESULTS AND ASSIGN OUTPUT PARAMETERS==========

/POST1

   SET,FIRST
   NSORT,U,Y                    ! Sorts nodes based on UY deflection
   *GET,DMAX,SORT,,MAX          ! Parameter DMAX = maximum deflection
   NSORT,S,EQV
   *GET,SMAX,SORT,,MAX          ! Parameter SMAXI = max. value of SMAX_I
   *GET,SMIN,SORT,,MIN
.
.
.
!!! Solve =============

/SOLU

   ANTYPE,STATIC
   SOLVE
save
FINISH

!!! RETEREIVE RESULSTS AND ASSIGN AS OUTPUTS
PARAMETERS==========

/POST1

   SET,FIRST
   NSORT,U,Y                    ! Sorts nodes based on UY deflection
```

```
   *GET,DMAX,SORT,,MAX         ! Parameter DMAX = maximum deflection
   NSORT,S,Z
   *GET,SMAX,SORT,,MAX         ! Parameter SMAXI = max. value of SMAX_I
   *GET,SMIN,SORT,,MIN

!!! BEGIN PROBABILSTIC PARAMETER DESIGNIATIONS =========

/PDS

   !!!! RANDOM INPUT PARAMETERS =======
   PDVAR,YOUNGX,LOG1,4.14e+010,.21e+010,0,0
   PDVAR,YOUNGY,LOG1,1.63e+010,.2e+010,0,0

   ! ASSIGN RANDOM OUTPUT VARIABLES =====
   PDVAR,DMAX,RESP
   PDVAR,SMAX,RESP
   PDVAR,SMIN,RESP

   PDANL,'shell7_Prob_Rev0.db','txt',' '

   PDMTHE,MCS,DIR              ! Defines Monte Carlo Direct Sampling Mtheod
   PDDMCS,240,,ALL,
   PDEXE,,SER

save
finish
```